Finite Element Modelling Of Mechanical Properties Of Polymer Composites

By

ELAHEH GHASSEMIEH

A Doctoral Thesis

Submitted in partial fulfilment of the requirements
For the award of Doctor Of Philosophy
By Loughborough University

December 1998

To those whose love kept my heart warm
and encouraged me all through my life, during the period of this study
and in near or far,
especially my dear mother Parichehr and my father Mehdi

Acknowledgements

Hereby I would like to thank my supervisor, Dr. V. Nassehi, for his assistance and advice during the course of this research and I wish to show my gratitude to all the members of staff and students in the Chemical Engineering Department of Loughborough University who accompanied me all over the way. I learned a lot from them and I enjoyed being with them.

A door to a new world was opened to me, an experience that will always be remembered.

ABSTRACT

Polymeric composites are used widely in modern industry. The prediction of mechanical behaviour of these material under different loadings is therefore of vital importance in many applications. Mathematical modelling offers a robust and cost effective method to satisfy this objective. In this project a comprehensive finite element model for particulate and fibre reinforced composites is developed.

The most significant features of this model are:

- The inclusion of slip boundary conditions.
- The inclusion of flux terms across the inter-phase boundaries to take the discontinuity of the material properties into account in the model.
- The use of penalty method in conjunction with Stokes flow equations which allow the application of the developed model to solid elasticity analysis as well as creeping viscous flows.

The predictions of this model are compared with available theoretical models and experimental data. These comparisons show that the developed model yields accurate and reliable data for composite deformation.

TABLE OF CONTENTS

Chapter Five

Chapter One

INTRODUCTION

Polymeric composites are amongst the most important new material resources. This is because of the relative low cost of manufacturing of these materials and the possibility of obtaining improved and unique properties from them. The bulk properties of polymeric composites obviously depend on their microstructure. Therefore the composite properties and their behaviour should be assessed and analysed considering microstructural responses of composites to external loading and conditions.

The main objectives of this project have been the analysis of the micromechanical behaviour of different types of polymeric composites using mathematical modelling. We have considered continuous fibre reinforced composite, short fibre reinforced composite and composites with hard or soft particles.

To understand the mechanical behaviour of composites, the mechanical behaviour of the constituent materials and the interactions of these constituents should be investigated.

Mathematical modelling offers a powerful prediction tool to carry out such investigation. In recent years a number of mathematical models for the microstructural behaviour of composites have been proposed. Most of these models are formulated in terms of mathematical equations, which cannot be solved analytically. Therefore in most cases the use of a numerical technique for the quantitative analysis of composite behaviour is required.

Finite element method combines robustness with flexibility and hence it is the method of choice in most applications. In this project we have considered the finite element schemes based on the 'displacement method' and the 'weighted residual method'. It is especially important to note that using the latter method a mathematical model for the microstructural analysis of composites can be developed which is based on equations similar to the fundamental equations of fluid dynamics. This approach has the advantage of using a single model for the analysis of composites in liquid or solid state. This thesis consists of five chapters. The introductory chapter describes the outline of the thesis and includes a summary of the properties of various composites investigated in the present work. In chapter two a thorough literature survey is given and the background of the present project is presented. In chapter three the development of the working equations of the model and the domain geometry are described. This chapter also includes explanation regarding the finite element mesh, the boundary conditions and the postprocessing calculations used. Chapter four is devoted to the computational results and discussion and the comparison with the available experimental data and the results generated by other models. Chapter four consists of the following sections:

In section one of this chapter the most important bulk property of composites, the modulus is studied. The effect of model assumptions and boundary conditions on the results obtained are discussed.

In section two the mechanical behaviour of epoxy resin filled with hard glass particles is studied as a typical composite filled with rigid particles. The addition of rigid particles to epoxy resins can result in a significant improvement in the properties of the resin and a considerable reduction in cost. There is invariably an increase in the stiffness of the resin but the effect of the particles upon the fracture behaviour is complex. The fracture behaviour of multiphase polymers has been reviewed and there has been considerable interest over the years in crack propagation in brittle materials reinforced with rigid filler particles. It is found that, in general, both the critical stress intensity factor and fracture energy increase with the addition of rigid particles, at least for low volume fractions of filler. The most generally accepted explanation of this

behaviour, using the analogy of a dislocation moving through a crystal, is that a crack in a body possesses "line tension" and that when it meets an array of a impenetrable obstacles it becomes pinned. In order to move past the obstacles the crack would have to bow out and this leads to an increase in fracture energy. The fracture energy reaches a maximum at a particular value of filler volume fraction and then falls with the further addition of particles, implying that there may be another mechanism which competes with crack front pinning at high volume fractions of filler.

Particulate filled composites are used in applications ranging from everyday usage, like automobile tires, to specific, such as solid rocket propellants. These materials exhibit interesting failure properties. Phenomena such as cavitation (the appearance of voids) and debonding (adhesive failure between matrix and filler particles) lead to gross nonlinearities in their stress-strain behaviour. Particulate composites subjected to large strains generally exhibit large degrees of debonding. The parameters that affect this failure include particle size, filler concentration, surface treatments, matrix and filler properties, superimposed pressure, and strain rate. Debonding of filler particles appears to be the dominant factor influencing both stress-strain and volumetric behaviour of particulate materials.

In section three the stress field in a composite with partially or fully debonded rigid particles is analysed. Bond degradation is often a critical factor in determining the ultimate strength of a composite material, as well as its fatigue resistance, impact resistance, and other important properties. The strength of the bonding between filler and matrix plays a major role in the ability of the composite to bridge cracks or deflect cracks along the interface and, thereby, contribute to composite fracture toughness. For such fracture toughening to occur, the filler matrix interface must exhibit just the right degree of bonding. If the bonding is too strong, the composite behaves like a monolithic material and cracks propagate through the material generally resulting in brittle fracture.

Improving adhesion at the interface increases the fracture strength of the composite , it is not entirely clear how this affects crack propagation. There have been reports of improving adhesion at the interface both increasing and decreasing the fracture energy, for crack propagation in particle reinforced composites.

With good adhesion it is found that the fracture strength of the composites is approximately the same as that of the unfilled matrices. On the other hand, with no surface pretreatments, or release agents, applied to the particles the strength decreases with increasing volume fractions of filler particles.

In the fourth section of chapter four the effects of adding rubbery particles on the mechanical characteristic of a matrix material such as epoxy resin are studied. The improvement of the impact properties of polymers is possible through incorporation of rubbery phase domains into a brittle polymer matrix. The increase in the toughness of glassy polymers with addition of rubber particles is believed to be due to induced wide-spread energy absorbing deformation processes, such as crazing and shear yielding, in the matrix material during fracture. Shear yielding is important; firstly, it is the factor which limits the strength of the composite if brittle fracture can be suppressed. A composite must have a high yield stress in order to be strong and if bulk, homogeneous yielding does occur the polymer is likely to be tough. Secondly, recent evidence suggests that shear yielding, in the form of microshear bands, plays a key role in the initiation of cracks. Shear yielding and crazing, both involve localised, or inhomogeneous, plastic deformation of the material which arises from strain softening and geometric considerations. The difference between the mechanisms is that shear yielding occurs essentially at constant volume whereas crazing occurs with an increase in volume. Thus, unlike shear yielding, crazing is a cavitation process in which the initiation step requires the presence of a dilatational component to the stress tensor and may be inhibited by applying hydrostatic pressure but enhanced in the presence of triaxial tensile stresses.

A craze is initiated when an applied tensile stress causes microvoids to nucleate at points of high stress concentrations in polymer. These microvoids are created by

scratches, flaws, cracks, dust particles, molecular heterogeneities. In general the microvoids develop in a plane perpendicular to the maximum principal stress but do not coalesce to form a true crack. Thus a microvoid is capable of transmitting loads across its faces. However, when cracks do initiate and grow they do so by means of the breakdown of the fibrillar structure in a craze. The importance of crazing is that it is frequently a precursor to brittle fracture. This is because, although considerable plastic deformation and local energy adsorption are involved in craze initiation, growth and breakdown, this micromechanism is often highly localised and confined to a very small volume of the material. However, it should be recognised that if stable crazes can be initiated in a comparatively large volume of the polymer, i.e. a multiple deformation mechanism is induced, then such multiple crazing may lead to a tough, and possibly even a ductile, material response.

Crazes are formed at the rubber particles whereas shear yielding takes place between the modifier particles.

The rubber inclusions cause a local stress magnification in the matrix material immediately surrounding the inclusions. This local stress magnification is believed to initiate crazing and shear yielding. A great deal of controversy still exists on the nature of the toughening mechanisms. Much of the dispute surrounds the issues of whether the rubber or the matrix absorbs most of the energy and whether the matrix undergoes massive crazing or simple voiding. Presumably, once the mechanisms responsible for the increased toughness are clearly identified, then the material parameters responsible for these mechanisms can be enhanced or modified to produce an optimal combination of properties.

The behaviour of the continuous fibre reinforced composites under tensile and shear loading is studied in section five of chapter four. High specific strength and stiffness properties of fibre reinforced composite materials have resulted in their widespread use in load bearing structures. These structures have complex geometries and are often subjected to multiaxial loadings. Monolithic material mechanical behaviour can be adequately described by a limited number of material properties and strength criteria as these materials present simple failure modes under different loading and boundary

conditions. Strength characterisation of composite laminate structures is more difficult to estimate because of the variety of failure modes and failure mode interactions. For a continuous fibre reinforced composite, the strength of the composite is derived from the strength of the fibres, but this strength is highly directional in nature. The longitudinal strength of the continuous fibre reinforced composites is much greater than the transverse strength. The compressive strengths associated with these directions may be different from the corresponding tensile strengths.

Failure of composite materials are determined not only by their internal properties such as properties of constituents and microstructural parameters but also by external conditions such as geometric variables, type of loading and boundary conditions. Critical failure modes for each composite material system under various loading conditions must be identified and a failure criterion should be established for each failure mode.

Finally the last section of chapter four presents the results of the analysis of the short fibre reinforced composites. Short fibre reinforced composites are not as strong or as stiff as continuous fibre reinforced composites and are not likely to be used in critical structural applications. However, short fibre composites do have several attractive characteristics that make them worthy of consideration for other applications. For example, in components having complex geometrical contours, continuous fibres may not be of practical use because they may not conform to the desired shape without being damaged or distorted from the desired pattern. On the other hand, short fibres can be easily mixed with the liquid matrix resin, and the resin/fibre mixture can be injection or compression moulded to produce parts having complex shapes. Such processing methods are also fast and inexpensive, which makes them very attractive for high volume applications. Composites having randomly oriented short fibre reinforcement are nearly isotropic, whereas unidirectional continuous fibre composites are highly anisotropic. In many applications the advantages of low cost, ease of fabricating geometrically complex parts, and isotropic behaviour are enough to make short fibre composites the material of choice.

Since the elastic modulus of the fibre is typically much larger than that of the matrix, the axial elastic displacements of the two components can be very different. In order to rationalise the design of reinforced materials, it is thus of primary importance to have a detailed knowledge of stress distribution induced by the applied load. Indeed, when discontinuous fibres are used, the attainment of good mechanical properties depends critically upon the efficiency of stress transfer between matrix and the fibres. That efficiency is often characterised by the critical length required of the fibre to build up a maximum stress equal to that of an infinitely long fibre.

The effective properties of fibre reinforced composites strongly depend on the geometrical arrangement of the fibres within the matrix. This arrangement is characterised by the volume fraction of fibres, the fibre aspect ratio and the fibre spacing parameter. Analytical equations for the variation of stress along discontinuous fibres in a cylindrically symmetrical model have been derived by Cox. In this approach the adhesion across the end face of the fibres is neglected and the local stress concentration effects near fibre ends have not been taken into account. The importance of these assumptions has been demonstrated by finite element approaches.

The overall conclusions of the present project are discussed in chapter five. The list of references quoted in the text is included at the end of the thesis.

The main objectives of this project can be summarised as:

- Developing a model to predict the mechanical properties of polymer composite
- Developing a code that can be used for studying the behaviour of the polymer composites in the both solid and liquid states.
- Including the boundary line integral terms in the model and investigating the effect of that on the final results of the computations for different shape of the fillers and composites.

- Imposing the slip boundary condition at the interface of the filler and matrix in order to simulate the level of adhesion at the boundary of a debonded filler particle.
- Applying the developed model for different types of composites such as composites filled with hard particles or soft particles, composite reinforced with continuous or short fibres. Using the proper geometry model and boundary condition for each case. Validating the results of the computation by comparing with experimental data and other well established model in each case in order to evaluate our model in qualitative and quantitative analysis.

Chapter Two

LITERATURE REVIEW

2.1 INTRODUCTION

A composite material is a combination of at least two chemically distinct materials with a distinct interface separating the components. Composites can offer a combination of properties and a diversity of applications unobtainable with metals, ceramics or polymers alone. Composites are also used when it is necessary to substitute the traditional materials. Substitution can be the result of legislation, performance improvement, cost reduction and expansion of product demand. For example the trend of legislation on minor impact damage has provided motivation for widespread substitution of plastics with metals in automobile bumpers. Improvement of mechanical properties such as load bearing and transfer, creep, fatigue strength and high temperature strength is also regarded as an important reason for designing and manufacturing of polymer composites. The enhancement of heat, abrasion, oxidation, corrosion and wear resistance which can protect the objects confronting environmental attacks is another reason for the increased use of composite materials. Improved electrical, magnetic and thermal conductivity properties can also be considered as objectives of the design of composite materials.

2.2 TYPES OF COMPOSITES

In polymeric composites the base or matrix is a polymer and the filler is an inorganic or organic material in either fibre or particulate form.

The properties of an advanced composite are shaped not only by the kind of matrix and reinforcing materials it contains but also by another factor which is distinct from composition. This factor is the geometry of reinforcement. Geometrically, composites can be grouped roughly by the shape of the reinforcing elements as particulate, continuous fibre or short fibre composites.

2.2.1 Polymeric composites filled with fibres

Addition of fibres to a polymer matrix enhances its stiffness, strength, hardness, abrasion resistance, heat deflection temperature and lubricity while reducing its shrinkage and creep. The fibre aspect ratio (i.e. the ratio of the characteristic length L to the characteristic diameter D of a typical fibre) and the orientation of fibres have profound influence on the properties of the composites. The most effective reinforcing fillers are fibres which intrinsically have a high elastic modulus and tensile strength. A superior composite is a material which can effectively transfer the applied load to the fibres.

Fibres can be made of organic material such as: Cellulose, Wood , Carbon / Graphite, Nylons and Polyester. At the present time however, for reasons of constitutional strength, stiffness, thermal stability, and sometimes cost, inorganic fibres are the most important reinforcement materials which are compounded with polymers. Recent developments in high modulus and thermally-resistant organic fibres are creating interest, especially where light weight materials are needed as in aerospace applications. Inorganic materials such as Asbestos, Glass, Boron, Ceramic, Metal filaments are commonly used in the production of fibres. Similar to organic fibres, these are produced using both natural and synthetic raw materials.

2.2.2 Polymeric composites filled with particulate fillers

This kind of filler embraces not only fillers with regular shapes, such as spheres, but also many of irregular shapes possibly having extensive convolution and porosity in

addition. However, the use of these types of fillers does not improve the ultimate tensile strength of the composites. In fact the tensile, flexural and impact strength of these composites are lowered, especially at higher filler contents. On the other hand hardness, heat deflection temperature and surface finish of particulate filled composites may be enhanced and their stiffness is mainly improved. Thermal expansion, mold shrinkage extendibility and creep are reduced too. The main advantage of using these fillers is that regardless of the bonding efficiency between particulate filler and matrix, the properties remain consistent. In addition the elastic modulus and the heat distortion temperature increases while structural strength decreases.

Wood flour, Cork, Nutshell, Starch, Polymers, Carbon and Protein are some of the commonly used organic particulate fillers.

Despite limited thermal stability, organic fillers have an advantage of being of low density and many have a valuable role as a cheap extender for the more expensive base polymer, as well as providing some incidental property such as reduction of mould shrinkage which is important in polymer processing.

Glass, Calcium carbonate, Alumina, Metal oxides, Silica and Metal powder are examples of the inorganic materials which are used as particulate fillers.

This class of fillers constitutes the more important group of particulate fillers in view of their low price and ready availability. Thus providing a basis for reducing the cost of moulded articles made with particulate filled composites without too much loss, if any, of desired properties (Sheldon, 1982).

2.3 MECHANICAL PROPERTIES OF POLYMERIC COMPOSITES

In many respects the mechanical properties of different polymers are their most important characteristics. Since whatever may be the reason for the choice of a particular polymer for an application, (whether it be thermal, electrical or even aesthetic grounds), it must have certain characteristics of shape, rigidity and strength. For polymer composites, improvement of mechanical behaviour is a prime requirement. Since by definition the polymer constitutes the continuous phase, the filler acts essentially through a modification of the intrinsic mechanical properties of

the polymer. Factors such as concentration, type, shape and geometrical arrangement of the filler within the matrix are the main contributors to the modification of the mechanical properties of polymer composites.

2.3.1 Mechanical properties of unfilled polymers

The most common way of recording mechanical properties of polymers is to carry out stress-strain, or more precisely load-extension tests. For amorphous polymers the finite natural relaxation rate of polymer chains results in the viscoelastic behaviour of these materials. The viscoelasticity of the polymers is itself a varying quantity relevant to the spectrum of chain movements within a particular polymer. Results of stress-strain tests for various types of polymers are shown schematically in *figure 2.1.*

Factors which affect the movement of polymer chains are responsible for changes in mechanical properties of polymers and can be listed as:

- ***Molecular weight:*** The first parameter to be considered is the molecular weight, which reflects in many cases the method of polymerisation of polymer and its origin. A lower average molecular weight invariably results in a softer polymer.

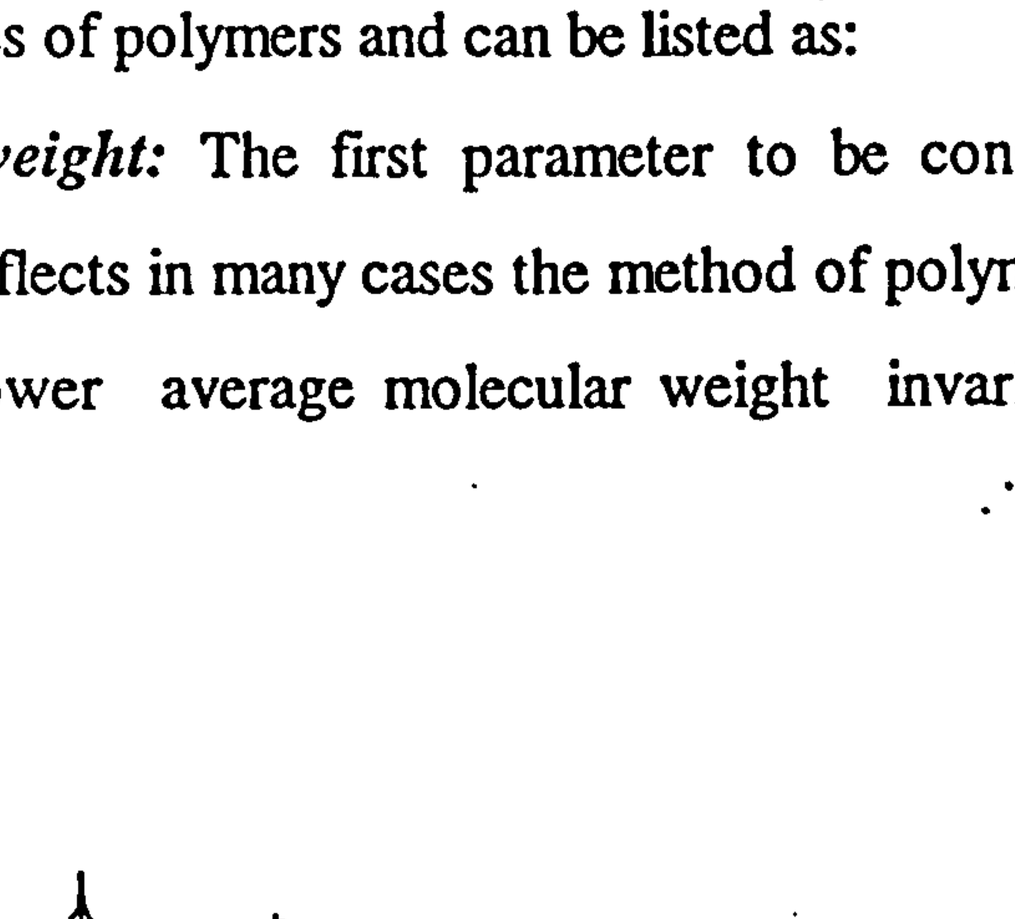

Fig2.1 Stress-Strain behaviour of polymers: (a) hard, brittle; (b) hard, strong (c)hard, tough; (d) soft, tough; (e) soft, weak

- ***Branching or cross-linking:*** Any cross-linking between polymer chains will push up the transition temperature.
- ***Crystallinity:*** Crystallinity in the polymer presents an intermediate case, with some of rigidity being retained through the stabilising effect of the crystalline regions which themselves only fail when the melting point is reached. The overall relaxation behaviour is affected by the restricted movement of those chains which are in crystalline regions, and a new type of time dependent response can arise through structural slippage within these regions.
- ***Impurities:*** The presence of impurities or low molecular weight additives such as moisture or organic liquids, will produce a softening as well as a weakening effect.
- ***Temperature:*** It is not exceptional for a polymer to transverse all five of the above classes of mechanical properties in a temperature range of no more than hundred degrees. For an amorphous polymer, the biggest transition in mechanical properties takes place at the glass transition temperature.
- ***Strain rate:*** The response of a polymer is affected by the rate of applying strain especially just above the glass transition temperature, when an increase of deformation rate causes an increase in apparent modulus and also usually gives rise to a more brittle-like failure of the polymer.

2.3.2 Mechanical properties of particulate filled polymers

A filler may be primarily used as an inexpensive extender, pigment or UV stabiliser. The produced composite must still have suitable mechanical properties for its intended application.

Based on a simple analysis it may be thought that the influence of a particulate filler on the deformability of a polymer may be purely hydrodynamic. This means that, it merely distorts the molecular flow pattern during the deformation of polymer, in practice however, specific interactions very often produce enhanced stiffening effects beyond what is expected from an unfilled polymer.

Figure 2.2a shows the stress-strain curves for a filled elastomer, while *figure 2.2b* and *2.2c* show typical data for a particulate-filled composite having a rigid matrix. In

both cases, as expected, the modulus increases with increased filler concentration. This may not always be the case, since if fabrication is accompanied by extensive void formation then the modulus of the produced composite may decrease. It can be seen in *figures 2.2a-2c* that the modulus increases for both soft and rigid matrices, while the tensile strength and elongation at break do not follow the same relationship. The tensile strength, however, particularly for a rigid matrix with rigid filler decreases with the increase of filler concentration. This is attributed to an increased concentration effect as well as the formation of microcracks either at the interface or locally in the matrix. In the case of a soft elastomeric-based composite, which is capable of dispersing stress more effectively, the tensile strength may very well increase as a result of higher filler concentrations. A maximum will be reached in this latter case, if

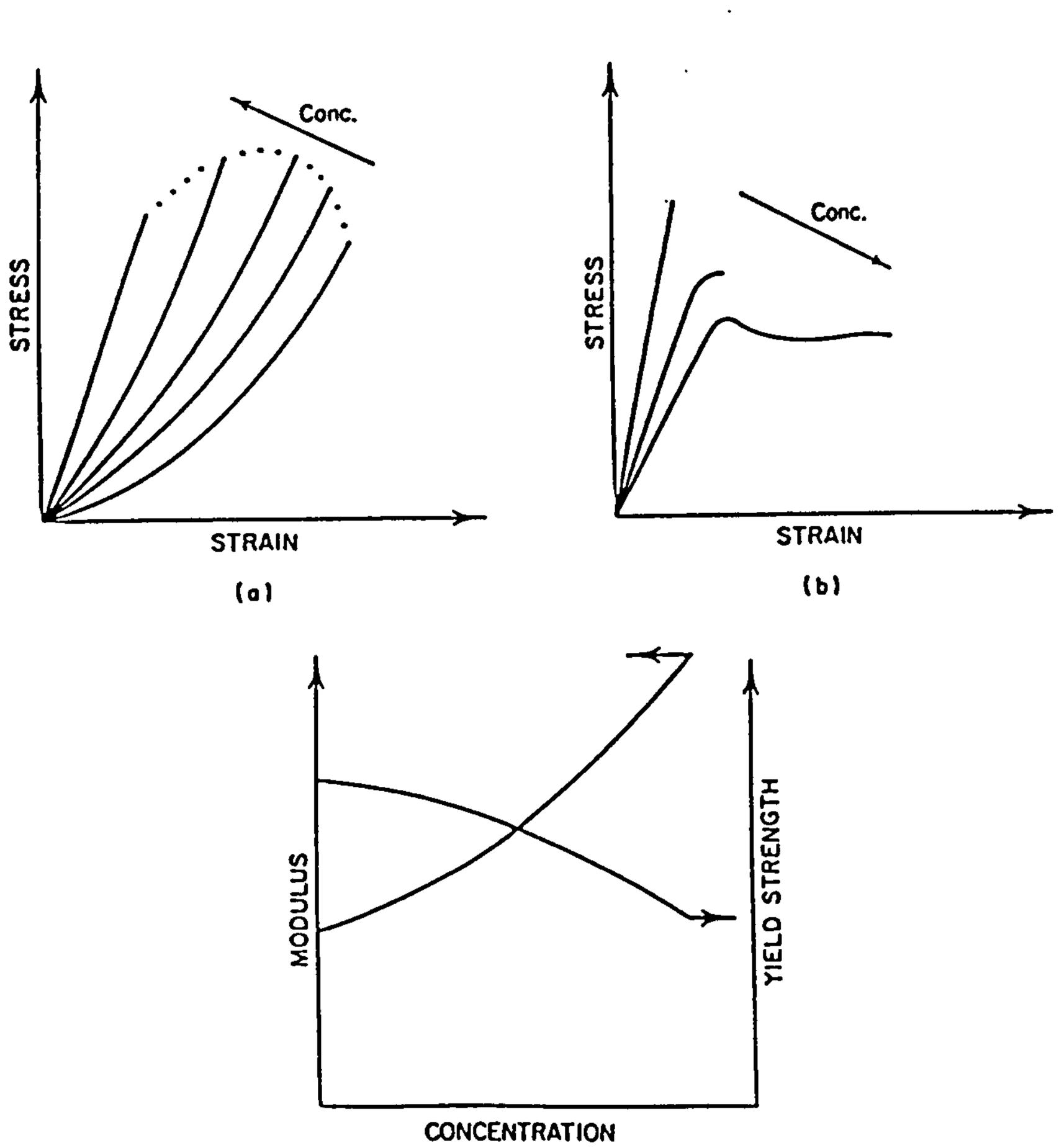

Fig.2.2 Stress-strain behaviour of polymer-particulate filler composites
(a) soft matrix, hard filler; (b) hard matrix, soft filler; (c) hard matrix, hard filler

for no other reason than that eventually the matrix continuity will be replaced by particle/particle contact. Thus mechanical coherence except for some agglomeration will be greatly reduced. On the latter point, it follows that improved dispersion can have an opposite effect on strength compared to modulus. Considering the other extreme property, i.e. elongation at break, it might be expected that this quantity will fall with increasing filler concentration. This is because proportionally, more strain is being applied to less polymer. However the use of soft fillers in a rigid matrix can give rise to an increase in elongation at break and also in impact strength. Part of this may be derived from the ability of some fillers to promote craze formation in deformed polymer prior to fracture.

Debonding and crack formation generally lower the strength of composites. In certain cases however, where cross-linked low energy brittle plastics such as polyesters and epoxides are involved, the actual fracture energy which is distinct from strength, may be increased by the presence of filler. The fracture energy increases up to quite high concentrations of filler after which it decreases again.

2.3.3 Non-linear behaviour of polymeric composites

It is usually assumed that composites have a linear mechanical behaviour to avoid the complexities involved in non-linear analysis. This can hardly be observed even for a pure polymer. The non-linear behaviour of a material is normally due to the following factors:

- ***Non linearity due to material behaviour:*** Although the first approximation of constitutive behaviour is usually based on a linear relationship between stress and strain, many common engineering thermoplastics exhibit a very non-linear stress-strain relationship. In order to define a non-linear stress-strain relationship, a finite set of stress-strain data generally provided by experiment, is considered. A mathematical software is then used to interpolate all other stress-strain values that are required during a broad analysis.
- ***Non linearity due to large displacements:*** A customary assumption in most engineering analysis is that the displacements are small. The elastic moduli of polymers are, however, usually as much as two orders of magnitude less than

those of materials with simpler behaviour such as metals. Furthermore, plastics will undergo as much as an order of magnitude more strain before incurring damage. These phenomena can often result in larger rotations and displacements in plastic structures than in metals.

- ***Non linearity due to the load-deformation interaction:*** A third type of non-linear behaviour is the result of the interaction of deformation with the application of load. Linear analysis assumes that the location and distribution of a load in a system do not change during its deformation. This assumption is not always valid, especially when deformations become large.

2.4 THEORETICAL MODELS FOR DETERMINATION OF THE MODULUS OF COMPOSITES

The micromechanical analysis of the mechanical behaviour in terms of the separate contributions of the two components(i.e. the polymeric matrix and inclusion) to mechanical properties is complicated. This complication arises not only from recognised complexities of the filler concentration, but also from uncertainties in the magnitude of interaction. Especially as the magnitude of interaction might itself vary as the polymer and filler are mechanically forced into greater contact during deformation. In addition there are uncertainties in filler size distribution, complicated by possible agglomeration, and the extent of void formation occurred during fabrication, and the related problem of imperfect interfacial contact between the matrix and filler. Nevertheless, theories which describe the mechanical properties of particulate filled polymers have been developed. Often one theory gives better account of one situation than other. Modulus of composites is a bulk property which depends primarily on the geometry, modulus, particle size distribution, and concentration of the filler and has been represented by a large number of theoretically derived equations.

2.4.1 Theories of rigid inclusions in a non-rigid matrix

2.4.1.1 Einstein equation and its modifications

Einstein equation: One of the earliest theories for the description of the behaviour of a composite system was developed for elastomers and is based on Einstein's equation (Einstein, 1956) for the viscosity of a suspension of rigid spherical inclusions and is given by:

$$\eta_C=\eta_m\left(1+K_E V_P\right) \tag{2.1}$$

where η_c and η_m are the viscosity of suspension and the matrix respectively. K_E is known as the Einstein coefficient and its value depends on the shape of the filler (it equals 2.5 for spheres) and V_P is the volume fraction of particulate filler. It has been assumed that a similar equation can be written for the shear modulus of composites (Smallwood, 1944; Hanson, 1965; Hashin, 1955) . Thus we have:

$$G_c = G_m(1+2.5V_P) \tag{2.2}$$

where G is the shear modulus and p , m and c refer to particle, matrix and composite, respectively. In the Einstein's equation, the stiffening action of a filler is assumed to be independent of its size. The equation also implies that it is the volume occupied by the filler, not its weight which is the important factor affecting the property of the composite. This equation is useful for low concentration of filler because it neglects the fact that by increasing the volume fraction of filler the flow or strain fields around particles interact. The difficulties associated with defining these interactions has led to several modifications of Einstein equation.

Mooney equation: Mooney (Mooney, 1951) made use of a functional equation which must be satisfied if the final viscosity of a suspension to be independent of the sequence of stepwise additions of partial volume fractions of the spherical particles to the suspension. For a monodisperse system the solution of his functional equation is:

$$G_c = G_m \exp(\frac{2.5 V_P}{1 - S V_P}) \qquad (2.3)$$

where S is the crowding factor that shows the volume occupied by the filler/true volume of the filler.

Guth equation: Guth's equation (Guth, 1951) is an expansion of Einstein's equation to take into account the interparticle interactions at higher filler concentrations.

$$G_c = G_m(1 + K_E V_P + 14.1 V_P^2) \qquad (2.4)$$

Thomas equation: Thomas's equation (Thomas, 1965) is an empirical relationship based on data generated with monodispersed spherical particles. The coefficients of different power series relating relative viscosity and volume fraction of solids were determined using a non-linear least square procedure.

$$G_c = G_m(1 + 2.5 V_P + 10.05 V_P^2 + A \exp(B V_P)) \qquad (2.5)$$

where A = 0.00273 and B = 16.6.

Quemada equation: Quemeda (Quemeda, 1977) introduces a variable coefficient to account for interparticle interactions and differences in particle geometry. Thus:

$$G_c = G_m(1 - 0.5 K V_P)^{-2} \qquad (2.6)$$

where K is usually 2.5 .

Frankel and Acrivos equation: An asymptotic expansion technique was used by Frankel and Acrivos (Frankle and Acrivos, 1977) to derive the functional dependence of effective viscosity on concentration for a suspension of uniform solid spheres. The result containing no empirical constant, is intended to complement the classical Einstein formula which is valid only at infinite dilution and is given by:

$$G_c = G_m(1+\frac{9}{8}[\frac{(V_P/\phi)^{1/3}}{1-(V_P/\phi)^{1/3}}]) \quad (2.7)$$

where φ is the maximum packing fraction of filler.

2.4.1.2 The Kerner equation and its modifications

One of the most versatile and elaborate equations for determining modulus of a composite material consisting of spherical particles in a matrix, is due to Kerner. For $G_p > G_m$, the Kerner equation (Kerner, 1956) simplifies to :

$$G_c = G_m(1+\frac{V_p 15(1-V_m)}{V_m(8-10V_m)}) \quad (2.8)$$

Nielsen equation: Halpin and Tsai (Tsai, 1968; Halpin, 1969) have shown that most of the equations for the elastic moduli of composite materials can be put into an equation of the general form as:

$$G_c = G_m(\frac{1+ABV_P}{1-BV_P}) \quad (2.9)$$

where A and B are constants for any given composite. The constant A takes into account such factors as geometry of the filler size and the Poisson's ratio of the matrix. The constant B takes into account the relative moduli of the filler and matrix phases, and is defined as:

$$B = \frac{(G_m/G_p)-1}{(G_m/G_p)+A} \quad (2.10)$$

Neilsen (Neilsen, 1970) has extended this equation to take the maximum packing volume fraction into account and to point out the relation between the constant A and the generalised Einstein coefficient k which depends on the Poisson's ratio. The equation that he finally derives is given as:

$$G_c = G_m\left(\frac{1+(k-1)BV_P}{1-BV_P}\right) \tag{2.11}$$

2.4.2 Theories of non-rigid inclusions in a non-rigid matrix

The random distribution of the constituent phases in a filled system demands a statistical approach, but this requires a knowledge of the distribution of the individual phases. Consequently, the problem is usually simplified to a two phase model in which average stresses and strains are considered to govern the behaviour of each phase.

The average behaviour of the composite is defined in terms of a representative volume element. When subjected to a gross uniform stress or strain, a uniform strain field is induced in the composite which can be used to estimate the elastic constant. The other approaches consist of the establishment of bounds for the moduli by the use of energy criteria in theory of elasticity.

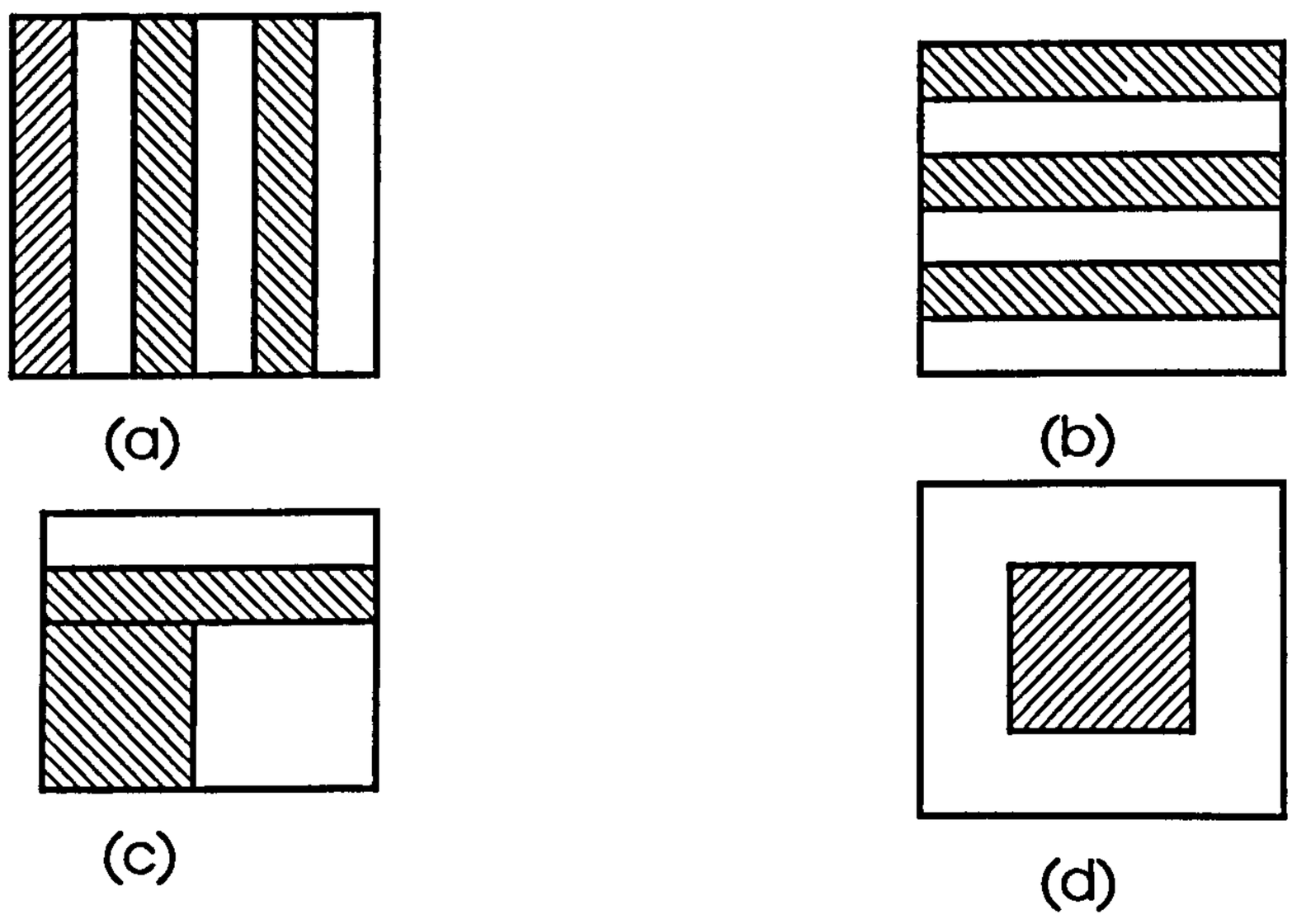

Fig.2.3 Models for particulate filled composites (a) Parallel model (b)series model (c) Hirsch's model (d) Counto's model

2.4.2.1 Series and parallel models

In the simplest case for a two-phase material, the arrangement of the phases is shown in *figures 3.a and 3.b*. For the parallel arrangement (case a), the uniform strain is

assumed in the two phase and the upper bound is given by (Broutman and Krock, 1967):

$$G_c = G_m V_m + G_P V_P \tag{2.12}$$

whereas in series arrangement (case b) the stress assumed to be uniform in the two phases. The lower bound is

$$G_c = \frac{G_P G_m}{G_P V_m + G_m V_P} \tag{2.13}$$

In *equation 2.12* it is assumed that the Poisson's ratios of constituent phases are equal. Whereas using *equation 2.13* υ_c , the corresponding Poisson's ratio should be given by:

$$\upsilon_c = \frac{(\upsilon_P V_P G_m + \upsilon_m V_m G_P)}{(V_P G_m + V_m G_P)} \tag{2.14}$$

The upper and lower bounds obtained from *equations 2.12* and *2.13* often do not represent the experimental data. This implies that the assumption of either a state of uniform strain or uniform stress in the individual phases of the filled system is not sufficient to describe the modulus.

2.4.2.2 The Hashin and Shtrikman model

Improved bounds for the modulus of two-phase media were obtained by Hashin and Shtrikman who took into account the Poisson contraction of the constituent phases. The overall response of the composite was assumed to be isotropic and linearly elastic. The equations for the lower and upper bounds of the composite modulus (Hashin, Shtrikman, 1963) are given, respectively, as:

$$E_c = \frac{9(K_m + \frac{V_p}{(1/K_p - K_m) + (3V_m/(3K_m + 4G_m))})(G_m + \frac{V_p}{(1/(G_p - G_m)) + (6(K_m + 2G_m)V_m/5(3K_m + 4G_m)G_m)})}{3(K_m + \frac{V_p}{(1/K_p - K_m) + (3V_m/(3K_m + 4G_m))}) + (G_m + \frac{V_p}{(1/(G_p - G_m)) + (6(K_m + 2G_m)V_m/5(3K_m + 4G_m)G_m)})} \tag{2.15}$$

$$E_c = \frac{9(K_p + \frac{V_m}{(1/K_m - K_p) + (3V_p/(3K_p + 4G_p))})(G_p + \frac{V_m}{(1/(G_p - G_m)) + (6(K_p + 2G_p)V_p/5(3K_p + 4G_p)G_p)})}{3(K_p + \frac{V_m}{(1/K_m - K_p) + (3V_p/(3K_p + 4G_p))}) + (G_p + \frac{V_m}{(1/(G_p - G_m)) + (6(K_p + 2G_p)V_p/5(3K_p + 4G_p)G_p)})} \quad (2.16)$$

where K and G are the bulk and shear moduli, respectively. The corresponding Poisson's ratio of the composite in this case is given by:

$$\nu_c = \frac{3K_c - 2G_c}{2(G_c + 3K_c)} \quad (2.17)$$

The separation of the Hashin upper and lower bound is dependent upon the modular ratio of particle to the matrix(**m=** $E_P = E_m$**).** When the moduli of the constituent phases are closely matched, the bounds predict values within 10%.

2.4.2.3 The Hirsch model

Hirsch (Hirsch, 1962) proposed a relation for G_c which is a summation of *equations 2.12* and *2.13* and is written as:

$$G_c = x(G_m V_m + G_P V_P) + (1 - x)\frac{G_P G_m}{G_P V_m + G_m V_P} \quad (2.18)$$

The model is illustrated in *figure 2.2.c.* Parameters x and 1-x are the relative proportions of material conforming to the upper and lower bound solutions, respectively. When x=0 *equation 2.18* reduces to *equation 2.13* which can be identified with a poorly bonded filler. For the perfectly bonded filler,(i.e. when x=1) the equation reduces to *equation 2.12.*

2.4.2.4 The Takayanagi model

Takayanagi (Takayanagi et.al, 1964) combined *equations 2.12* and *2.13* and proposed a series-parallel model given by:

$$G_c = \left(\frac{\alpha}{(1-\beta)G_m + \beta G_P} + \frac{(1-\alpha)}{G_P}\right)^{-1} \qquad (2.19)$$

where parameters α and β represent the state of parallel and series coupling in the composite, respectively. *Equation 2.19* was developed to predict the modulus of a crystalline polymer. The basic problem with this model is the determination of values for α and β. The arrangement of the series and parallel element is, however, an inherent difficulty in all of the proceeding models and there are conceptual difficulties in relating these models to real systems.

2.4.2.5 The Counto model

A simpler model, for a two phase system is proposed by Counto (Counto, 1964) and assumes perfect bonding between the particle and the matrix. The modulus of the composite is given by:

$$\frac{1}{G_c} = \frac{1-V_p^{1/2}}{G_m} + \frac{1}{(1-V_p^{1/2})/V_p^{1/2}G_m + G_P} \qquad (2.20)$$

This model predicts moduli which are in good agreement with a wide range of experimental data. It should be noted that when x takes a value of 0.5 in *equation 2.18* it coincides with the values predicted from *equation 2.20*.

2.4.3 Limitations of the theoretical models

Equations 2.12 and 2.13 assume that the individual phases are under uniform strain or stress. In practice, however, the filler particles may not be completely separated from one another and the reinforcement element may, on the microlevel, effectively be an aggregate of smaller particles. Thus in response to the applied load the stress will be distributed unevenly between the particles and aggregates and the assumption of either uniform strain or stress is clearly an oversimplification. To account for the complex stress and phase distribution, Hirsch and Takayanagi considered differing combinations of the upper and lower bounds of the laws of mixtures. All of these

require an empirical factor which is determined by a curve fitting routine to furnish a phenomenological description of the experimental data.

Theories which deal with filled systems indicate that the elastic modulus for a given particle and matrix depends only upon the volume fraction of filler and not the particle size. The modulus however, increases as the particle size decreases.

The properties of the composites may also be affected by changes in particle shape. This effect is especially pronounced with larger or non-spherical particles where a preferred orientation can modify the particle deformation behaviour.

The particle size distribution affects the maximum packing fraction ϕ_m. Mixtures of particles with differing sizes can pack more densely than monodispersed particles because the small ones can fill the space between the closely packed large particles to form an agglomerate. These aggregated particles may be able to carry a large proportion of the load than the primary particles to yield a higher modulus, at the same volume fraction.

Most of the theories which explain the reinforcing action of a filler assume perfect adhesion between the filler and the polymer matrix. The case of imperfect adhesion was, however, discussed theoretically by Sato and Furukawa (Sato and Furukawa, 1963). They assumed that the non-bonded particles act as holes and, therefore, predicted a decrease in modulus with increasing filler content. One can argue that the non-bonded particles do not act entirely as holes since they also restrain the matrix from collapsing. A change of the matrix-filler adhesion has a smaller effect on modulus than on strength. The latter is much more dependent on surface pretreatment. In fact, the degree of adhesion does not appear to be an important factor as long as the frictional forces between the phases are not exceeded by the applied stress. In most filled systems there is a mismatch in the coefficients of thermal expansion which is reflected as a mechanical bond resulting from thermally induced stresses. Brassell (Brassell and Wischmann, 1974) found that the degree of bonding between the phases does not appear to have any influence on mechanical properties at liquid nitrogen temperature and this was attributed to the compressive stresses on the filler particle. In most cases even if the adhesion between phases is poor the theories remain valid as

long as there is not a relative motion across the filler-matrix interface(no slip case) (Ahmed and Jones, 1990).

2.5 MICROMECHANICAL ANALYSIS OF POLYMERIC COMPOSITES

It would be an impossible task to analyse composite materials behaviour by keeping track of the strains, strain rates and strain gradients within and around each and every inclusion in the material. At the other end of the scale, we could simply assume that the individual phases do not exist, measure the macroscopic properties and proceed with the structural design task(macromechanical analysis). This approach, while practical, ignores the main opportunity and challenge of composite materials, namely to tailor the microscale features and characteristics to achieve desired and optimal macroscopic behaviour. Thus we are naturally led to the problem of averaging the microscale effects and characteristics to predict the macroscopic behaviour and to investigate the effects of microstructure, particle size, particle distribution and interface on the final properties (micromechanical analysis).

The microscale geometry of composite materials involves both deterministic and statistical features. In proceeding with micromechanical analysis, a cell size is selected and averaging is done on this scale. The scales for different methods are approximately:

atomic, molecular	$10^{-8}-10^{-9}$ m
microscale	10^{-5} m
macroscale	$10^{-1}-10^{-2}$ m

The microscale dimension reflects the typical filler diameters, as well as being characteristic of many particulate inclusion dimensions. The microscale is thus nearly equally spaced in between the atomic and the macroscale behaviour. Understanding the behaviour of composites on the microscale offers considerable promise for improving their bulk material properties. Obviously the cell size to be used in a volume averaging operation must be larger than the characteristic microscale dimension. An upper limit for the cell size must relate to the macroscopic strain gradients in the material. In particular, the cell size must be small compared with a dimension that is

characteristic of the inverse of the strain gradient. Averaging is done with regard to cell sizes on the scale of the inhomogeneity. Further to statistical averaging certain features of the composites such as isotropic behaviour of system with no preferred orientation are usually used to develop microstructural models (Christensen, 1982).

2.5.1 Qualitative description of the microstructure

2.5.1.1 Geometric models

The procedure typically used to determine macroscopic properties involves the analysis of a representative cell or volume element of the material. Most of the cell geometries apply equally well to the cases of fibres or particulate inclusions when viewed in either cylindrical or spherical coordinates. The composite sphere model was introduced by Hashin and the corresponding composite cylinders models by Hashin and Rosen (Hashin and Rosen 1964). A gradation of sizes of cells is assumed such that a volume filling configuration is obtained. A fixed ratio of cylinders' radii is assumed such that the analysis of single sphere can be taken to be the representative of the entire composite system.

There is a more complicated model known as self-consistent scheme. In this model, the average stress and strain in each phase are determined by solution of a separate problem. The material outside the inclusion is assumed to have the effectively unknown macroscopic properties. The solution of the problems shown in *figure 2.4.a* then allows us to determine the macroscopic properties.

A third major type of model is that of the three phase model, shown in *figure 2.4.b*, which involves taking the inclusion as a system to be surrounded by an annulus of matrix material in turn embedded in an infinite medium with unknown effective macroscopic properties.

In a fourth model type a regular arrangement of inclusions is considered. In this case, single size cylindrical inclusions are taken as arranged in regular patterns, usually with either square or hexagonal packing. These models are usually used in finite element analysis. Although non-uniform distribution of particles has also been investigated by Guild and Davy (Davy and Guild, 1989) with application of a combination of finite

element and statistical calculations. The described geometrical models are usually used to formulate the finite element analysis of stress-strain behaviour of composites.

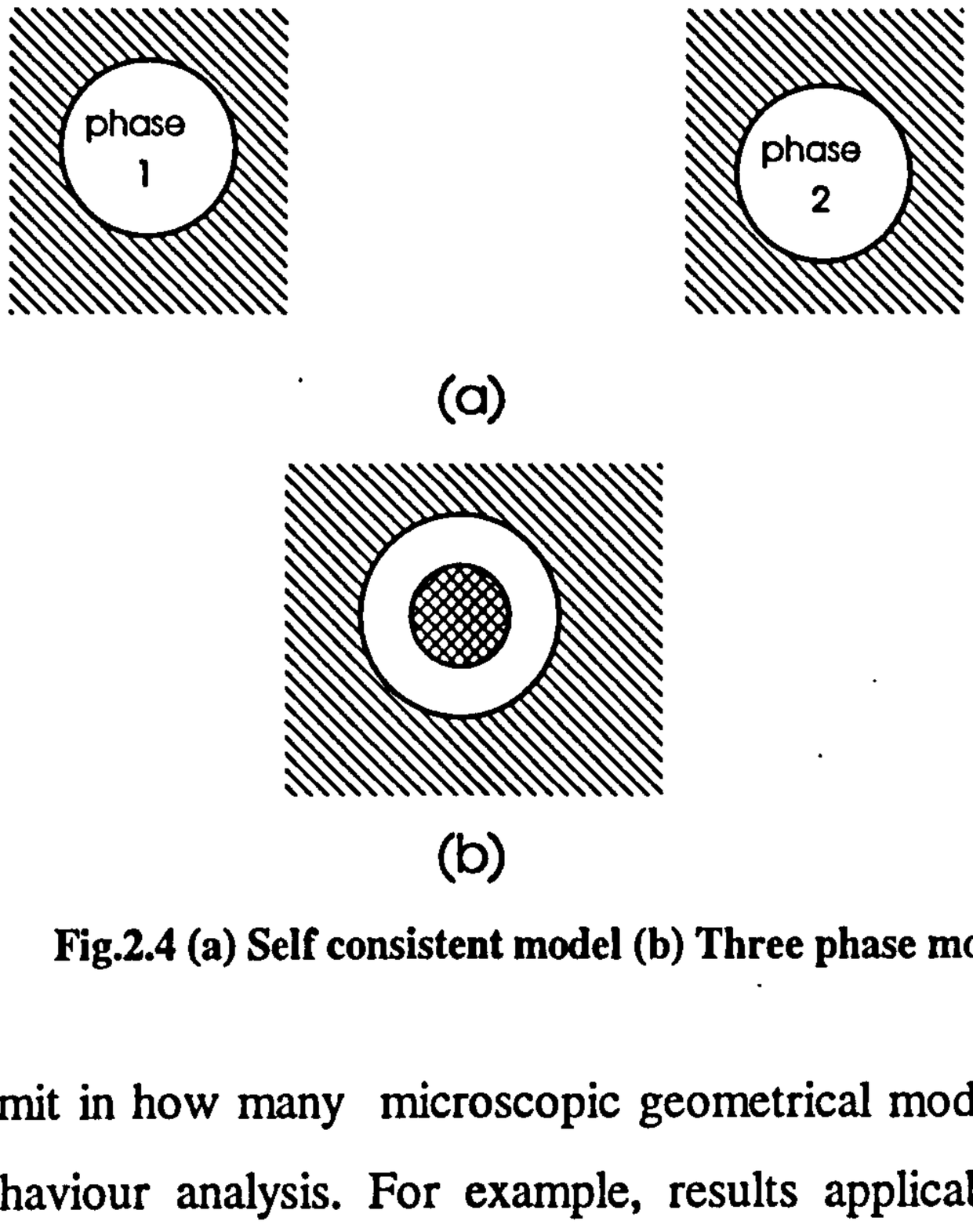

Fig.2.4 (a) Self consistent model (b) Three phase model

There is no limit in how many microscopic geometrical models can be designed for composite behaviour analysis. For example, results applicable to second order in volume fraction can be obtained by the analysis of just two interacting inclusions in an infinite medium. At dilute concentrations, ellipsoidal inclusions can be used to represent a variety of geometric shapes. Also, ellipsoidal inclusions are also directly related to the self-consistent scheme (Christensen, 1982).

2.5.1.2 Geometric model used in finite element modelling of composites

Although usually a periodic distribution of particles are chosen, there is possibility of studying nonuniform distribution through using statistical calculations such as the model due to Guild and Davy. In this model, spherical particles of equal diameter are assumed to be randomly distributed within an infinite matrix. Finite element analysis is performed for a cylinder of resin, radius equal half-height, R, containing a single sphere at its centre, radius r. This cylinder can be represented by the plane ABCD using axisymmetric elements (*figure 2.5*).

The value of the sphere radius, r, was kept constant and cylinder radius was varied. The statistical model has been used in order to calculate the distribution of the distance from a sphere centre to boundary of its Voronoi cell which indicates the interparticle distance (Christensen 1982).

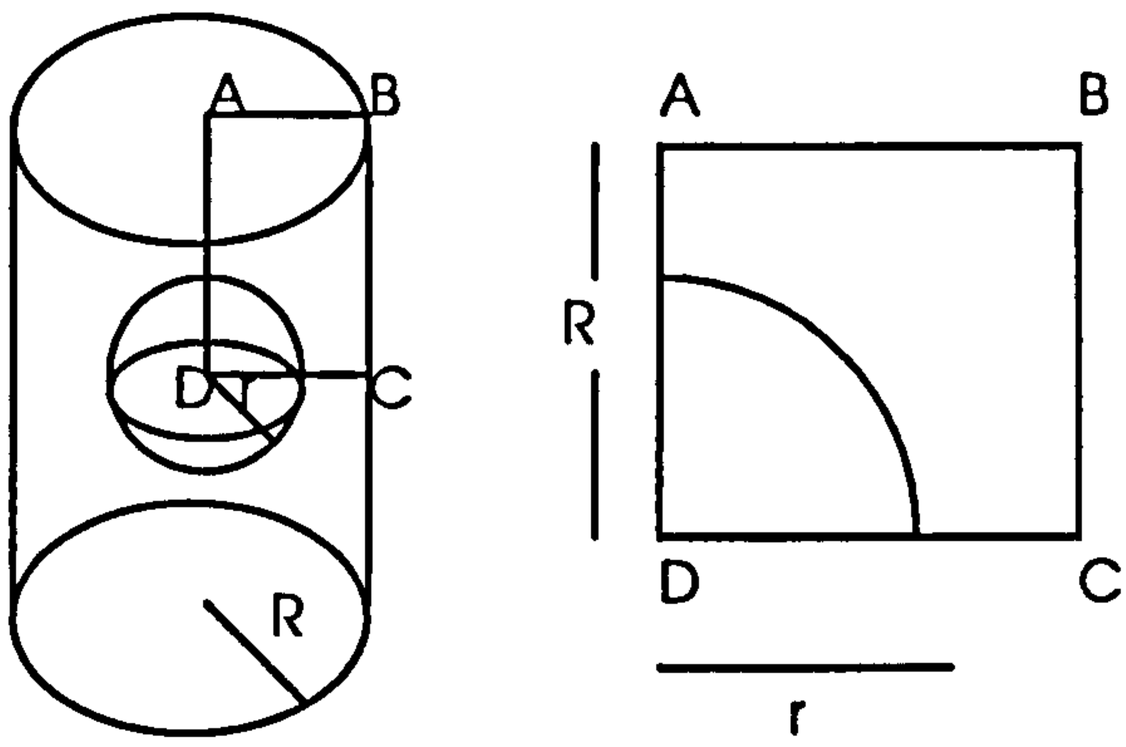

Fig.2.5 Guild-Davy model

However in most of the finite element analysis, a specific packing geometry is assumed in formulating a micromechanical analysis, dictated by the necessity of establishing suitable boundary conditions on the region to be analysed. Two geometries typically assumed are indicated in *figures 2.6.a and 2.6.b*, a square array and a hexagonal array being special cases of these two geometries. By utilising a regular periodic array, a typical repeating unit (such as that indicated by the dashed lines can be isolated for detailed analysis. In fact if symmetry with respect to both the x and y axes is maintained, only one quadrant (solid lines) of this repeating element needs to be analysed. Because of the complex boundary conditions which must be satisfied even when such symmetry is maintained, closed form analytical solutions are not suitable. Of the several numerical analysis procedures which are available, e.g., finite differences, finite elements, truncated series and boundary collacation, the finite element method has emerged as the most generally useful (Hashin and Rosen, 1964). The material region to be analysed is resolved into an array of subregions. According to the order of interpolation and the type of element considered the strain variation across an element can be modelled.

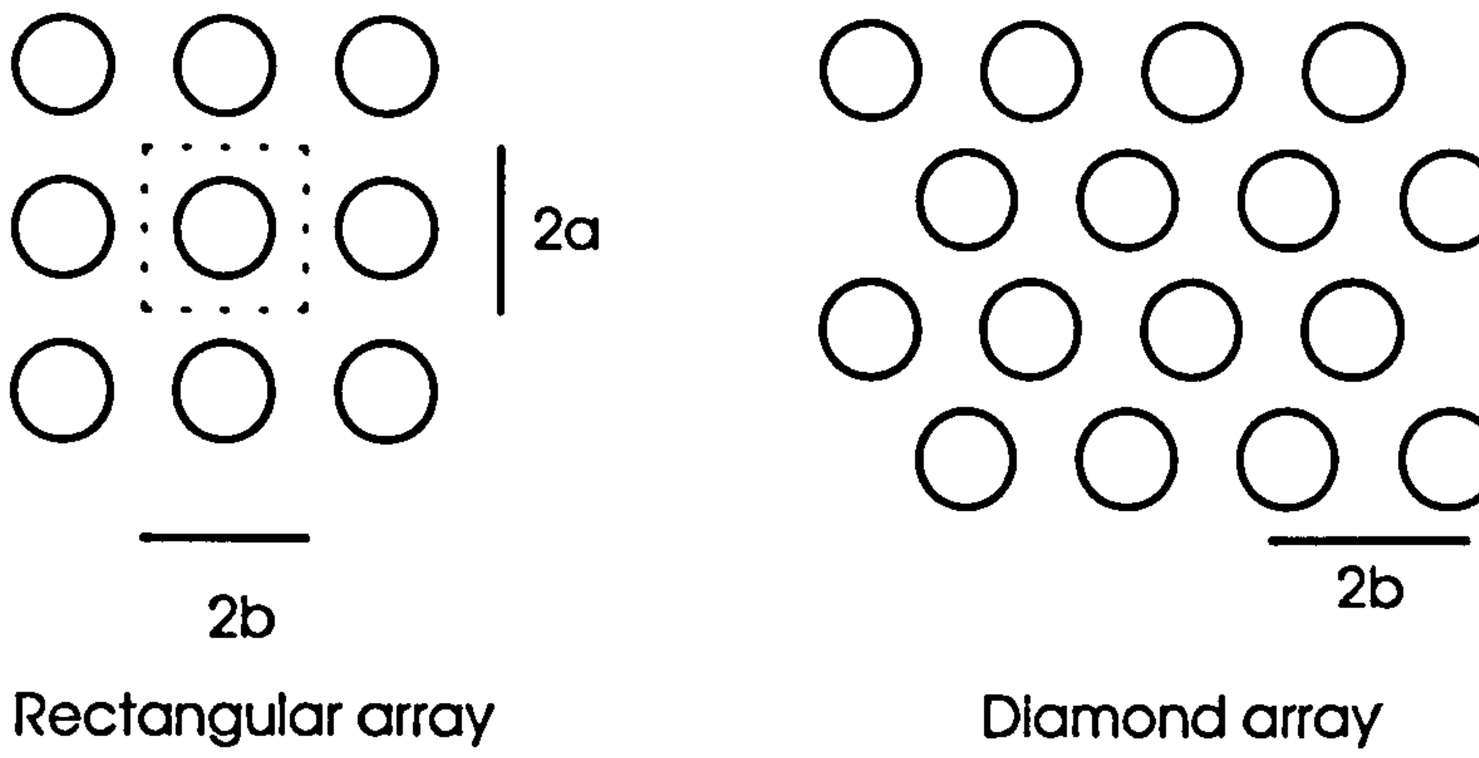

Fig.2.6 packing geometries

2.5.1.3 Structural descriptors

Various types of composite materials, ranging from aligned continuous fibre laminates to particulate filled systems, may be distinguished as special cases of microstructures described in terms of (i) aspect ratios (a_e) and (ii) the orientation of the reinforcing agents(f). The following comparison points out the relatively simple microstructure of continuous fibre laminates. For this special material system, the continuity ($a_e \longrightarrow \infty$) of the collimated (f = 1) fibres assures the simplifying condition that the strain parallel to the aligned fibres is essentially uniform. As a consequence the longitudinal properties may be predicted from the simple rule of mixtures; however, the variation of the fields transverse of the fibre direction must be taken into account to obtain relationships which predict the transverse properties and shear moduli.

Particulate filled systems represent the next level of complexity because unlike fibres, particulate fillers have a low aspect ratios, often approximating those of spheres or plates. In most particulate filled composites, the reinforcing agents are spherical (or near spherical) so that the aspect ratio is unity. The marked discontinuity of particulate filled systems introduces significant fluctuations in the internal fields which complicate the analysis of properties. On the other hand, simple reinforcing geometry precludes a dependence on the orientation of the reinforcing agent so that the consideration of this structural feature is not required in the analysis of these materials.

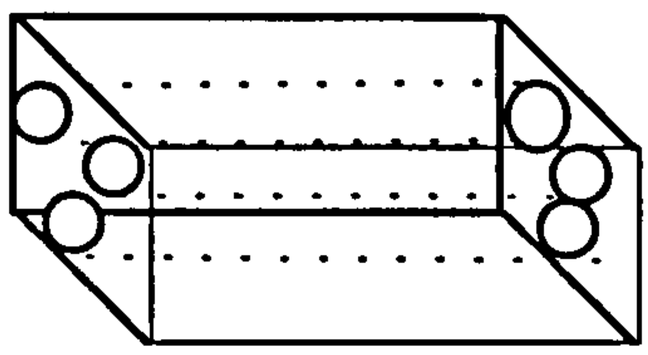

continlous fibres

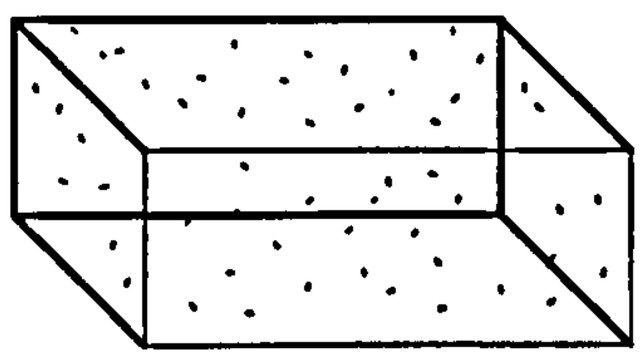

particles

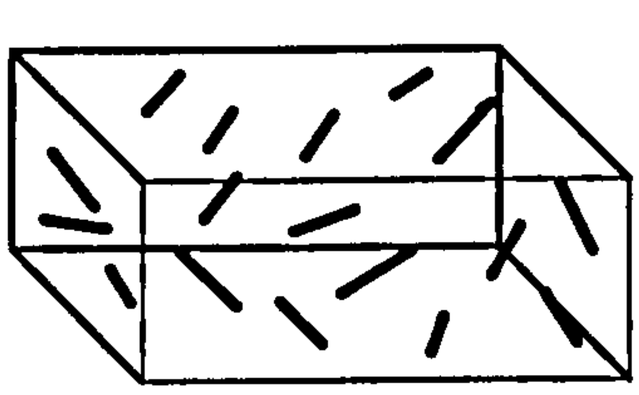

Short fibres

Symmetry	Microstructure
Orthotropic Transversley Isotropic	Aspect ratio --> Orientation Aligned
Isotropic	Aspect ratio =1 Orientation: Independent
orthotropic Transversley Isotropic	1< Aspect ratio Planar Random (f=0) < Orientation (f) < Aligned (f=1)

Fig2.7 schematic definition of the structural features

Short-fibre reinforced materials represent yet a higher level of complexity since variation in both the aspect ratio and fibre orientation must be taken into consideration. Short fibre systems can be further distinguished according to the microstructural features induced by fabrication procedures (Sato and Furukawa, 1963).

2.5.1.4 Size of particles

The use of smaller particles results in rapid increase in the value of modulus. This may be due to a greater total surface of interaction or to a change in the value of maximum packing fraction. Agglomeration of particles, arising from strong particle-particle interactions, might dissociate trapped polymer from the main polymer matrix and in so doing produce an effect of increased stress for a given strain.

Larger particles give rise to greater stress concentrations and lower tensile strength, than the smaller particles. Where bonding is weak, then at some critical strain, debonding takes place and the composite exhibits opacity. But where a suitable bonding agent has been employed, a greater level of stress will be required to produce breakdown of interfacial adhesion. In fact, if the interaction is extremely strong, fracture of matrix or even filler may occur first.

2.5.2 Interface-adhesion

Recently, there has been much renewed interest regarding the role of the interface in composite material behaviour. This is due largely to the realisation that any interaction occurring between the primary constituents must propagate through a common interfacial boundary. Intuitively, it is reasonable to expect that a better understanding of the interfacial region could lead to the design and preparation of improved composite structures. The interphase represents an interfacial region of finite volume wherein the material properties vary continuously between those of bulk matrix and bulk filler. Such an interface might be the result of processing conditions, for example, which impart the unique material properties to the region. Also the morphology of a matrix polymer or resin may be quite different in the region adjacent to the fibre. This can give an interphase region with properties quite different from that of the bulk matrix. Alternatively, an interphase may encompass an interlayer of some composition which is deliberately introduced into the composite structure in order to improve the load transfer properties of the interface (Brassell and Wischmann, 1974). An inconsistent interphase causes a poor distribution of stress concentration centres which results in the premature failure of the composite or growing of cracks. An optimal interphase coating maximises the composite strength. The level of bonding of inclusions to the matrix is also one of the dictating aspects in load transfer.

Interfacial bonding in composites can be divided into three levels: weak, ideal, and strong. Factors leading to a good polymer-filler bonding are as follows:

- Low viscosity of resin at time of its application.
- Increased pressure to assist flow.
- High viscosity after application.

- Clean and dust free surface on filler.
- Absence of cracks and pores on filler surface.
- Moderate roughening of filler surface.
- For impermeable filler solvent -based resins should be avoided
- Use of resins less rigid than filler.
- Similarity of the coefficient of thermal expansion of components.

2.6 FINITE ELEMENT MODELLING OF THE MECHANICAL PROPERTIES OF COMPOSITES

The finite element techniques which are commonly used in solid and fluid mechanics can be broadly categorised as: Least-square, Weighted residual and Variational methods.

2.6.1 Finite element methods based on variational principles

Generally in these techniques a variational principle characteristic of the system under study is formed and minimised to obtain a solution for the system unknowns. This is the oldest of the finite element methods and it is developed by the engineers who wanted to solve complex structural problems using a section by section approach. for a solid system simple variational principles can be formed on the basis of load or force displacement relationships. Depending on the form of the basic governing equation of a system equations different approaches can be derived. These are called: displacement (stiffness), force (flexibility) and hybrid (mixed) methods.

Each of these approaches is equivalent to a variational principle that is, the minimisation of an appropriate system property. The three most commonly used variational principles are the principle of minimum potential energy (displacement method), the principle of complementary energy (force method) and the Reissner principle (mixed method). In all of these methods, it is necessary to identify the physical condition of the system. In any physical situation then, an expression for the total energy could be obtained and minimised to find the equilibrium solution. Now,

we consider different steps of displacement method as the most commonly used one in this category. A brief outline of the most important techniques based on 2-D domains is given in the following sections.

2.6.1.1 Displacement method

In the most commonly used form of this method a general two dimensional structure is divided into a number of 2-D, triangular finite elements and associated nodes. When a load is applied to the structure, all of the elements must deform in a fashion that guarantees equilibrium of forces between the elements. In addition, the deformation of the modelled structure must remain compatible in order to ensure that discontinuities in displacement do not develop at element boundaries.

The first step in developing these equations is to establish the expression for element stiffness, relating forces and displacements at the nodes of an element. The sequence in this process is as follows:

(i)Assume an approximate displacement function for the element. This function is defined in terms of the displacements at the nodes of the element and should ensure compatibility of displacements with neighbouring elements along its entire boundary.

(ii)Apply the kinematic equations defining strain in terms of the approximate displacement functions.

(iii)Use the constitutive relationship appropriate for the material to determine stresses in terms of strains.

(iv)Develop equilibrium equations relating internal element nodal forces to externally applied nodal forces.

Displacement function

The displacement function characterises the displacements within an element as a function of space. The choice of displacement function affects the accuracy of the element in approximating actual displacement, strain, and stress behaviour over the volume of the element. Since strain is a first order derivative of displacements, a linear displacement function leads to the approximation of constant strains and stresses

within the element. Similarly, a quadratic displacement function simulates linear strain and stress fields within an element. For the three node, triangular element, we will designate the x axis to lie along one edge of the triangle. With displacements (u_i, v_i) in two coordinate directions (x, y) at each node(i) there are a total of six nodal displacements (degrees of freedom) in terms of which the deformation field for the element can be defined. In order to define the displacements within the element in terms of these six nodal displacements, functions with a total of six coefficients are required. A natural set of choices for this element is

$$u = a + bx + cy \tag{2.21}$$

$$v = d + ex + fy \tag{2.22}$$

where a, b, c, d, e, and f are unknown constants.

Element displacements in terms of nodal displacements

Using *equations 2.21 and* 2.22 to evaluate the displacement at each node (i),

$$V_k = d + e X_k + f Y_k \tag{2.23}$$

$$U_k = a + b X_k + c Y_k \tag{2.24}$$

(k=1,2,3)

where X_k, and Y_k define known coordinate locations. A similar set of equations can be written to define the coefficients d, e, and f in terms of the nodal y displacements. Using matrix manipulation it is possible to represent the u and v displacements within an element in terms of nodal displacements as

$$\begin{Bmatrix} u(x,y) \\ v(x,y) \end{Bmatrix} = [N] \begin{Bmatrix} U_i \\ V_i \\ U_j \\ V_j \\ U_k \\ V_k \end{Bmatrix} = [N]\{\delta\} \tag{2.25}$$

where the $[N]$ is the shape function matrix that can be formed by using *equation 2.23* and *equation 2.24*, and $\{\delta\}$ is the vector of nodal displacements.

Strain as a function of nodal displacements

The two dimensional definitions of strain in terms of displacement are:

$$\xi_x = \frac{\partial u}{\partial x} \tag{2.26}$$

$$\xi_y = \frac{\partial v}{\partial y} \tag{2.27}$$

$$\gamma_{xy} = \frac{\partial u}{\partial y} + \frac{\partial v}{\partial x} \tag{2.28}$$

These relations are then used to calculate the strain within the element in terms of its nodal displacements. Using matrix notation again, this relationship can be expressed as

$$\{\xi\} = \begin{Bmatrix} \xi_x \\ \xi_y \\ \gamma_{xy} \end{Bmatrix} = [B]\{\delta\} \tag{2.29}$$

Where [B] is a matrix that can be defined in terms of derivatives of the shape functions using *equations 2.26, 2.27 and 2.28.*

Stresses in terms of strains

In order to relate stresses to strains, a material constitutive model is necessary. For simple linear elasticity, the plane-stress constitutive relations are

$$\sigma_x = \frac{E}{1-\nu^2}(\xi_x + \nu\xi_y) \tag{2.30}$$

$$\sigma_y = \frac{E}{1-\nu^2}(\xi_y + \nu\xi_x) \tag{2.31}$$

$$\gamma_{xy} = \frac{E}{2(1+\nu)}\gamma_{xy} \tag{2.32}$$

where E is the elastic modulus and ν is Poisson's ratio. Using matrix notation,

$$\begin{Bmatrix} \sigma_x \\ \sigma_y \\ \tau_{xy} \end{Bmatrix} = [D]\begin{Bmatrix} \xi_x \\ \xi_y \\ \xi_{xy} \end{Bmatrix} = [D][B]\{\delta\} \tag{2.33}$$

where [D] is the material matrix formed using *equations 2.30, 2.31 and 2.32.*

Nodal forces in terms of displacements

Load is transmitted from one element to another through forces at nodes of the elements, which can be represented as {F}. These nodal forces in two coordinate directions are related to the nodal displacements through a set of element equilibrium equations. These equilibrium equations can be defined by equating the external work accomplished by the nodal forces when subjected to an arbitrary set of nodal virtual displacements, $d\{\delta\}$, to the internal energy stored in the element's volume as its stress field subjected to the virtual strain field resulting from the same virtual nodal displacements. This relationship can be expressed as

$$(d\{\delta\})^T\{F\} = \int_{Vol} d\{\varepsilon\}^T\{\sigma\}dVol \tag{2.34}$$

Since the virtual strains can be related to the virtual nodal displacements as

$$d\{\varepsilon\} = [B]d\{\delta\} \tag{2.35}$$

the element equilibrium *equation 2.32* takes the form

$$d\{\delta\}^T\{F\} = d\{\delta\}^T\int_{Vol}[B]^T[D][B]dVol \tag{2.36}$$

equation 2.36 now takes the form of a relationship between the nodal forces {F} and the nodal displacements $\{\delta\}$,

$$\{F\} = [K]_e \{\delta\} \tag{2.37}$$

Where $[K]_e$ is the elemental stiffness matrix defined as:

$$[K]_e = \int_{Vol} [B]^T [D][B] dVol \tag{2.38}$$

Global equilibrium

Equation 2.37 establishes the relationship between the nodal displacements of an element and the corresponding nodal forces. When individual elements are joined at common nodes to model a structure, global equilibrium must be ensured at each node. This requirement means that the summation of the forces associated with all elements attached to that node must be equal in magnitude and opposite in direction to the externally applied force at that node.

To construct these equations, individual element stiffnesses are assembled using algebraic techniques into a global stiffness matrix representing the stiffness of the entire structure. This global set of equations relates all the nodal degrees of freedom in the structure to the externally applied nodal forces. If the externally applied nodal forces are known, a solution for the nodal degrees of freedom can be obtained using linear algebra once the required boundary conditions are applied. When the displacements of all the nodes are known, the state of deformation of each element is also defined. Thus the state of the stresses and strains can be calculated using *equations 2.29 and 2.33*. However, since equilibrium is only guaranteed at a finite number of nodal points in the structure, the finite element method is a numerical approximation rather than an exact solution. (McCullough, 1982)

2.6.2 Least-square and Weighted residual method

In this approach, instead of finding the variational principle explicitly, we start with the governing partial differential equations derived from the conservation laws of physics. These equations are used to formulate a functional statement. In the least square method the functional is the least square of errors generated by the substitution of the unknown function in the governing equation with an approximation. In the weighted residual methods, on the other hand a more general approach based on projection methods is used to derive a functional as a weak statement. Generally these functional statements are obtained without directly determining an expression for the total energy of the system. The advantages of these methods over the simple variational techniques are:

- The procedure can be considered as a mathematical technique independent of the physics of the problem under study.
- It is more flexible and can deal with different conditions without being concerned about proving different physical relationships. Consequently, the non-isotherm condition and non-linear cases can be studied easily and in each case the corresponding equation will be added to the set of equations.

2.6.2.1 A brief outline of Galerkin method

The Galerkin method has been judged to be the most powerful technique for generating finite element representation of non-linear differential equations (Oden, 1972). The method is a special case of the method of weighted residuals. Consider the non-linear equation,

$$Y(f) = P \tag{2.39}$$

where (f) is a solution of *equation 2.39* and Y represents a non-linear operator. The approximate solution of this non-linear equation is assumed to be a combination of trial functions, say

$$\bar{f} = \sum_{i=1}^{p} \phi_i f_i \tag{2.40}$$

The substitution of $\bar{f}$ into *equation 2.39* gives

$$Y(f) - P = r(f) \tag{2.41}$$

where r represents the error or residual due to the approximate solution.

The method of weighted residuals involves the identification of a set of weight functions

$W_w(f)_{,w=1,\ldots,P}$, so that $r(f)$ vanishes in some weighted average sense over the solution domain Ω. Generally the requirement is written

$$\int_{\Omega} W_w(f) r(f) d\Omega = 0 \tag{2.42}$$

Galerkin suggested a rational choice of weight functions. In this method the weighting functions are chosen to be the same as the shape functions (or trial functions). Thus, over each element *equation 2.42* becomes

$$\int_e \phi_l \left[Y(\sum_{i=1}^{P} \phi_i f_i) - P \right] de = 0 \tag{2.43}$$

where $l = 1,\ldots P$. The system of P equations generated above are then solved to determine values of f_i

Chapter Three

DEVELOPMENT OF THE PREDICTIVE MODEL

This chapter deals with the derivation of the working equations and different aspects of the development of a mathematical model to predict the behaviour of composites under various types of loadings. The main advantage of the penalty method which is used in this study is that it can cope with both fluid and solid state behaviour of composites. This is particularly important considering that polymeric composites are in liquid state under high stress and temperature condition.

3.1 MODEL EQUATIONS

3.1.1 Axisymmetric stress condition

The problem of stress distribution in bodies of revolution (axisymmetric solids) under axisymmetric loading is of considerable practical interest. Axisymmetric formulation is expressed in terms of cylindrical coordinates, r the radial coordinate and z the axial coordinate and θ the circumferential coordinate.

The basic hypothesis of axisymmetry is that all functions under consideration are independent of θ. That is, they are functions of r and z only.

Thus three dimensional problem is reduced to a two dimensional

one.(Zienkiewicz and Taylor, 1988)

In this form of stress distribution any radial displacement automatically induces a strain in the circumferential direction, and as the stresses in this direction are certainly non-zero, this fourth component of strain and its associated stress need to be considered. Here lies the essential difference in the treatment of the axisymmetric situation.

Equilibrium equations in r and z directions in axisymmetric case are:

$$\frac{\partial \sigma_{rr}}{\partial r}+\frac{\partial \sigma_{rz}}{\partial z}+\frac{\sigma_{rr}-\sigma_{\theta\theta}}{r}=0 \tag{3.1}$$

$$\frac{\partial \sigma_{rz}}{\partial r}+\frac{\partial \sigma_{zz}}{\partial z}+\frac{\sigma_{rz}}{r}=0 \tag{3.2}$$

The matrix equation which defines the stress and strain relations can be written as follows :

$$\sigma = D\varepsilon \tag{3.3}$$

where the stress matrix is defined as:

$$\sigma=\begin{Bmatrix}\sigma_{zz}\\ \sigma_{rr}\\ \sigma_{\theta\theta}\\ \tau_{rz}\end{Bmatrix} \tag{3.4}$$

and

$$D=\frac{E(1-\nu)}{(1+\nu)(1-2\nu)}\begin{bmatrix} 1, & \frac{\nu}{1-\nu}, & \frac{\nu}{1-\nu}, & 0 \\ & 1 & \frac{\nu}{1-\nu}, & 0 \\ & & 1 & 0 \\ & & & \frac{1-2\nu}{2(1-\nu)} \end{bmatrix} \tag{3.5}$$

and the strain matrix can be presented as follows:

$$\varepsilon = \begin{Bmatrix} \varepsilon_{zz} \\ \varepsilon_{rr} \\ \varepsilon_{\theta\theta} \\ \gamma_{rz} \end{Bmatrix} = \begin{Bmatrix} \dfrac{\partial v}{\partial z} \\ \dfrac{\partial u}{\partial r} \\ \dfrac{u}{r} \\ \dfrac{\partial u}{\partial z} + \dfrac{\partial v}{\partial r} \end{Bmatrix} \tag{3.6}$$

where ν is the Poisson ratio, u and v are the displacement components in r and z directions. By substituting the stress terms in the equilibrium equations by the above constitutive relations the model equilibrium equations in terms of the strain in r and z directions are found as:

$$-\frac{\partial}{\partial r}\left(\frac{\partial v_r}{\partial r}+\frac{v_r}{r}+\frac{\partial v_z}{\partial z}\right)+\frac{\partial}{\partial r}\left(2\mu\frac{\partial v_r}{\partial r}\right)+\frac{2\mu}{r}\frac{\partial v_r}{\partial r}-\frac{2\mu v_r}{r^2}+\frac{\partial}{\partial z}\left[\mu\left(\frac{\partial v_r}{\partial z}+\frac{\partial v_z}{\partial r}\right)\right]=0 \tag{3.7}$$

$$-\frac{\partial}{rz}\left(\frac{\partial v_r}{\partial r}+\frac{v_r}{r}+\frac{\partial v_z}{\partial z}\right)+\frac{\partial}{rz}\left(2\mu\frac{\partial v_r}{\partial r}\right)+\frac{\mu}{r}\left(\frac{\partial v_z}{\partial r}+\frac{\partial v_r}{\partial z}\right)+\frac{\partial}{\partial z}\left[\mu\left(\frac{\partial v_r}{\partial z}+\frac{\partial v_z}{\partial r}\right)\right]=0 \tag{3.8}$$

The Galerkin weighted residual method is used to write the weak formulation of the above equations and Green's theorem is applied in order to reduce the order of the integration. Then the weak forms are obtained in r direction as :

$$\int_{\Omega}[\lambda(\frac{N_j N_i}{r^2}+\frac{N_j}{r}\frac{\partial N_i}{\partial r}+\frac{N_i}{r}\frac{\partial N_j}{\partial r}+\frac{\partial N_j}{\partial r}\frac{\partial N_i}{\partial r})$$

$$+\mu(\frac{2N_j N_i}{r^2}+\frac{N_j}{\partial r}\frac{\partial N_i}{\partial r}+\frac{\partial N_j}{\partial z}\frac{\partial N_i}{\partial z})]U_i\,rdrdz$$

$$+\int_{\Omega}\lambda[(\frac{\partial N_j}{\partial r}\frac{\partial N_i}{\partial z}+\frac{1}{r}N_j\frac{\partial N_i}{\partial z})+\mu(\frac{\partial N_j}{\partial z}\frac{\partial N_i}{\partial r})]V_i\,rdrdz$$

$$+\oint_{\Gamma}(\mu N_i\frac{\partial N_j}{\partial z}r\,n_z+2\mu N_i\frac{\partial N_j}{\partial r}r\,n_r-\lambda N_i\frac{\partial N_j}{\partial r}r\,n_r-\lambda N_i N_j n_r)U_i\,d\Gamma$$

$$+\oint_{\Gamma}(\mu N_i\frac{\partial N_j}{\partial r}r n_z-\lambda N_i\frac{\partial N_j}{\partial z}n_r)V_i d\Gamma=0 \qquad (3.9)$$

and in z direction as below:

$$\int_{\Omega}\lambda[(\frac{\partial N_j}{\partial z}\frac{\partial N_i}{\partial r}+\frac{1}{r}N_i\frac{\partial N_j}{\partial z})+\mu(\frac{\partial N_j}{\partial r}\frac{\partial N_i}{\partial z})]V_i r dr dz$$

$$+\int_{\Omega}\lambda[(\frac{\partial N_j}{\partial z}\frac{\partial N_i}{\partial z})+\mu(2\frac{\partial N_j}{\partial z}\frac{\partial N_i}{\partial r})]V_i r dr dz$$

$$+\oint_{\Gamma}(\mu N_i\frac{\partial N_j}{\partial z}r n_r-\lambda N_i\frac{\partial N_j}{\partial r}r n_z-\lambda N_i N_j n_z)U_i d\Gamma$$

$$+\oint_{\Gamma}(2\mu N_i\frac{\partial N_j}{\partial z}r n_z+\mu N_i\frac{\partial N_j}{\partial r}r n_r-\lambda N_i\frac{\partial N_j}{\partial z}r n_z)V_i d\Gamma=0 \qquad (3.10)$$

In the above equations μ is shear modulus, λ is penalty parameter, n_z, n_r are components of unit vector, N_I, N_j are the weight and shape functions.

An equivalent formulation for the stress distribution can be derived starting from the Stokes flow equation for incompressible fluids in conjunction with so called Penalty method using appropriate penalty parameter. For steady state and axisymmetric flow the equations of motion and continuity are:

$$-\frac{\partial P}{\partial z}+\mu\left[\frac{1}{r}\frac{\partial}{\partial r}(r\frac{\partial v_r}{\partial r})+\frac{\partial^2 v_z}{\partial z^2}\right]+\rho g_z=0 \qquad (3.11)$$

$$-\frac{\partial P}{\partial r}+\mu\left[\frac{\partial}{\partial r}(\frac{1}{r}\frac{\partial}{\partial r}(r v_r))+\frac{\partial^2 v_r}{\partial z^2}\right]+\rho g_r=0 \qquad (3.12)$$

$$\frac{\partial v_r}{\partial r}+\frac{v_r}{r}+\frac{\partial v_z}{\partial z}=0 \qquad (3.13)$$

where v_r, v_z are velocity components, P is the pressure, μ represents fluid viscosity, ρ is fluid density and g_r, g_z are the components of body force vector.(Huebner and Thornton, 1982)

In a penalty method approach the pressure is eliminated as an unknown field variable through the use of a penalty parameter and modified momentum equations are solved for the velocity components. The pressure is represented by

$$P = -\lambda\left(\frac{\partial v_r}{\partial r} + \frac{v_r}{r} + \frac{\partial v_z}{\partial z}\right) \tag{3.14}$$

where $\lambda > 0$ is a parameter. This means that the incompressibility condition (i.e. the continuity equation) can be treated as a constraint on the momentum equation. In a viscous flow if the parameter λ is specified to have a large numerical value in the solution, the incompressibility condition will be satisfied. The main advantage of penalty formulation is that the additional variable P is eliminated and the working equation take a more compact form. The final matrix form can be written as:

$$[[C]+[K]+\lambda[L]]\begin{Bmatrix} v_z \\ v_r \end{Bmatrix} = \begin{Bmatrix} R_{v_z} \\ R_{v_r} \end{Bmatrix} \tag{3.15}$$

For an incompressible flow we must seek a solution to the above matrix equation as $\lambda \to \infty$. Since the matrices [C] and [K] are finite, as λ becomes large the solution tends to :

$$\lambda[L]\begin{Bmatrix} v_z \\ v_r \end{Bmatrix} = \begin{Bmatrix} R_{v_z} \\ R_{v_r} \end{Bmatrix} \tag{3.16}$$

The special consideration that is required in the penalty function approach is that [L] must be a singular matrix. Most commonly used conforming elements produce a nonsingular [L] if the integrals are evaluated exactly. The procedure used to make [L] singular is to evaluate [L] approximately by using reduced Gauss integration.

Now if we define the penalty parameter as follows, the equation of flow will result in the equations similar to the equations of equilibrium.

$$\lambda = 2v\mu / (1-2v) \tag{3.17}$$

In our study we have based our model on Stokes flow equation and the penalty method. This gives us the flexibility to switch the model from the analysis of flow to solid material deformation under applied load. Since most composite materials are in fluid state at the processing time and are in solid state when they are used, this approach offers the advantage of the ability of predicting the material behaviour in both cases through one model.

When establishing the element mesh for axisymmetric problems, care should be taken to avoid positioning elements in such a way that two nodes have the same or nearly the same radial coordinates. If two radial coordinates are close, the calculated difference between them may be grossly in error, and if $r_i = r_j$ some of the integrals in *equations 2.9 and 2.10* become infinite. Another problem can arise in case where nodes lie on the z axis, (i.e. r=0), because this result in the appearance of infinite terms in the working equations of the scheme. This can be avoided by introducing a small core hole along the axis and assigning low values to the radial coordiantes that would normally be zero. The radial displacements along the core are then set to be zero to simulate the actual condition of zero radial displacement at r=0.

3.1.2 Plain strain condition

In the plain strain problem the displacement field is uniquely given by the u and v displacements in directions of the, orthogonal Cartesian x and y axes. It should be noted that the only strains and stresses that have to be considered are the three components in the xy plane. The stress in a direction perpendicular to the xy plane is not zero. However, by definition, the strain in that direction is zero, and therefore no contribution to internal work is made by this stress, which if desired can in fact be explicitly evaluated from the three main stress components at the end of all computations.

Equilibrium equations in x and y directions in plain strain case:

$$\frac{\partial \sigma_{xx}}{\partial x} + \frac{\partial \sigma_{xy}}{\partial y} = 0 \qquad (3.18)$$

$$\frac{\partial \sigma_{xy}}{\partial x} + \frac{\partial \sigma_{yy}}{\partial y} = 0 \qquad (3.19)$$

The matrix equation which defines the stress and strain relations can be written as follows

$$\sigma = D\varepsilon \tag{3.20}$$

where the stress matrix can be defined as:

$$\sigma = \begin{Bmatrix} \sigma_{zzx} \\ \sigma_{yyr} \\ \tau_{rz} \end{Bmatrix} \tag{3.21}$$

$$D = \frac{E(1-\nu)}{(1+\nu)(1-2\nu)} \begin{bmatrix} 1 & \frac{\nu}{1-\nu} & 0 \\ \frac{\nu}{1-\nu} & 1 & 0 \\ 0 & 0 & \frac{1-2\nu}{2(1-\nu)} \end{bmatrix} \tag{3.22}$$

and the strain matrix can be presented as follows:

$$\varepsilon = \begin{Bmatrix} \varepsilon_{xx} \\ \varepsilon_{yy} \\ \gamma_{xy} \end{Bmatrix} = \begin{Bmatrix} \frac{\partial v}{\partial x} \\ \frac{\partial u}{\partial y} \\ \frac{\partial u}{\partial x} + \frac{\partial v}{\partial y} \end{Bmatrix} \tag{3.23}$$

By substituting the stress terms in the equilibrium equations by the above constitutive relations the model equilibrium equations in terms of the strain in x and y directions are resulted as:

$$-\lambda \frac{\partial}{\partial x}\left(\frac{\partial v_x}{\partial x} + \frac{v_y}{\partial y}\right) + \left(2\mu \frac{\partial v_x}{\partial x}\right) + \frac{\partial}{\partial y}\left\{\mu\left(\frac{\partial v_x}{\partial y} + \frac{v_y}{\partial x}\right)\right\} = 0 \tag{3.24}$$

$$-\lambda \frac{\partial}{\partial y}\left(\frac{\partial v_x}{\partial x} + \frac{v_y}{\partial y}\right) + \left(2\mu \frac{\partial v_y}{\partial y}\right) + \frac{\partial}{\partial x}\left\{\mu\left(\frac{\partial v_x}{\partial y} + \frac{v_y}{\partial x}\right)\right\} = 0 \tag{3.25}$$

The Galerkin weighted residual method is used to derive the weak formulation of the above equations and Green's theorem is applied in order to reduce the order of the integration. Thus the weak variational forms are obtained in x and y directions, respectively, as :

$$\int_{\Omega}[(\lambda+2\mu)\frac{\partial N_j}{\partial x}.\frac{\partial N_i}{\partial x}+\mu\frac{\partial N_j}{\partial y}.\frac{\partial N_i}{\partial y}]V_i dxdy$$

$$+\int_{\Omega}\lambda\frac{\partial N_j}{\partial x}.\frac{\partial N_i}{\partial y}+\mu\frac{\partial N_j}{\partial y}.\frac{\partial N_i}{\partial x}]U_i dxdy$$

$$+\oint_{\Gamma}(\mu N_i\frac{\partial N_j}{\partial y}n_y+2\mu N_i\frac{\partial N_j}{\partial x}n_x-\lambda N_i\frac{\partial N_j}{\partial x}n_x)U_i d\Gamma$$

$$+\oint_{\Gamma}(\mu N_i\frac{\partial N_j}{\partial r}r n_z-\lambda N_i\frac{\partial N_j}{\partial z}n_r)V_i d\Gamma=0 \qquad (3.26)$$

and

$$\int_{\Omega}\mu\frac{\partial N_j}{\partial x}.\frac{\partial N_i}{\partial y}+\lambda\frac{\partial N_j}{\partial y}.\frac{\partial N_i}{\partial x}]V_i dxdy$$

$$\int_{\Omega}[\mu\frac{\partial N_j}{\partial x}.\frac{\partial N_i}{\partial x}+(\lambda+2\mu)\frac{\partial N_j}{\partial y}.\frac{\partial N_i}{\partial y}]U_i dxdy$$

$$+\oint_{\Gamma}(\mu N_i\frac{\partial N_j}{\partial z}r n_r-\lambda N_i\frac{\partial N_j}{\partial r}r n_z)U_i d\Gamma$$

$$+\oint_{\Gamma}(2\mu N_i\frac{\partial N_j}{\partial z}r n_z+\mu N_i\frac{\partial N_j}{\partial r}r n_r-\lambda N_i\frac{\partial N_j}{\partial z}r n_z)V_i d\Gamma=0 \qquad (3.27)$$

3.2 MODEL GEOMETRY AND BOUNDARY CONDITIONS

3.2.1 Modelling of the particulate filled composites

In the finite element approximation of axisymmetric solids, the continuous structure or medium is replaced by a system of axisymmetric elements interconnected at nodal points. It is assumed that the composites filled with particles(assumed to possess symmetry) could be approximated by a unit cell shown in *figure 3.1.a.* When this unit cell is rotated 360° around axis AD, a hemisphere embedded in a cylinder is produced. (Zienkiewics and Taylor, 1989)

The interparticle spacing is equal to $2(r_1-r_2)$. The volume fraction of the filler can be calculated from the ratio r_2/r_1. For a square or cubic array the relation of volume fraction and

the ratio r_2/r_1 is defined as:

$$V_f = \frac{\pi}{6}(\frac{r_2}{r_1})^3 \tag{3.28}$$

and for hexagonal array it is modified as:

$$V_f = \frac{\pi}{3\sqrt{3}}(\frac{r_2}{r_1})^3 \tag{3.29}$$

This form of axisymmetric representation of the composite only approximates its real packing and structure. These axisymmetric cells are not actual repetitive units but are related in their dimensions to the interparticle spacing. The maximum volume fraction for hexagonal and square array in this case is 0.74 and 0.52 respectively. (Agrawal and Broutman, 1973)

For rod like particles, the unit cell is defined as shown in *figure 3.2.a.* When this unit cell is rotated 360° around axis AD, a cylinder embedded in a cylinder is produced.

Different parameters used are:

l_f, d_f, r_f: length, diameter and radius of the fibre

l_m, d_m, r_m: length, diameter and radius of the cell

a_f fibre aspect ratio: $a_f = l_f / d_f$

s_f fibre tip spacing: $l_m - l_f = s_f l_f$

x_f fibre spacing parameter: $l_m - l_f = x_f d_f$

Then the dimensions of the cell are related to the volume fraction of the fibres in the composite through the expressions: (Berthelot et al, 1993)

$$(\frac{r_m}{r_f})^2 = \frac{1}{V_f(1 + x_f / a_f)} \tag{3.30}$$

The boundary conditions imposed for analysing the tensile load applied on the particulate filled composite are as follows: (Christman et al, 1989)

$$v_z = 0 \qquad \text{on } Z=0 \tag{3.31.a}$$

$$v_z = V \qquad \text{on } Z=b_o \tag{3.31.b}$$

$$v_r = U \qquad \text{on } r=R_o \tag{3.31.c}$$

$$v_r = 0 \qquad \text{on } r=0 \tag{3.31.d}$$

Here V is a prescribed constant while U is determined from the condition that the average lateral traction rate vanishes, i.e.

$$\int_0^{b_o} \sigma_{rr}\, dZ = 0 \qquad \text{on } r=R_o \tag{3.32}$$

These conditions can be applied to unit cell of spherical particulate and rod shape particulate filled composites shown in *figure 3.1.a* and *figure 3.2.a* respectively. In addition to the boundary conditions 3.31.a-d, there is the requirement that displacement components vanish on the surface of the rigid fibre.

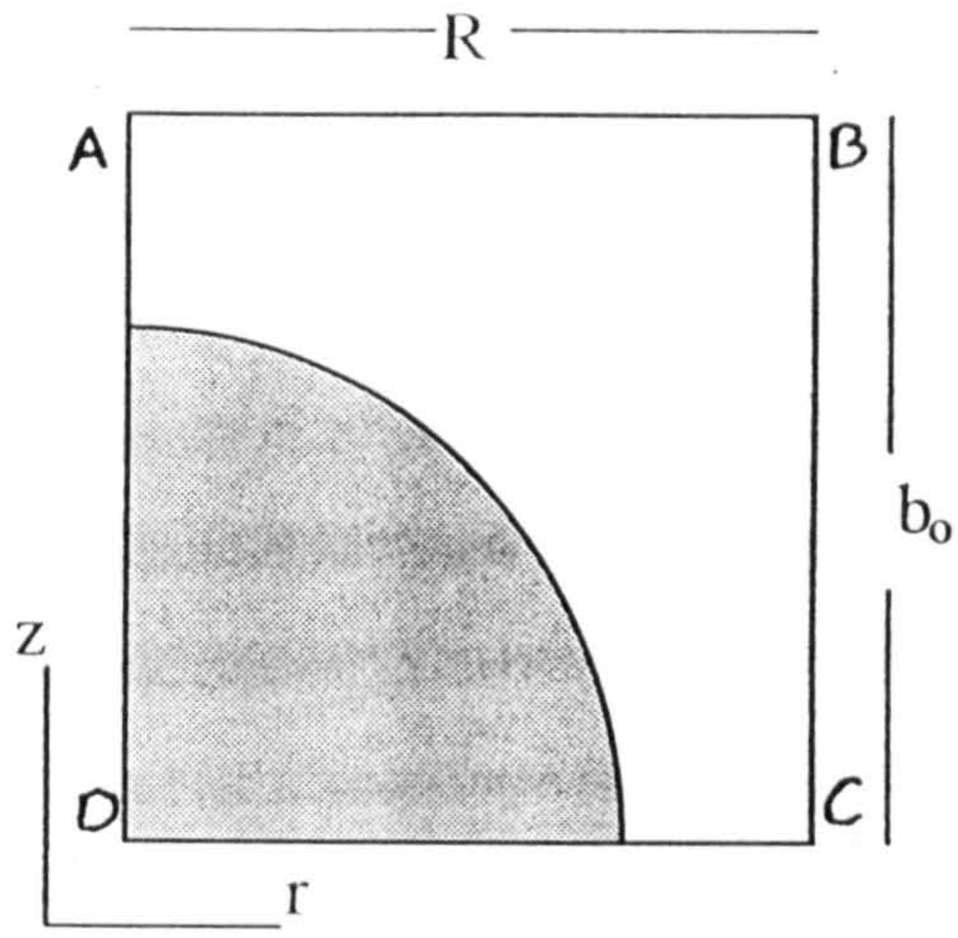

Fig.3.1.a: Axisymmetric unit cell for spherical particulate filled composite

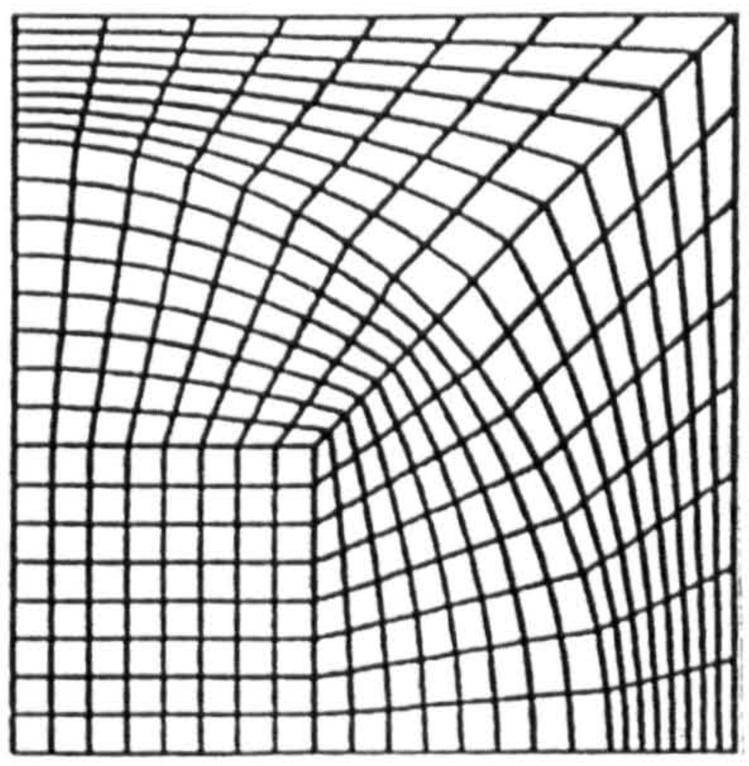

Fig:3.1.b: Mesh for spherical particulate filled composite

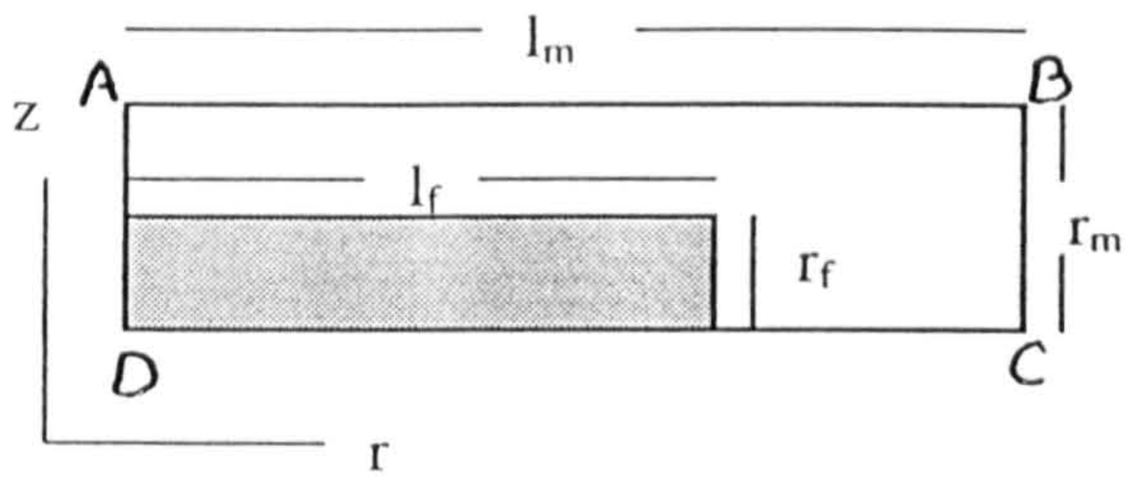

Fig.3.2.a: Axisymmetric unit cell for rodlike particulate filled Composite

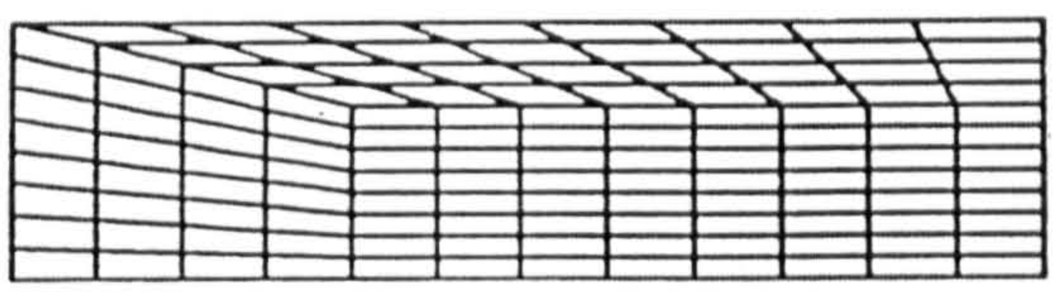

Fig.3.2.b: Mesh for rodlike particulate filled composite

In some calculations, a second set of boundary conditions is employed consisting of 3.31.a and 3.31.b, but with 3.31.c and 3.31.d replaced by $\sigma_{rr} = 0$ on $r=R_o$. So that every point along $r=R_0$ is stress free. Under these conditions the outer sidewall of the cell does not remain straight and vertical. Of course, for the entire tension specimen, $\sigma_{rr} = 0$ on the outer boundary of the specimen. Relaxing boundary conditions 3.31.c and 3.31.d permits, in a highly approximate manner, consequences of deviations from this highly constrained fibre distribution to be explored. Predictions based on 3.31.c and 3.31.d are referred to as result "with constraint" and predictions based on $\sigma_{rr} = 0$ on $r=R_o$ are referred to as results "without constraint".

To satisfy the first set of boundary conditions (with constraint) , the following procedure is used.

1) The stress and displacement distribution is found such that:

$$v_{z1} = 0 \qquad \text{on } Z=0 \qquad (3.33.a)$$

$$v_{z1} = 1 \qquad \text{on } Z=b_o \qquad (3.33.b)$$

$$v_{r1} = 0 \qquad \text{on } r=R_o \qquad (3.33.c)$$

$$v_{r1} = 0 \qquad \text{on } r=0 \qquad (3.33.d)$$

2) The stress and displacement is found such that :

$$v_{z2} = 0 \qquad \text{on } Z=0 \qquad (3.34.a)$$

$$v_{z2} = 0 \qquad \text{on } Z=b_o \qquad (3.34.b)$$

$$v_{r2} = 1 \qquad \text{on } r=R_o \qquad (3.34.c)$$

$$v_{r2} = 0 \qquad \text{on } r=0 \qquad (3.34.d)$$

3) These stress and displacement distributions are superimposed to obtain

$$\sigma = \sigma_1 + k\,\sigma_2 \qquad (3.35)$$

and

$$v = v_1 + k\,v_2 \tag{3.36}$$

where k is determined such that the net force in the r direction along bc is zero. (Agrawal et al , 1971) thus

$$(F_r)_{BC} = \int_{BC} (\sigma_{r1} + k\,\sigma_{r2})dz = |BC|(\sigma_{r1} + k\,\sigma_{r2})_{BC} = 0 \tag{3.37}$$

so that

$$k = -\left(\frac{\sigma_{r1}}{\sigma_{r2}}\right)_{BC} \tag{3.38}$$

The stress on AB is thus

$$(\sigma_z)_{AB} = (\sigma_{z1})_{AB} - \left(\frac{\sigma_{r1}}{\sigma_{r2}}\right)_{BC} (\sigma_{z2})_{AB} \tag{3.39}$$

and the displacement is

$$(u_z)_{AB} = (u_{z1})_{AB} - \left(\frac{\sigma_{r1}}{\sigma_{r2}}\right)_{BC} (u_{z2})_{AB} = (u_{z1})_{AB} \tag{3.40}$$

since $(u_{z2})_{AB} = 0$.

3.2.2 Fibre reinforced composite

The plain strain analysis can be used for the fibre reinforced composite. *Figure 3.3.a* shows the unit cell for the cubic array configuration of fibre reinforced composite. The following expression defines the relation between the unit cell dimensions and the volume fraction:

$$V_f = \frac{\pi\, r_2^2}{4\, r_1^2} \tag{3.41}$$

Figure 3.4.a shows the unit cell employed for the hexagonal array configuration. Numerous choices exist for the unit cell geometry. The unit cell tested is rectangular in

shape with dimension $2L_1*2L_2$, with $L_2=\sqrt{3}\,L_1$. Then the volume fraction of the fibres is related to the cell geometry according to

$$V_f=\frac{\pi}{2\sqrt{3}}\left(\frac{R}{L}\right)^3 \qquad (3.42)$$

The maximum volume fractions for the square and hexagonal array in the fibre reinforced composite analysis are 0.907 and 0.785 respectively. (Gibson, 1994)
Using the square array and hexagonal unit cells the composite response to transverse tensile and shear loading is examined.

2.2.1.1 Tensile loading

The boundary conditions imposed for analysing the tensile load applied on the fibre reinforced composite are as follows:

$$v_y=0 \qquad \text{on } y=0 \qquad (3.43.a)$$

$$v_y=V \qquad \text{on } y=Y_0 \qquad (3.43.b)$$

$$v_x=U \qquad \text{on } x=X_o \qquad (3.43.c)$$

$$v_x=0 \qquad \text{on } x=0 \qquad (3.43.d)$$

Here V is a prescribed constant while U is determined from the condition that the average lateral traction rate vanishes, i.e.

$$\int_0^{b_o}\sigma_{xx}\,dy=0 \qquad \text{on } x=X_o \qquad (3.44)$$

These conditions can be applied to unit cell of square and hexagonal array of fibre reinforced composites shown in *figure 3.3.a* and *figure 3.4.a*.

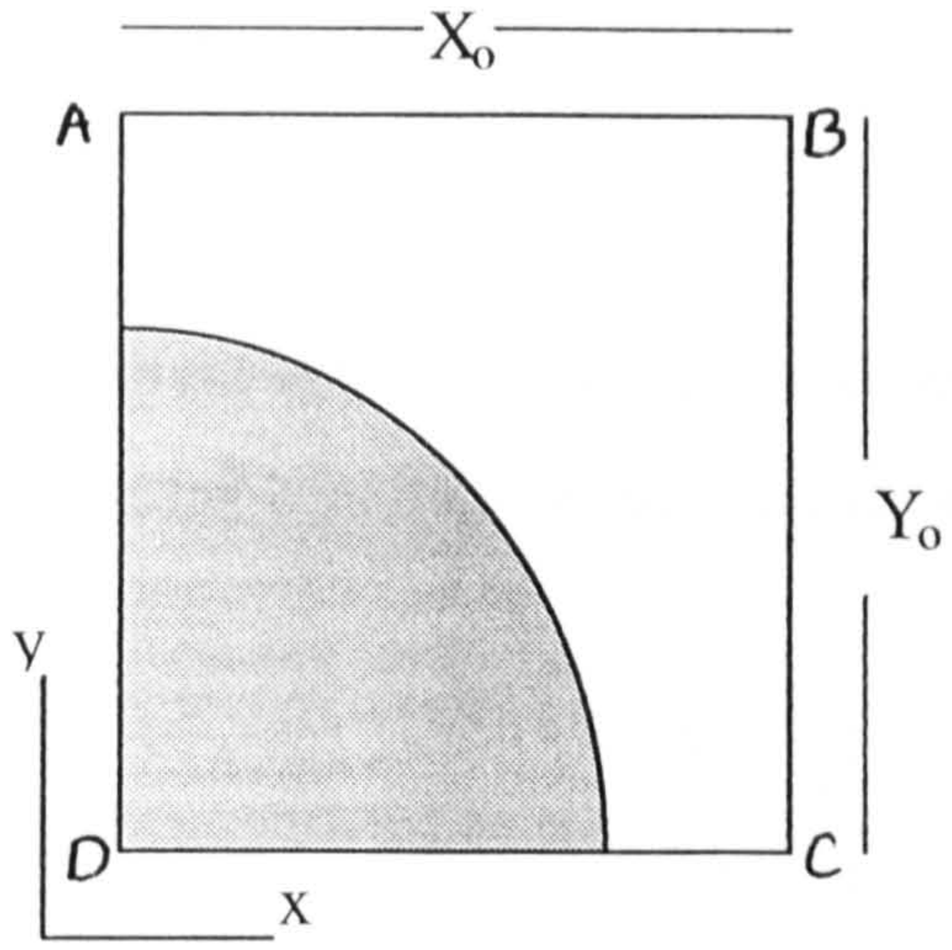

Fig.3.3.a: Unit cell of square array for fibre reinforced composite

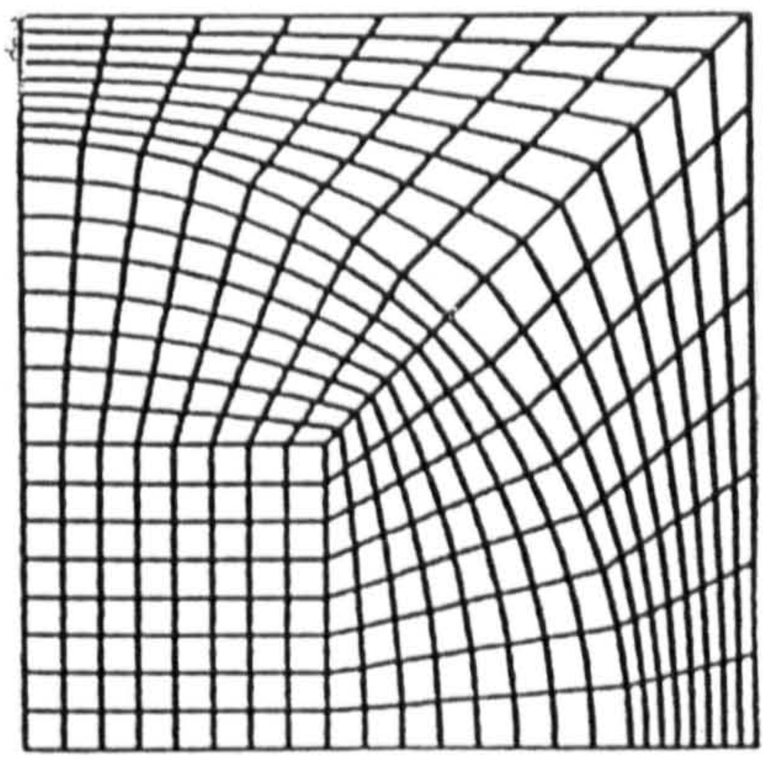

Fig.3.3.b: Mesh for fibre reinforced composite (square array)

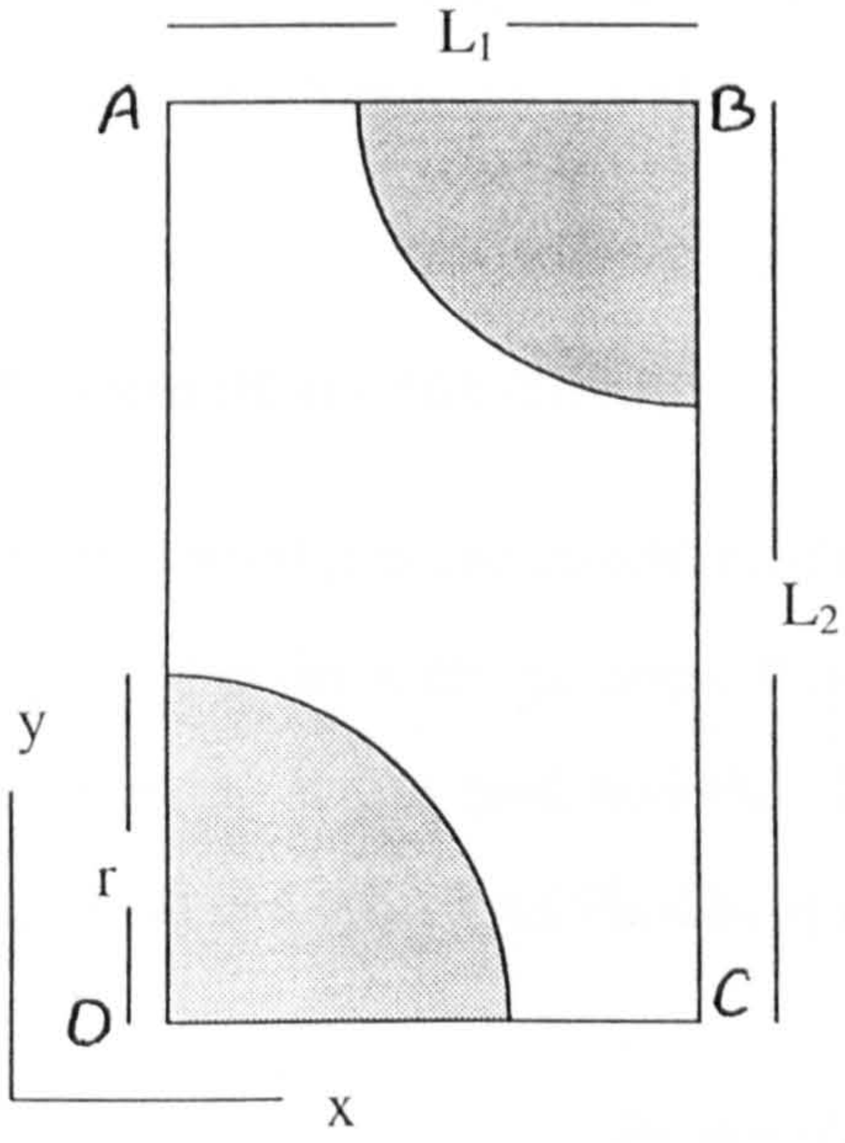

Fig.3.4.a: Unit cell of hexagonal array for fibre reinforced composite

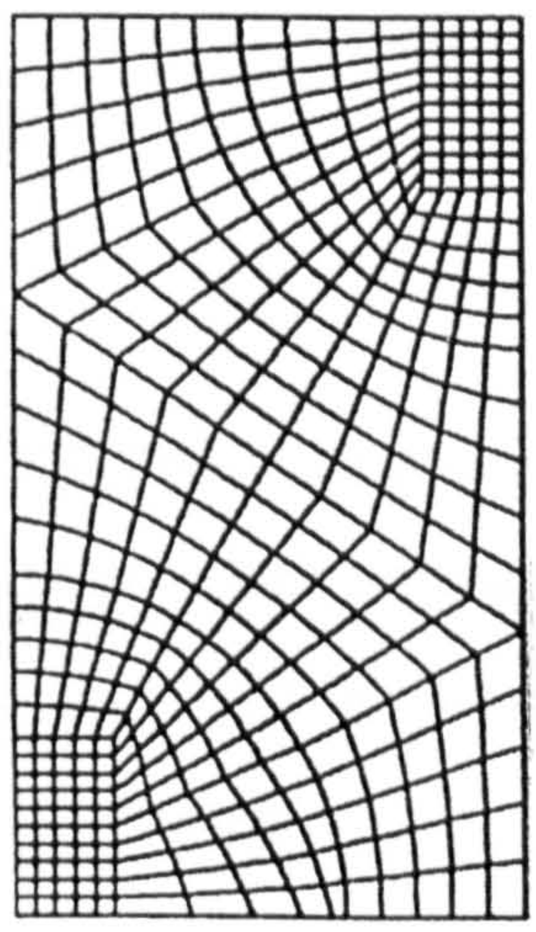

Fig.3.4.b: Mesh for fibre reinforced composite (hexagonal array)

In addition to the boundary conditions 3.31.a-d, there is the requirement that displacement components vanish on the surface of the rigid fibre.

3.2.2.2 Shear loading

The response of the fibre reinforced composite to transverse shear load is simulated with the following boundary conditions imposed on the unit cells shown in *figure 3.3.a* or *figure 3.4.a*:

$$\left.\begin{aligned} v_y &= 0 \\ v_x &= 0 \end{aligned}\right\} \qquad \text{on } y=0 \qquad (3.45.a)$$

$$v_x = V \qquad \text{on } y=Y_0 \qquad (3.45.b)$$

$$v_y = 0 \qquad \text{on } x=X_0 \qquad (3.45.c)$$

$$v_y = 0 \qquad \text{on } x=0 \qquad (3.45.d)$$

Here V is a prescribed constant in addition to the boundary conditions 3.31.a-d, there is the requirement that displacement components vanish on the surface of the rigid fibre.(Eischen and Torquato, 1993)

3.2.3 Slip boundary conditions

When there is no slip at the interface of the matrix and filler, the relative displacement of the two phases is the same as zero. Whereas in the case of slip the relative displacement of the two phase is not zero and the boundary condition is described by Naviers slip relation, which is a third kind (Robin or convective) boundary condition:

$$(\beta\tau.\mathbf{n}+\mathbf{v}).\mathbf{t}=0 \qquad (3.46)$$

Complementary with the above boundary condition is the following relation which ensures there is no relative radial displacement of the two phase.

$$\mathbf{v}.\mathbf{n}=0 \qquad (3.47)$$

Where:

β = slip coefficient

τ = stress tensor

$\mathbf{n}$ = Unit vector normal to the interface

$\mathbf{t}$ = Unit vector tangential to the interface

$\mathbf{v}$ = relative displacement of the two phase

From the slip boundary equations and the usual stress and velocity relations the components of the slip velocity are obtained as follows:

$$v_1 = -\mu\beta n_2[2(\frac{\partial v1}{\partial x1} - \frac{\partial v2}{\partial x2})n_1 n_2 + (\frac{\partial v1}{\partial x2} + \frac{\partial v2}{\partial x1})(n_2^2 - n_1^2)] \qquad (3.48)$$

$$v_2 = \mu\beta n_1[2(\frac{\partial v1}{\partial x1} - \frac{\partial v2}{\partial x2})n_1 n_2 + (\frac{\partial v1}{\partial x2} + \frac{\partial v2}{\partial x1})(n_2^2 - n_1^2)] \qquad (3.49)$$

We discretise the domain and write the weak formulation of the slip velocity relations. The interpolation points are chosen inside the elements adjacent to the slip boundary. The resulting stiffness matrices are assembled with other elemental matrices obtained from the flow equations, to form the global stiffness matrix representing the entire domain.

The matrix representation of these equations for an element located at the slip boundary results in the following equation:

$$\begin{bmatrix} a_{11}^{ij} & a_{12}^{ij} \\ a_{21}^{ij} & a_{22}^{ij} \end{bmatrix} \begin{bmatrix} v1j \\ v2j \end{bmatrix} = \begin{bmatrix} 0 \\ 0 \end{bmatrix} \qquad (3.50)$$

The members of the above stiffness matrix are given as:

$$a_{11}^{ij} = \int_{\Omega} N_i N_j d\Omega + 2n_1 n_2^2 \int_{\Omega} \mu\beta N_i N_{j,1} d\Omega$$

$$+(n_2^2 - n_1^2) \int_{\Omega} \mu\beta N_i N_{j,2} d\Omega$$

$$a_{12}^{ij} = -2n_1 n_2^2 \int_{\Omega} \mu\beta N_i N_{j,2} d\Omega$$

$$+(n_2^2 - n_1^2) n_2 \int_{\Omega} \mu\beta N_i N_{j,1} d\Omega$$

$$a_{21}^{ij} = -2n_2 n_1^2 \int_{\Omega} \mu\beta N_i N_{j,1} d\Omega$$

$$-(n_2^2 - n_1^2) n_1 \int_{\Omega} \mu\beta N_i N_{j,2} d\Omega$$

$$a_{22}^{ij} = \int_{\Omega} N_i N_j d\Omega + 2n_2 n_1^2 \int_{\Omega} \mu\beta N_i N_{j,2} d\Omega$$

$$-(n_2^2 - n_1^2) \int_{\Omega} \mu\beta N_i N_{j,1} d\Omega \quad (3.51)$$

3.3 CALCULATIONS

3.3.1 Composite modulus of elasticity and Poisson's ratio

To calculate the stiffness or modulus of elasticity of the filled composite, the average stress on the boundary AB is calculated: (Agrawal et al., 1971)

$$\sigma_z = \frac{\int_A \sigma_z \, dA}{A} = (\sigma_z)_{AB} \tag{3.52}$$

where A is the area of the top of the cylinder in the finite element analysis and the integral is replaced as a summation as follows:

$$\int_A \sigma_z \, dA = 2\pi \int_0^{r1} \sigma_z \, r dr = 2\pi \sum_{i=1}^{n} 1/2(r_i^2 - r_{i-1}^2)\sigma_z \tag{3.53}$$

where r_i and r_{i-1} are the radii to the nodal circles that define the elements on the top of the cylinder, n is the number of such circles, and σ_z is the corresponding normal stress in each element.

The modulus is defined as $E=\sigma_z/\varepsilon_z$ where the strain used is calculated from the specified boundary displacement, $\varepsilon_z = (U_z)_{AB} / |BC|$. Poisson's ratio was calculated from the displacements using the equation $u = u_1 + ku_2$. The displacement of boundary AB is $(u_z)_{AB} = (u_{z1})_{AB}$, and the displacement of boundary BC is $(u_r)_{BC} = (u_{r1})_{BC} + k(u_{r2})_{BC}$, but $(u_{r1})_{BC} = 0$; thus, $(u_r)_{BC} = k\,(u_{r2})_{BC}$. Poisson's ratio can be written as

$$\upsilon = \frac{|(u_r)_{BC}| / AB}{|(u_z)_{AB}| / BC} = \frac{|k|(u_{r2})_{BC} BC}{(u_{z1})_{AB} AB} \tag{3.54}$$

and since $(u_{r2}) = (u_{z1})_{AB} = 1$

$$\upsilon = |k|\frac{BC}{AB} = |k|(BC = AB) \tag{3.55}$$

3.3.2 Composite strength

In order to calculate the composite strength, it was assumed that the composite would fracture as soon as an element of the matrix reached a large enough value of stress to cause fracture of the matrix. Since the matrix is subjected to combined stresses (triaxial) a suitable failure criterion has to be used in order to predict matrix failure under combined stresses. The Von Mises failure criterion or distortion energy theory was selected. (Sahu and Broutman, 1972)

This criterion is then applied by determining which element has the maximum value of distortion energy for the applied stress. This value of energy may not exceed the value needed to fail the matrix material (σ_{ys}^2) and thus the composite strength is calculated from

$$S_c = \sigma_z \frac{\sigma_{ys}}{(U_{\max})^{1/2}} \tag{3.56}$$

where $U_{\max}$ is the maximum value of distortion energy determined for the arbitrary specified displacement which produces the average stress σ_z and S_c is the composite strength. The accuracy of the strength results is particularly affected by the assumption that composite failure occurs by the first matrix failure.

3.3.3 Stress calculations(Variational recovery)

The displacement formulation has frequently resulted in an unrealistic stress prediction, giving interelement stress jumps even if the true stresses were continuous. Resort to nodal averaging of element stresses is frequently made in practice to make the results more meaningful to the user. However, it is possible to obtain a better stress picture by a projection or variational recovery process which in itself is another way of applying a mixed formulation.

In this method we obtain displacements **u** by an irreducible formulation. The stresses σ are approximated, (Zienkiewicz and Taylor, 1989)

$$\hat{\sigma} = DB\bar{u} \tag{3.57}$$

We compute a set that is interpolated by

$$\dot{\sigma} = N_\sigma \bar{\sigma} \tag{3.58}$$

which in the weak sense approximates to σ. We write this approximation as

$$\int_\Omega N_\sigma^T(\sigma^* - \hat{\sigma})d\Omega = 0 \tag{3.59}$$

or

$$(\int_\Omega N_\sigma^T N_\sigma d\Omega)\bar{\sigma} = (\int_\Omega N_\sigma^T DB\bar{u})d\Omega \tag{3.60}$$

It is interesting to note that the projection of the above equation is equivalent to the least square fit or minimisation of

$$\Pi = \int_\Omega (\sigma^* - \hat{\sigma})^2 d\Omega \tag{3.61}$$

The fact that smoothed and thus more accurate, stresses are a least square fit of computed stresses provides a clue as to the location of points at which the sampling or evaluation of stress is optimal.

Stresses at the interface of the spherical filler and continous fibre are calculated from the following equations:

$$\sigma_\theta = \sigma_z \cos^2\theta + \sigma_r \sin^2\theta - \tau_{rz} \sin 2\theta \quad \text{(hoop stress)}$$

$$\sigma_{rr} = \sigma_z \sin^2\theta + \sigma_r \cos^2\theta + \tau_{rz} \sin 2\theta \quad \text{(radial stress)}$$

$$\tau_{r\theta} = \tau_{rz} \cos 2\theta - \frac{1}{2}(\sigma_r - \sigma_z)\sin 2\theta \quad \text{(shear stress)}$$

$$\sigma_{\psi\varphi} = \sigma_\phi \quad \text{(tangentail stress)}$$

Chapter Four

RESULTS AND DISCUSSION

INTRODUCTION

In this chapter the numerical analysis results are presented and the following topics are discussed:

- **Modulus of composites**

A general review of modulus of composites found by numerical analysis and other methods is presented. The strengths, weaknesses and assumptions made in different methods are discussed and compared.

- **Composites filled with rigid particles**

The imposition of the tensile load on a composite filled with particles much stiffer than the matrix is simulated. The modulus, stress distribution and the strength of these types of composites are predicted. The tensile stress obtained by our model is compared with the Papanicolaou model which includes the effects of taking the particle diameter

into account. The tensile strengths predicted by different models are compared with the outcome of our model.

- **Composites filled with debonded rigid particles**

Composites with a weak interface between the filler and matrix which are susceptible to interfacial crack formation are studied. This condition can be distinguished as partially bonded inclusion. Another case arises when there is no bonding between the inclusion and the matrix. In this latter case the slip boundary condition is imposed on the section of the interface which remains closed. The state of stress and displacement fields are obtained for both cases. The location of any further deformation through crazing or shear band formation is identified as a crack tip. Completely unbonded inclusion with the partial slip at a section of the interface reduces the concentration of the stress at the crack tip.

The effect of debonding on the strength of the composite is studied.

- **Composites filled with soft particle**

The behaviour of the rubber filled composites under the tensile load is studied. The effect and the importance of the use of different filler properties on the outcome of the numerical analyses are discussed. Two types of toughening mechanisms, namely shear banding and cavitation, are identified and the fracture behaviour of the composites is studied.

- **Continuous fibre reinforced composites**

The responses of the fibre reinforced composites under tensile and shear loads are investigated. The Young's modulus and shear modulus are calculated. The stress distribution at interface and throughout the matrix is analysed. Different failure modes are defined and discussed.

- **Short fibre reinforced composite**

The effect of different geometrical parameters such as aspect ratio and fibre spacing on the modulus of the short fibre reinforced composites is examined. The critical fibre

length for achieving the maximum reinforcement is described. The interfacial shear and tensile stress are predicted and compared with the shear lag and modified shear lag models. The model equations are modified by considering the boundary flux terms. The model predictions for the composite properties and stress fields are obtained with and without boundary fluxes. The possibility of the composite failure either by interfacial debonding and fibre breakage is investigated.

4.1 MODULUS

4.1.1 Equal stress and equal strain bounds

Modulus is a bulk property of composites that depends primarily on the geometry, modulus, particle size distribution, and concentration of the filler.

The Hashin's bounds and rule of mixture bounds are compared with our prediction in *figures 4.1a-c* for a particulate filled composite. The rule of mixture bounds predict that the modulus of a two phase composite should fall between the upper bound of:

$$E_c = V_m E_m + V_f E_f \tag{4.1}$$

and the lower bound of:

$$E_c = \frac{E_m E_f}{V_m E_f + V_f E_m} \tag{4.2}$$

The epoxy matrix and glass beads (filler) properties, which are used in our model, are given in table 4.1.

	Input Properties	
Phase	**E (GPa)**	**Poisson's Ratio, ν**
Matrix	3.01	0.35
Glass Sphere	76.0	0.21

Table 4.1. Elastic Material Properties Used in the Predictive Models

The modulus predictions agree well at low filler volume fractions. At higher filler volume fractions the Hashin's bound and rule of mixture bounds become widely spaced, and therefore they are of limited predictive value. However, these bounds can still serve as a useful test for the approximate theories, since any solution outside these bounds must be regarded as invalid. From a mechanical viewpoint, the upper bound represents the situation in a two phase material in which both phases strain equally.

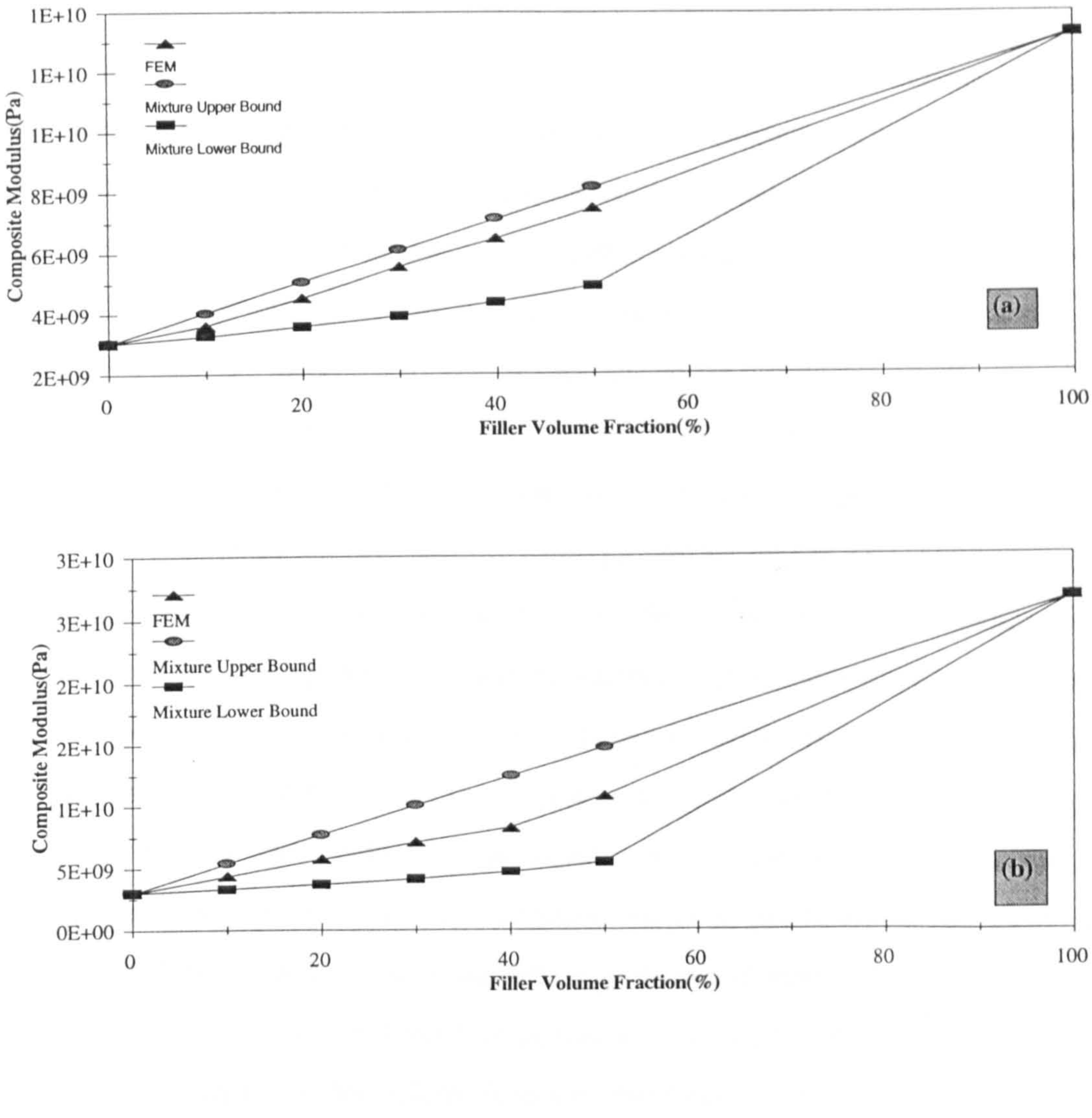

Fig4.1: Comparison of the FEM modulus predictions of filled composite for different relative properties of filler and matrix with rule of mixture bounds and Hashin's bounds.

The lower bounds represent the case in which the phases are stressed equally under an applied load. This situation is typified by particles in a matrix, with no hydrostatic stress present. The relative position of the modulus values in the bounds depends on the relative properties of the particle and the matrix. When a two-phase particulate filled composite is deformed under an applied load, the matrix, which is usually softer than the particulate reinforcement, tends to deform at lower stresses than the dispersed particles. However, since the matrix is rigidly bonded to the harder particles, it cannot deform in the same manner as it would in the absence of the filler.

The restriction of matrix deformation imposed by the hard reinforcing particles results in the generation of a hydrostatic state of stress in the matrix. The magnitude of this hydrostatic constraint and the determination of whether the generated stress is purely hydrostatic depends on the relative clast properties of the two phases (i.e. elastic modulus and Poisson's ratio of phases). As the disparity between hardness and the strength of the two phases in these composites becomes greater, the hydrostatic constraint factor cannot be extended as much as it does in the composites with phases having closer properties. Therefore a greater relative modulus of particles and matrix results in a composite modulus closer to the lower bound, ie; equal stress prediction.

In *figures 4.1a-c* the modulus of composite has been predicted by the finite element model for three different relative moduli of particle and matrix. It can be seen that as the relative value increases from 2.14 in *figure 4.1a* to 25 in *figure 4.1c.*, the modulus values at the range of filler volume fraction shift from the upper equal-strain bound to the lower equal-stress bound. The bounds are more widely spaced when the relative modulus rises. However, in all cases the Hashin bounds are spaced closer than rule of mixture bounds.

The advantage of the finite element prediction is that it can be used for any shape of particles and interface conditions.

The lower and upper bound assume that individual phases are under uniform stress or strain. In practice, however, the filler particles may not be completely separated from one another and the reinforcement element may, on the microlevel, effectively be an aggregate of smaller particles. Thus in response to the applied load the stress will be

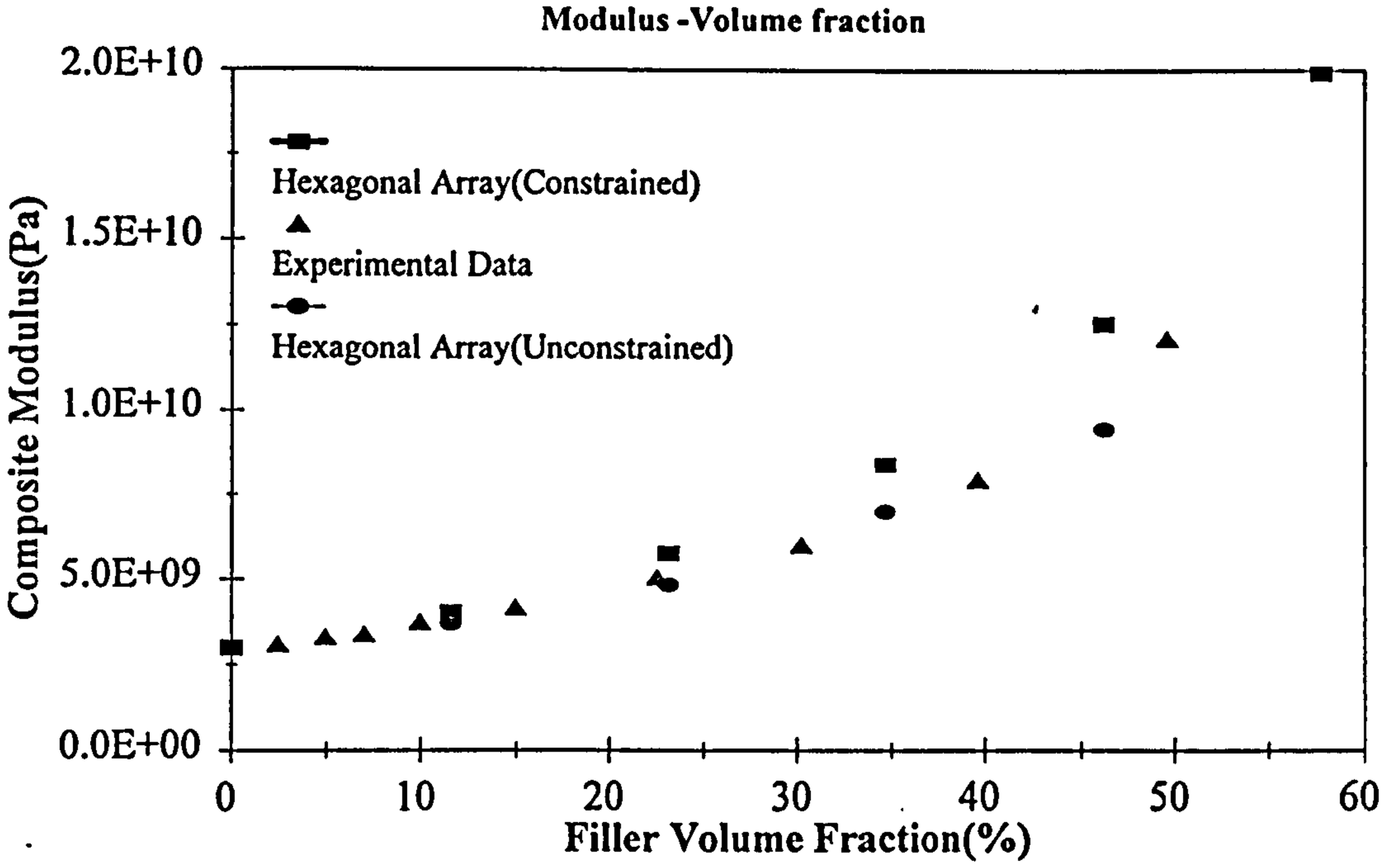

Fig.4.2: Variation of the tensile modulus versus volume fraction for particulate filled composite. Results of FEM are for hexagonal array with constrained and unconstrained boundary conditions.

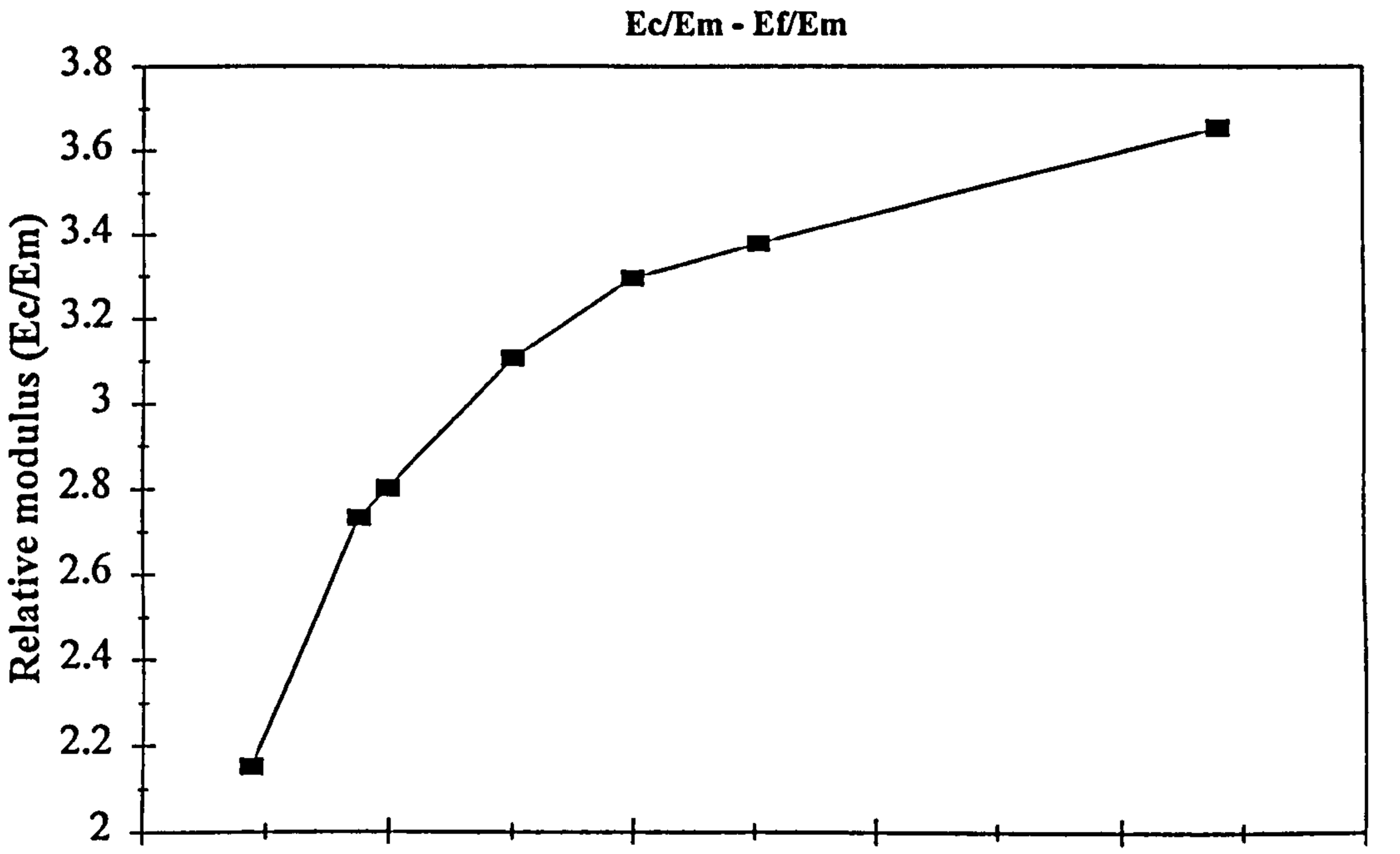

Fig.4.3: Effect of Ef/Em on the Ec/Em for particulate filled composite. Volume fraction studied is

distributed unevenly between the particles and aggregates and the assumption of either uniform stress or strain (uniform particle size and distribution) will be an over-simplification.

4.1.2 Model predictions and experimental results

Accurately measured values of Young's modulus for epoxy resin reinforced with glass spheres are available from literature. These experimental results agree well with our finite element predictions as shown in *figure 4.2*. The differences can be attributed to the assumptions that have been made in the model. The discrepancy between model predictions and the experimental results may be due to ignoring the following factors in the model.

4.1.2.1 Agglomeration

The filler particles may aggregate to form agglomerates much larger than the filler particles. Agglomerates tend to contain voids and air filled spaces so that their apparent volume is considerably greater than the true volume of the filler material.

If the agglomerates are hard and have appreciable mechanical strength, they will not easily be broken and considering the weight of material added as filler, the filled material can have a modulus greater than expected. Because the volume of the aggregates in this case is larger than the true volume of the filler particles. Soft and easily disintegrating aggregates, on the other hand, would be expected to give rise to an opposite effect. The agglomeration of particles have a considerable effect at higher volume fractions of filler and therefore this factor become more significant at higher volume fractions.

4.1.2.2 Dewetting

At high concentration of fillers, all the individual particles might not be wetted by matrix phase resulting in a poorer dispersion of the filler within the composite. Instead, the particles tend to aggregate. Dewetting and poor dispersion are amongst

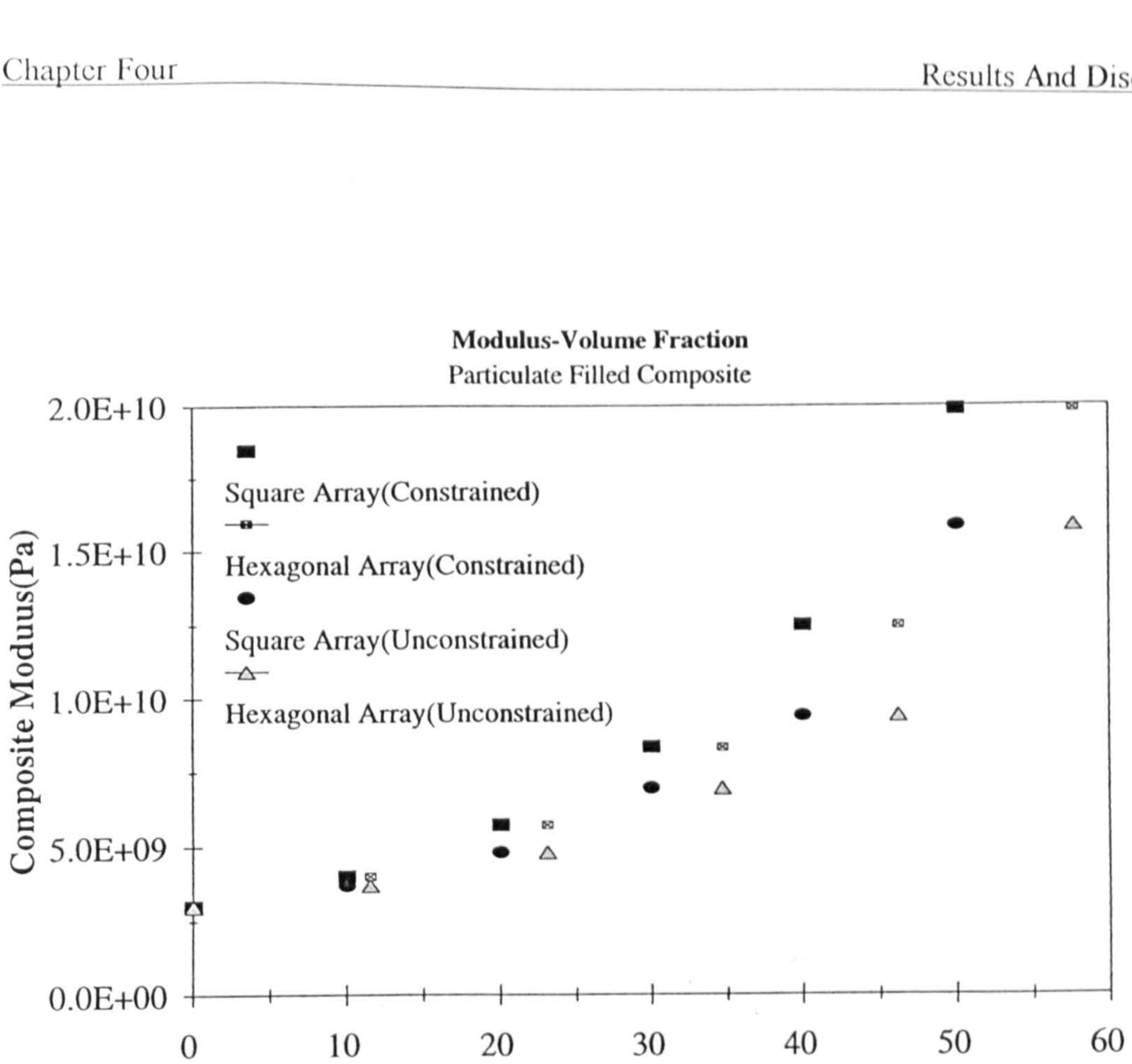

Fig.4.4: Comparison of FEM results for the modulus-volume fraction variations for square and hexagonal arrays, constrained and unconstrained boundary conditions.

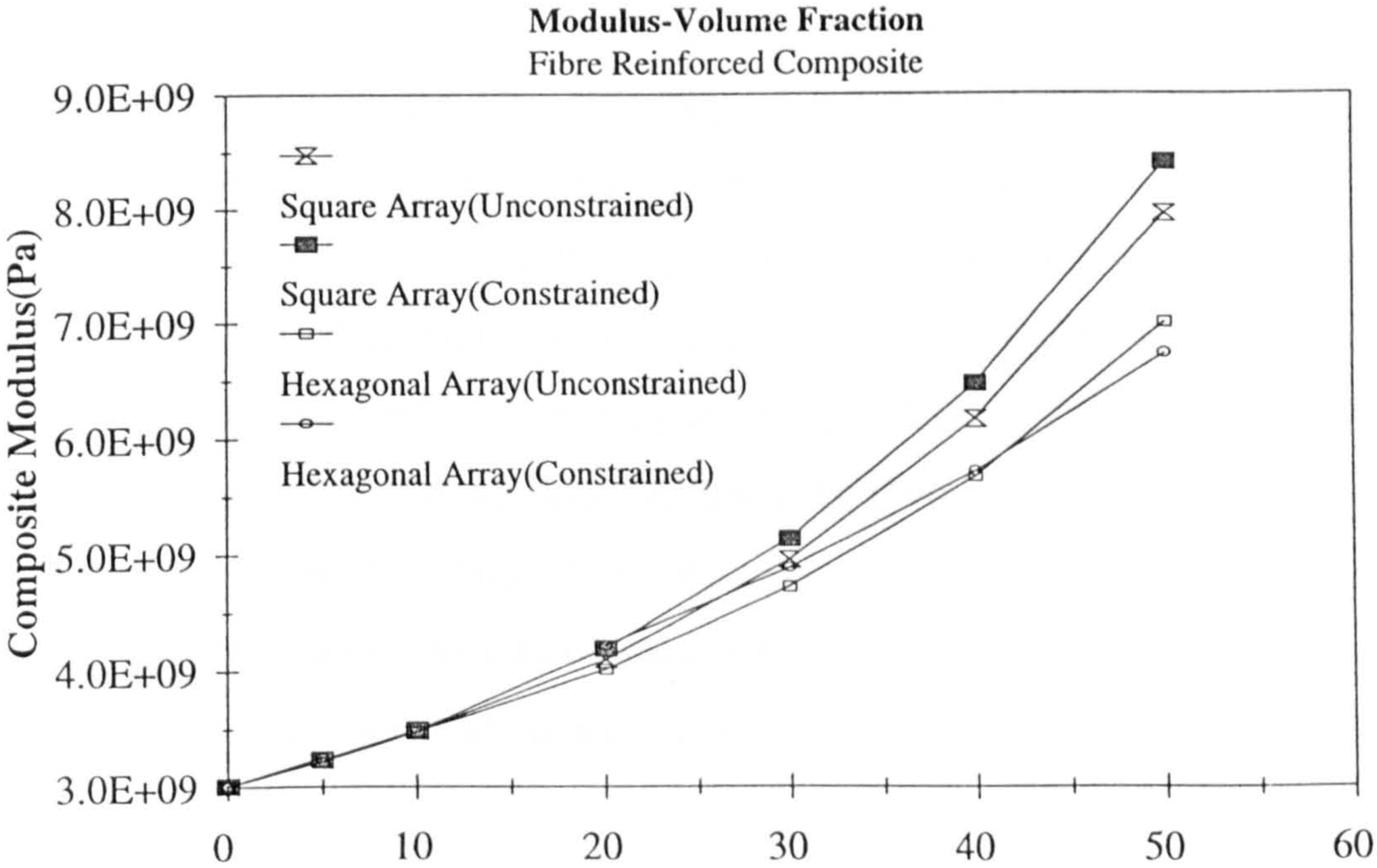

Fig.4.5: The variation of the continous fibre reinforced composite with volume fraction of the fibres for square and hexagonal array arrangement of the fibres. Comparion of constrained and unconstrained boundary conditions.

the reasons that make the production of composites with very high filler volume fractions impractical.

4.1.2.3 Adhesion and bonding

In theoretical analysis of the behaviour of the composites it is generally assumed that the adhesion between the filler and the polymer matrix is perfect. By perfect adhesion it is meant that there is no relative movement of the phases across the interface under the applied loads. At higher applied stresses, however, the interfacial bond may break, and the adhesion is no longer perfect. Thus, the magnitude of the applied stresses often determines whether there is a perfect adhesion or not. In reality, the degree of adhesion does not appear to be an important factor as long as the frictional forces between the phases are not exceeded by the applied stress. In most filled systems there is a mismatch between thermal expansion coefficients of the phases which results in a mechanical bond due to thermally induced stresses.

In many practical cases it cannot be assumed that there is a perfect adhesion between the filler and the matrix. In extreme cases of debonded particles it can be assumed that the particles act as holes and, therefore can seriously decrease the composite modulus with increasing filler content. It can be argued that the unbonded particles do not act entirely as holes, since they also restrain the matrix from collapsing.

If the bond or adhesion between filler and polymer is weak, the bond may break when a load is applied. The polymer will then deform more than the filler so that unsymmetrical cavities and voids develop around each filler particle.

A change of the matrix-filler adhesion has a smaller effect on composite modulus than its strength. The latter is much more dependent on the pre-treatment of the filler surface. Thus the filler is less efficient as a reinforcing agent, and in extreme cases the modulus of the composite can be reduced rather than being increased by the addition of filler.

4.1.2.4 Arrangement

In practice the arrangement of the filler particles in a composite can never be uniform and the interparticle spacing varies in different parts of the composite. It has been

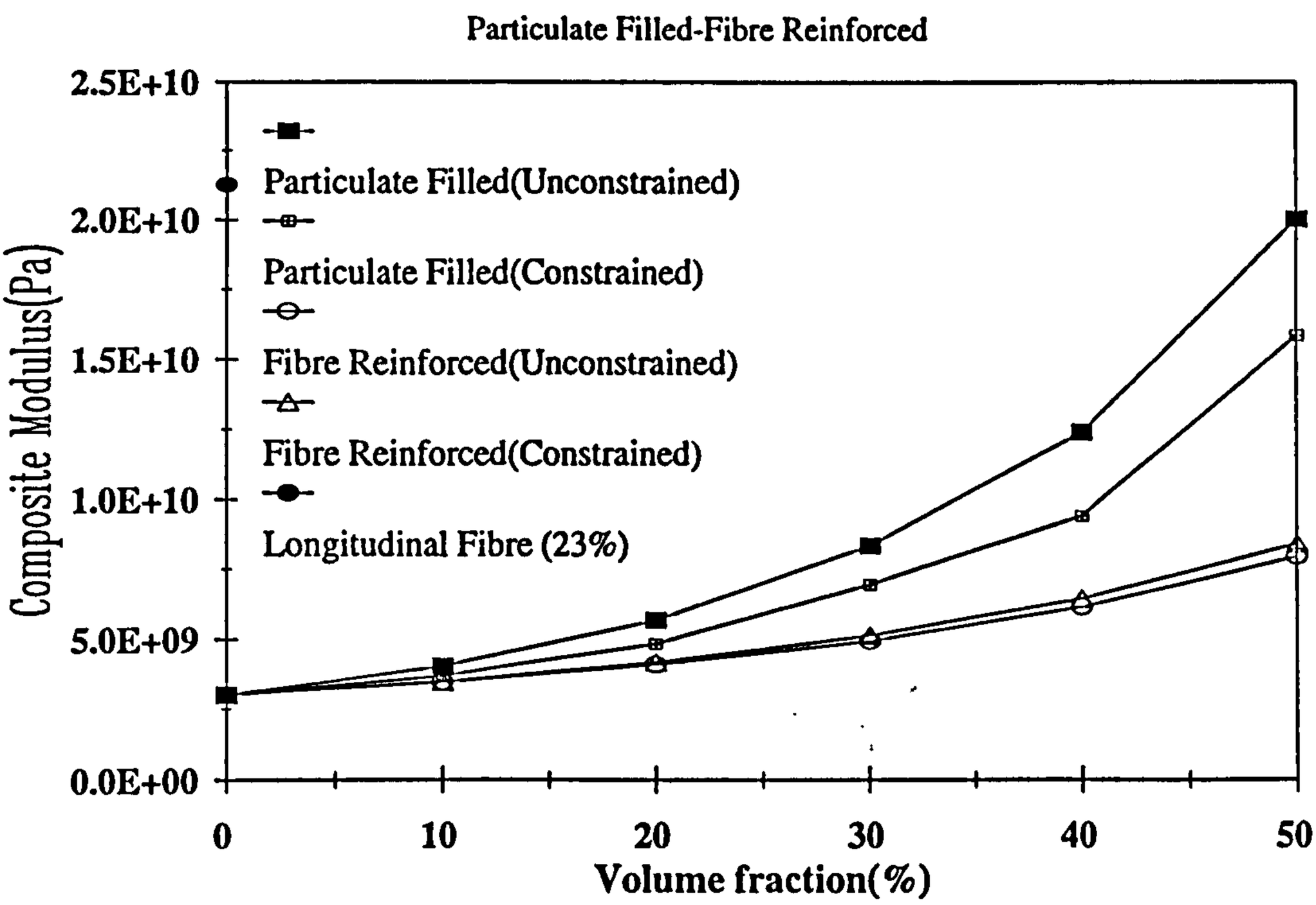

Fig.4.6: Comparison of the stiffness obtained by pariculate filled and fibre reinforced composites. FEM results for square array arrangement and constrained and unconstrained boundary

shown that when particles are distributed randomly, a lower composite modulus is obtained. A combination of finite element modelling and spatial statistical techniques has been used in the simulation of composites with randomly distributed filler particles.

In this project two different types of particle arrangements in the form of square and hexagonal arrays are examined to show the effect of the particle distribution on the final physical properties of the composite. The results are shown in *figure 4.4* for a particulate filled composite. The same comparison of the effect of the arrangement of reinforcing phase can be seen in *figure 4.5* for a fibre reinforced composite. In both cases the hexagonal array gives lower composite modulus for the same filler volume fraction and the hexagonal array gives a higher volume fraction for the same particle spacing. The hexagonal array can be considered to be a more random arrangement compared to the square array.

4.1.2.5 Filler particle shape

In our model we assume that the particles are spherical and of the same size. Practically the filler particles are not uniform in size and only a few fillers are spherical in shape. However, since most particles have nearly the same dimensions in all directions, they can be approximated by sphere. Deviations of experimental results from the model may be caused by more important factors than small deviations of the particles from spherical shapes.

Despite the described simplifying assumptions our model predictions compare closely with the experimental results. The agreement between model predictions and experimental results is more obvious when unconstrained boundary conditions is imposed and hexagonal packing is chosen to show the distribution of the particles.

It can be shown that the addition of particles produces a substantial increase in composite modulus. However, as *figure 4.3* indicates the effect of increase in particle modulus gradually diminishes becoming asymptotic to the modulus of an infinitely rigid particle.

4.2.3 Boundary conditions used in the finite element model

The conditions at the boundary of the cell which is perpendicular to the boundary under tensile load can affect the result of the analysis. When boundary conditions with constraint are imposed, for each point of the modulus-volume fraction curve we need to follow two steps of loading. The results of these steps are superimposed and the total and final point is calculated. Under this set of boundary conditions we enforce geometric compatibility and therefore the outer sidewall of the cell remains straight. When the unconstrained boundary conditions is employed, every point along the sidewall is stress free. However, since the constraints are released, the sidewalls do not remain straight. The results obtained for these sets of boundary conditions are compared for both particulate and fibre reinforced composites and are shown in *figure 4.6*. The results predicted using unconstrained boundary condition are lower than the results found for the constrained boundary conditions.

4.2 COMPOSITES FILLED WITH RIGID PARTICLES

In this section the response of epoxy resin filled with glass particles to tensile and compressive loading is studied. The physical properties of the epoxy resin and glass filler used as the input values for the finite element program are presented in table 4.1.

4.2.1 Young's modulus

The predicted values of the Young's modulus for composites filled with hard particles are compared with experimental data in *figure 4.4*. The theoretical models which are used to explain the variations of the modulus of polymer composites with volume fraction do not normally include the effect of filler particle size. However, experimental observations of Spanoudakis and Young (Spanoudakis and Young, 1984) show that there is a clear reduction in the modulus of a composite with increasing particle size for a given volume fraction of particles.

Relatively low values of Young's modulus for large particle sizes have been attributed to the "skin" effect. Lewis and Neilsen suggested that in the moduli measurements, the properties of the surface are emphasised at the expense of the interior of the composite. This leads to a higher error for larger particles where the surface "skin" is depleted of particles. This could explain the drop in modulus with increasing particle size. The error due to "skin" effect can be removed by the extrapolation of measured values for particles with zero size (i.e. points).

4.2.2 Stress distribution

4.2.2.1 Concentration of direct stress

The maximum direct stress concentration which is the maximum principle stress is found to be in the resin above the pole of the sphere. The precise position and value of the maximum stress concentration of the applied stress vary with the volume fraction of the filler. The magnitude of the stress concentration of applied stress increases with volume fraction of added glass particles which is due to increasing interactions

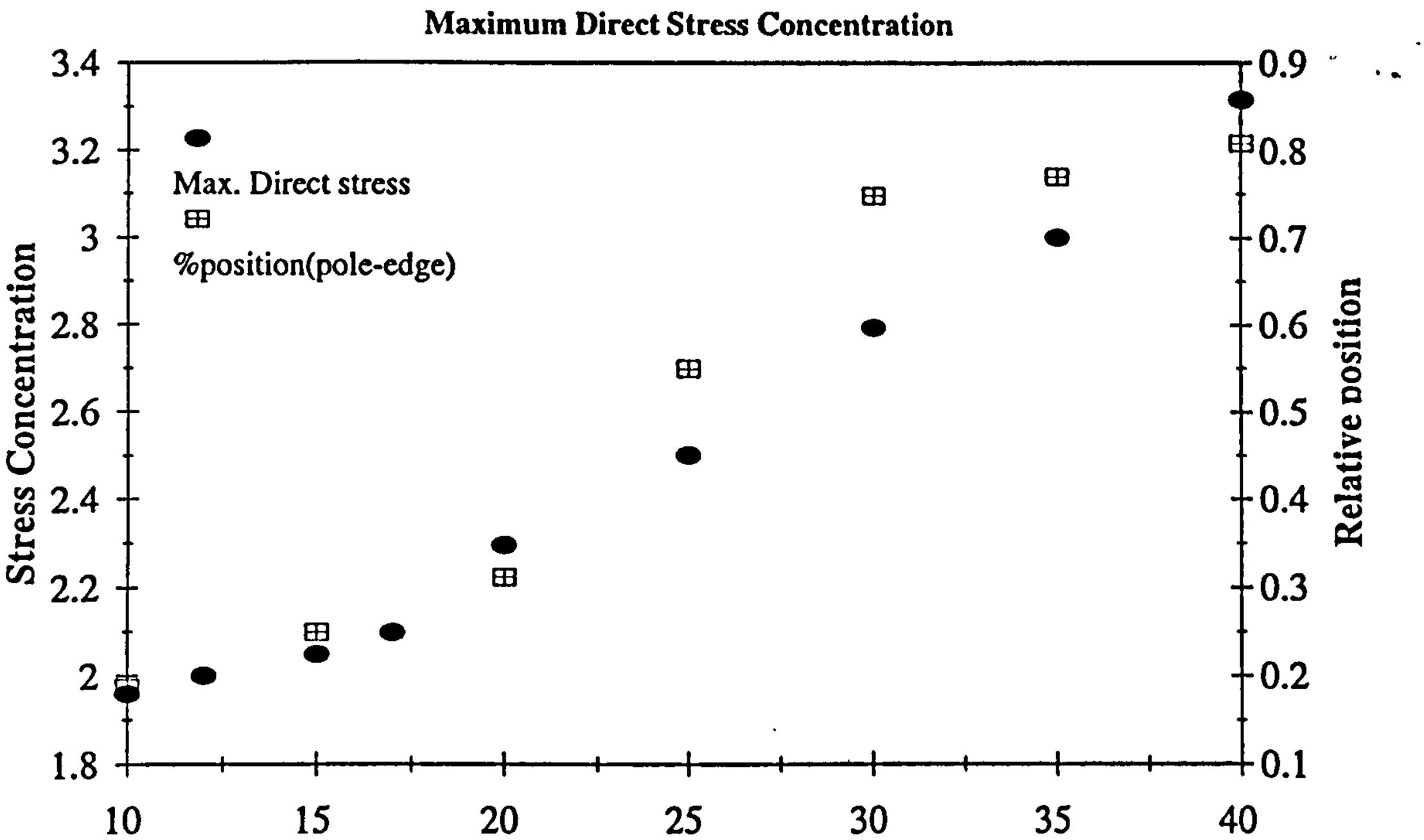

Fig.4.7: Maximum direct stress concentration and position versus filler volume fraction.

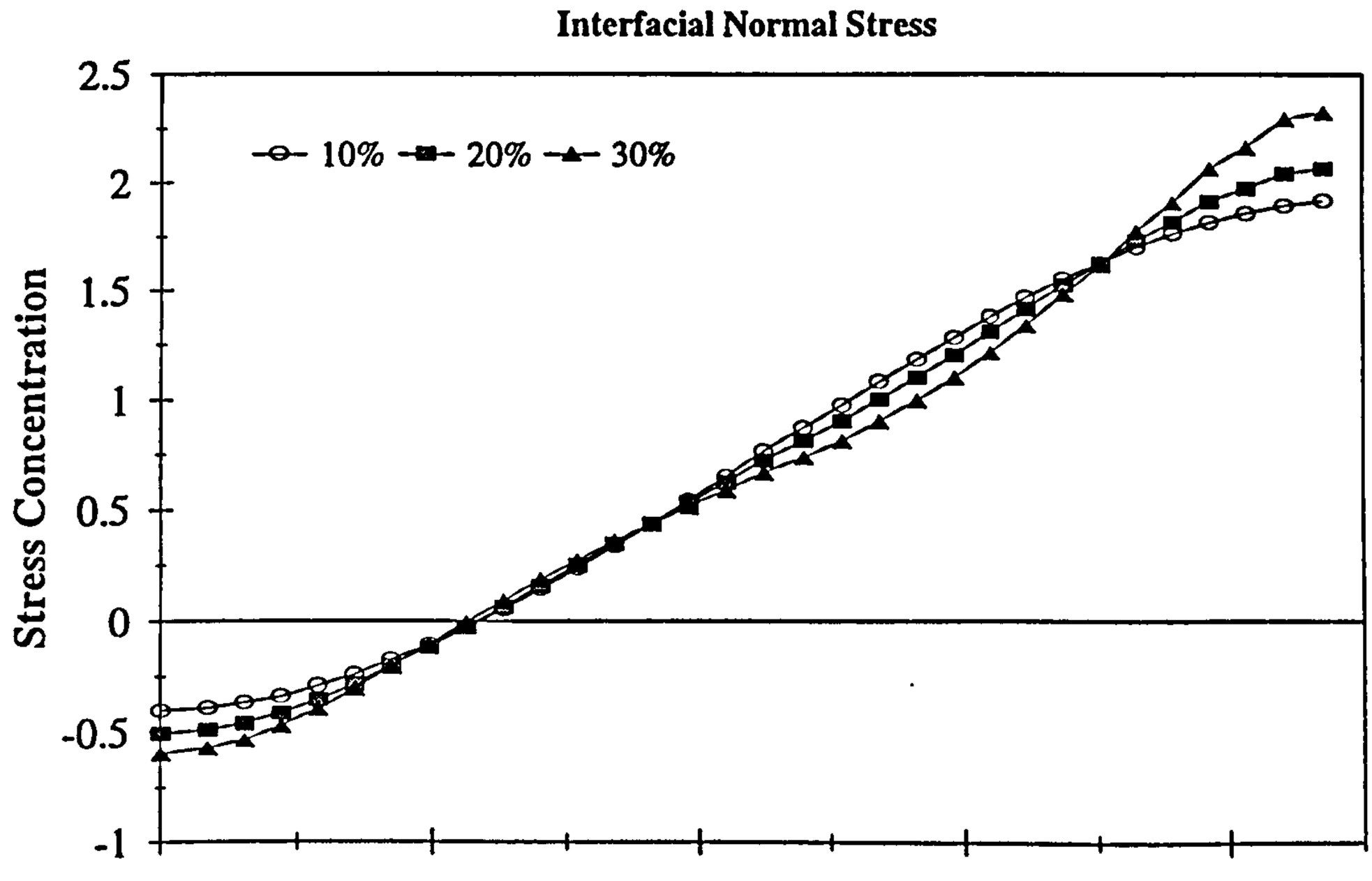

Fig.4.8a: Radial stress concentration at the interface of the filler particle and matrix.

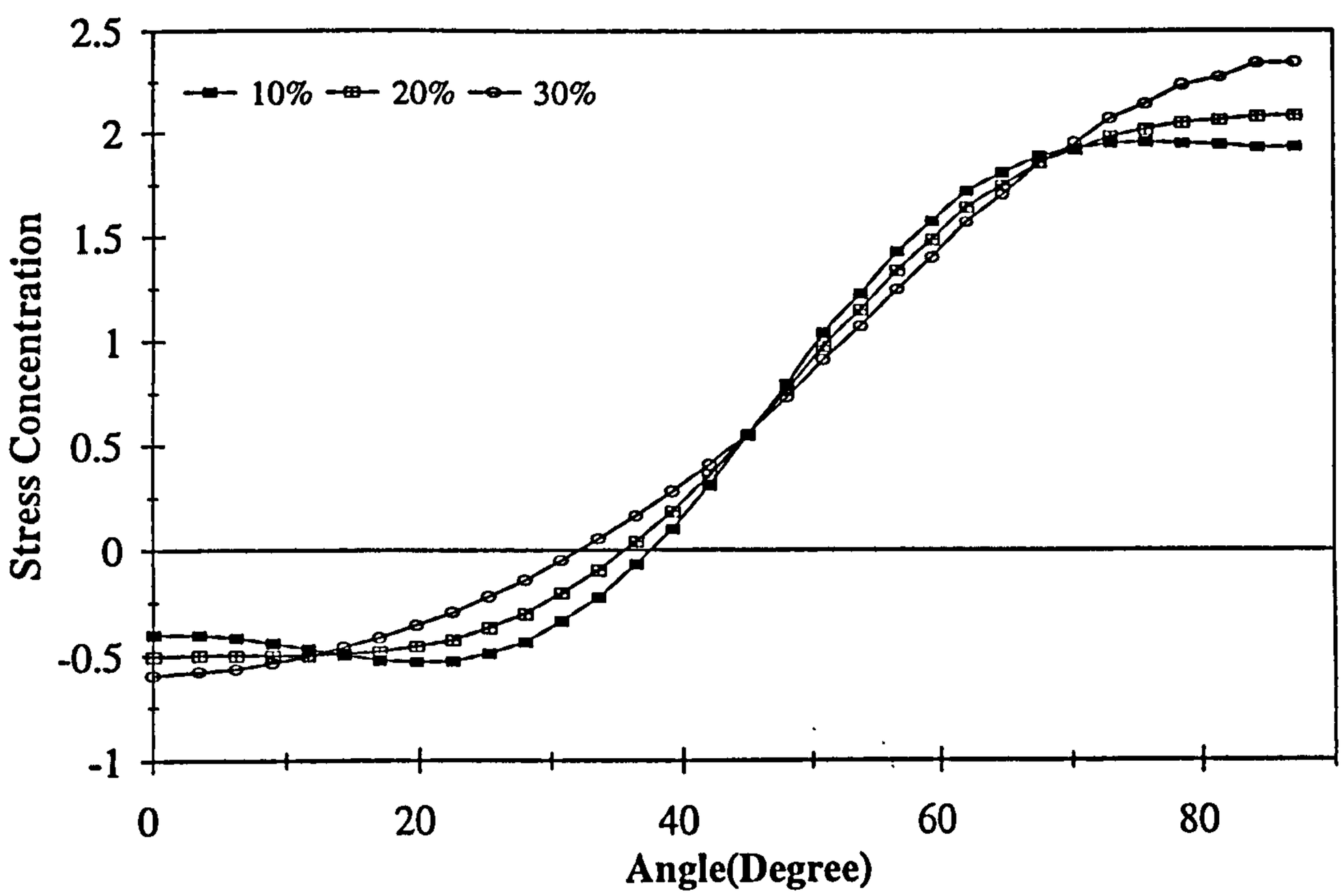

Fig.4.8b: Tangential stress concentration at the interface of the filler particle and matrix.

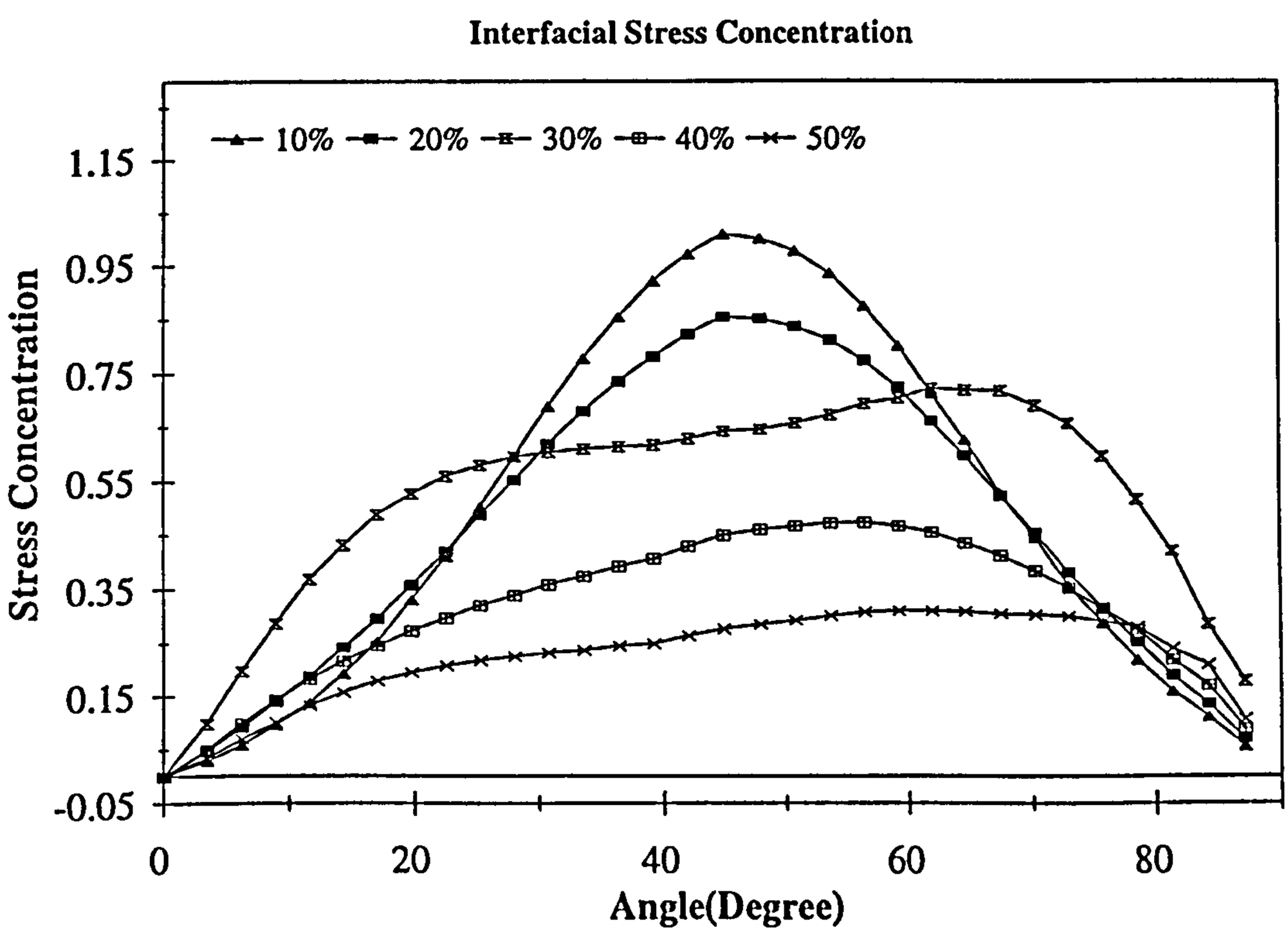

Fig.4.8c: Shear stress concentration at the interface of the filler particle and matrix.

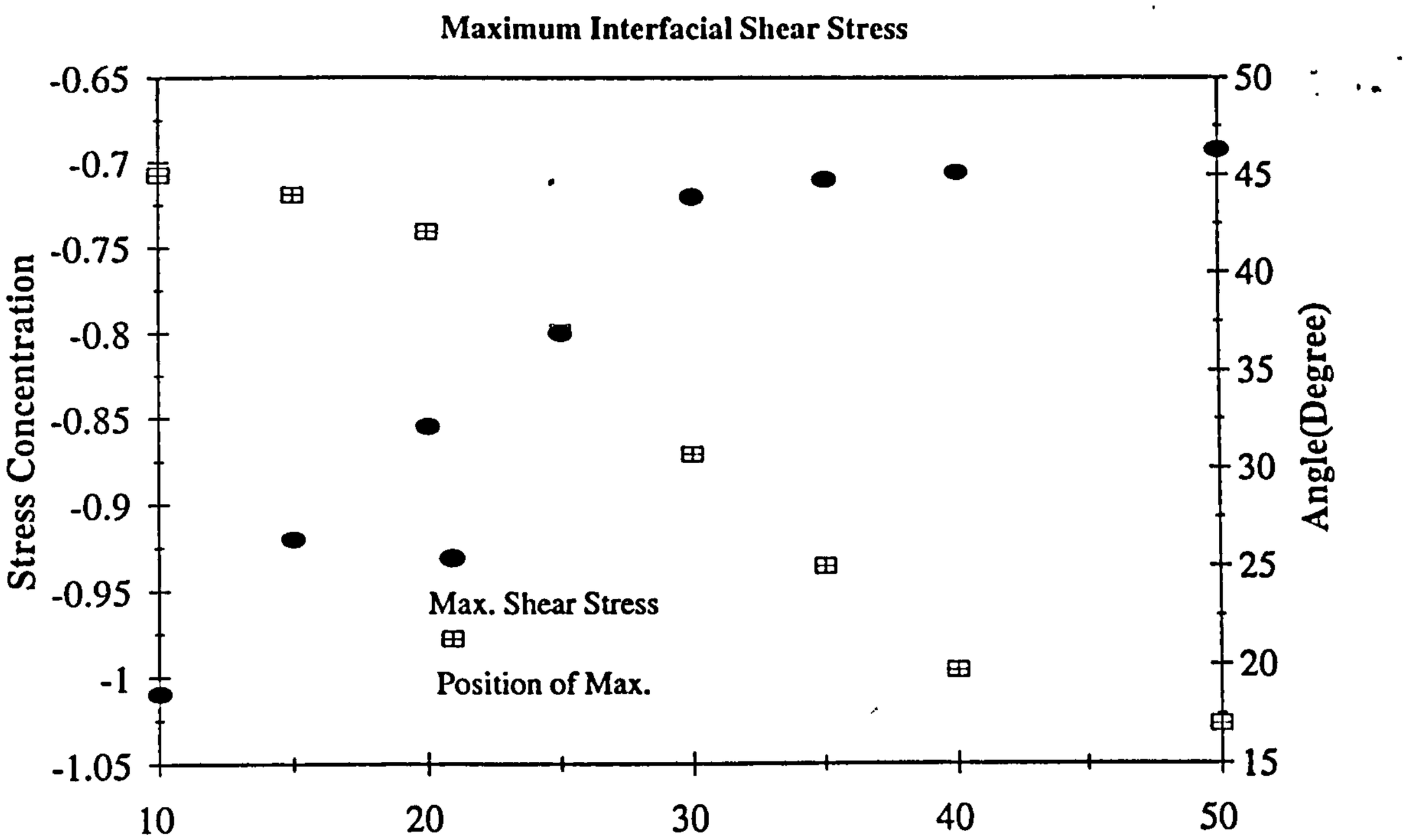

Fig.4.9: Maximum interfacial shear stress concentration and its position.

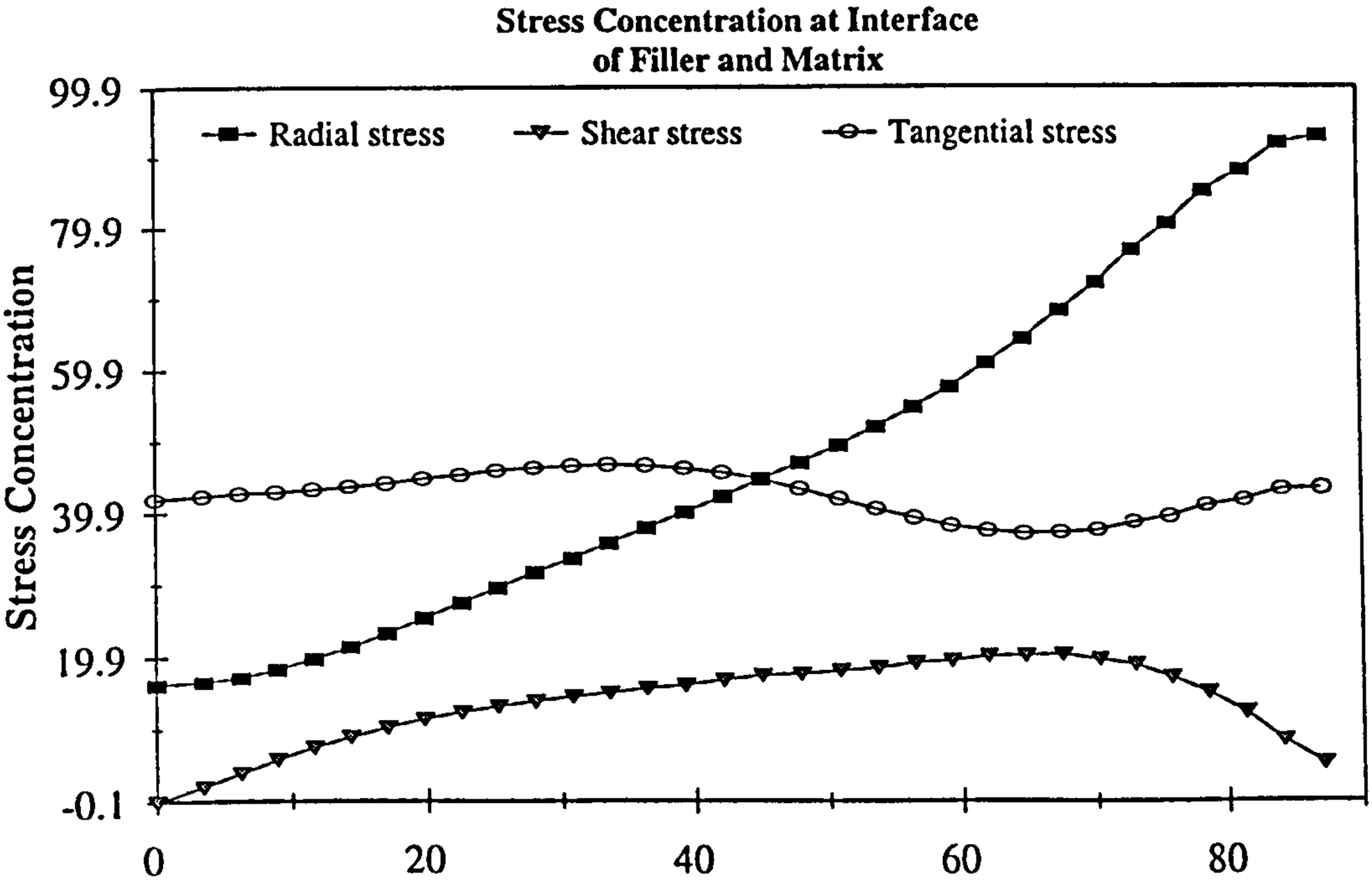

Fig.4.10: Stress concentrations at the interface of the particle and matrix for the composite under compression.

between the stress fields around the filler particles as their separation decreases.

Stress concentration in this work is defined as the stress value normalised by the stress applied to the composite and the relative position is the distance from the pole normalised by the pole-edge distance.

The position of maximum stress concentration factor of the applied stress varies in the studied cases. This is shown in *figure 4.7*. At high filler volume fractions the position is at the edge of the grid, which is the midway between the particles. At lower volume fractions the position is relatively closer to the particle in the cylinder under analysis, which is further away from its adjacent particles. Taking into account that the distances between adjacent particles for different volume fractions is variable, the maximum distance between the position of stress concentration and adjacent particle was calculated. This distance decreases rapidly with increasing filler volume fraction.

4.2.2.2 Stresses at the interface

Stresses around the interface are transformed to polar coordinates. Radial and shear stresses on either side of the interface, in the glass and resin are identical. It is found that the stress transferred to the glass sphere is substantial. This leads to a sharp increase in the stiffness with increasing volume fraction of particles.

As *figure 4.8a* shows the maximum radial stress is at the pole of the particle sphere for all volume fractions. The variations of the value of this stress concentration with filler volume fraction is similar to that of the maximum stress concentration. Radial stress is tensile at the pole and compressive at the equator for a spherical particle. At position $\theta = 22°$ the stress is zero for all volume fractions. The variation of the tangential stress in the matrix at the interface is shown in *figure 4.8b*.

There is a maximum in radial-tangential shear stress as it can be seen in *figure 4.8c*. Both the value and the position of this stress concentration vary with volume fraction. The absolute value of the stress concentration factor decreases with increasing volume fraction. This decrease is explained by considering the source of this stress concentration, which is the difference between the moduli of the particle and its surrounding material. As the volume fraction of spheres increases this difference decreases, and hence the rate of this decrease becomes significantly ($\approx$ 4 times) smaller

than the rate of the increase of the concentration of applied stress. *Figure 4.9* indicates that at higher volume fractions the site of this maximum concentration of shear stress moves closer to the pole of the sphere.

Stresses around the interfaces of spherical particles have previously been considered by Dekkers and Heikens (Dekkers and Heikens, 1983). For a poorly bonded interface they postulate that a crack will form around the interface because of the tensile radial stress. Using the constituent material properties very close to those we have used, they predicted that the interfacial crack should grow up to an angle of $\theta = 68°$ to 70°, depending on the remaining friction of the debonded interface. The magnitude of the radial stress concentration at the pole is not much smaller than the maximum concentration of the applied stress. Therefore for the tensile loading, debonding from the pole is expected. Under tensile applied stress the radial stress at the equator is compressive.

4.2.3 Compression

The radial stress would be tensile at the equator of the particle interface if the applied stress is compressive. *Figure 4.10* shows the distribution of the stresses at the particle and matrix interface. Although the absolute value of this stress at the equator is almost an order of magnitude smaller than its value at the pole it may however be sufficient to cause debonding from the equator of the sphere under the condition of the applied compression.

4.2.4 Concentration of yield stress

The contour diagrams of the Von Mises stress, direct stress and shear stress concentrations are shown in *figures 4.11a-c*. In the contour diagram of the Von Mises stress two positions where Von Mises stress reaches its maximum are found: the first point is in the resin above the pole of the sphere in the close vicinity of the position of the maximum direct stress concentration; the second point is near to the position of the maximum shear stress at the interface. The values of these stress concentration factors vary with volume fraction as is shown in *figure 4.12*. Their positions vary in the same directions as the positions of the associated concentrations of the direct stresses. *Figure 4.13* shows that the magnitudes of the maximum concentrations of

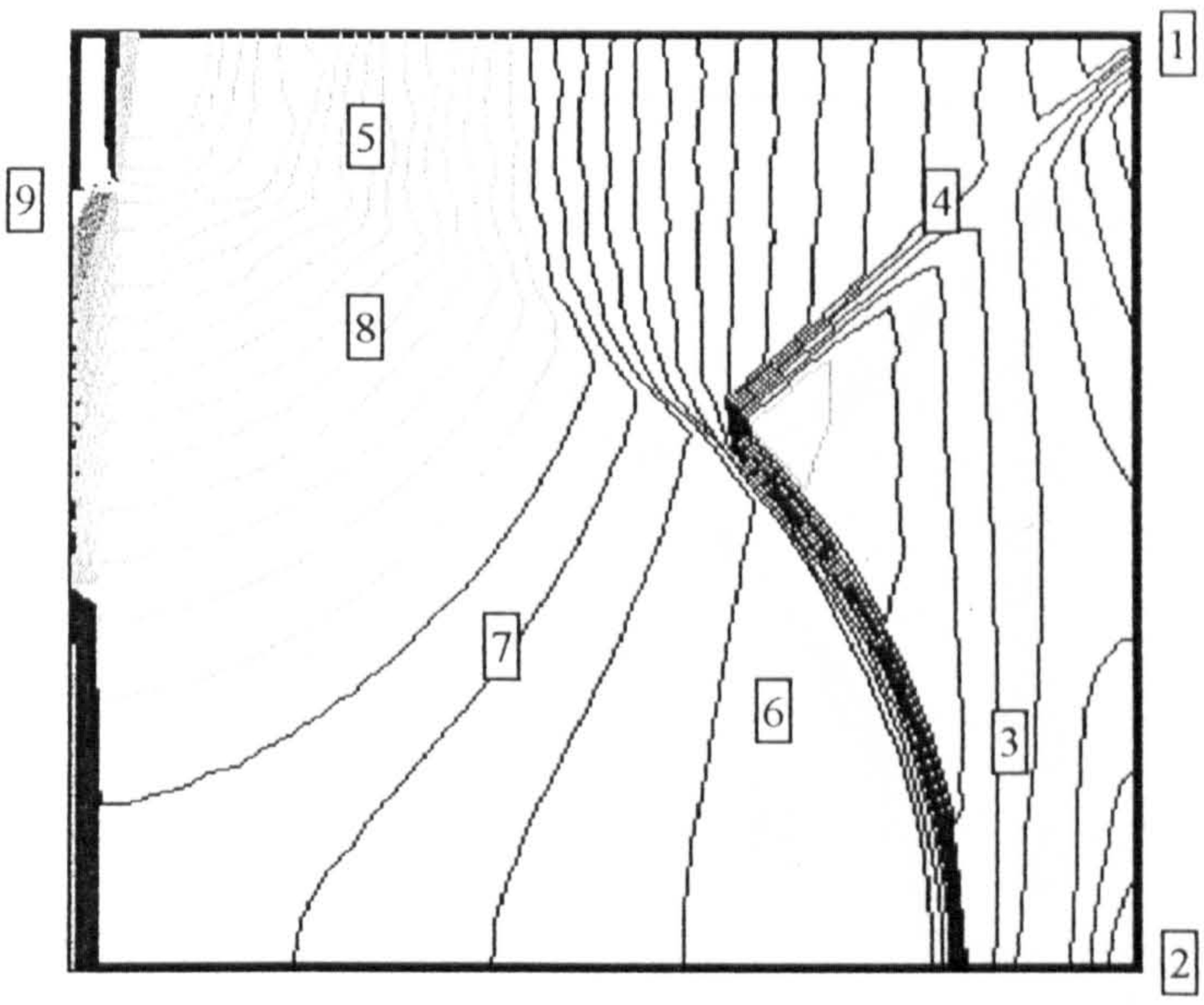

1	0.144E7
2	0.222E7
3	0.260E7
4	0.313E7
5	0.120E8
6	0.488E7
7	0.801E7
8	0.113E8
9	0.335E8

Fig 4.11a : Contour diagram of the direct stress field of the composite filled with 30% of hard filler particles

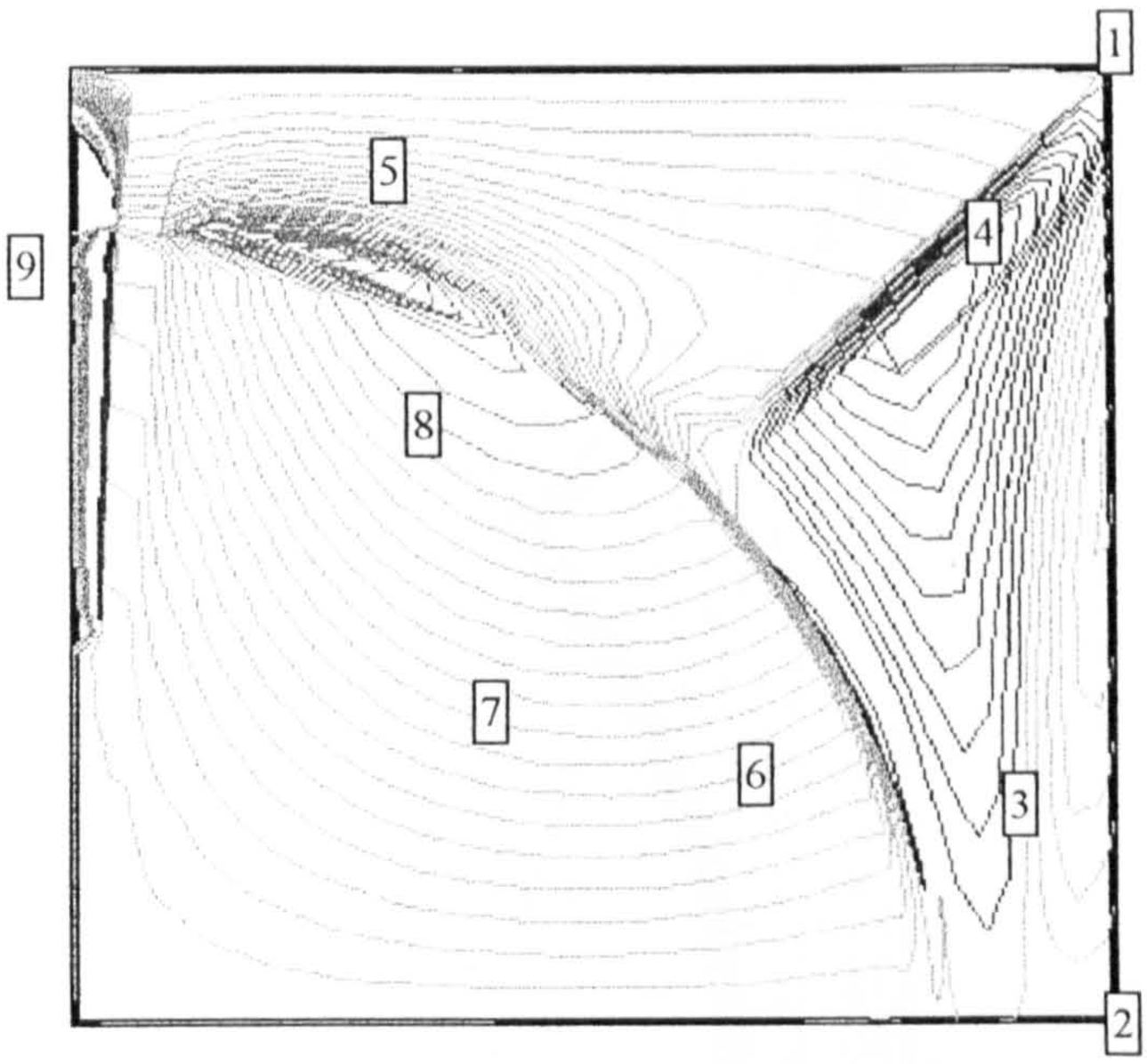

1	0.968E4
2	-0.216E4
3	0.336E6
4	-0.452E6
5	-0.452E6
6	0.219E6
7	-0.162E7
8	-0.227E7
9	0.175E8

Fig 4.11b : Contour diagram of the shear stress field of the composite filled with 30% of hard filler particles.

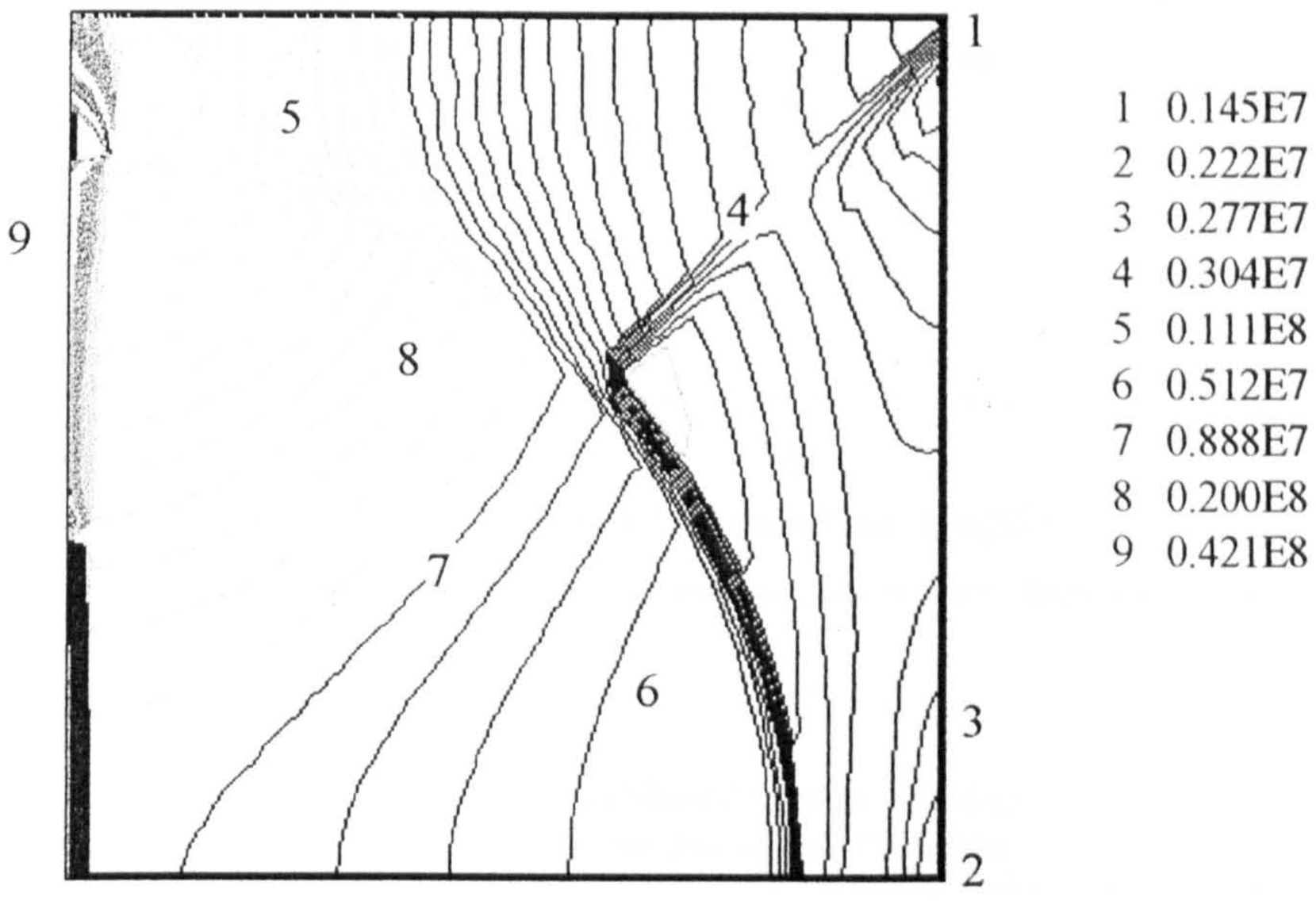

Fig 4.11c : Contour diagram of the Von Mises stress field of the composite filled with 30% of hard filler particles

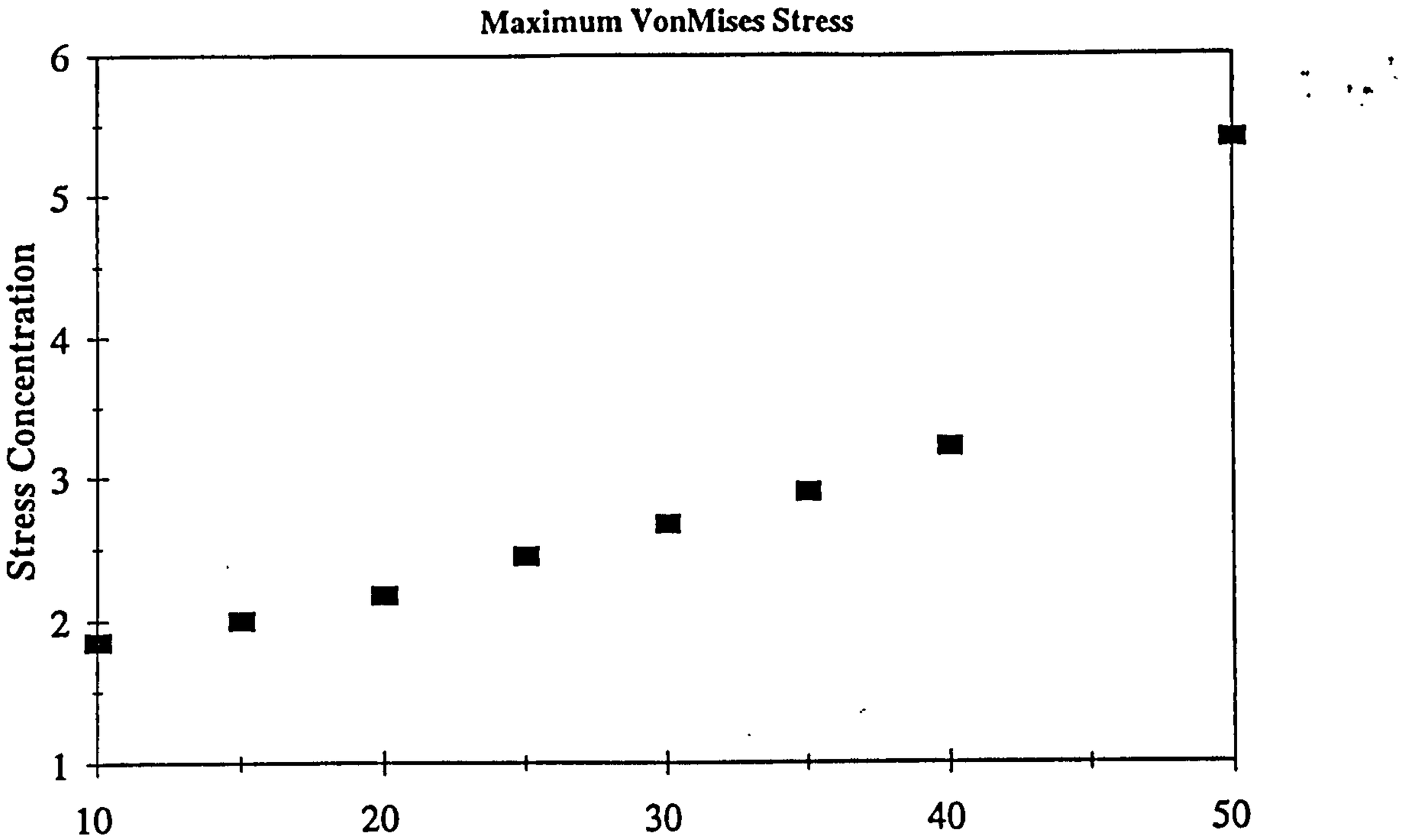

Fig.4.12: Maximum Von Mises stress concentration at the range of filler volume fraction.

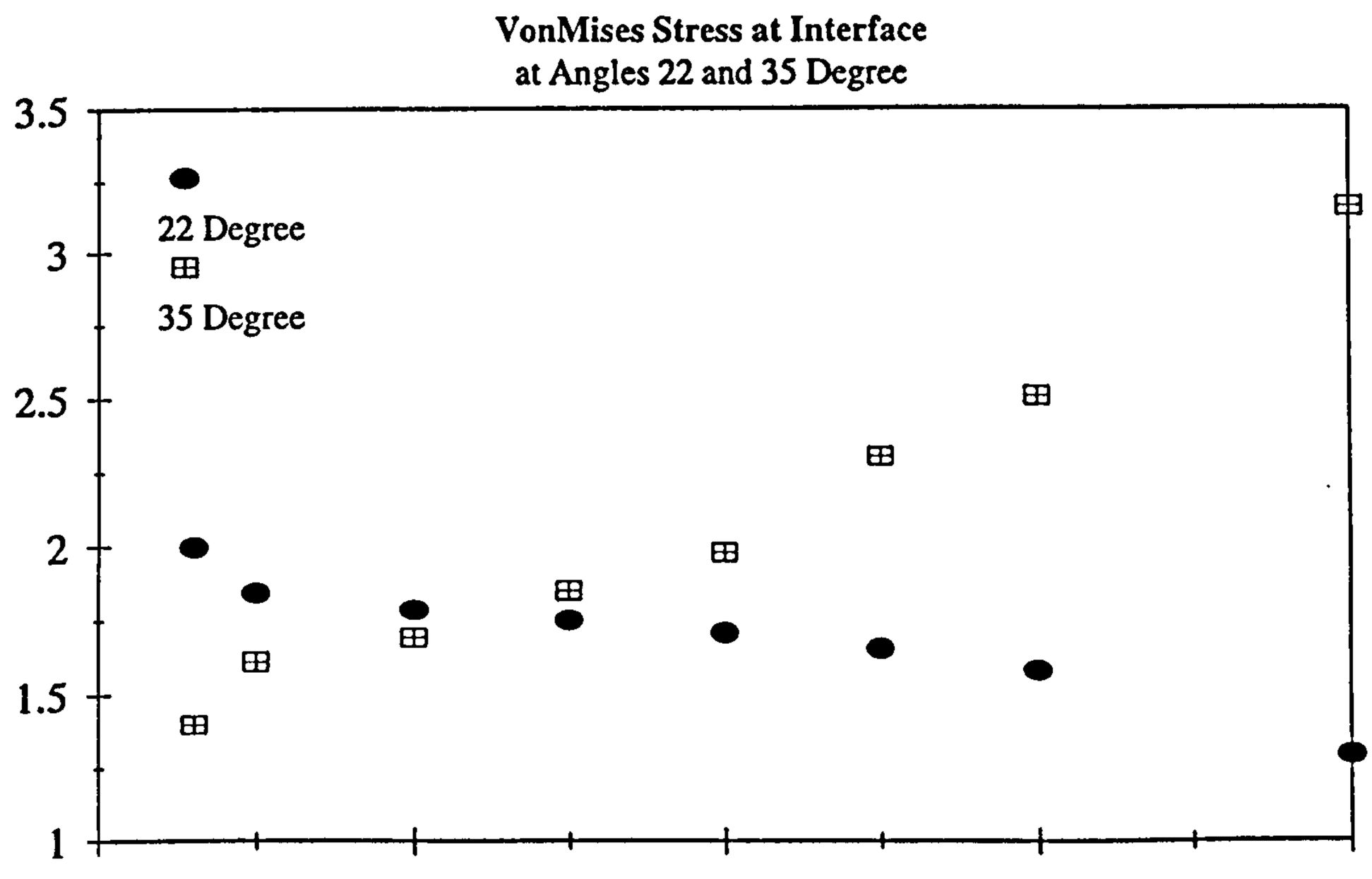

Fig.4.13: VonMises stress concentration at angle 22 and 35 of the interface of the filler particle and matrix.

the Von Mises stress vary with volume fraction in the same way as the associated stress concentrations, although the range of the variation of Von Mises stress is very small. The stress peak located above the pole is greater at higher volume fractions of the filler, but at volume fractions below about 15% the maximum located at the interface is greater. Dekkers and Heikens (Dekkers and Heikens, 1983) studied the shear band formation for very low volume fractions of glass beads in various polymer matrices. They found shear band formation at the interface, at $\theta = 45^{\circ}$. The results of our finite element analysis for similar composites are given in *figure 4.14* which show that at low volume fractions the maximum concentration of Von Mises stress is at the interface, at $\theta = 40^{\circ}$.

The Von Mises stress at which yield occurs is dependent on the hydrostatic stress as explained earlier in this chapter. The hydrostatic stress values corresponding to the points of maximum Von Mises stress were calculated. Under the application of tensile stress the hydrostatic stress is tensile. The hydrostatic stress concentration remains almost constant up to around 20% volume fraction of filler, but it increases rapidly for higher volume fractions. The maximum hydrostatic stress concentration occurs at the pole of the particle.

4.2.5 Fracture behaviour

Crack growth is generally considered to move in the direction of the position of maximum direct stress. Our model predicts that the position of maximum direct stress is above the pole. These predictions correspond with the experimental observations (Spanoudakis and Young, 1984).

For a well bonded sphere, at low volume fractions, crack growth is developed towards the resin above the pole of the sphere. Smearing of resin around the pole of the sphere is observed. This type of fracture appearance contrasts with the observed crack growth in epoxy resin containing poorly bonded glass particles which is found to be attracted to the equator of the sphere. The stress distribution in composite with poorly bonded filler particle is similar to that of a composite containing holes. The site of the maximum stress concentration is found to be at the equator of the sphere.

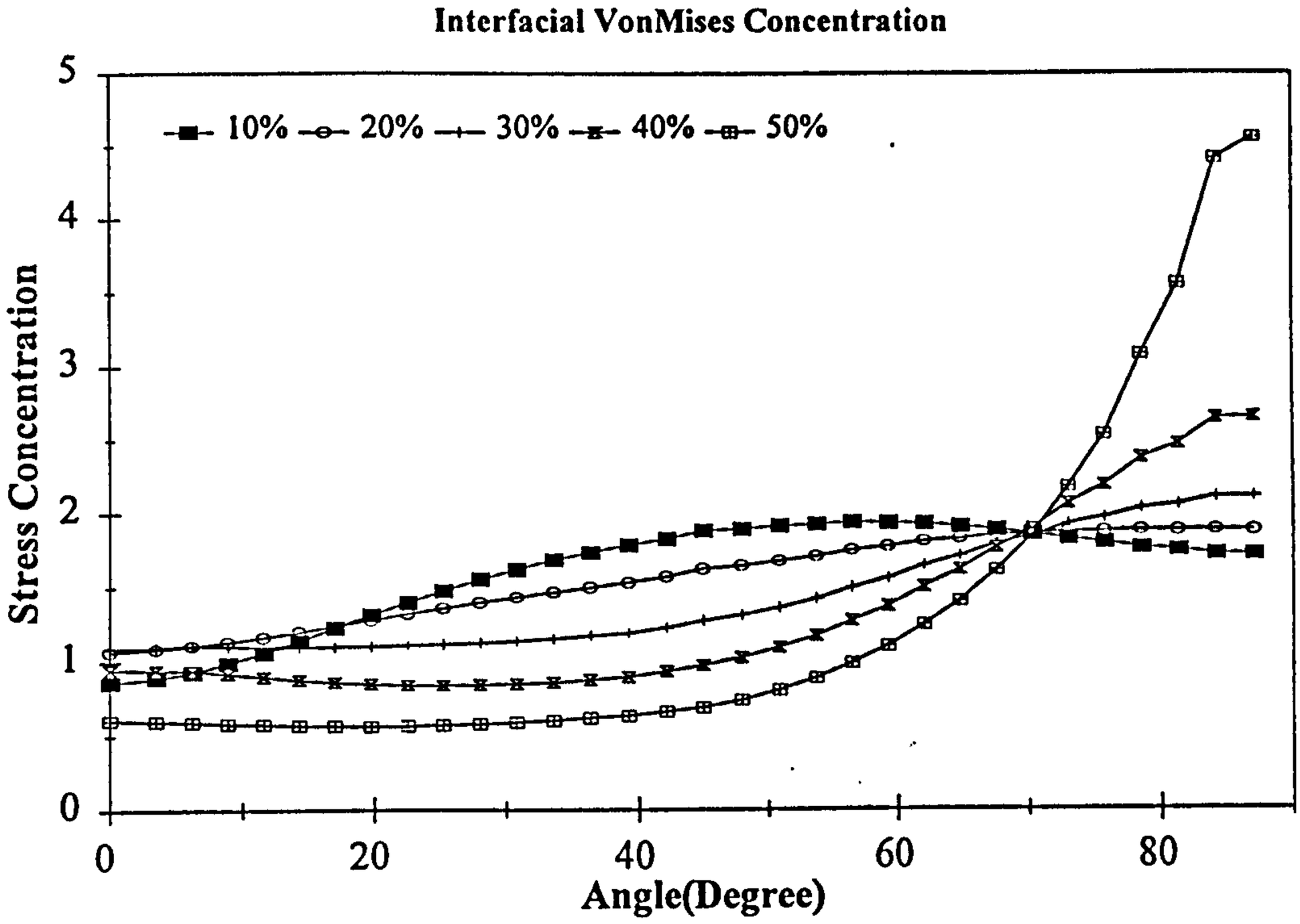

Fig.4.14: VonMises Stress concentration at the interface of the filler and matrix.

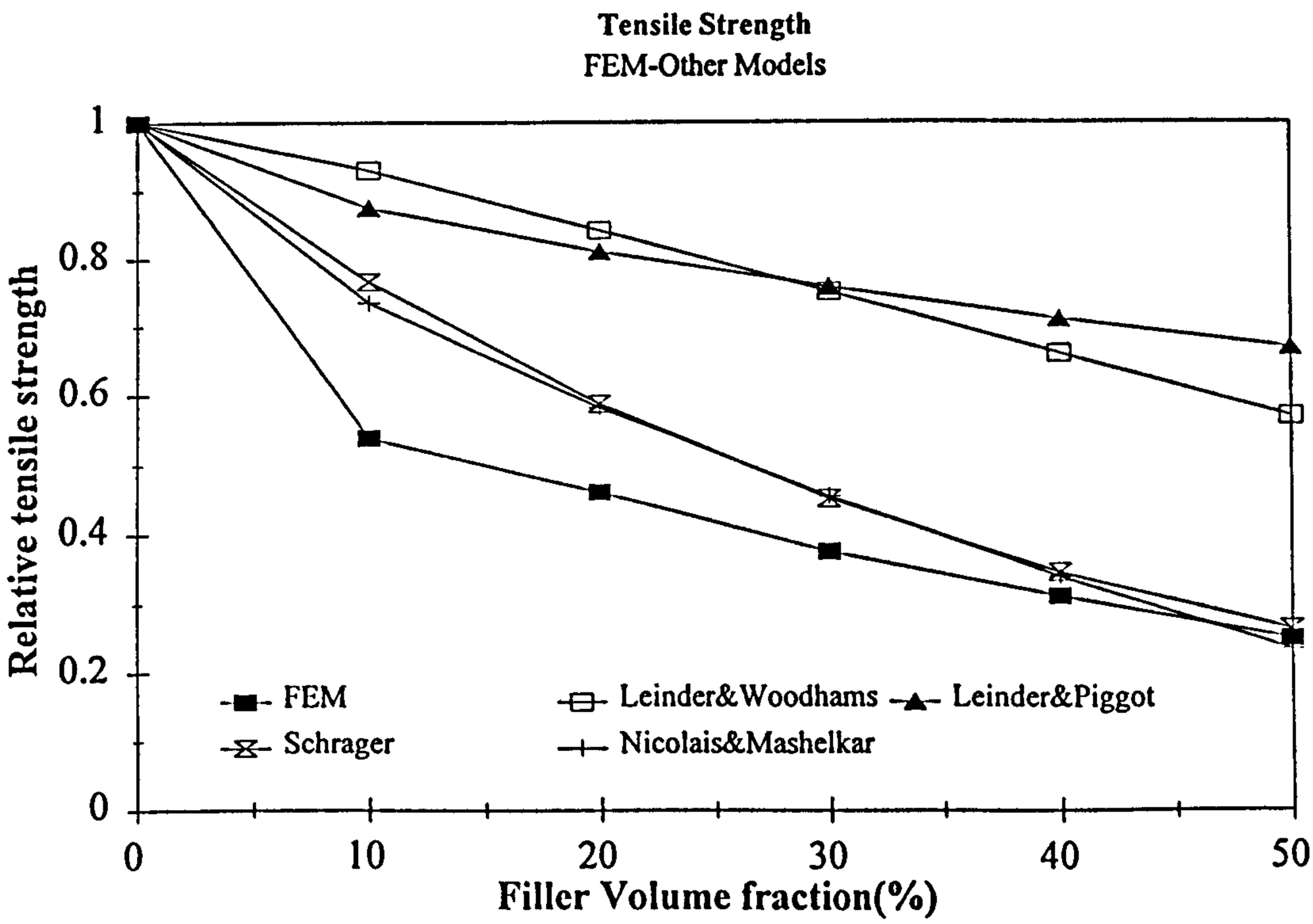

Fig.4.15: Prediction of the ratio of the tensile strength of composite to the tensile strength of matrix t the range of filler volume fraction by FEM and other models.

The amount of resin smearing around the pole of a well bonded sphere would be dependent on the position of the crack with respect to the sphere. Our results show that at low volume fractions the maximum distance is much further away from the sphere than for high volume fractions. Thus the model predicts that more smearing would occur if there are no spheres visible in the fracture surface. Greater smearing at low volume fractions has been observed. (Spanoudakis and Young, 1984)

It is found that besides matrix properties, strain rate and temperature, the degree of interfacial adhesion has a profound effect on the competition between craze and shear band formation. In cases where the beads adhesion are perfect craze formation is favoured, whereas for poorly adhering beads shear band formation is dominant. This effect is caused by the difference in local stress situation, craze formation becomes the controlling factor under a triaxial stress state and shear band formation becomes the dominant factor under a biaxial stress state. In the case of an excellently adhering glass bead, the crazes form near the pole. Stress analysis shows that these are regions of maximum dilatation and maximum principle stress. At a perfectly bonded glass bead experimental observations show that the shear bands form near the surface of the bead at 45° from the poles which are defined by the axis of symmetry maximum principal shear stress and the density of maximum distortion energy. Our results confirm these observations.

In the case of poor interfacial adhesion between glass beads and matrix, both craze and shear band are preceded by dewetting along the interface between bead and matrix. At dewetting a curvilinear interfacial crack is formed, starting at the pole and propagating in the direction of the equator until, at an angle of about 60° from the pole, a craze or shear band originates at the tip of the interfacial crack.

Neilsen suggested a very simple model based on the assumption of Hookean behaviour up to breaking strains. In this case the following relation can be written:

$$\sigma_c = E_c \varepsilon_c \qquad (4.3)$$

where E is the tensile modulus and ε_c is the elongation at breaking point, and ε_c may be expressed as:

$$\varepsilon_c = \varepsilon_m (1 - V_f^{1/3}) \tag{4.4}$$

where ε_m is the elongation at the breaking point of the matrix. Using the above relations the relative strength of the composite is found as:

$$\sigma_{rel} = \frac{E_c}{E_m}(1 - V_f^{1/3}) \tag{4.5}$$

The ratio E_c/E_m can be calculated by the finite element model.

There are other theoretical models which predict the strength of the filled composites and a few of them are brought to attention for comparison with the results of our finite element model. The constants in the following models are given for the glass filled epoxy composite.

1. Leidner and Woodham (Leidner and Woodham, 1978):

$$\sigma_c = 0.83 pa V_f + K\sigma_m(1 - V_f) \tag{4.6}$$

where pa=1540 psi, K=0.8 or 0.9.

2. Piggot and Leidner (Piggot and Leidner, 1974):

$$\sigma_c = \sigma_m(1 - 0.5 V_f^{0.6}) \tag{4.7}$$

3. Nicolais and Mashelkar (Nicolais and Mashelkar, 1976):

$$\sigma_c = \sigma_m - b V_b^n \tag{4.8}$$

with b=1.21 and n=0.66

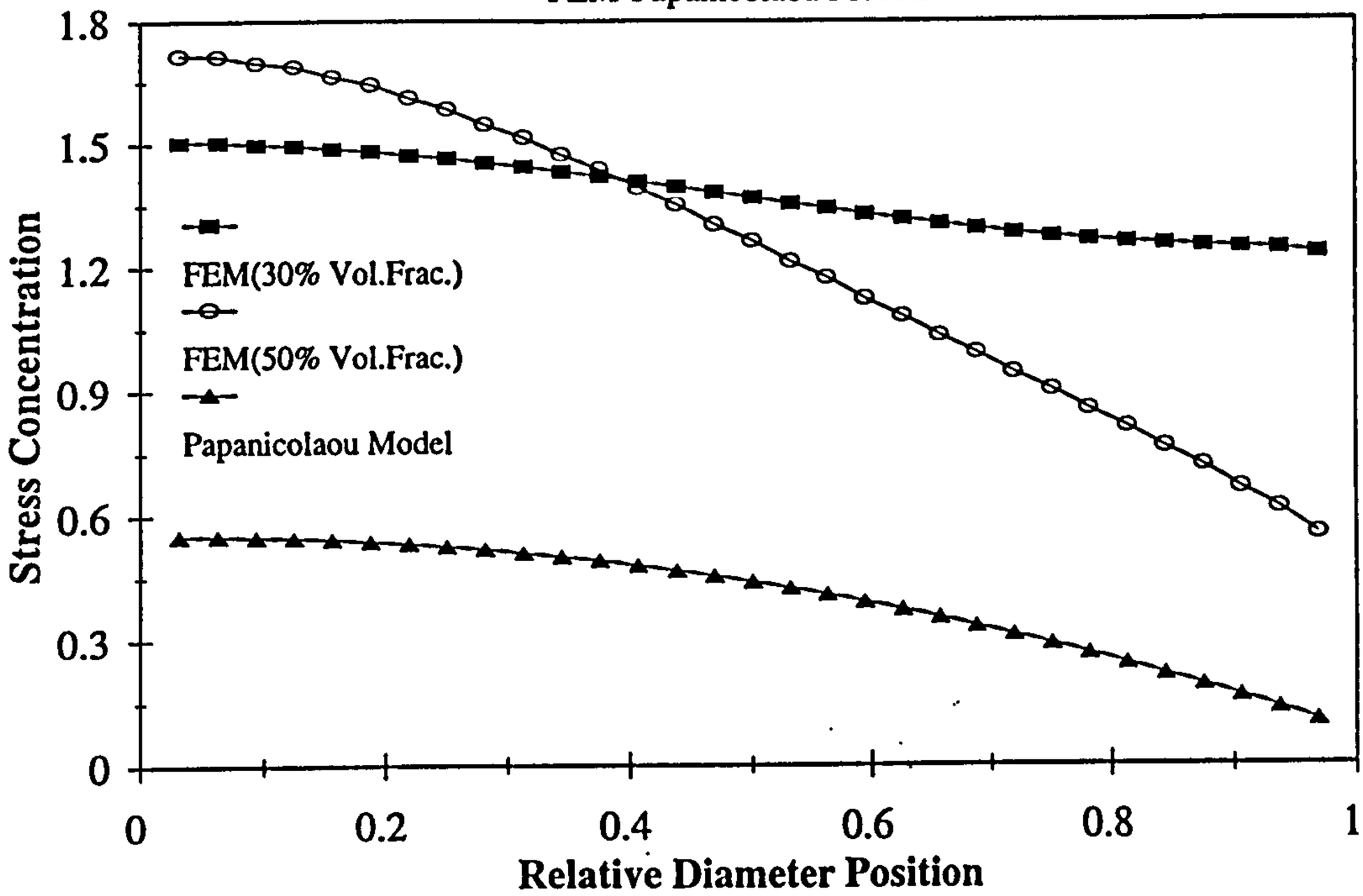

Fig.4.16: Tensile stress along particle diameter predicted by FEM and Papanicolaou models.

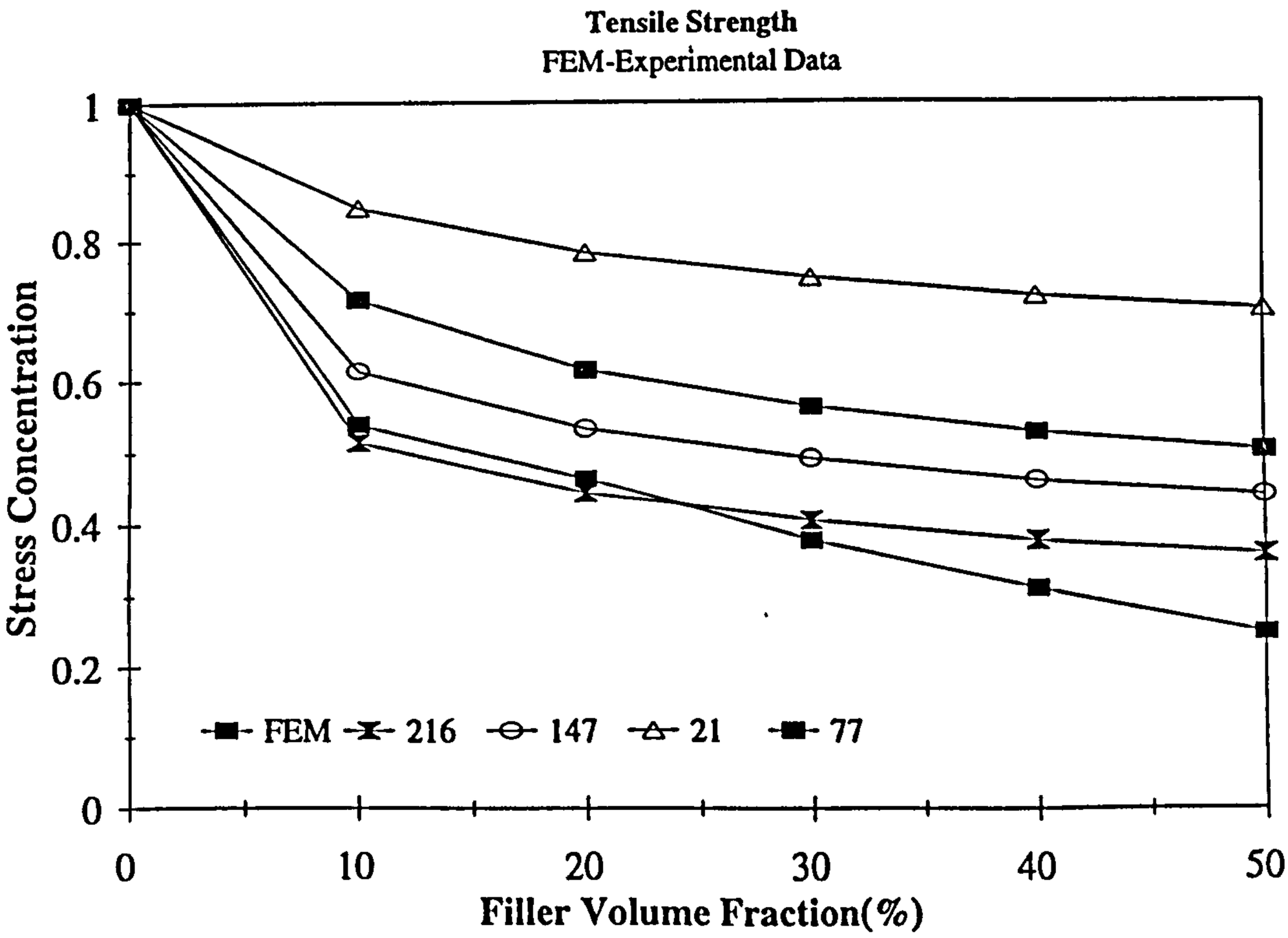

Fig.4.17: Relative tensile strength by FEM and experimental results for different particle diameters.

4. Schrager (Schrager, 1978):

$$\sigma_c = \sigma_m \exp(-2.66 V_b) \qquad (4.9)$$

The results obtained using the above equations are given in *figure 4.15* and are compared with the results of our model. All of these models except the Neilsen's model show a decrease in the strength of the composite with increasing volume fraction of the filler. The Neilsen's predictions depend strongly on the model which is used to obtain the modulus of the composite at different filler volume fractions.

The finite element model gives rather low tensile strengths for cases corresponding to the described models. In the finite element analysis, it is assumed that composite failure occurs when the first element fails. A more realistic assumption would be that composite failure does not occur until several of the highly stressed elements fail. This allows for 'crack arrest' by neighbouring inclusions and also takes into account the statistical increase in the strength for the small volume of material which is subjected to the stress concentration. The use of this averaging technique will results in an increase in the theoretical strength of the composite.

Papanicolaou et al (Papanicolaou and Bakos, 1992) have proposed a model for the prediction of the tensile strength of the particulate filled polymers. They have used a modified Cox model to find the stress distribution along a particle diameter. The load which is carried by the inclusions is calculated and used to estimate the tensile strength of the composite. The variations of the tensile stress concentration along the particle diameter of the inclusion are presented in *figure 4.16*. The trend of model predicted variations is similar to that obtained by Papaicolaou. Although the curve predicted by the finite element model shows a shift to higher values compared to the curve found using modified Cox model (Cox, 1952).

The experimental results show that the strength of the composite depends on the size of the filler particles (London et al, 1977). In *figure 4.17* the experimental results for four different particle diameters, 216 μm, 147 μm, 77 μm and 21 μm are compared

with our model. It can be seen that for the range of particle diameters studied the composite strength diminishes at higher volume fractions. The results also indicate that smaller particles show higher strength. The reason for this phenomenon is not entirely clear, but the increase in interfacial area per unit volume of filler for smaller particles must be an important factor. A second factor which may also be important, is that the stress fields near a particle are independent of the size of the particle, nevertheless the volume of polymer that experiences a given stress concentration increases with particle size. Therefore the probability of finding a large flaw within this volume increases. If a large flaw exists within an area of stress concentration, the tensile strength will be reduced according to Griffith's theory. In most of the aforementioned theoretical models, the effect of particle size cannot be investigated. In our finite element model we also assume that the composite is flawless and hence it predicts the strength of the composite through the stress fields which are independent of the particle size. *Figure 4.17* confirms once again that our finite element model provides a somewhat conservative prediction of the strength for the composite.

4.3 COMPOSITES FILLED WITH DEBONDED RIGID PARTICLES

Rigid spherical inclusions in glassy polymers induce inhomogeneous stress fields and thus act as stress concentrators. Consequently, plastic deformation processes such as craze and shear band are formed at these inclusions. The mechanisms of craze formation and shear band formation are investigated for small glass spheres embedded in matrices subjected to uniaxial tension. These microscopic studies have revealed the profound effect of the degree of interfacial adhesion on the mechanism of craze (Wellinghoff and Baer, 1978; Donald and Kramer, 1982) and shear band formation (Kinloch and Young, 1983). In the cases where the adhesion of glass sphere and polystyrene matrix is perfect, the crazes are found near the poles of the sphere. From stress analysis around a completely bonded sphere it appears that these are regions of maximum dilatation and of maximum principal stress. For perfectly adhering glass spheres in a polycarbonate matrix the shear bands are found to form around the surface of the sphere at an angle of 45° from the poles defined by the axis of symmetry of the stressed sphere. These are regions of maximum distortional strain energy density and maximum principal shear stress. In the case of poor interfacial adhesion between the glass sphere and the polymer matrix, both craze and shear band formation are found to be preceded by dewetting along the interface between sphere and matrix. During dewetting a curvilinear interfacial crack is formed, starting at the pole and propagating along the interface in the direction of the equator until, at an angle of about 60° from the pole, a craze or shear band originates at the tip of this crack. The results of these studies prompted us to analyse the stress conditions near the tip of a curvilinear interfacial crack between a glass sphere and a polymer matrix.

4.3.1 Boundary conditions at the interface

Figure 4.8a indicates that for all volume fractions of the filler the normal stress has negative value and is compressive in the part of the interface which starts from the equator and ends at about $\theta = 22°$. At this point the normal stress is about zero and from this point towards the pole of the particle it continues to rise to its maximum

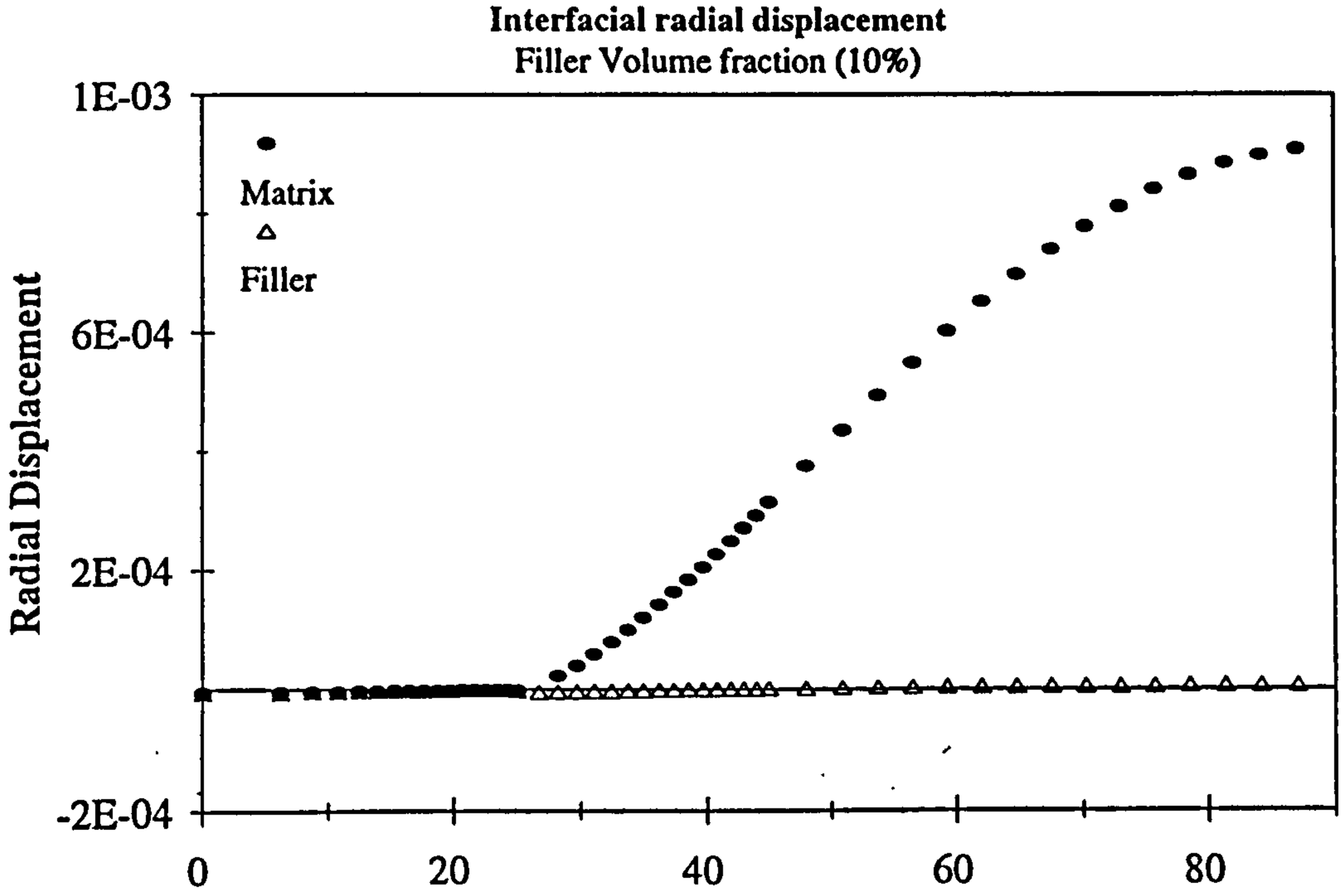

Fig.4.18: Radial displacement of the matrix and filler at the interface of the partly debonded particle

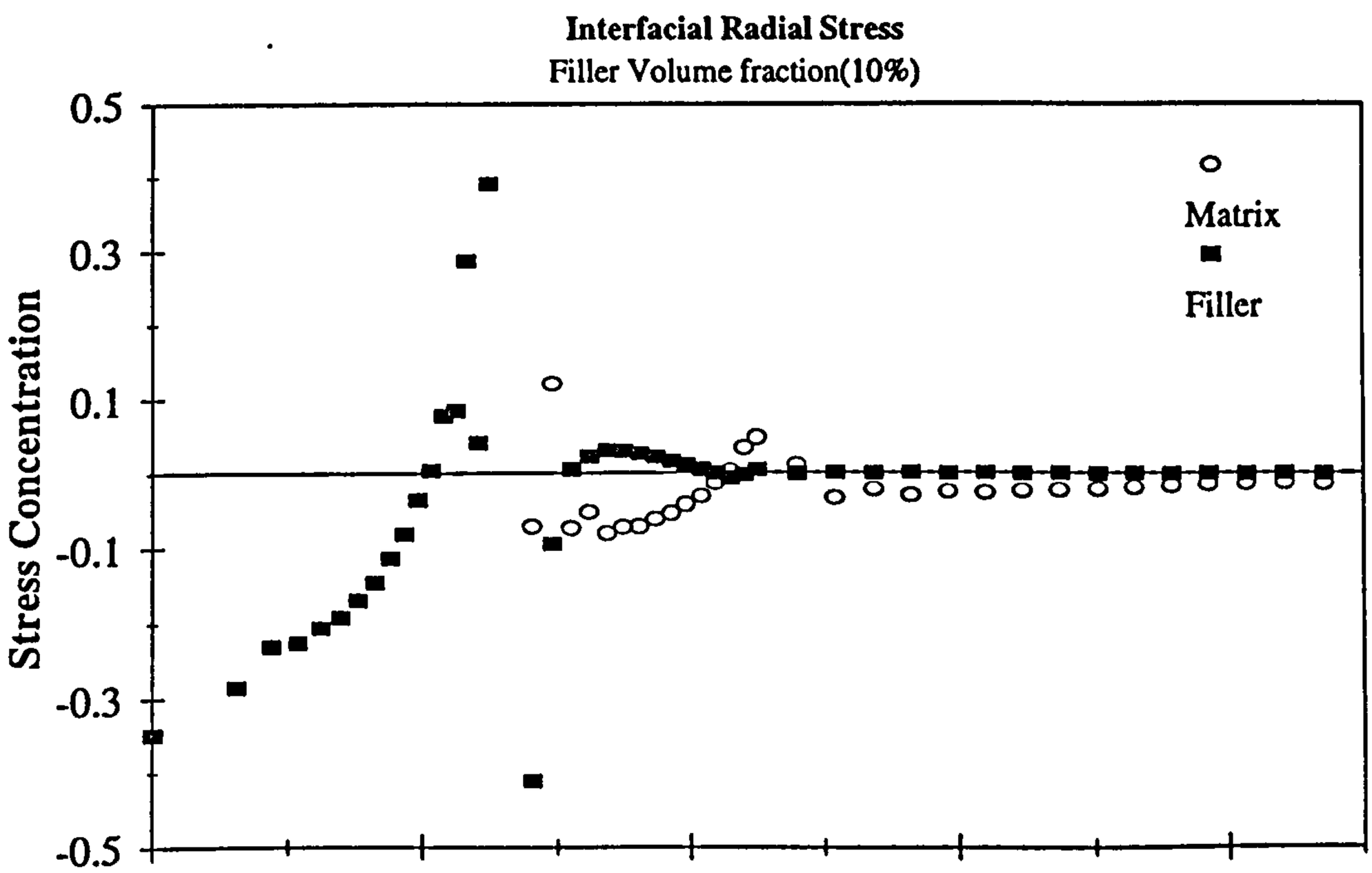

Fig.4.19: Radial stress concentration of matrix and filler at the interface of a partly debonded particle

value at the pole. From this analysis it can be concluded that in the case of debonded filler or when dewetting occurs in a bonded filler, from the pole up to a length of the unbonded region represented by $\theta = 22^{\circ}$, the entire unbonded region may be regarded as an interfacial crack.

Here we consider two cases. In the first case the remainder of the interface is bonded and there is no relative displacement of the matrix. In the second case we investigate the situation in which all the interface is debonded and from $\theta = 22^{\circ}$ to the equator of the particle there can be a relative tangential displacement of the matrix depending on the frictional force at the interface. If the frictional force acting on the interface is high enough it can prevent the particle and matrix to have relative tangential movement. Therefore under this condition the model will be similar to the first case. If the frictional force is weak the tangential displacement occurs and hence slip boundary condition is imposed for this case. The slip coefficient controls the extent of relative movement of the matrix and the filler particle.

4.3.2 Displacement

Figure 4.18 shows the normal displacement of the filler and the matrix at the interface. The radial displacement of the matrix and the filler from the equator to $\theta = 22^{\circ}$ is negative and much smaller than the displacement of the other segment of the interface(nearly zero). This negative value confirms that even in the case of debonding of the filler at this part, the two phases remain in contact and the stress can be transferred from the matrix to the filler. From the point of $\theta = 22^{\circ}$ to the pole the radial displacement of the matrix is positive and increases to its maximum at the pole. The filler displacement in this part is nearly zero.

4.3.3 Interfacial stresses

The interfacial radial stress concentration in matrix and filler is shown in *figure 4.19* for volume fraction of 10%. The results indicate that the normal stress is negative and compressive at the interface from the equator (i.e. $\theta = 0$) to $\theta = 22^{\circ}$. In higher volume fractions this stress become closer to zero. The normal stress concentration has its

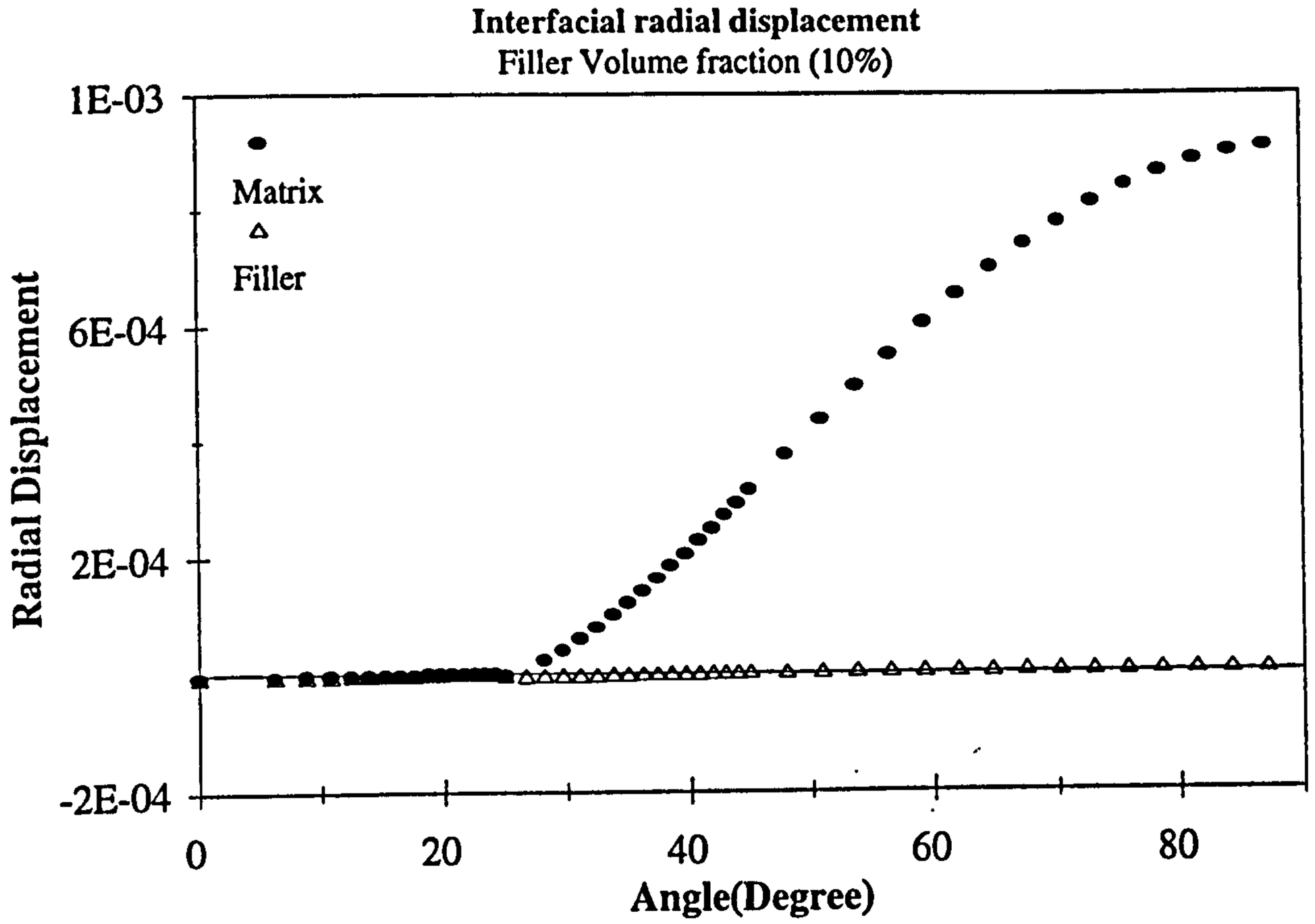

Fig.4.18: Radial displacement of the matrix and filler at the interface of the partly debonded particle

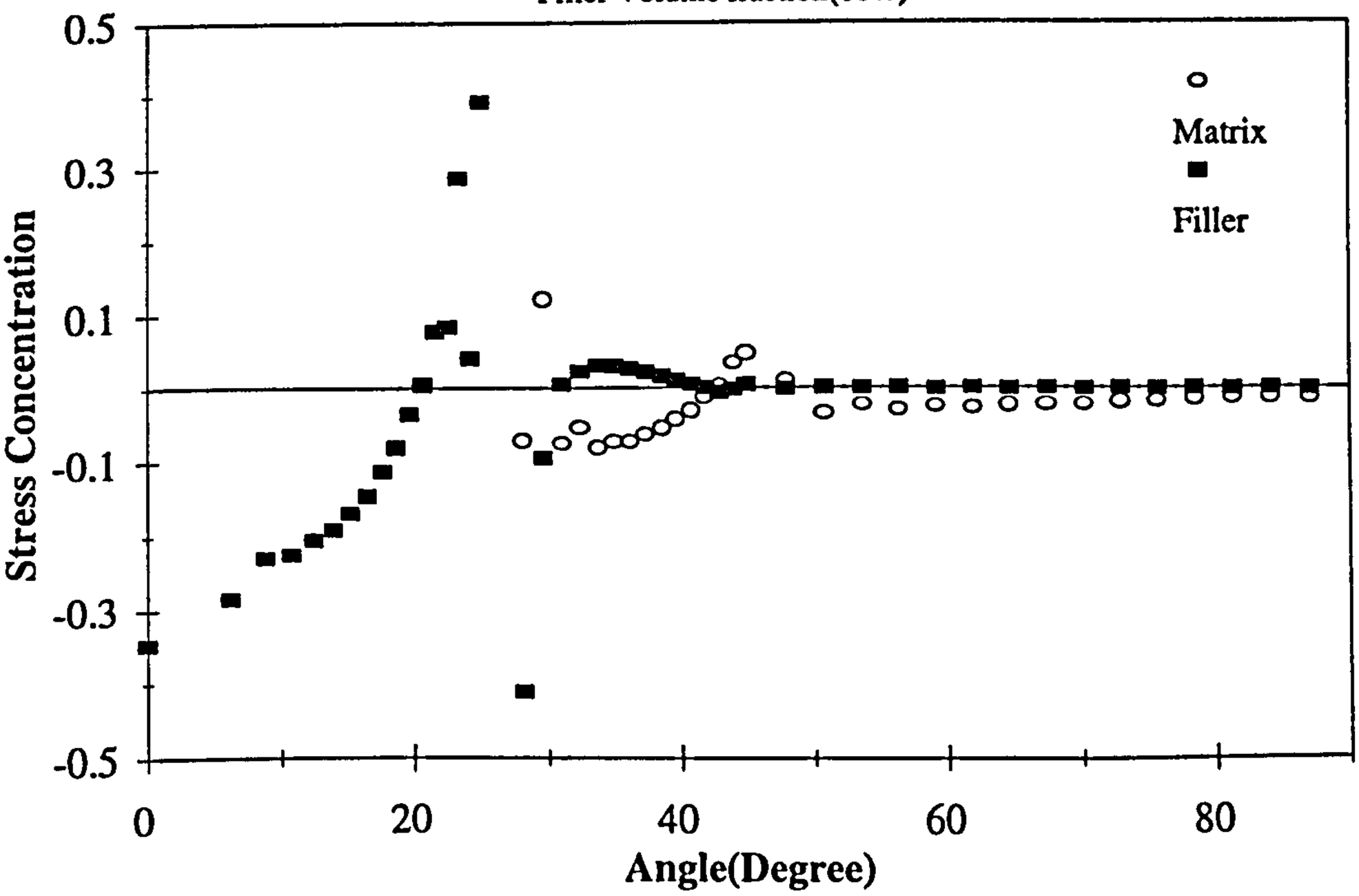

Fig.4.19: Radial stress concentration of matrix and filler at the interface of a partly debonded particle

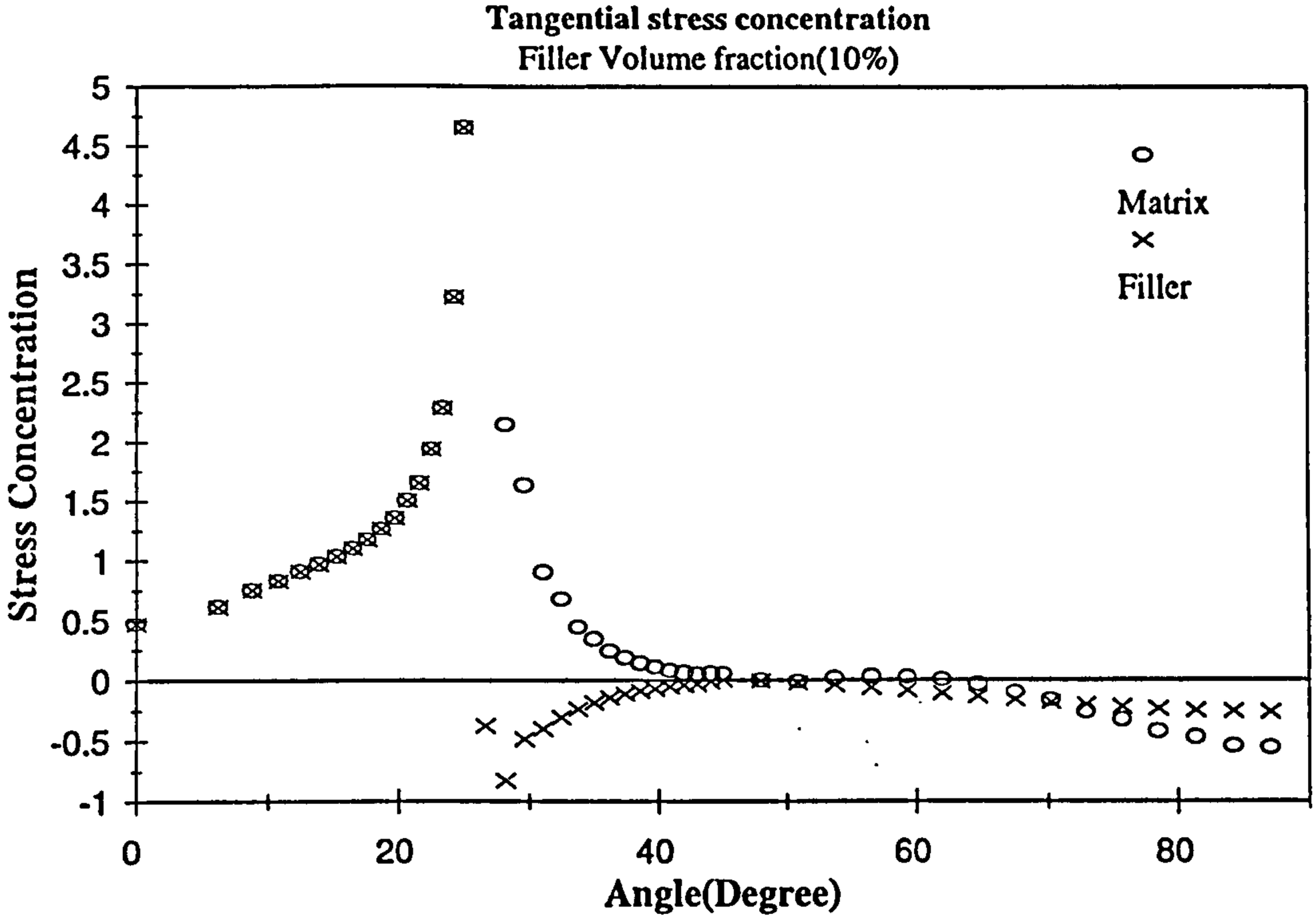

Fig.4.20: Tangential stress concentration of matrix and filler at the interface of the partly denonded Particle

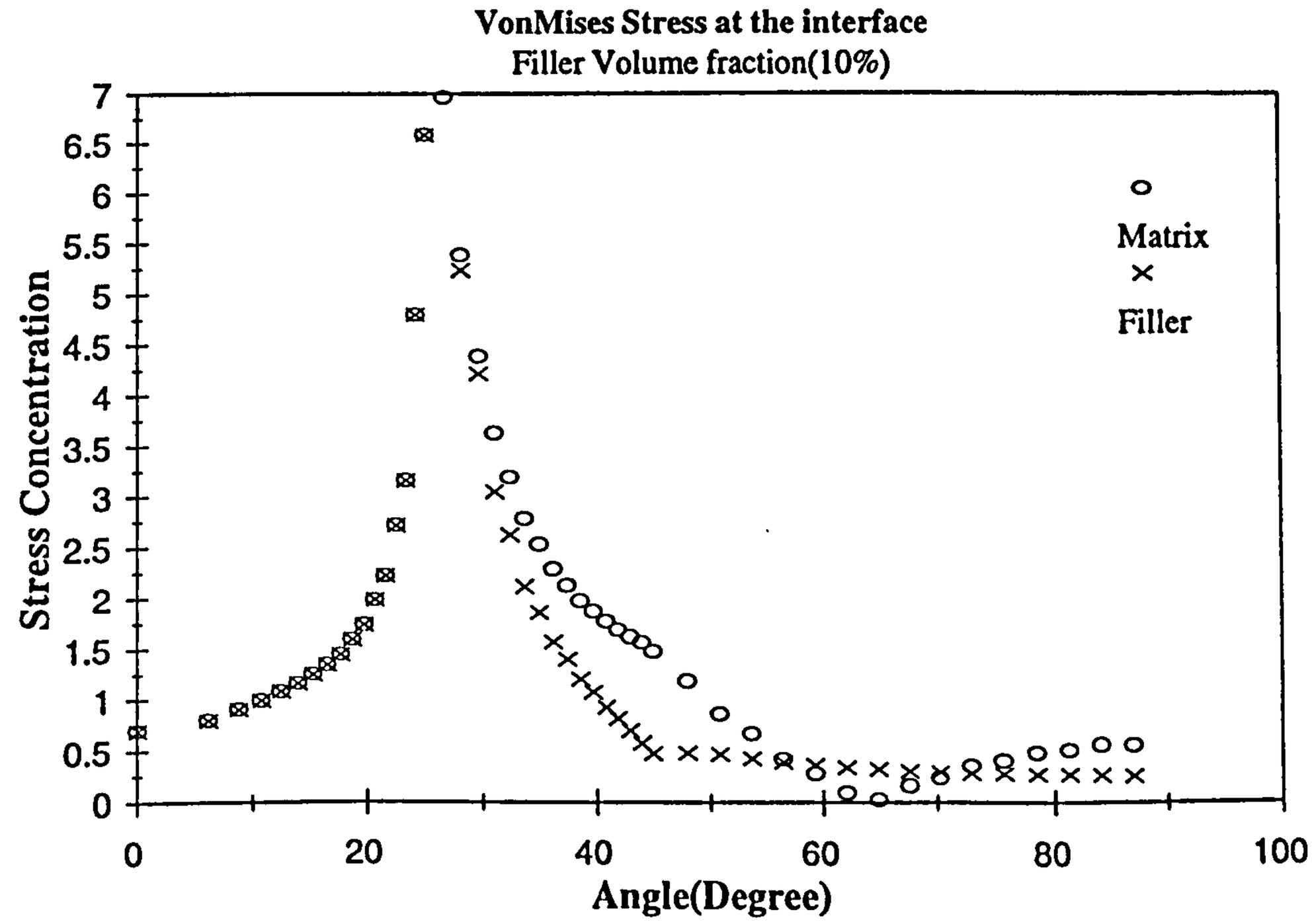

Fig.4.21: Von Mises stress concentration of matrix and filler at the interface of the partly debonded particle

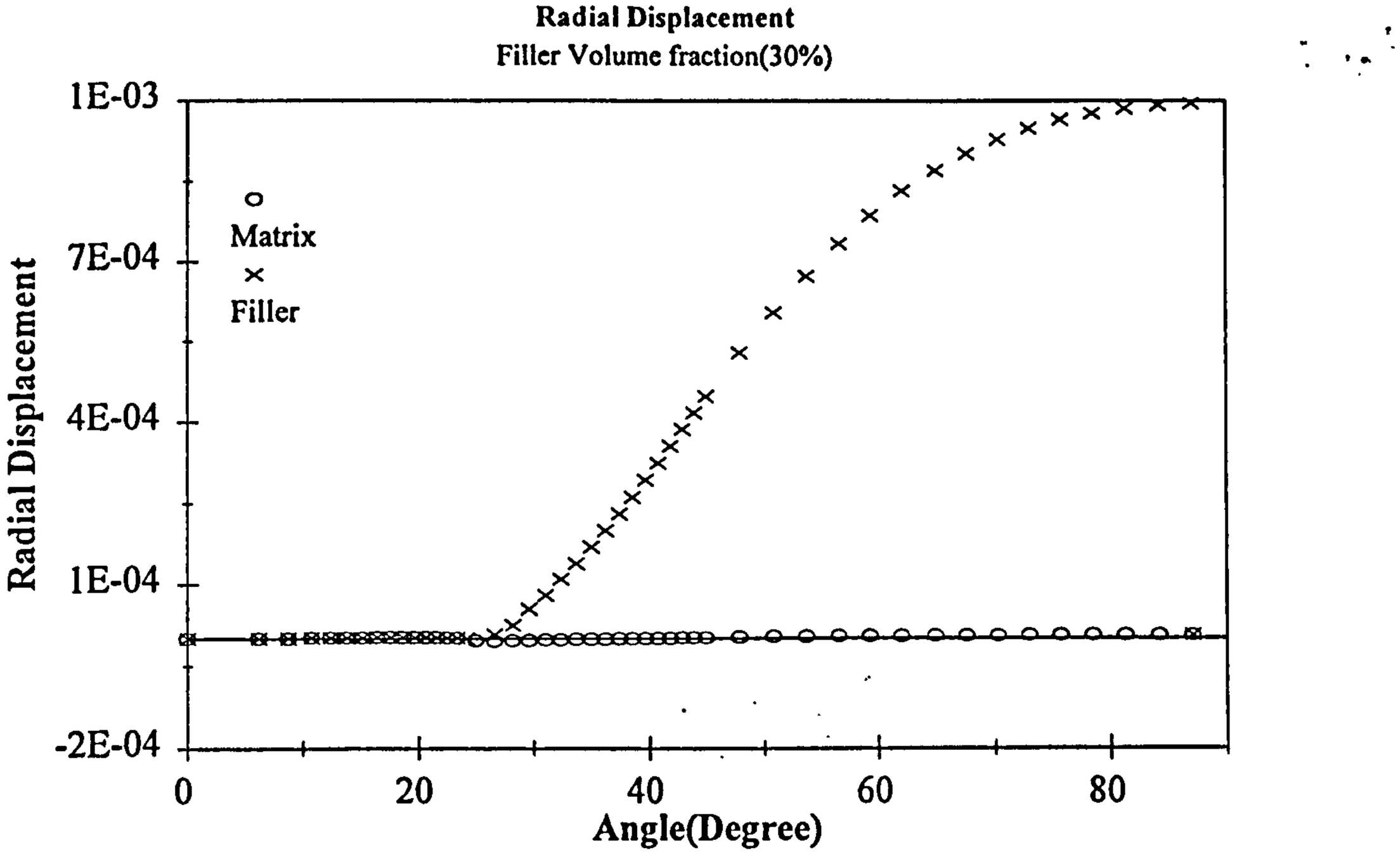

Fig.4.22: Radial displacement of the matrix and filler at the interface of the partly debonded particle

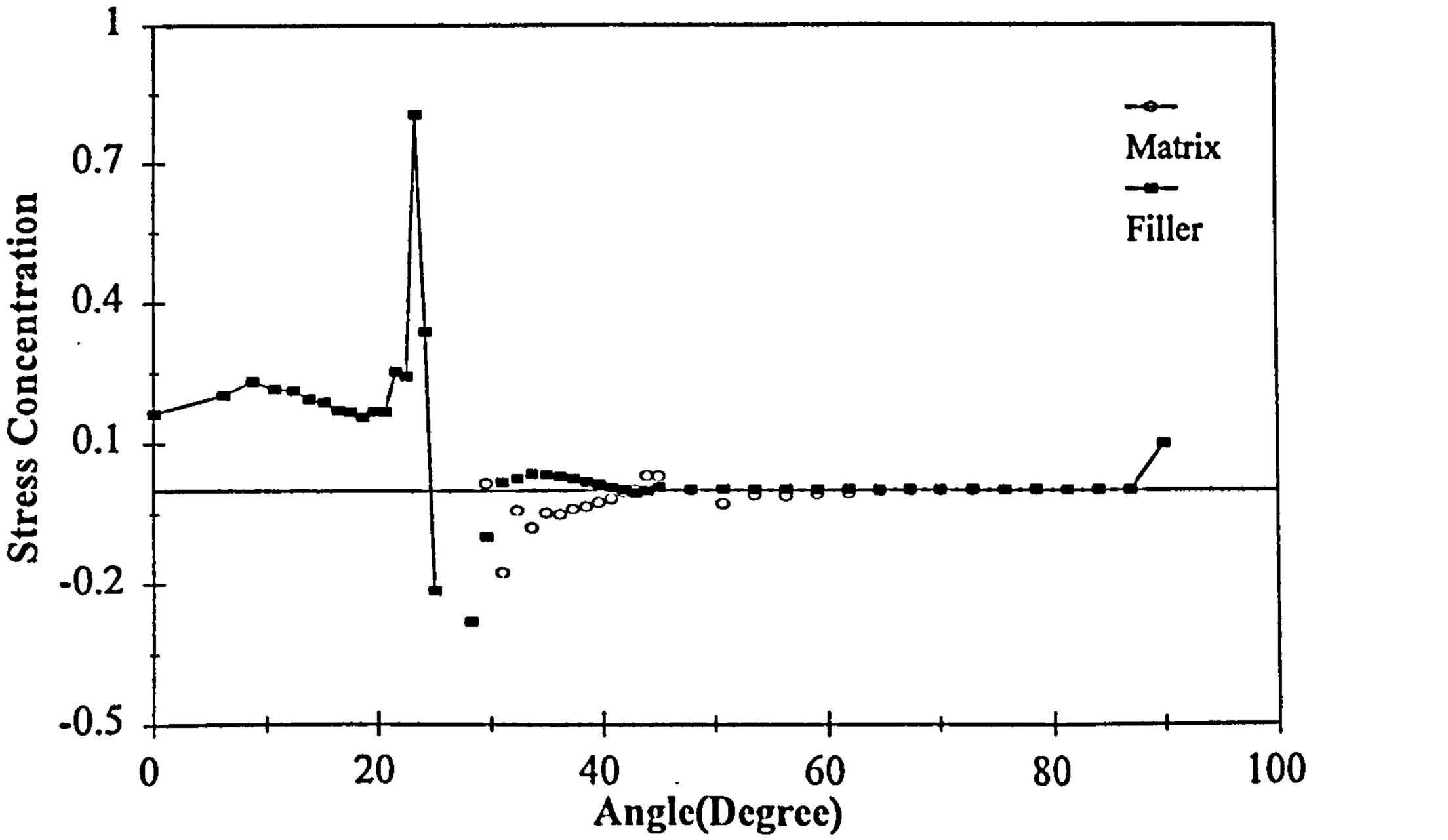

Fig.4.23: Radial stress concentration of the matrix and filler at the interface of the partly debonded particle

maximum value at the tip of the crack or unbonded region. This stress is nearly zero in both matrix and filler at the other part of the interface from the crack tip to the pole. The frictional force is proportional to the normal stress acting on the interface. Therefore in the segment closer to the pole, it is equal to zero which shows that no stress transfer occurs. In the other segment which experiences a compressive stress, the frictional force rises. This frictional force acts in the opposite direction to the tangential stress and is proportional to the normal stress so that:

$$F_t = \mu F_n \qquad (4.10)$$

The value of frictional force determines whether there is any relative tangential displacement between filler and matrix or not.

The tangential stress concentration distribution is shown in *figure 4.20*. The maximum stress is at the crack tip and the value is much higher than the normal stress. The tangential stress of cracked segment is zero close to the crack tip and shows a small negative value close to the pole.

In *figure 4.21* the variation of Von Mises stress concentration is presented. The maximum of this stress is found at the crack tip. The stress concentration distribution at the interface shows the maximum values for direct and Von Mises stress at the crack tip. This confirms that any further plastic deformation through crazing or shear band formation starts from the crack tip.

Figures 4.22 and 4.23 show the radial displacement and radial stress concentration for an epoxy composite 30% filled with glass beads. The radial displacements have positive values very near to zero in the bonded region. These values are negative for filler volume fractions up to 12% (*figure 4.19*). As it can be seen in *figure 4.23* the radial stresses at this part are also positive. Therefore there can be a possibility for the growing of a crack towards the equator for higher volume fraction of glass beads. The negative values of displacement and compressive stresses at lower volume fractions

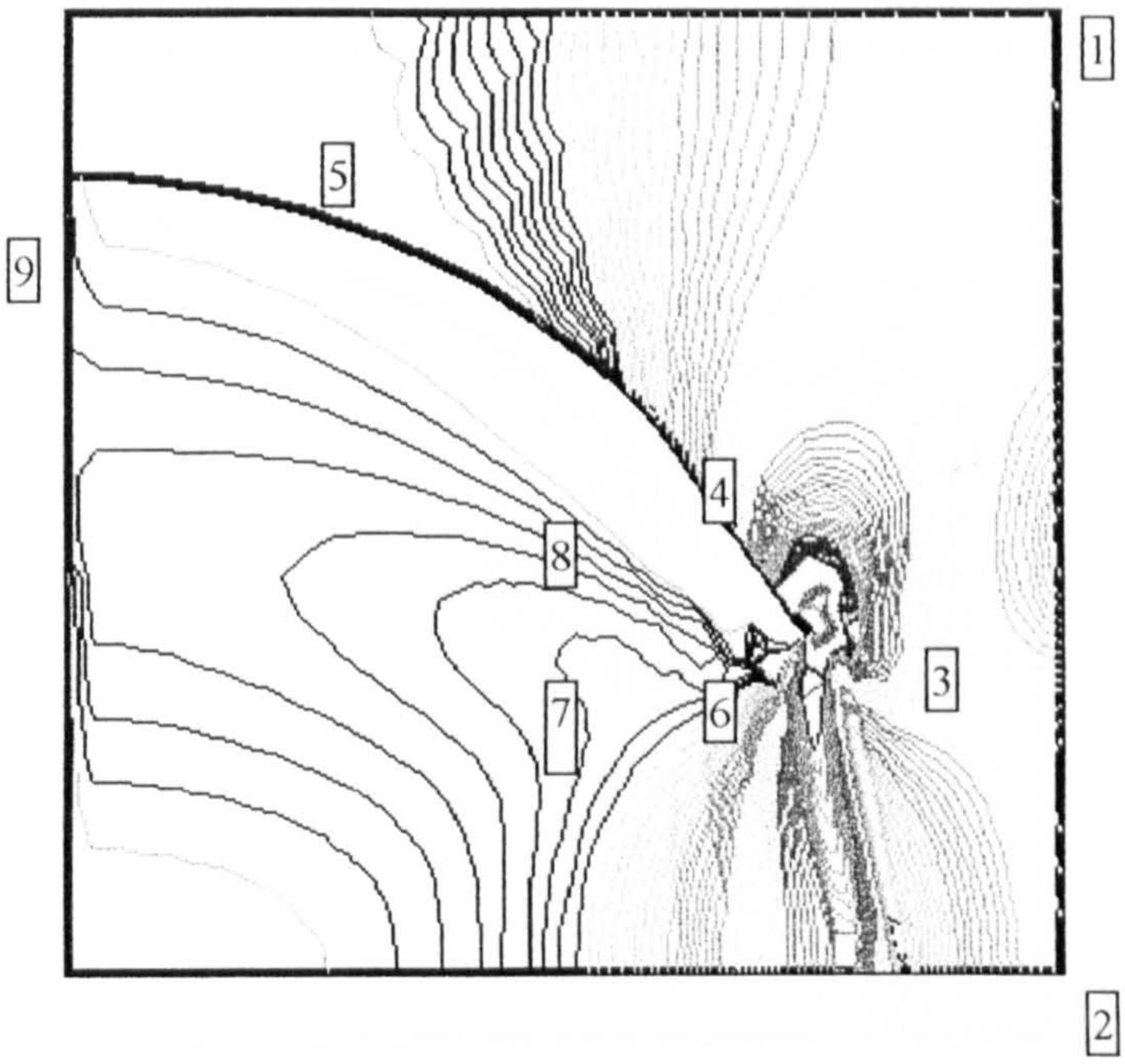

1	0.312E7
2	0.285E7
3	0.281E7
4	0.276E7
5	0.105E5
6	0.525E4
7	0.182E7
8	-0.121E6
9	-0.134E7

Fig.4.24a: Contour diagram of the direct stress field of the partly debonded composite with 30% of hard filler particles

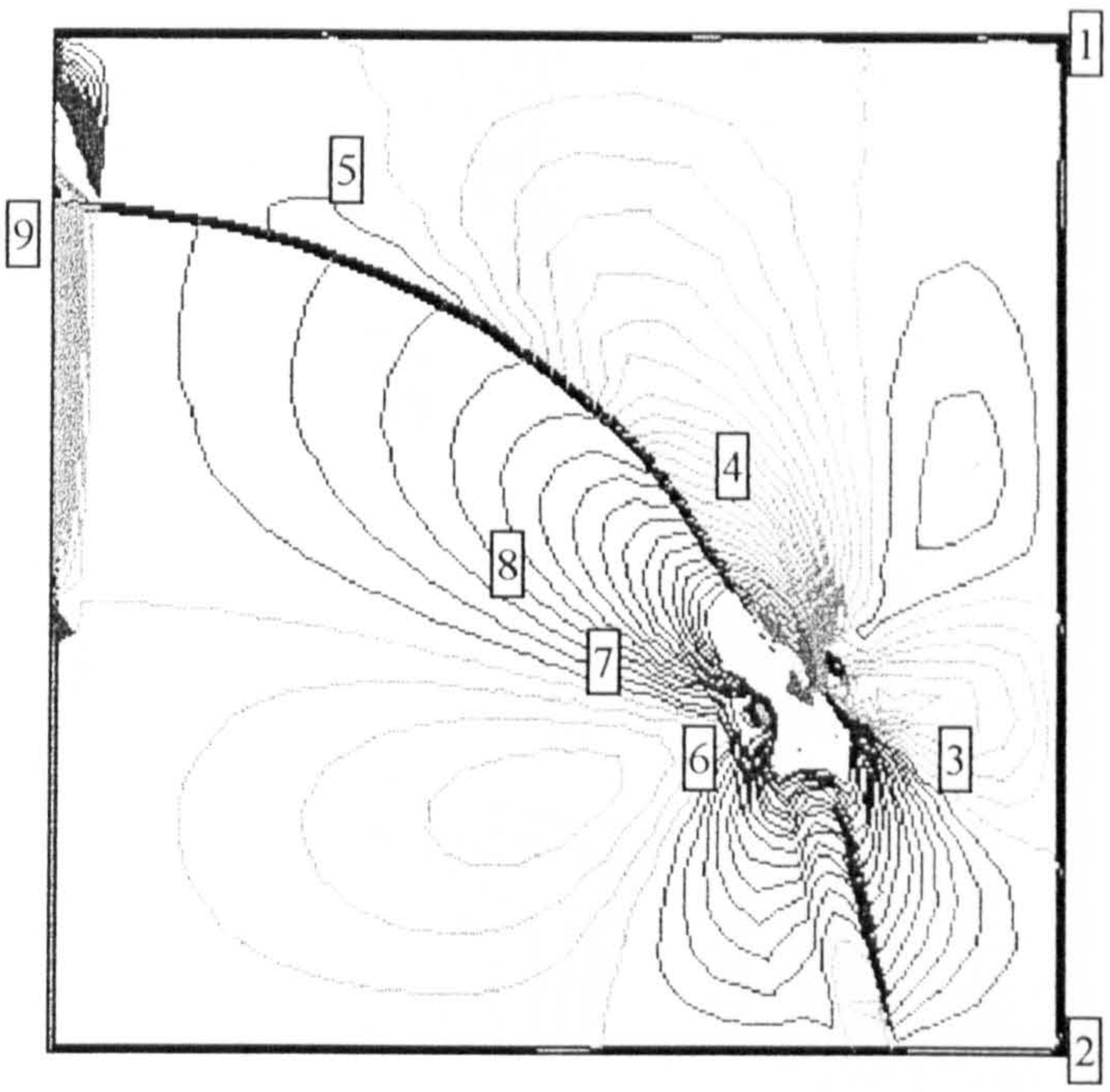

1	-0.167E4
2	-0.644E3
3	-0.219E6
4	0.447E5
5	0.162E5
6	0.220E7
7	-0.889E6
8	0.188E6
9	-0.164E8

Fig.4.24b: Contour diagram of the shear stress field of the partly debonded composite with 30% of hard filler particles

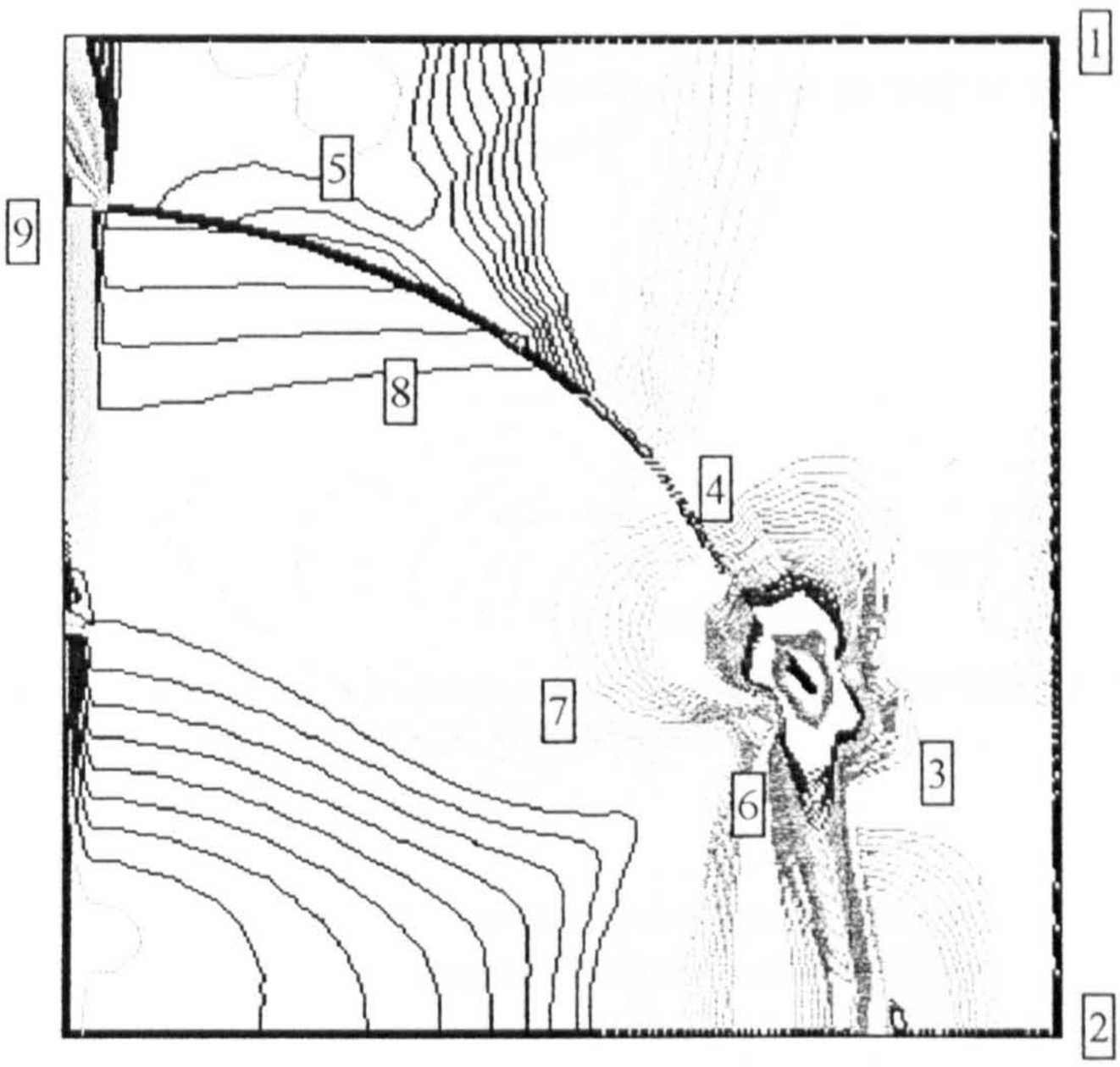

1	3.12E06
2	2.85E+06
3	2.85E+05
4	2.85E+06
5	5.25E+05
6	6.77E+06
7	2.24E+06
8	4.81E+05
9	3.26E+07

Fig.4.24c: Contour diagram of the Von Mises stress field of the partly debonded composite with 30% of hard filler particles

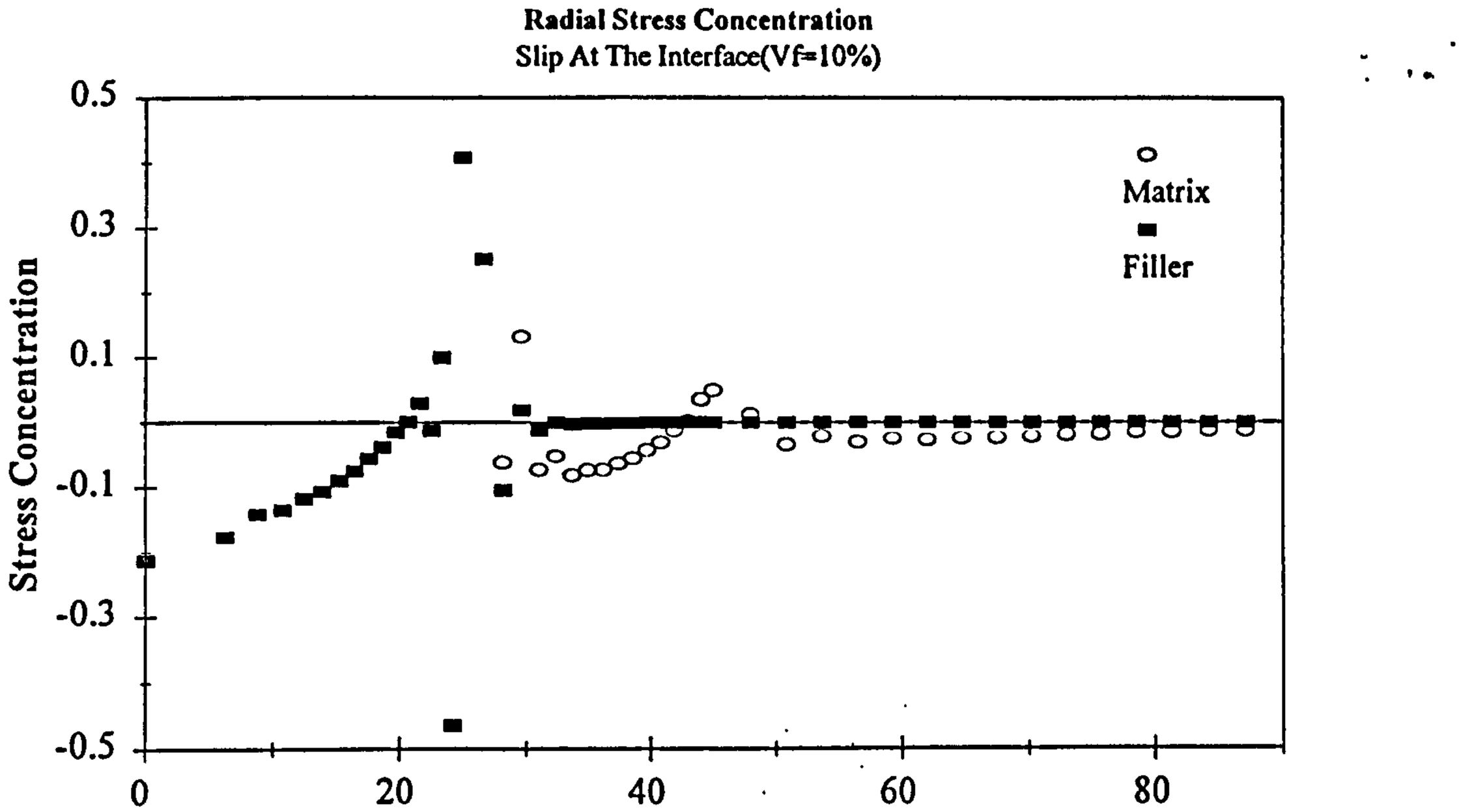

Fig.4.25: Radial displacement of the matrix and filler at the interface of the partly debonded particle with slip condition at the closed segment of the interface

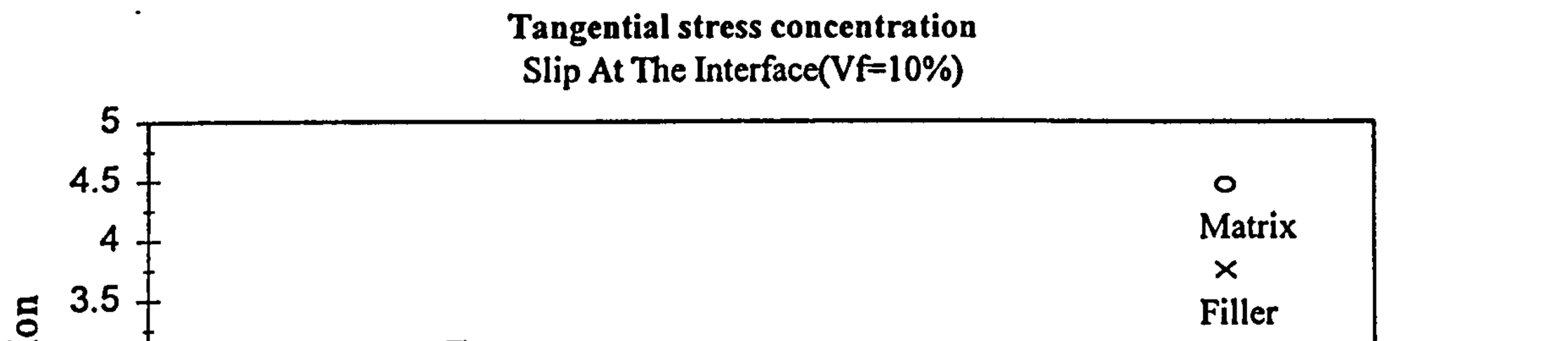

Fig.4.26: Tangential stress concentration at the interface of partly debonded particle with slip condition at the closed segment of the interface

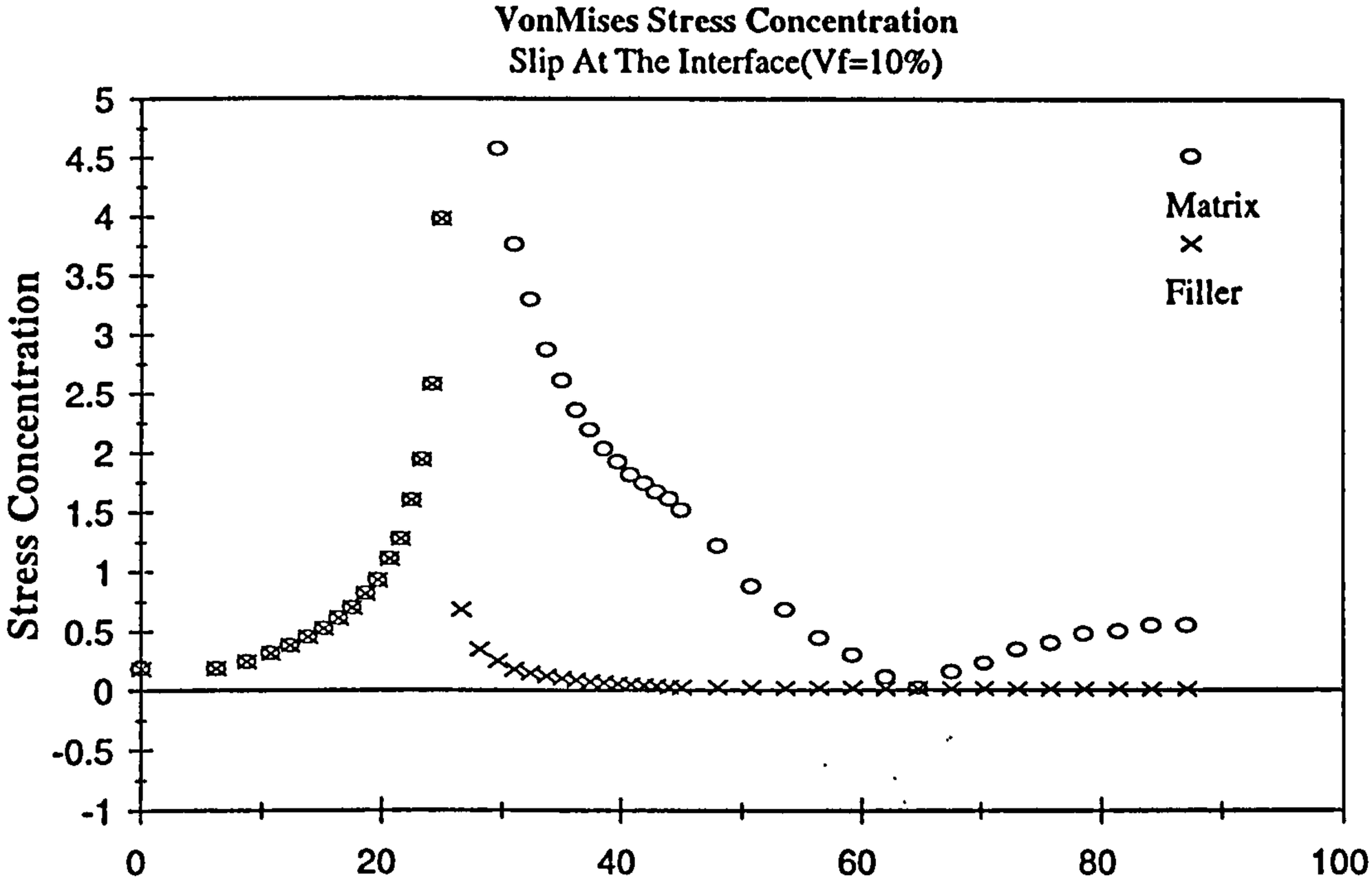

Fig.4.27: VonMises stress concentration at the interface of partly debonded partilce with slip condition at the closed segment of the interface.

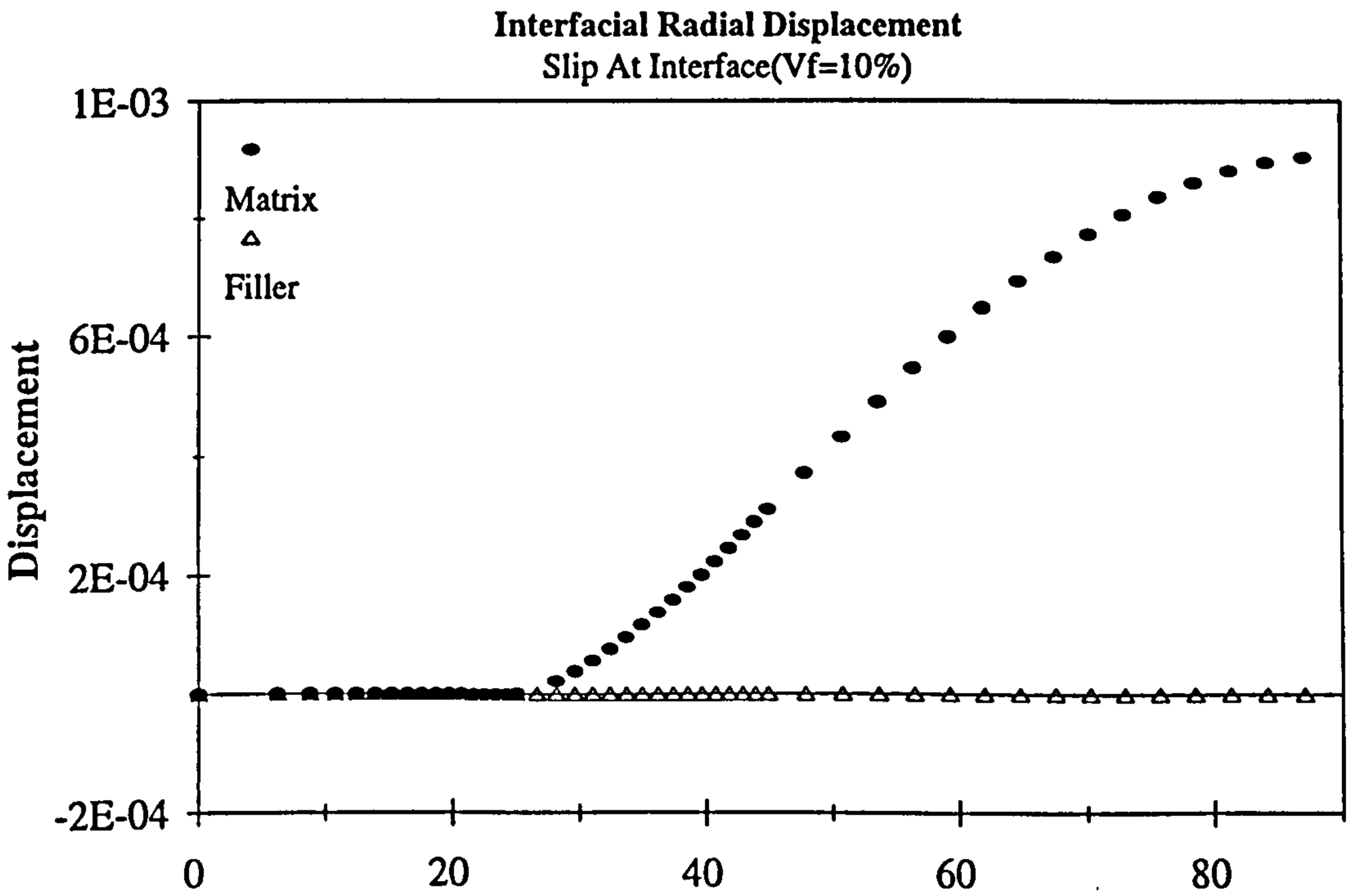

Fig.4.28: Radial displacement of the matrix and filler at the interface of the partly debonded particle with slip condition at the closed segment of the interface

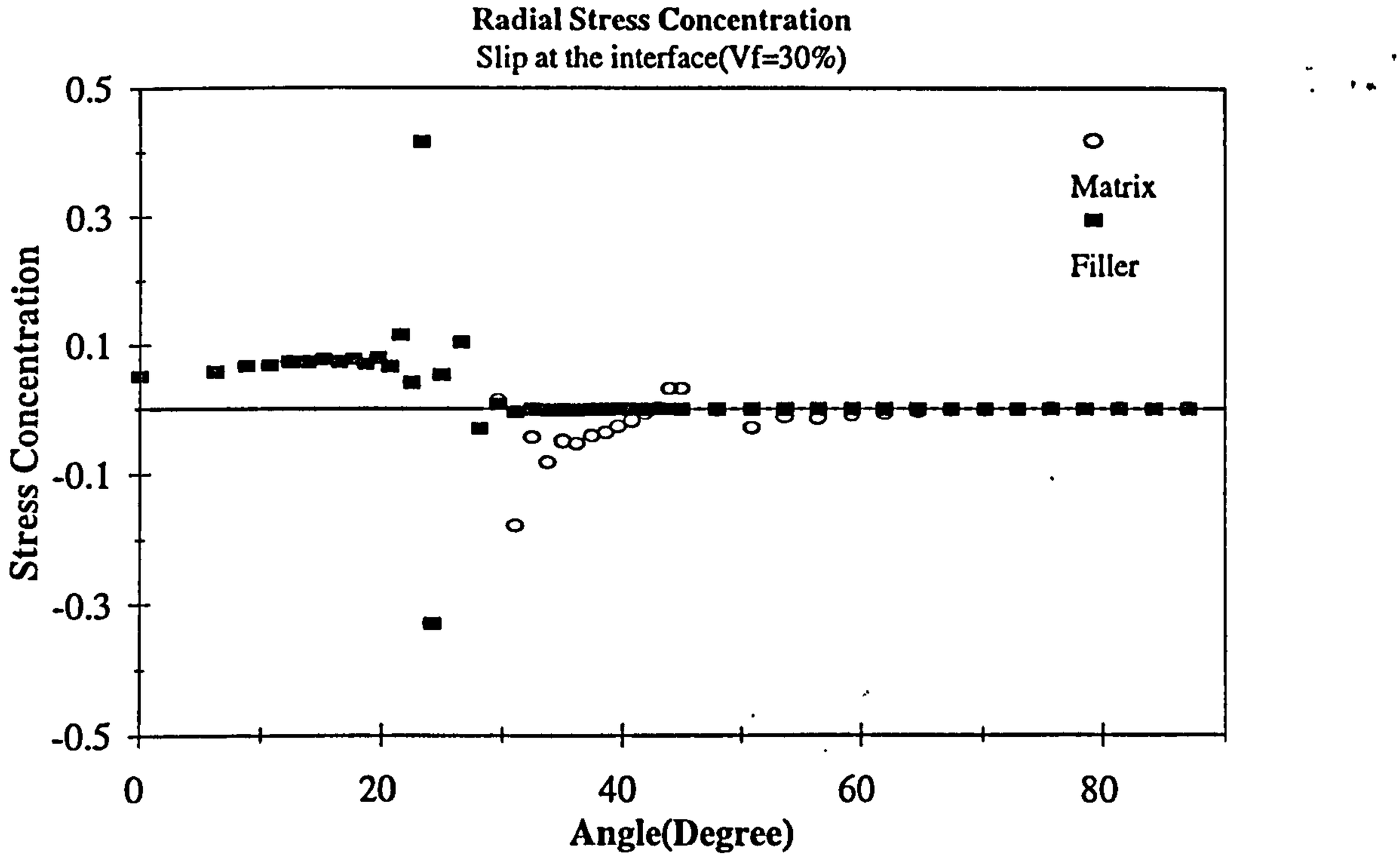

Fig.4.29: Radial displacement of the matrix and filler at the interface of the partly debonded particle with slip condition at the closed segment of the interface

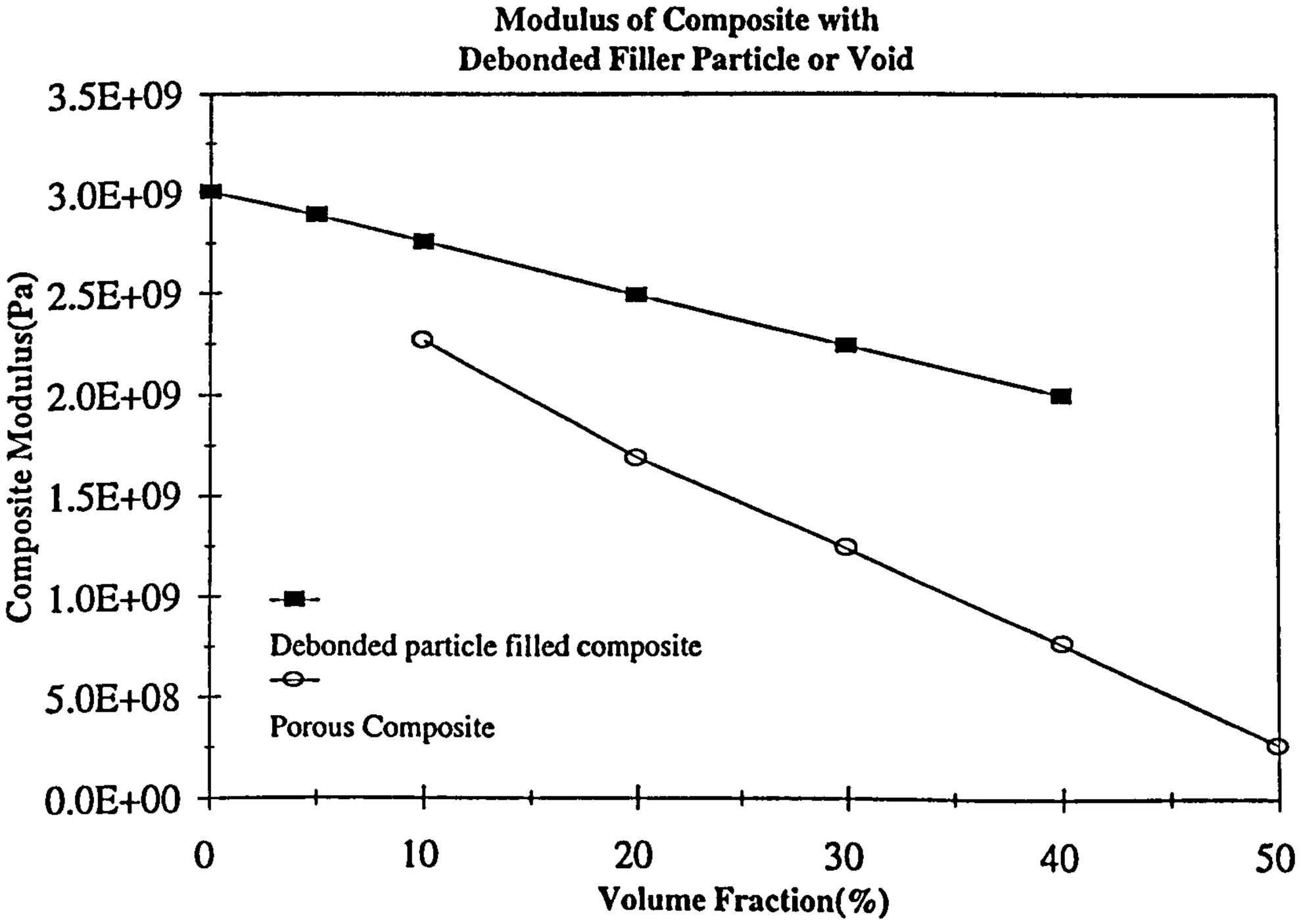

Fig.4.30: Modulus of composite filled with debonded filler particle or void

exclude the possibility of growing or opening of the crack further than θ =22° towards the equator.

The contour diagrams of the direct stress, shear stress and Von Mises stress concentrations are shown in *figure 4.24a-c*. Maximum stress concentration in all of the above cases can be found at the crack tip.

4.3.3 Slipping of the particle at part of the interface

Figures 4.25-28 show the stress and displacement variations at the interface for epoxy composite filled with 10% of glass beads while slip condition is imposed on the segment of the particle from θ =22° to the equator. Since a low slip coefficient is used, the stress and displacement fields follow more or less the same trend as the no slip case. However, the maximum radial, tangential and Von Mises stresses decrease compared to the non slip case. Using the same slip coefficient in a composite with 30% volume fraction of filler the results are shown in f*igure 4.29*. The stress concentrations shows noticeable decrease at this volume fraction.

In *figure 4.30* the modulus of the composite filled with the unbonded particles and the composite containing voids are compared for the range of volume fractions.

4.3.4 Strength

The tensile strength of the composites with perfectly bonded and unbonded interfaces and composites with voids are calculated using finite element model. The results are compared in *figure 4.31*. The decrease of the tensile strength with increasing volume fraction can be observed in all cases. The graph shows the strength of composite with unbonded interface is between the upper bound curve which is for the bonded interface and the lower bound curve which represents the composites with voids.

In *figure 4.32* the strength predicted by the finite element analysis is compared with the following models proposed by Neilsen and Nicloais&Narkis.

Different theoretical models are suggested for the unbonded or no adhesion case. A commonly reported model is due to Nicolais and Narkis (Nicolais and Narkis, 1971) which is based on the assumption that the unbonded particle cannot carry any of the

load and the yielding occurs in the minimum cross section of the continuous phase. They presented the following equation for the yield stress of the composite.

$$\sigma_c = \sigma_m(1-1.21V_f) \qquad (4.11)$$

Another model suggested by Neilsen (Neilsen, 1966) gives the yield stress in a composite assuming no adhesion between polymer and filler, expressed as :

$$\sigma_c = \sigma_m(1-V_f^{2/3})S \qquad (4.12)$$

where S is the stress concentration function which can be determined by the finite element analysis. The Neilsen's prediction is very close to the finite element prediction for voided composites and it is also closer to the unbonded composite. But the Nicolasis and Narkis's model gives a much higher values for the strength.

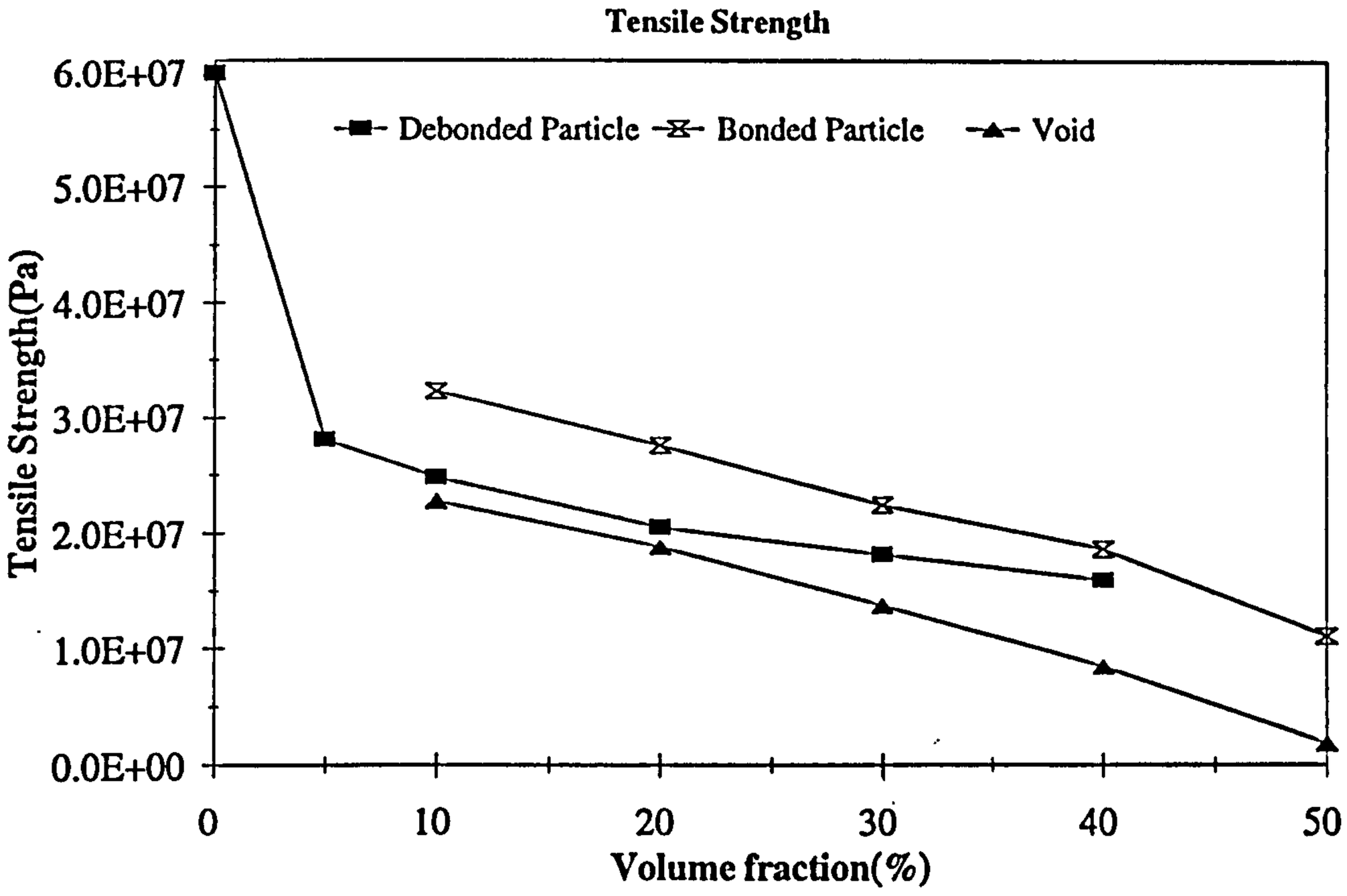

Fig.4.31: Prediction of tensile strength of composite filled with perfectly bonded particles, debonded particles and voids.

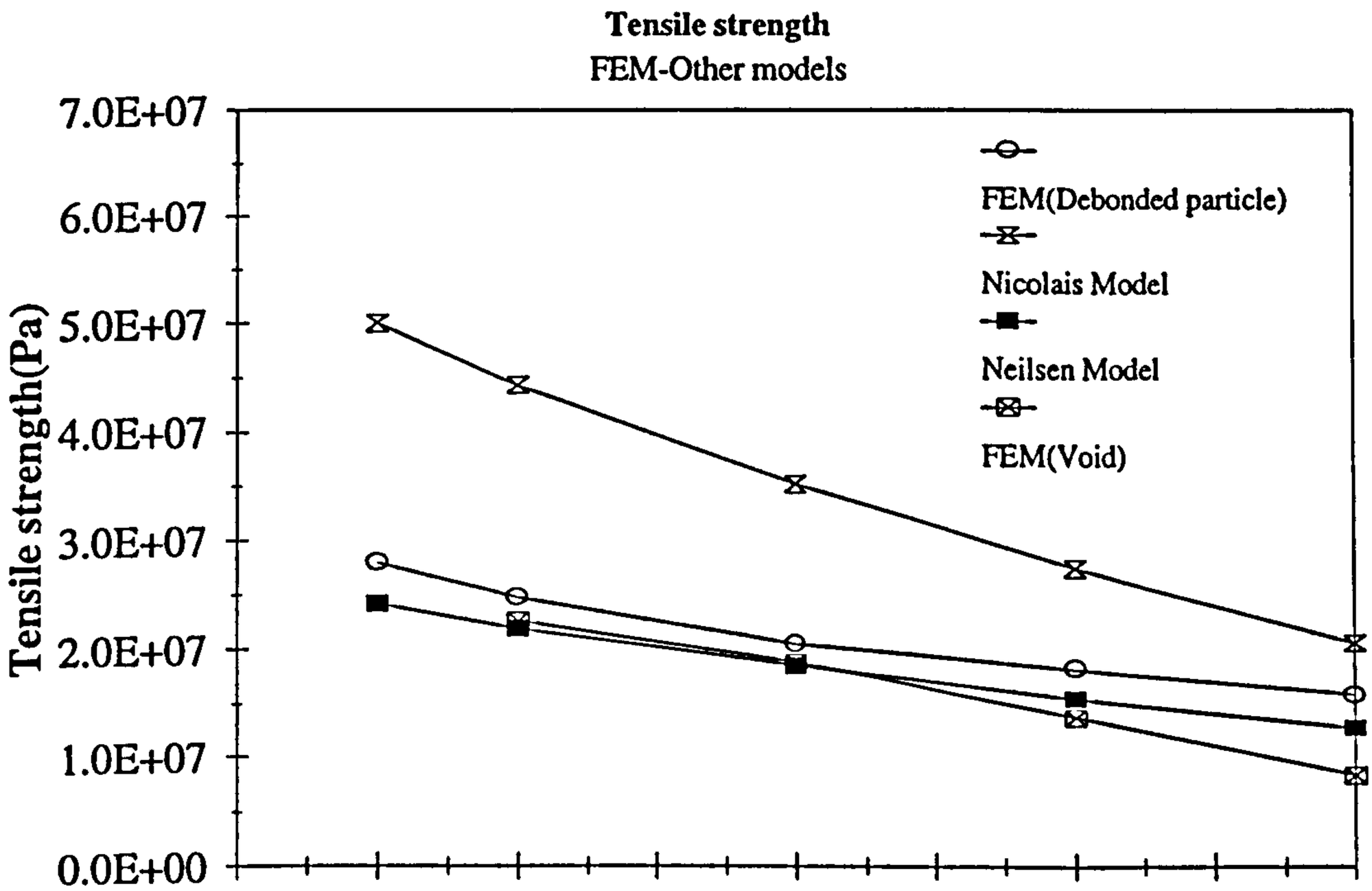

Fig.4.32: Comparison of the predicted tensile strength of the composite with debonded particles and voids with other models predictions

4.4 COMPOSITES FILLED WITH SOFT PARTICLES

4.4.1 Material properties

The results presented in this section include the linear-elastic behaviour of the rubbery phase and the epoxy matrix. The input values used to obtain stress concentrations and the composite toughness via a linear elasticity model are shown in table 4.2.

	Input Properties		Derived Properties	
Phase	**E (GPa)**	**Poisson's Ratio, ν**	**K (GPa)**	**G (GPa)**
Epoxy	3.0	0.35	3.333	1.119
Rubber	0.0004	0.490-0.4999	0.006-0.667	0.000134-0.00026

Table 4.2. Elastic Material Properties Used in the Predictive Models

Material properties for typical epoxy type polymer are well-known. However, the value of E for the rubbery phase is more difficult to establish; A sensible range of values of ν was selected for the rubber. The upper value chosen for ν is very close to the maximum theoretical value of 0.5. It should be noted that the finite element analysis package that was employed fails if ν = 0.5 is used. However, the maximum value of ν used in the present work is 0.4999. Such relatively high values may now be used because of improved precision of the finite element code.

The most important advantage of being able to use values of the Poisson's ratio close to 0.5 is that in this way we can substitute high values of K(i.e. bulk modulus of the rubber particle). Indeed, the input values E 0.4 MPa and ν 0.4999 imply a value of K of about 0.667 GPa, which is of the order expected for a rubbery polymer (Brandrup and Immergut, 1989).

4.4.2 Young's modulus

As it is shown in *figure 4.33* the relationship between the modulus of the composite and volume fraction of the filler is nearly linear. The measured Young's modulus for

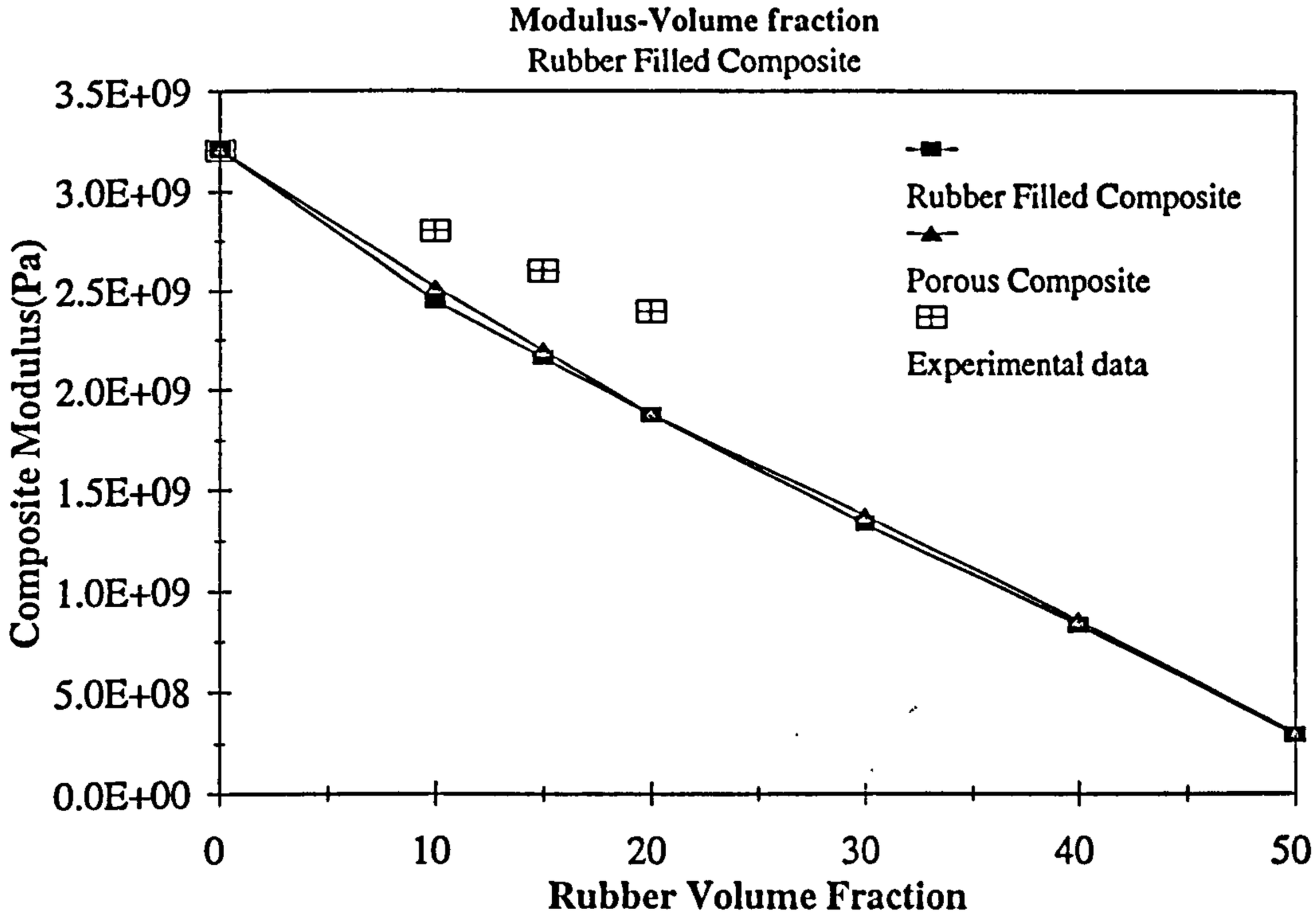

Fig4.33: The modulus of the rubber filled composite, porous composite and experimental data

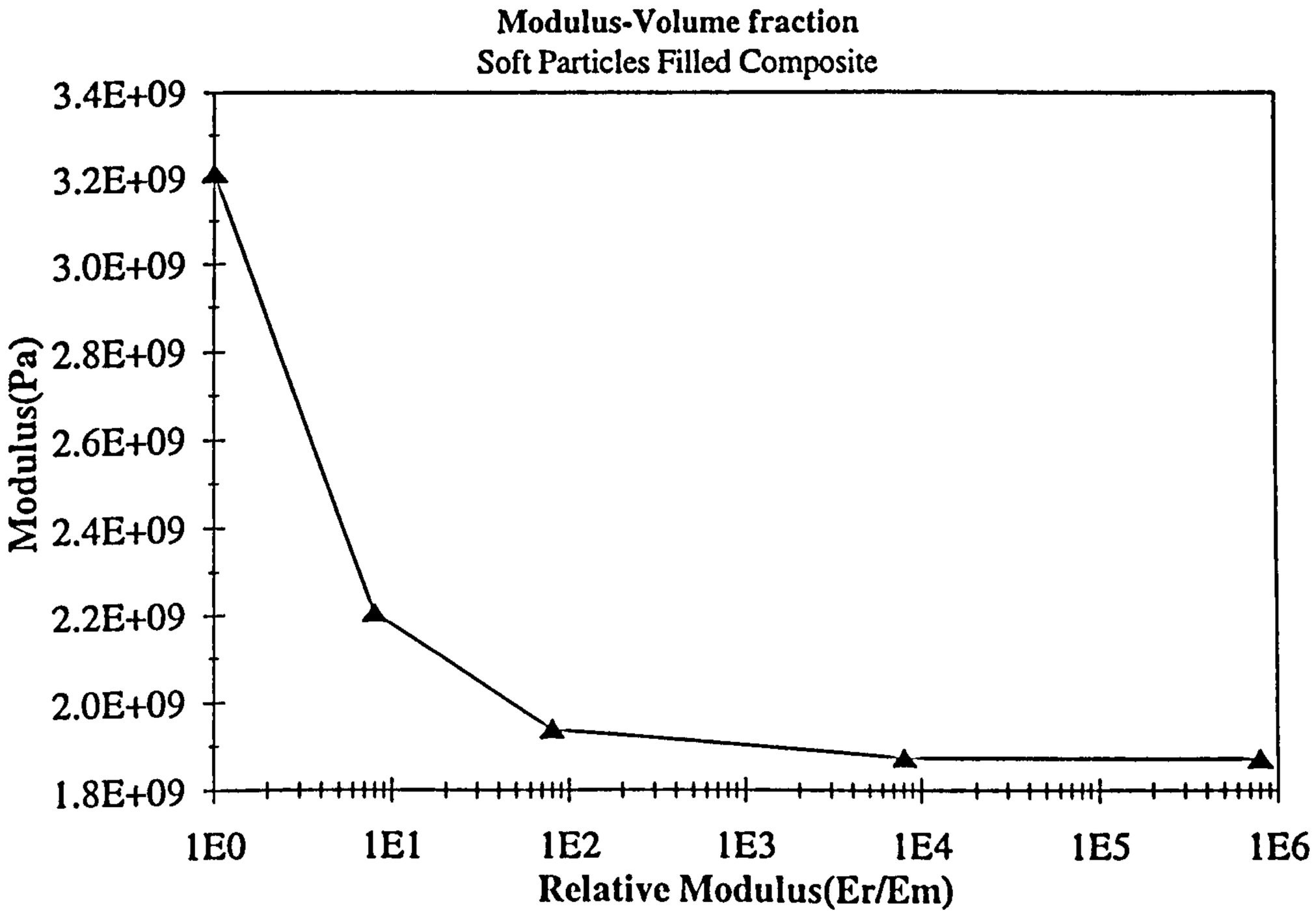

Fig4.34: Variation of the rubber filled composite modulus with the relative modulus(Er/Em)

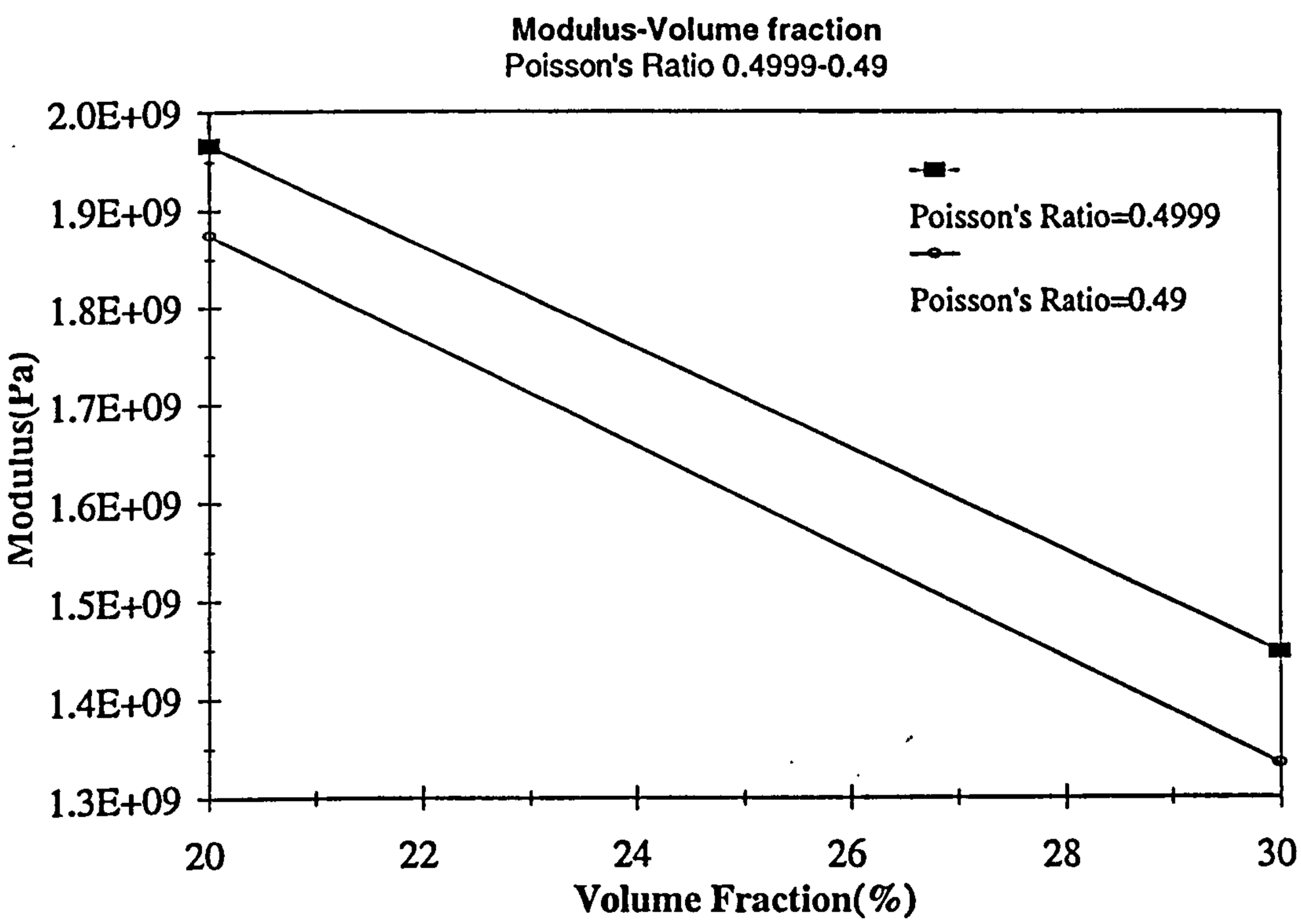

Fig4.35: The effect of Poisson's ratio of rubber on the final result of FEM.

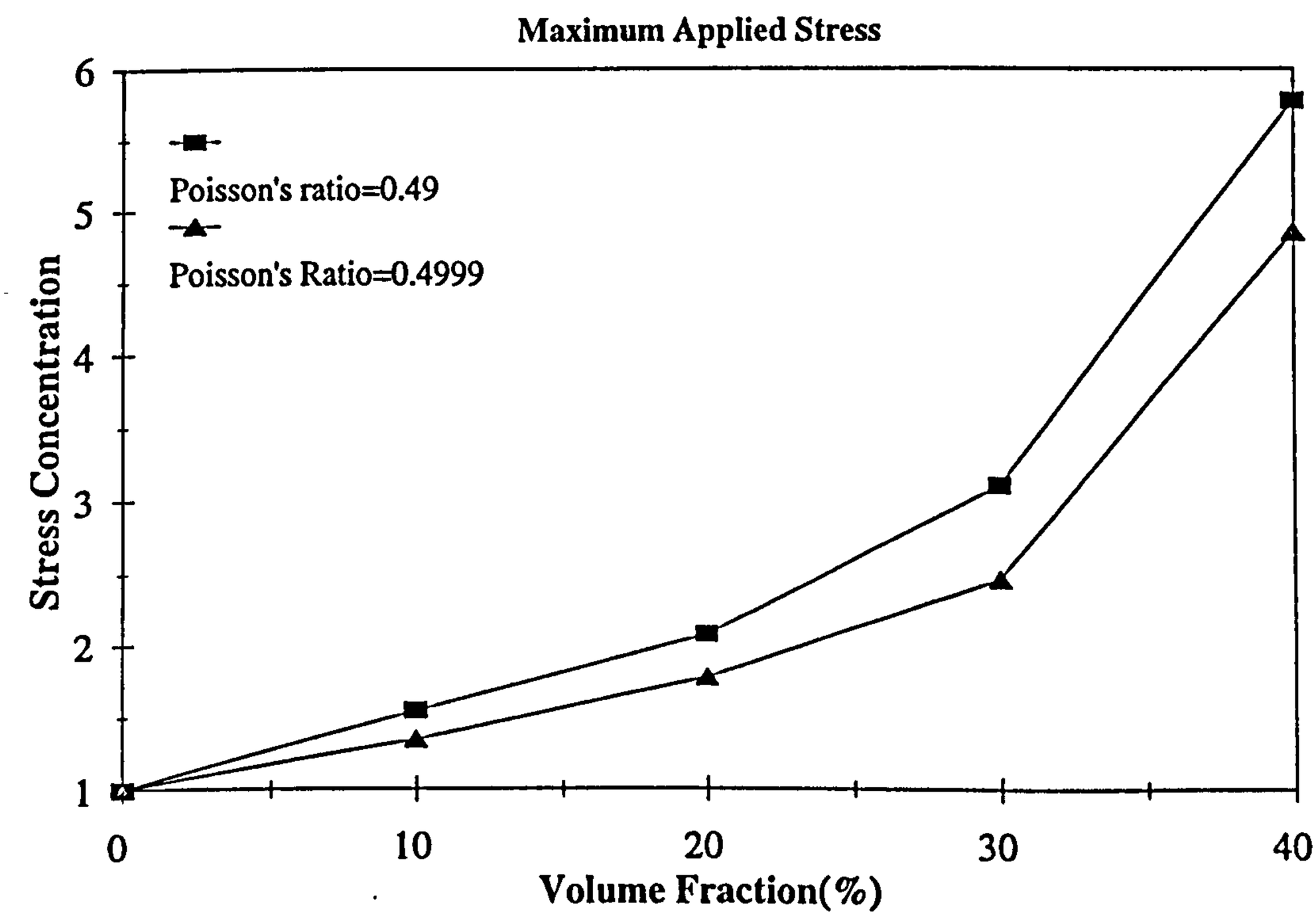

Fig4.36: Concentration of maximum applied stress for different filler volume fractions.

epoxy resin reinforced with 15% volume fraction of rubber spheres is also included. The measured value is significantly higher than the predicted range by our model. The lack of precise agreement between experimental and numerical results could arise from the inaccuracy in description of the rubber properties and the assumption that the phases are perfectly separated. Beyond a volume fraction of about 0.2, there are no experimental data available for comparison, because when higher concentrations of rubber are used, phase inversion of the multiphase polymer normally occurs.

Figure 4.34 shows predictions of our model for the Young's modulus of the multiphase rubber-toughened epoxy as a function of log(Em/Er), where Ep and Em are the Young's modulus of the rubber and epoxy respectively. A volume fraction of 20% has been assumed for the rubber phase. In the calculations, the Poisson's ratio of the rubber is considered to be 0.49. Initially the Young's modulus of the two phase material decreases sharply with an increase in the value of log(Em/Er). When this value approaches 3.0, the Young's modulus has a constant lower bound of 1.87 GPa. The predicted values of the overall modulus are relatively insensitive to the changes of the value of the rubber modulus.

The predicted overall modulus is found to increase by 5% at 20% volume fraction and 7% at 30% of volume fraction if the Poisson's ratio of the rubber is increased from the value used 0.49 to 0.4999 as is shown in *figure 4.35*. Therefore the properties of rubber could probably be best described using a Poisson's ratio of 0.5, but this causes a problem for the finite element analysis.

The experimental values reported for rubber filled composites are in comparison higher than our model predictions, this is probably because of some stiffening of the rubber via the epoxy, the inadequate description of the Poisson's ratio of the rubber in the model, and incomplete phase separation leading to a lower rubber volume fraction than the expected theoretical value. The onset of plasticity during the experimental measurements as well as any experimental errors can also cause some discrepancy between the measured and the predicted values. In some cases the reason for the

experimental value to be higher than the predicted results can be the skin effect. The restrictions imposed by the walls of molds, leads to an excess polymer at the surface of the test specimens. Thus, in torsion or flexural tests where the maximum stress is at the surface, the properties of the surface is dominant and determine the behaviour of the whole sample. This error can be corrected by using thicker specimens which can be extrapolated to infinite thickness, or by using particles of smaller size and extrapolation to zero particle size. The skin effect can produce errors as large as ten to twenty percent depending on the thinness of the specimen.

Despite the discrepancy between the experimental and the model results, it should be noted that almost linear relationship between Young's modulus and volume fraction is very similar to the relationship measured experimentally by Yee and Pearson.

4.4.3 Stress distribution

4.4.3.1 Concentration of direct stress

The contour diagrams of the direct stress, shear stress and Von Mises stress concentrations are given in *figures 4.37a-c.*

The contour diagram for the concentration of the applied stress indicates that the maximum stress concentration is found at the interface at the equator of the sphere. The examination of other contour diagrams confirms that this is the maximum principle stress predicted in the system. The position of maximum stress concentration, at the equator of the sphere, is in agreement with previous theoretical predictions and experimental results (Spanoudakis and Young, 1984). As it can be seen in *figure 4.36* the values of the maximum stress concentration, varies sharply with the volume fraction of rubber spheres. The stress concentration decreases with increasing Poisson ratio of rubber, since the effect of the difference between matrix and physical properties of the particle is diminished. In *figure 4.36* the direct stress concentration versus volume fraction can be compared for rubber Poisson's ratios, of 0.49 and 0.4999.

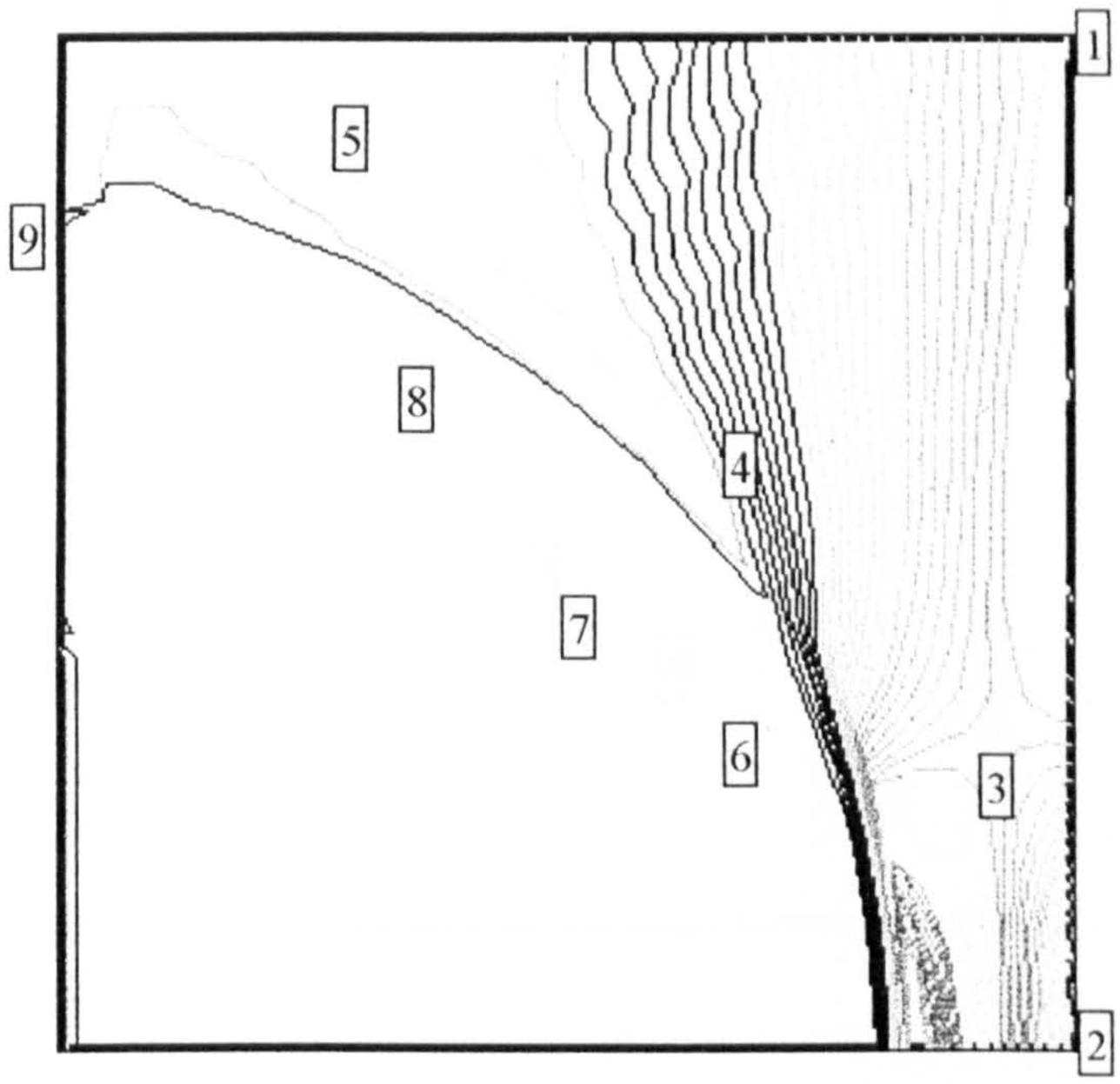

1	2.61E06
2	5.09E06
3	2.28E06
4	1.81E06
5	1.18E05
6	6.33E05
7	2.56E05
8	1.53E05
9	2.56E05

Fig.4.37a: Contour diagram of direct stress field of composite with 30% of soft filler particles

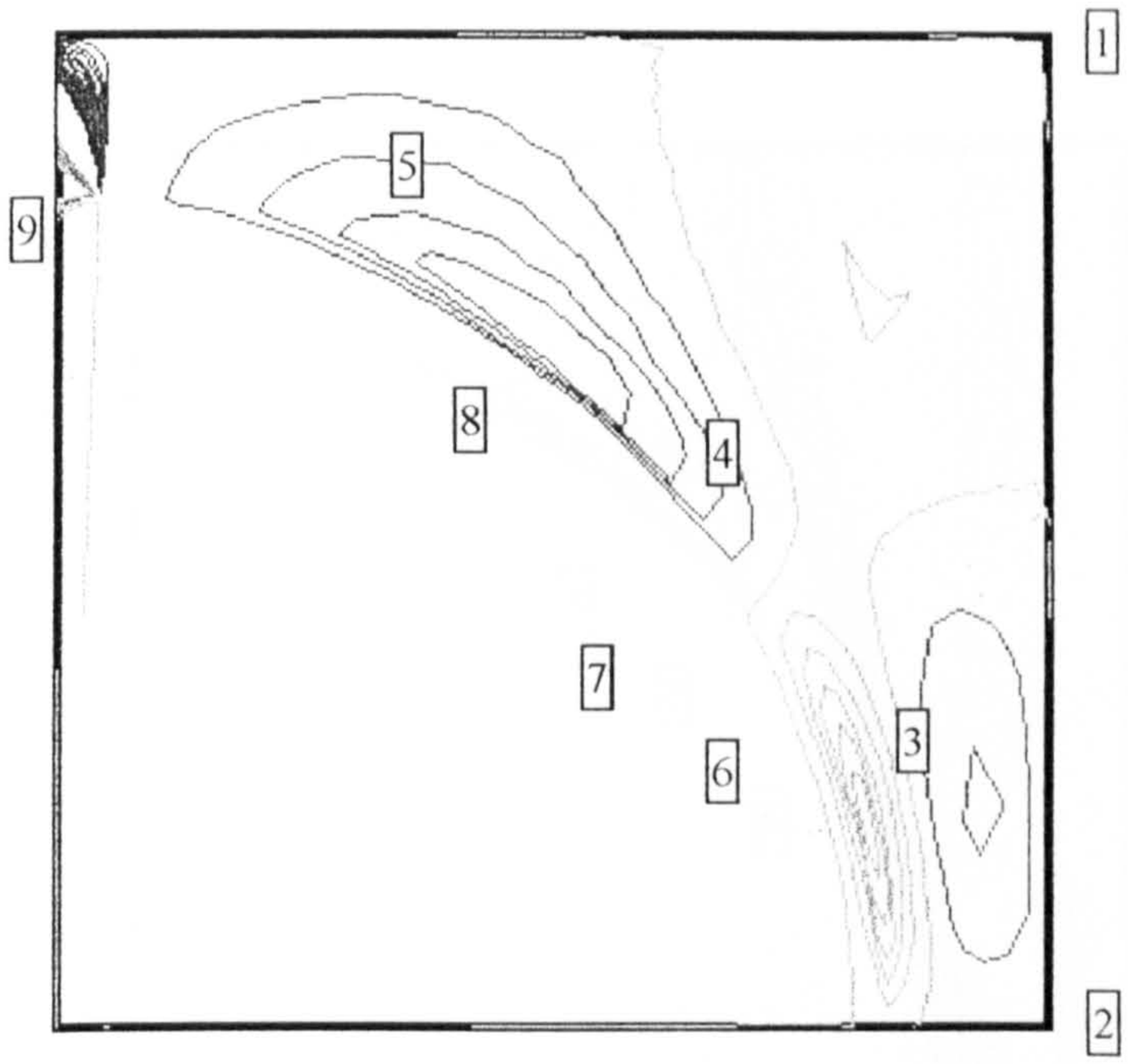

1	2.17E03
2	6.03E04
3	1.08E05
4	-8.28E04
5	1.68E05
6	-1.70E05
7	1.49E02
8	2.09E05
9	1.57E02

Fig.4.37b: Contour diagram of shear stress field of the composite with 30% of soft filler particles

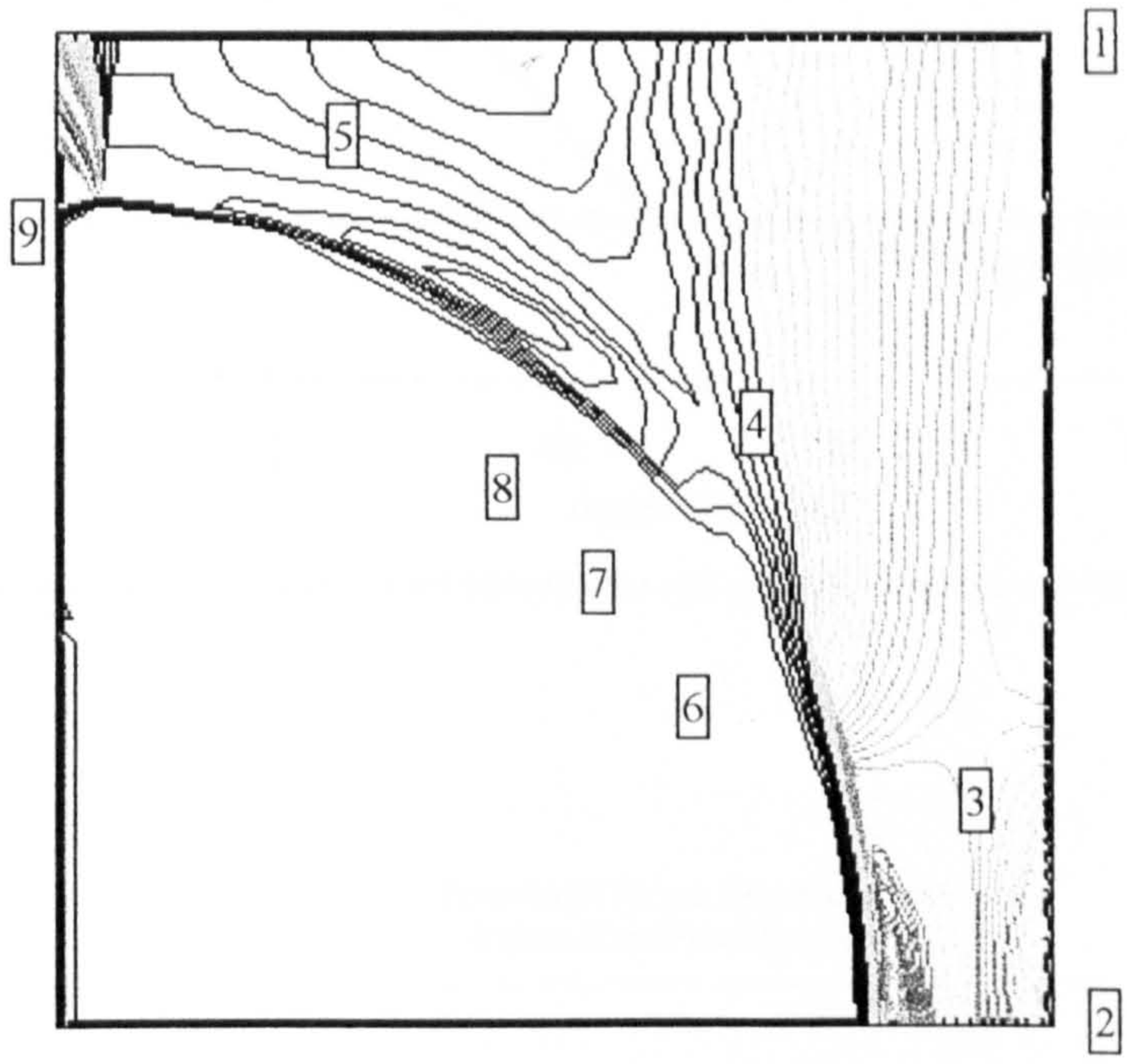

1	0.261E7
2	0.922E6
3	0.228E7
4	0.184E7
5	0.411E6
6	0.623E6
7	0.255E6
8	0.462E6
9	0.979E6

Fig.4.37c: Contour diagram of Von Mises stress field of composite with 30% of soft filler particles

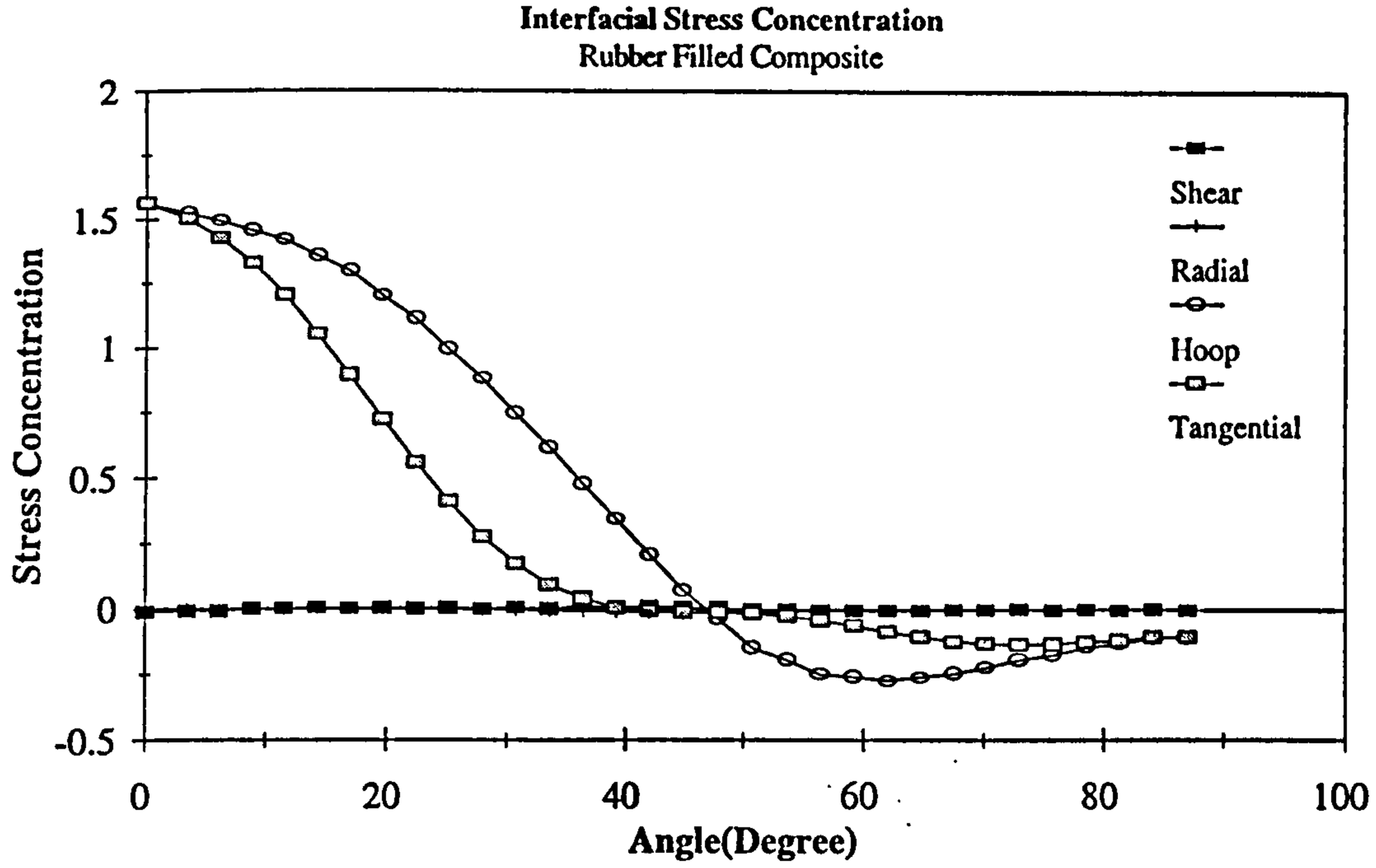

Fig.4.38: Stress concentration at the interface in the soft particle filled composites (Vf=20%).

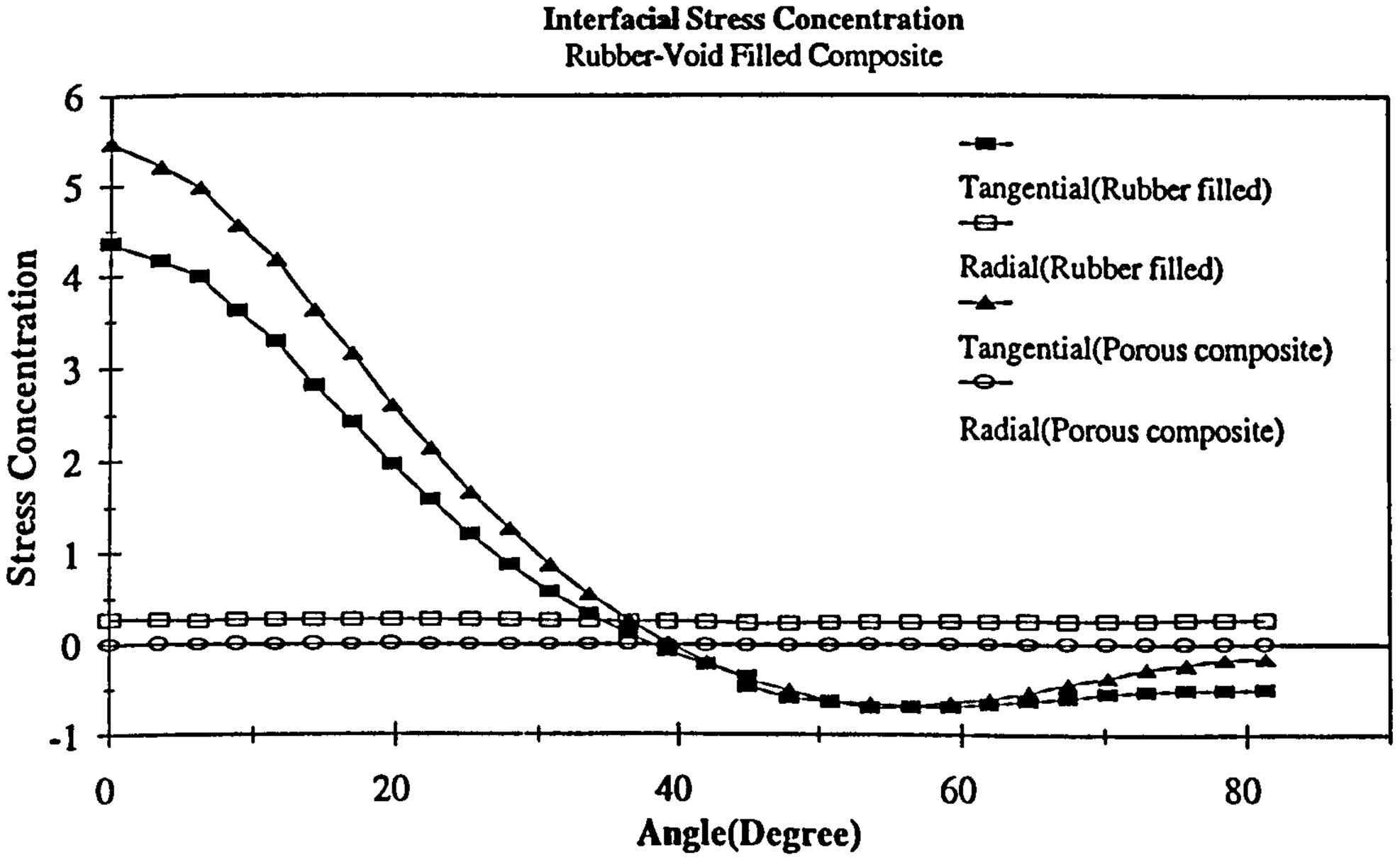

Fig.4.39: Comparison of interfacial stress concentration of rubber filled and porous composites (Volume fraction of rubber or voids=30%).

4.4.3.2 Stresses at the interface

Stresses around the interface of the matrix and filler are converted to polar coordinates. The shear stresses in both the resin matrix and the rubber sphere are zero. The only high stress is the tangential stress in the resin matrix, which has its maximum at the equator of the rubber sphere. *Figure 4.38* shows the concentration of different stresses at the interface for a composite with 20% rubber volume fraction. The radial stresses in the resin and rubber are equal and constant around the interface; the tangential stresses are also identical in the matrix and rubber particle. We note that the radial stress at the interface for the soft particles is far smaller than that found for the hard particles. This indicates that there is no tendency for debonding at the interface in the composites, which is in contrast to the tendency for debonding in the glass filled material. The low value of stress transmitted to the rubber, shows that the rubber sphere is acting like a hole. The concentration of stresses at the interface is compared in *figure 4.39* for the matrix filled with 30% of rubber and matrix having 30% of voidage. The similarity of the behaviour of the composites filled with rubber or voids is confirmed by the values of matrix maximum stress concentration, at the equator for epoxy resin containing holes or rubber spheres. The values are hardly changed by the presence of rubber.

4.4.3.3 Hydrostatic stress in the rubber particle

Examination of the stresses in the rubber shows that the whole particle is in uniform pure hydrostatic tension. The variation of the hydrostatic stress concentration factor with volume fraction is shown in *figure 4.40*. The magnitude of this stress is uniform throughout the sphere within accuracy of the prediction. Although the value of this stress concentration is about two orders of magnitudes smaller than the maximum stress concentration in the resin, it may still be significant since the difference in moduli of two phases is around five orders of magnitude. The magnitude of hydrostatic stress concentration in rubber increases with its volume fraction. Initially there is a little increase by increasing volume fraction up to around 20% and then it increases by a factor of 2 between 20% and 50% of filler volume fraction. The Poisson's ratio of the rubber has a significant effect on the predicted values of the

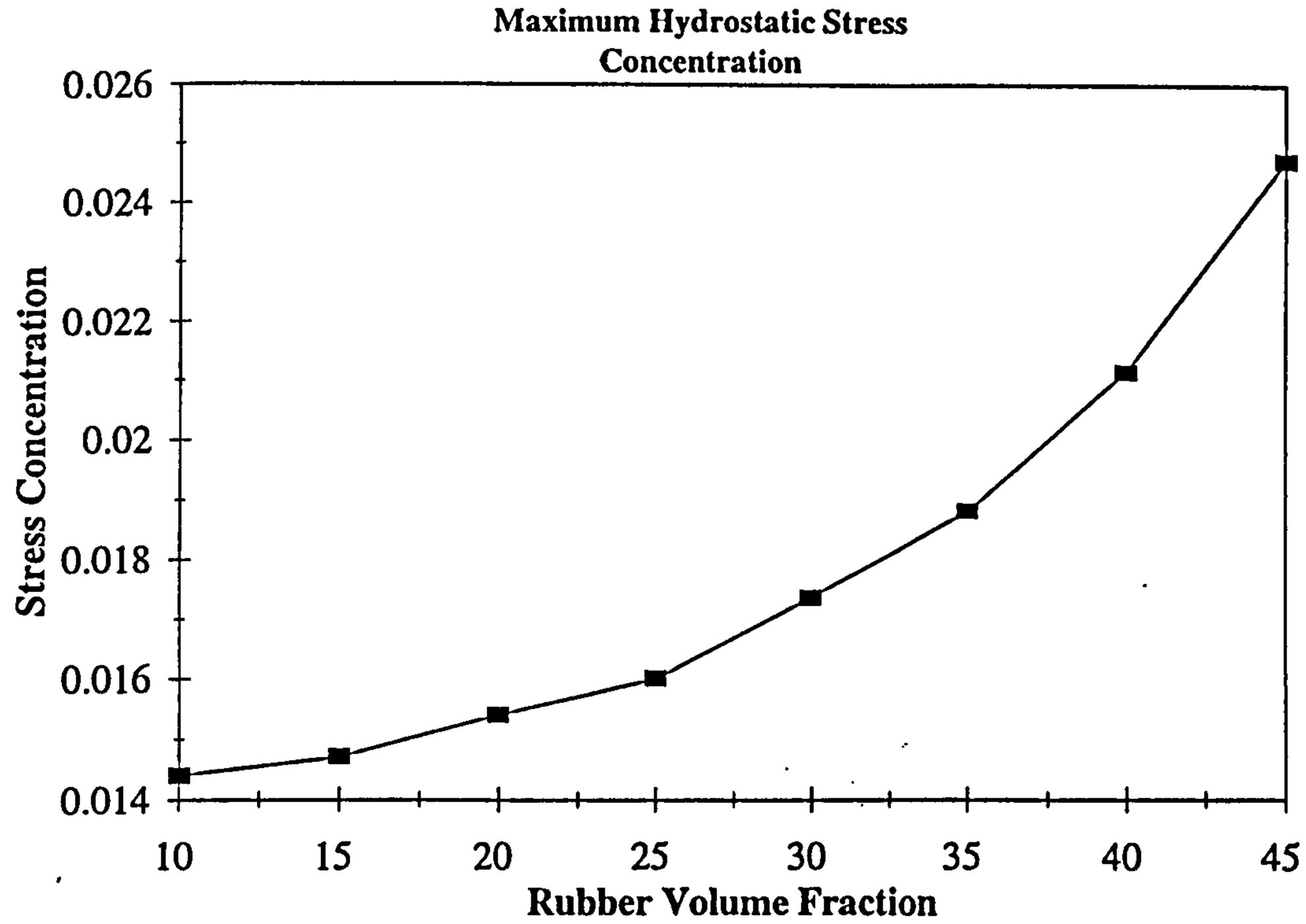

Fig.4.40: Maximum hydrostatic stress concentration in rubber particle.

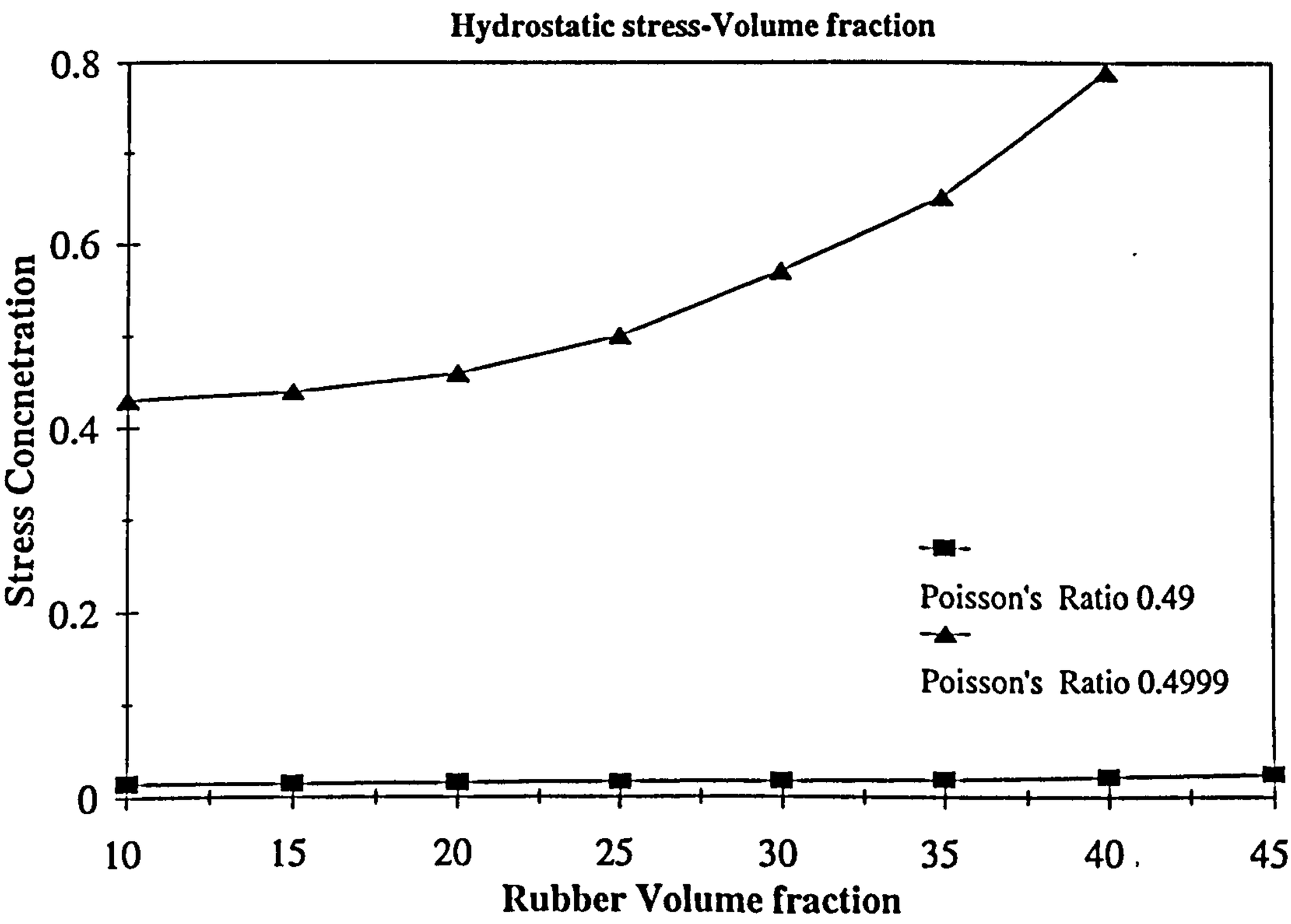

FIG.4.41: Effect of Poisson's ratio in FEM calculations of the hydrostatic stress.

hydrostatic stress in the rubber. The variation of the hydrostatic stress concentrations as a function of the volume fraction of the rubber phase for two values of Poisson's ratio, 0.49 and 0.4999 are presented in *figure 4.41*. These values of the Poisson's ratios gives the bulk modulus of the rubber as 0.006 GPa and 0.667 GPa at the same Young's modulus.

4.4.3.4 Concentration of yield stress

As it is shown in *figure 4.37c* the maximum Von Mises stress is found at the interface, at the equator of the sphere, which is the identical position to the maximum direct stress. The position of the maximum Von Mises stress remains unchanged for different volume fractions but the magnitude of the stress concentration factor increases sharply with increased volume fraction as can be seen in *figure 4.42*.

As it is mentioned earlier in this chapter the magnitude of the hydrostatic stress at the equator is less dependent on the volume fraction. We can compare the change in applied stress required for yield between 10% and 20% volume fraction of rubber. Our predictions show an increase in stress concentration from 1.50 to 2.00 over this range. Assuming that yield occurs when the stress within the material reaches a given level, and bearing in mind that hydrostatic stress over this range changes slowly, this increase in stress concentration predicts that applied stress at 20% rubber volume fraction should be 85% of the applied stress at 10% rubber volume fraction; the measured reduction is found to be from 55 to 50 MPa i.e. 91% (Yee and Pearson, 1986). Shear bands in the resin are expected to grow from the point of maximum concentration of Von Mises stress, which is predicted to be at the equator of the sphere.

4.4.3.5 Stresses in the matrix

The stresses in the matrix on the lower side of the cell from the equator to the edge of the grid are shown in *figure 4.43a*. The stress concentrations for direct stress and Von Mises stress reach maximum at the equator and decrease towards the edge of the cell. The shear stress on the other hand is almost zero. The variation of stress concentration

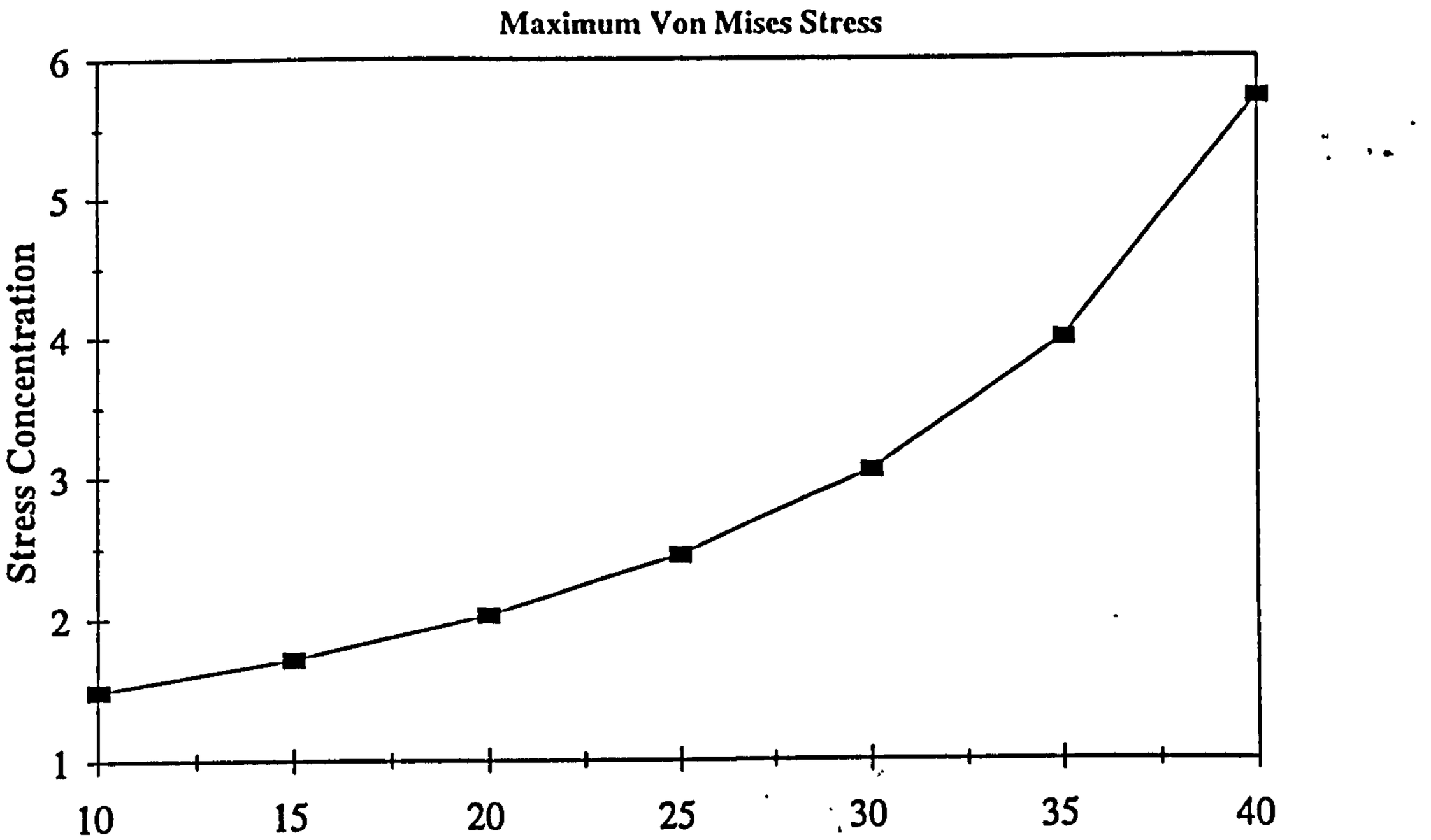

Fig.4.42: Maximum Von Mises stress concentration at the range of rubber volume fraction.

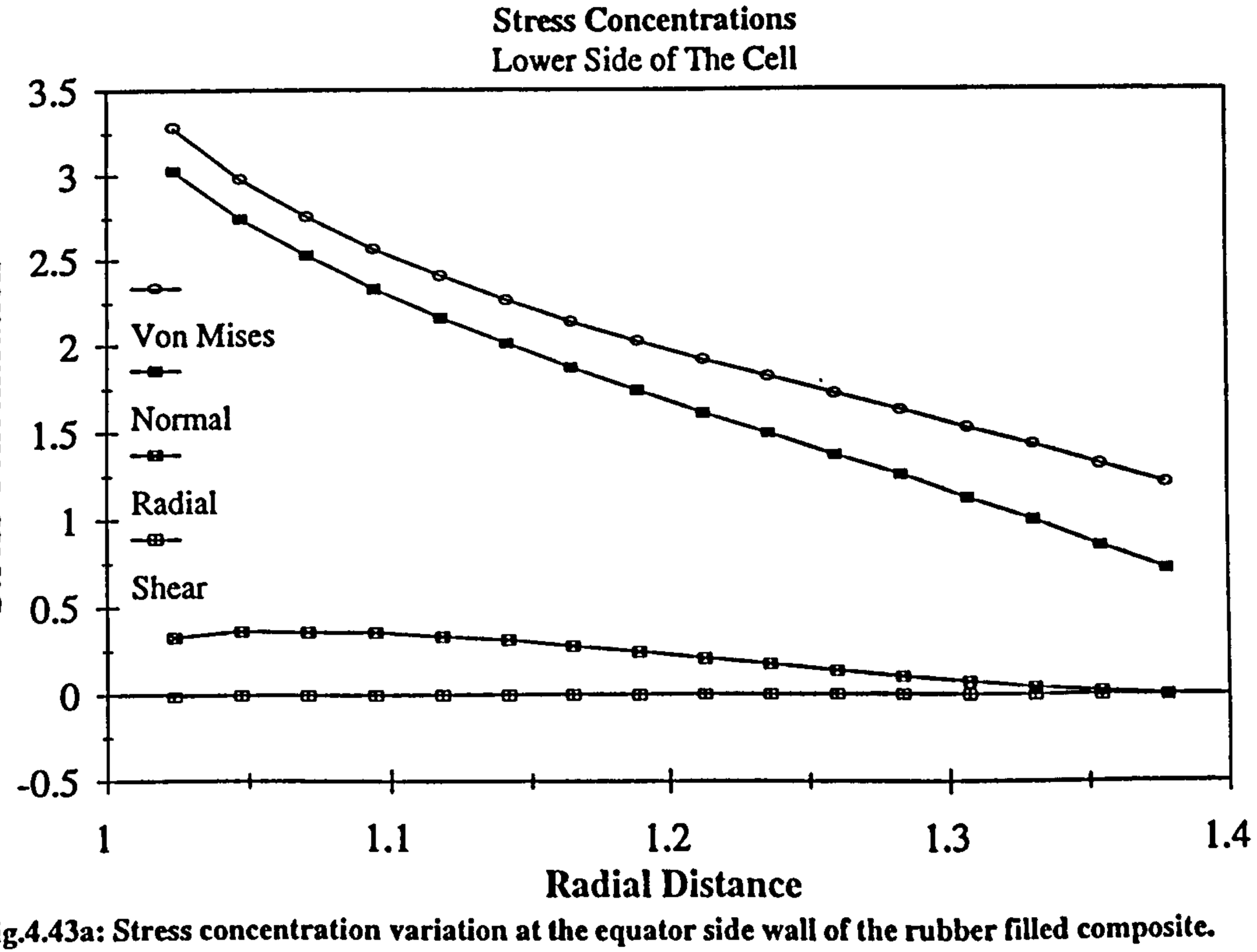

Fig.4.43a: Stress concentration variation at the equator side wall of the rubber filled composite.

on the diagonal of the cell follows an opposite trend and decreases from the particle surface towards the upper right corner edge of the cell, as it can be seen in *figure 4.43b.*

4.4.4 Fracture behaviour

Two important toughening mechanisms have been identified for the two phase material under study which consists of a rubbery phase dispersed in a matrix of cross-linked polymer. The first mechanism is localised shear yielding, or shear banding, which occur between rubber particles at an angle of approximately 45° to the direction of the maximum principal tensile stress. Owing to the large number of particles involved, the volume of thermoset matrix material which can undergo plastic yielding is effectively increased compared to the single-phase polymer, consequently, far more irreversible energy dissipation is involved and the toughness of the material is improved. The second mechanism is internal cavitation or interfacial debonding of the rubbery particles. The mechanism enables the subsequent growth of the voids formed by plastic deformation of the epoxy matrix. This irreversible hole-growth in the epoxy matrix in turn dissipates energy and therefore contributes to the enhancement in the fracture toughness of the composite.

Gent and Lindley (Gent and Lindley, 1959) have shown that cavitation of rubber can occur at relatively low stresses. Their analysis was later extended to include surface energy effects for small holes. Surface energy effects are important for initial holes smaller than 0.1 μm radius. The hydrostatic stress required for cavitation from an initial hole with radius greater than about 0.1 μm has been shown to be approximately close to the modulus of the rubber that is about 0.4 MPa. For an initial hole of radius 0.01 μm the stress required for cavitation increases by a factor of 40.

Internal cavitation of the rubbery particles or debonding of the particles from the matrix leads to voids (cavities) being formed. By neglecting any plastic void growth at this stage, the void can be treated as a particle with zero modulus, and a similar analysis to the one that is described above can therefore be done to calculate the stress concentration around the voids and the Young's moduli of the voided epoxy polymer. The formation of voids due to internal cavitation of the rubbery particles or debonding

of the particles from the matrix does not significantly change the level of the stress concentration in the epoxy matrix.

The described mechanisms are triggered by the different types of stress concentrations that act within the overall stress field in the two-phase material. For example, initiation and growth of the shear bands are largely governed by the concentration of Von Mises stress in the matrix, whereas cavitation, or interfacial debonding, of the rubber particles is largely controlled by the hydrostatic (dilatational) tensile stresses. To analyse the stress field accurately, it is necessary to employ a numerical technique such as the finite element method.

The yielding of the glassy polymers is usually dependent on the hydrostatic stress component, and therefore the simple Von Mises criterion is not strictly satisfied. Instead the Von Mises criterion should be modified as:

$$\tau_{vm} = \tau_y - \mu_m P \tag{4.13}$$

where τ_{vm} is the Von Mises shear stress, as defined in *equation 4.14*, τ_y is the yield stress under pure shear, μ_m is a material constant and P is the hydrostatic stress, Thus

$$\left[(\sigma_1-\sigma_2)^2+(\sigma_2-\sigma_3)^2+(\sigma_3-\sigma_1)^2\right] = 2\sigma_{vm}^2 = 6\tau_{vm}^2 \tag{4.14}$$

and

$$P = \frac{1}{3}(\sigma_1+\sigma_2+\sigma_3) \tag{4.15}$$

where σ_{vm} is the Von Mises tensile stress and the value of μ_m has been reported to be between 0.175 and 0.225. In this study this value is taken to be 0.2. It is obvious from *equation 4.13* that the stress required for the material to shear yield under tensile loading is reduced compared to the prediction of the unmodified Von Mises criteria. Hence, the relative size of the plastic zone will be increased. The tensile strength of the rubber toughened epoxy is shown in *figure 4.44*.

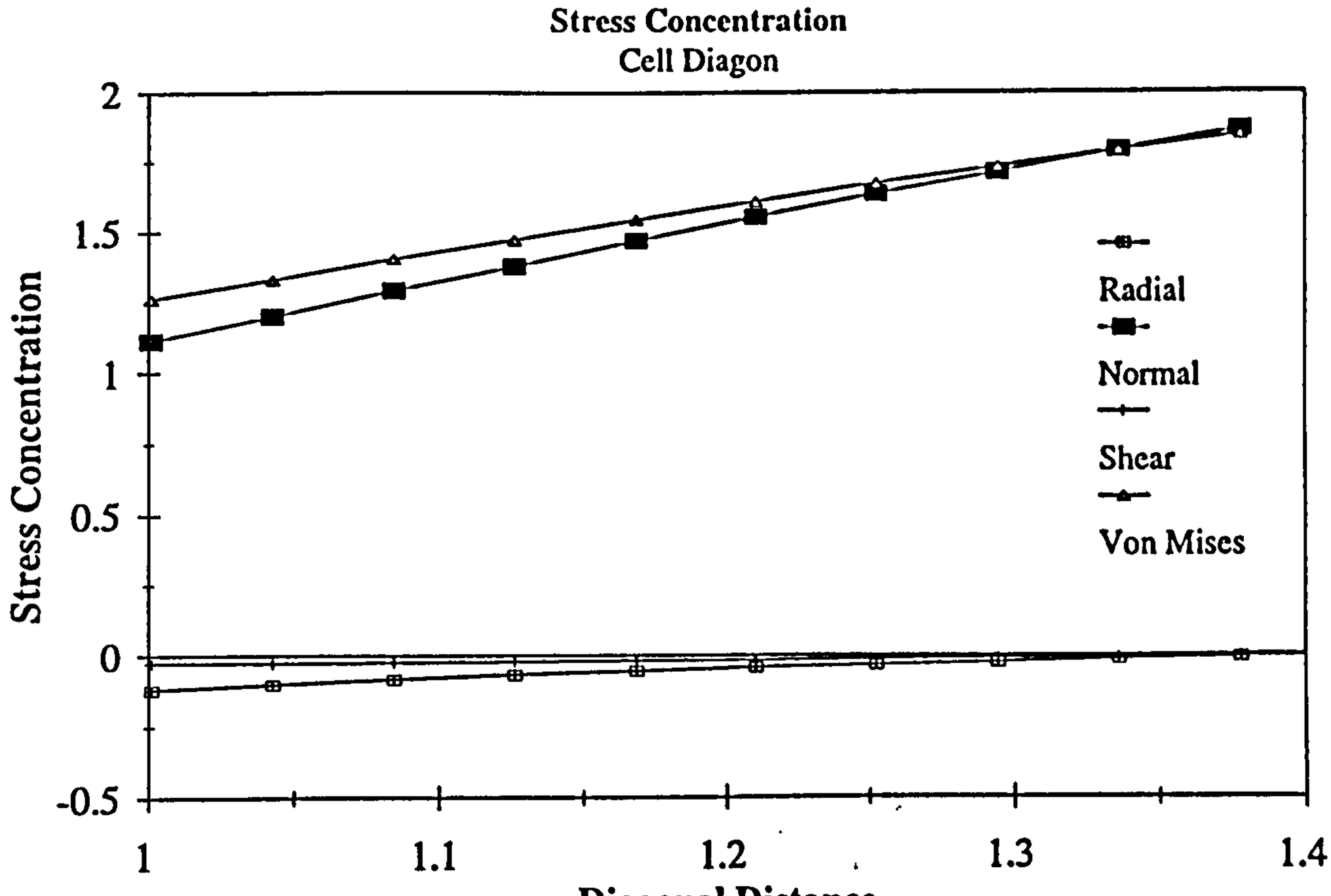

Fig.4.43b: Stress Concentration on the diagonal line of the cell in the matrix.

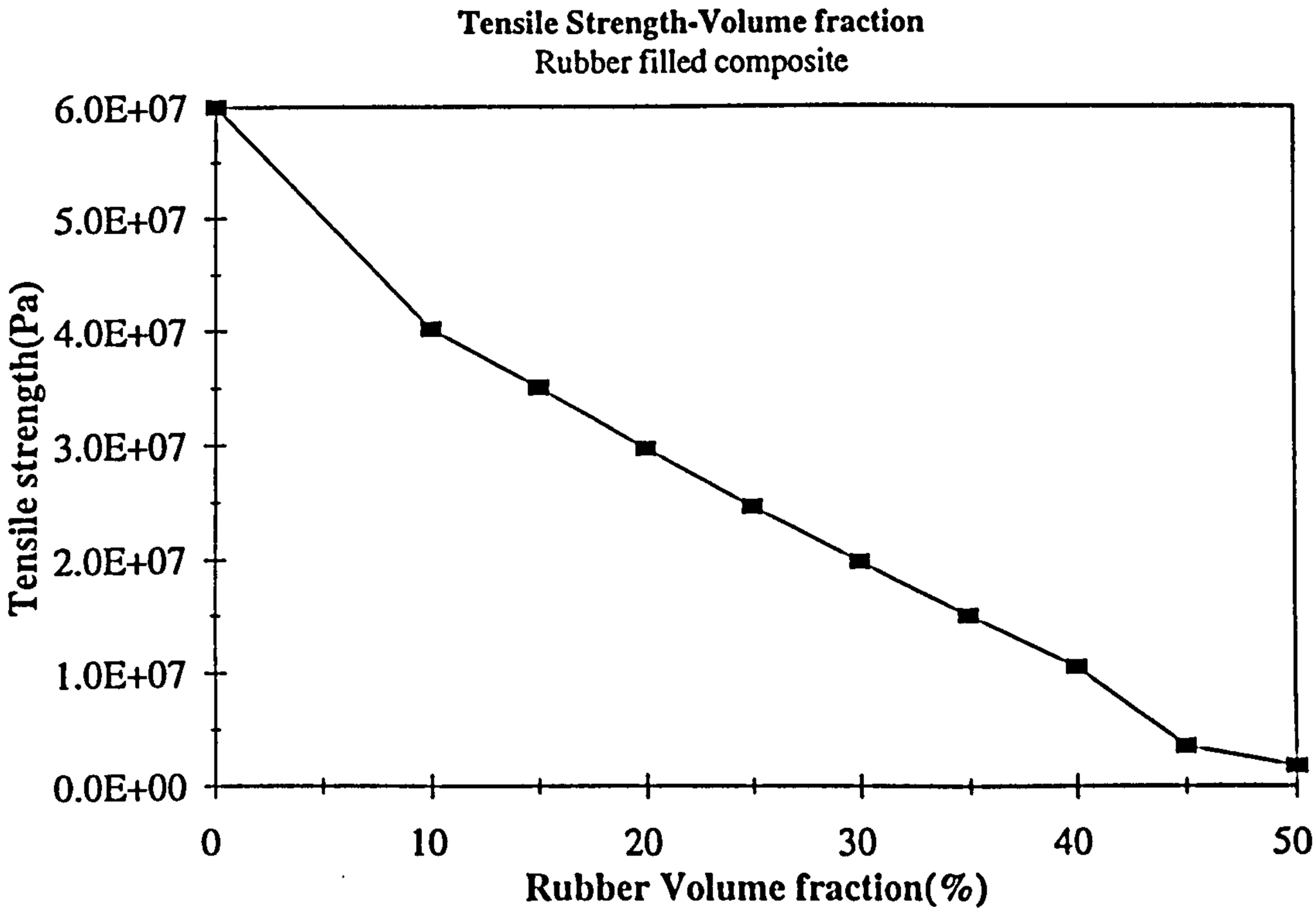

Fig.4.44: Tensile strength prediction using Von Mises stress comcentration criteria.

Schwier et al (Schwier et al , 1985) in their experimental investigation of polystyrene filled with polybutadiene rubber spheres, concluded that intrinsic cavitation of rubber spheres occurred at about an overall hydrostatic tension of 60 MPa.

Our results predict that for 20% volume fraction of rubber the concentration factor of hydrostatic tension in the rubber is about 0.025. Shear band formation probably occurs at about 30 MPa stress for epoxy resins. Keeping the average applied tensile stress at this level would subject the rubber spheres to a further 1 MPa hydrostatic tension. Cavitation of rubber particles on fracture surfaces is generally found to start from the centre of the sphere. Our predictions do not indicate a preferred point of initiation but clearly show that the imposition of an overall tensile stress of the order of the matrix yield stress places the rubber particles in sufficient hydrostatic tension to initiate cavitations from small flaws. These flaws may be areas of rubber which are not fully polymerised and cannot be observed by conventional microscopic techniques. There is some argument as to whether or not the cavitation of the rubber particles is necessary for shear bands to form. The exact stress levels for shear band formation and cavitation will depend on the values of stress required to form matrix shear bands and cause rubber cavitation for the system under study.

Epoxy resin reinforced with rubber spheres may be described as an inherently tough material since the position of maximum stress concentration, where a crack would be likely to develop, is at the equator of the sphere. The sphere acts as a barrier to any further growth of the crack. However, the maximum stress concentration rise sharply at high volume fractions. A simple description of toughness could be that yield is the preferred mechanism to the growth of the crack. Considering the very high stress concentration of applied stress at high volume fraction, crack growth could become more dominant at high volume fractions leading to the decreased toughness of composites filled with rubber particles. This effect was noted by Kunz (Kunz et al, 1982) who found a rapid increase in toughness until around 5 pbw (parts by weight) rubber, around 10% volume fraction, followed by a plateau. A similar effect is found by Spanoudakis and Young (Spanoudakis and Young, 1984) for epoxy resin reinforced with glass spheres treated with a release agent; the sphere must be behaving as a stable hole, and stress distribution in the resin must be similar to our prediction here; the

observed crack growth for glass spheres treated with a release agent supported the expected maximum stress concentration at the equator of the sphere. They found that fracture toughness decreased with volume fraction above 30% for this material. Although for glass spheres coupled to the resin matrix the toughness increased throughout the range of filler volume fraction.

Stress distribution in the matrix for resin containing rubber spheres has been found to be very similar to that of a resin containing holes. Shear band formation in the resin would occur in a similar way for the two materials. However, epoxy resin containing holes is known to be a very poor material. We therefore can postulate that shear band formation is not the only important fracture mechanism for this material. Our results have shown that cavitation of the rubber particles is likely to occur, in agreement with experimental observations; after cavitation the rubber may be stretched. It appears that the process of rubber cavitation and stretching may make important contributions to the overall fracture energy. The magnitude of these contributions is dependent on the modulus of the rubber. Further contributions to the fracture energy of epoxy resin containing rubber spheres may arise from the physical presence of the rubber which would act as a crack stopper to a growing crack attracted to the equator of the sphere by either the concentration of direct stress or the initiation of shear bands.

4.5 FIBRE REINFORCED COMPOSITES

In this section the response of epoxy resin reinforced with glass fibres to transverse tensile and shear loading is studied. The physical properties of the epoxy resin and glass fibres are presented in table 4.1.

4.5.1 Transverse tensile loading

4.5.1.1 Modulus

A tensile loading in the transverse direction of the fibres is applied to the composite. The modulus of particulate filled composites is compared with the moduli of transverse and longitudinal fibre reinforced composite having the same constituents in *figure 4.6.* As expected the longitudinal modulus of the fibre composite is much higher than that of the particulate composite, while the transverse modulus is lower. Maximum volume fractions of the fibres are 0.785 and 0.907 for square array and hexagonal array, respectively. These values reduce to 0.57 and 0.74 for square and hexagonal array in particulate composites. Therefore a higher volume fraction and modulus can be reached in fibre composites.

It is observed that the addition of fibres produces a substantial increase in the transverse modulus of the binder material; however, the effect of an increase in fibre modulus is a gradually diminishing one becoming asymptotic to the value obtained for the infinitely rigid fibre. Therefore, at high values of the fibre modulus, The ratio of transverse Young's modulus to longitudinal Young's modulus becomes relatively small which is one of the significant structural problems associated with the use of high modulus filaments in composite structures. If multiple oriented fibre arrays are utilised to solve the problem of low stiffness in the transverse direction, a decrease in the major stiffness of the fibrous composite follows.

4.5.1.2 Concentration of applied stress

Contours of the direct stress and Von Mises stress are obtained for fibre reinforced composites as shown in *figures 4.45a-b.* These contour diagrams indicate that the

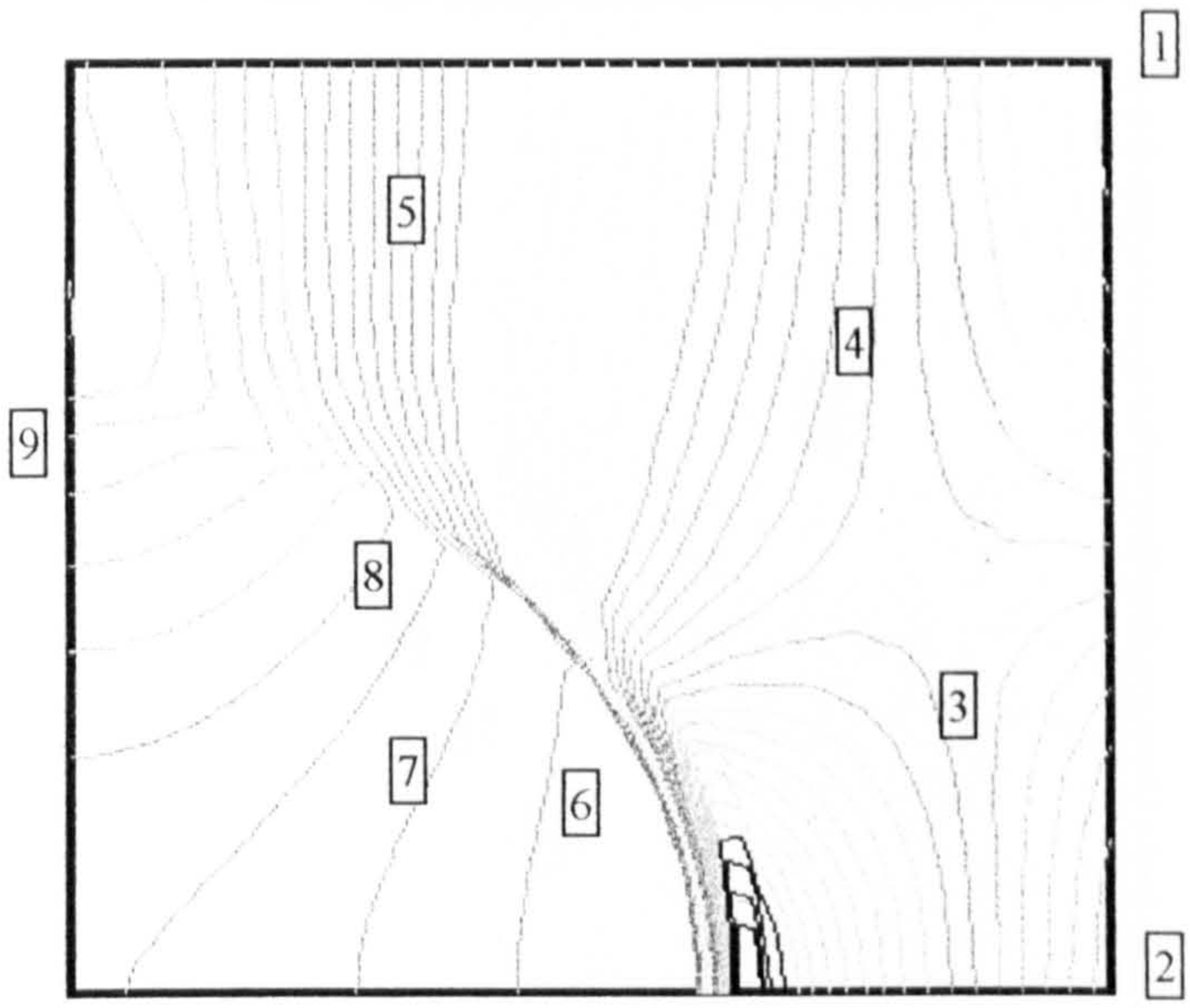

1	.125E7
2	.246E7
3	.367E7
4	.196E7
5	.189E7
6	.387E7
7	.403E7
8	.428E7
9	.186E7

Fig 4.45a : Contour diagram of the direct stress field for the fibre reinforced composite

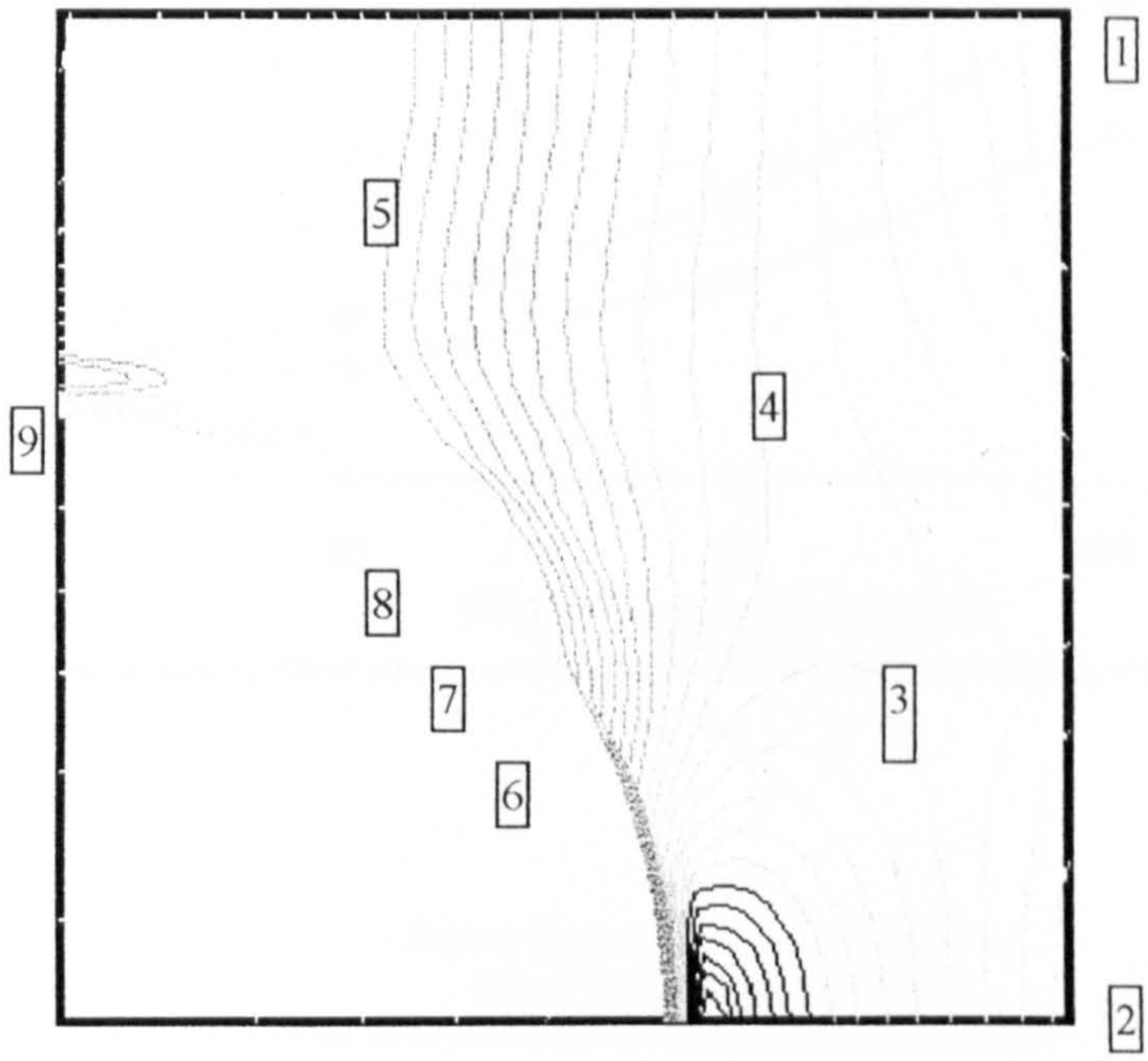

1	0.889E6
2	0.174E7
3	0.137E7
4	0.104E7
5	0.267E7
6	0.197E7
7	0.301E7
8	0.319E7
9	0.269E7

Fig.4.45b: Contour diagram of the Von Mises stress field of the continuous fibre reinforced composite with 30% of fibres.

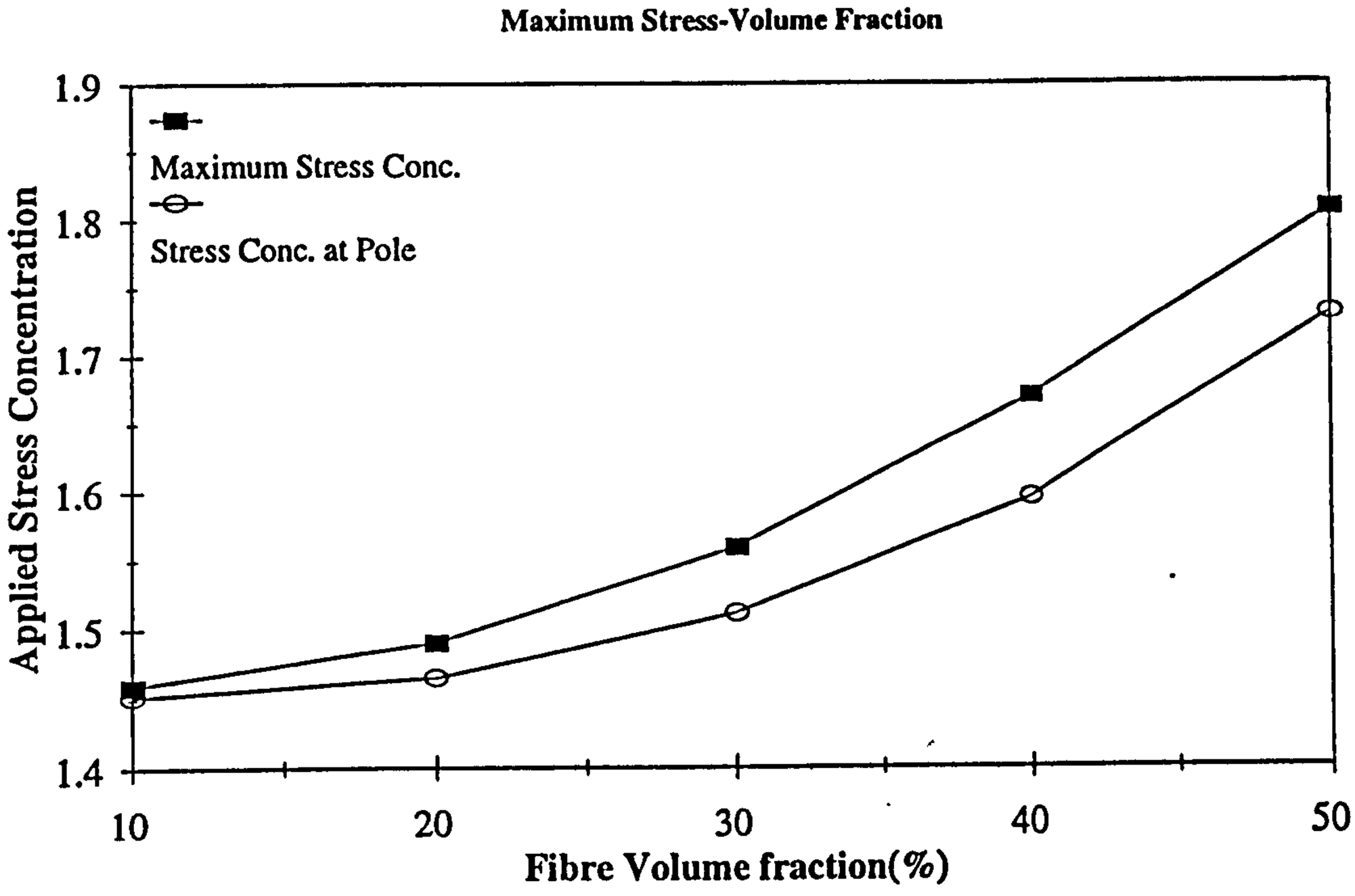

Fig.4.46: The maximum applied stress concentration in the matrix and at the pole of the fibre reinforced composite

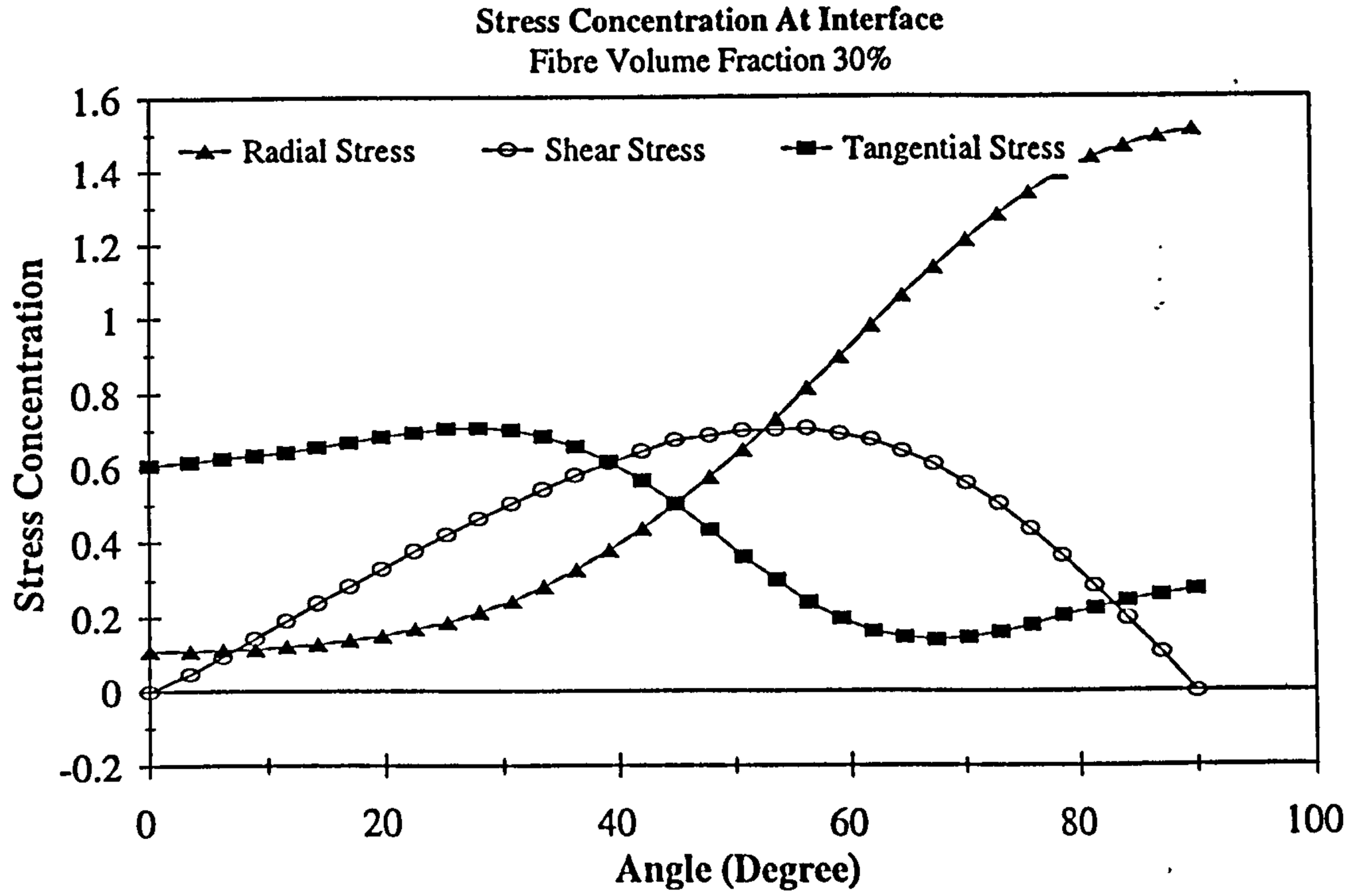

Fig.4.47: Stress concentration at the interface of fibre and matrix for the 30% volume fraction of fibre reinforced composite.

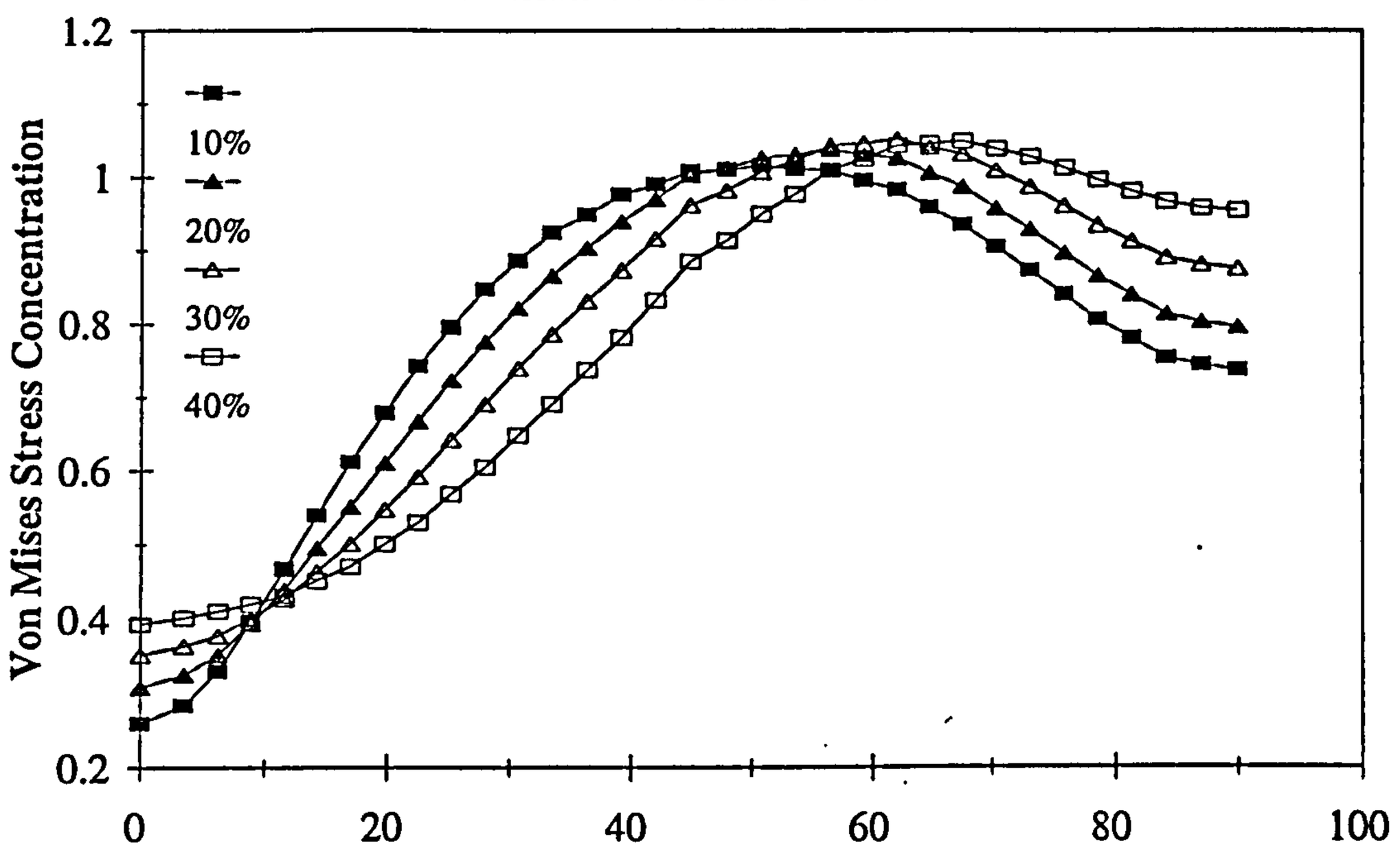

Fig.4.48: Von Mises stress Concentration at interface of fibre and matrix for different fibre volume fractions.

concentration of applied stress in the matrix for a typical fibre reinforced composite is very similar to that of a particulate filled composite. *Figure 4.46* indicates that the maximum concentration of the applied stress is in the matrix above the pole. The precise position of maximum concentration varies for different fibre volume fractions. For higher volume fractions of fibre the position of the maximum is at the edge of the grid, centred between neighbouring fibres. However this maximum is not much higher than the stress concentration at the pole. Since the failure strength of the interface is expected to be lower than failure strength of the resin, the stress concentration at the interface is considered to be more important for the study of the fracture behaviour than the stress concentration above the pole. The stress distribution in the fibre is almost constant for all volume fractions. The stress concentration reaches a small maximum at the pole. The concentration of stress may lead to failure via the failure of the fibres in the transverse direction.

The values of the stress concentration increase with increasing volume fraction of fibres for both matrix and fibre. This result is expected and may be attributed to increasing interactions between the stress fields as the inter-fibre separation decreases. It means that increasing disorder increases the stress concentration.

4.5.1.3 Stresses at interface

Stresses in the xy plane around the interface within the fibre and matrix were extracted and transformed to polar coordinates. The results for 30% volume fraction of fibres are shown in *figure 4.47*.

The trend of these results is a stringent check of the accuracy of the finite element analysis. *Figure 4.47* shows that the necessary conditions are, in general, well satisfied. Shear stress is zero at the pole and equator. The maximum stress at the interface is the radial stress at the pole. The results shown in *figure 4.47* are comparable with the results obtained for composites filled with spherical particles.

The variations of Von Mises stress at the interface for different volume fractions of fibres are shown in *figure 4.48*. The value of the maximum Von Mises stress concentration increases slightly for the range of the volume fraction studied and is

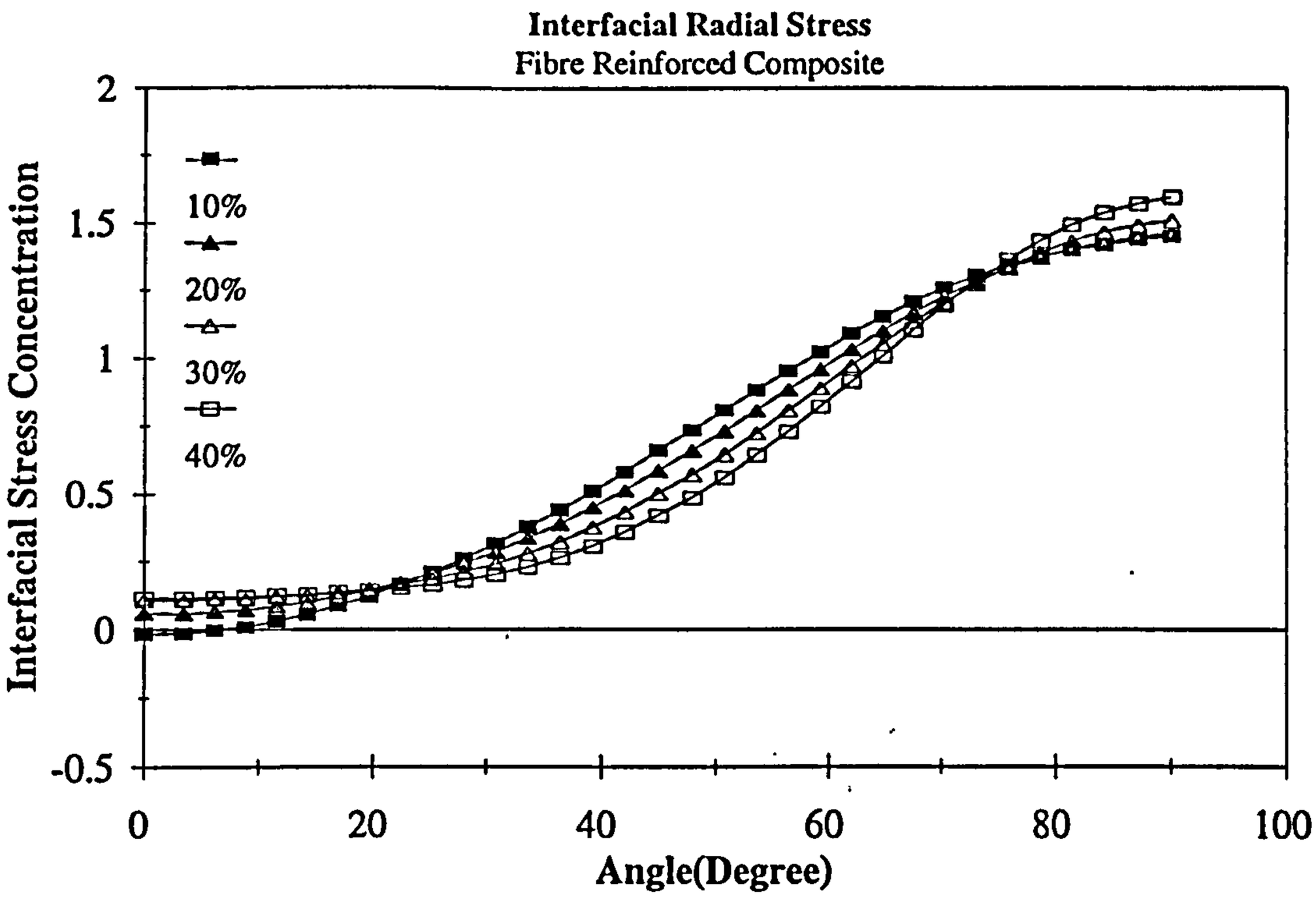

Fig.4.49: Radial stress concentration at the interface of the fibre and matrix for composites with different fibre volume fractions

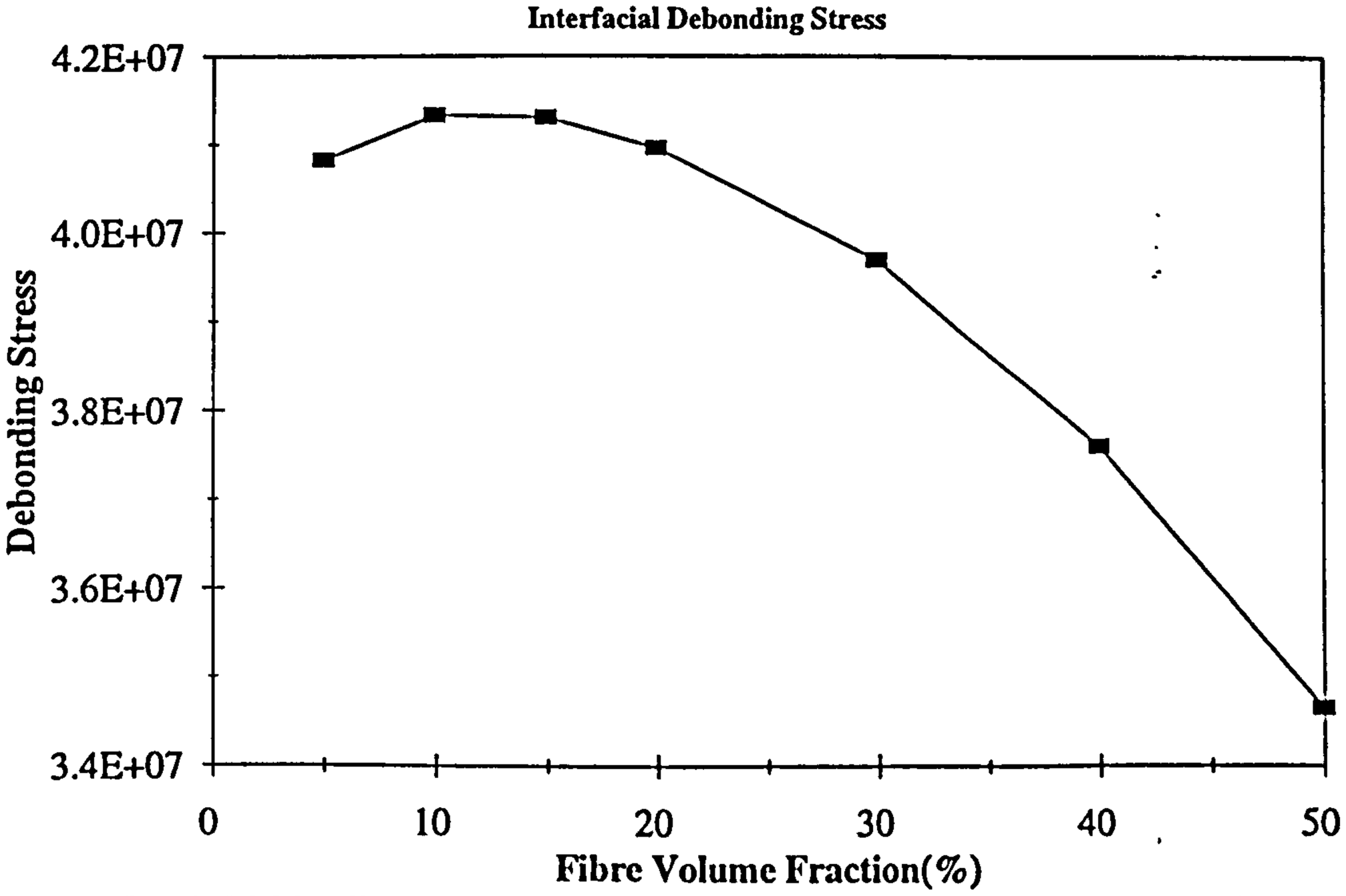

Fig.4.50: Interfacial debonding stress versus volume fraction of fibres for fibre reinforced composites

almost constant. However, the position of the maximum at the interface moves from about 40° at low volume fraction towards the pole for the higher volume fractions.

4.5.1.4 Fracture strength

The overall stress distribution for the matrix and fibre may be used to deduce the failure mechanisms of this type of composites. It is assumed that failure is essentially brittle, and takes place when local stress reaches a critical level. The concentration of the stress in the fibre may lead to failure via transverse splitting of the fibres. The concentration of applied stress in the radial direction at the interface may lead to tensile failure of the interface. The radial stress variations at the interface are shown for different volume fractions in *figure 4.49*. The position of the maximum is at the pole over the range of the volume fraction. The increasing values of stress concentration with volume fraction imply a reduction in overall applied stress required for failure. Thus the fracture strength of the material is predicted to fall with increasing fibre volume fraction. Although the rise of the maximum stress concentration is relatively slow.

The transverse strength of the glass fibres is about 2758 MPa which is much higher than that of the epoxy resin which is about 60 MPa (Gibson, 1994). Since the concentration of applied stress at the pole is the same in the fibre and the matrix at the interface, failure is predicted to occur at the interface at the pole via failure of the matrix. Assuming the strength of the interface equals the strength of the resin (i.e. assuming good bonding), the overall applied stress for which the interface failure is expected can be calculated from the concentration of the radial stress at the pole.

The initiation of a fibre/matrix debond is analysed using an interfacial failure criterion, proposed by Sun and Zhou (Sun and Zhou, 1988) for free edge delamination of composite laminates, which here is modified to accommodate the cylindrical geometry of the fibre matrix interface,

$$\left(\frac{\sigma_r}{R}\right)^2+\left(\frac{\tau_{r\theta}}{S}\right)^2=1 \qquad (4.16)$$

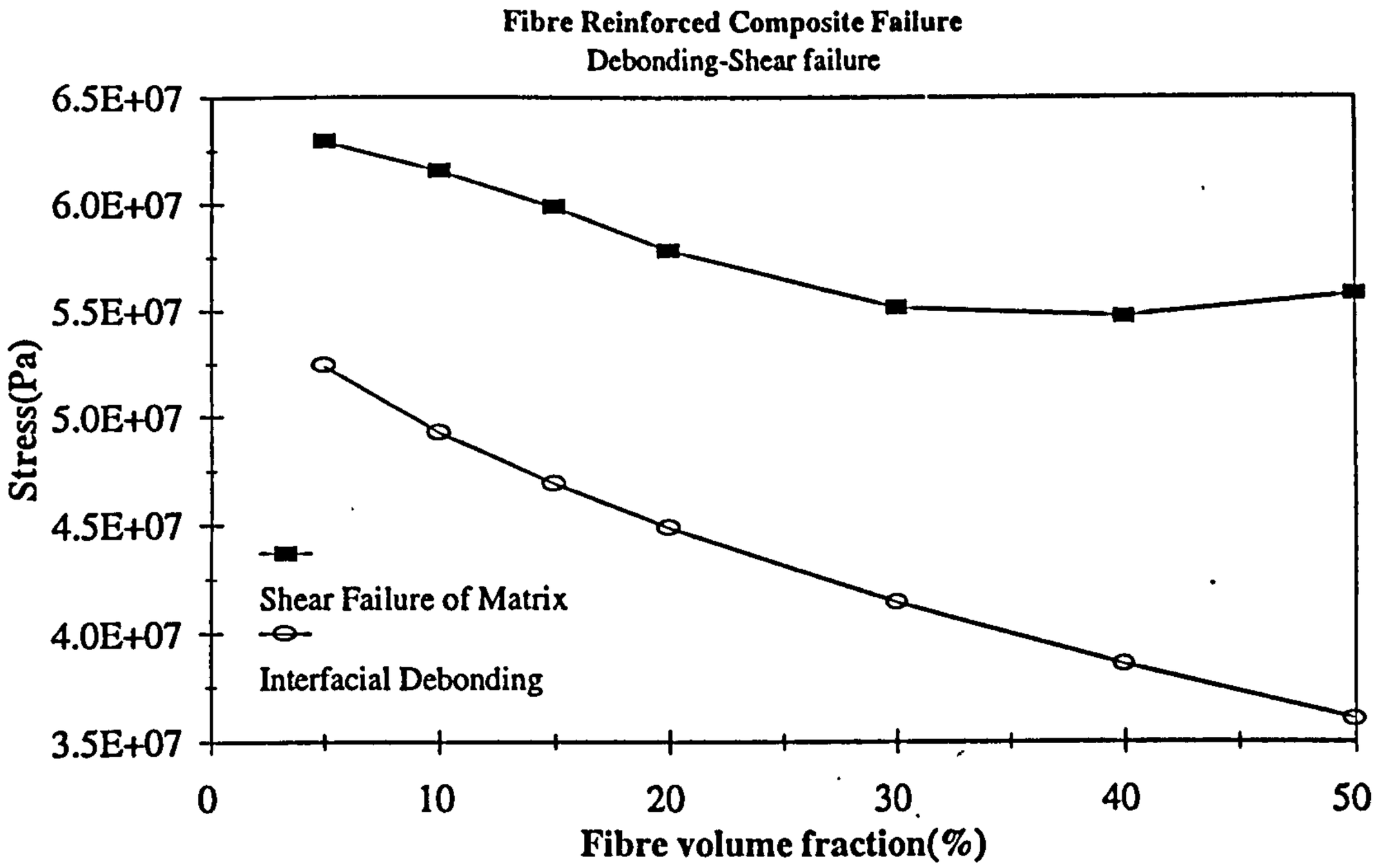

Fig.4.51: Comparison of the stresses required for interfaial debonding and matrix failure at different volume fractions of fibre.

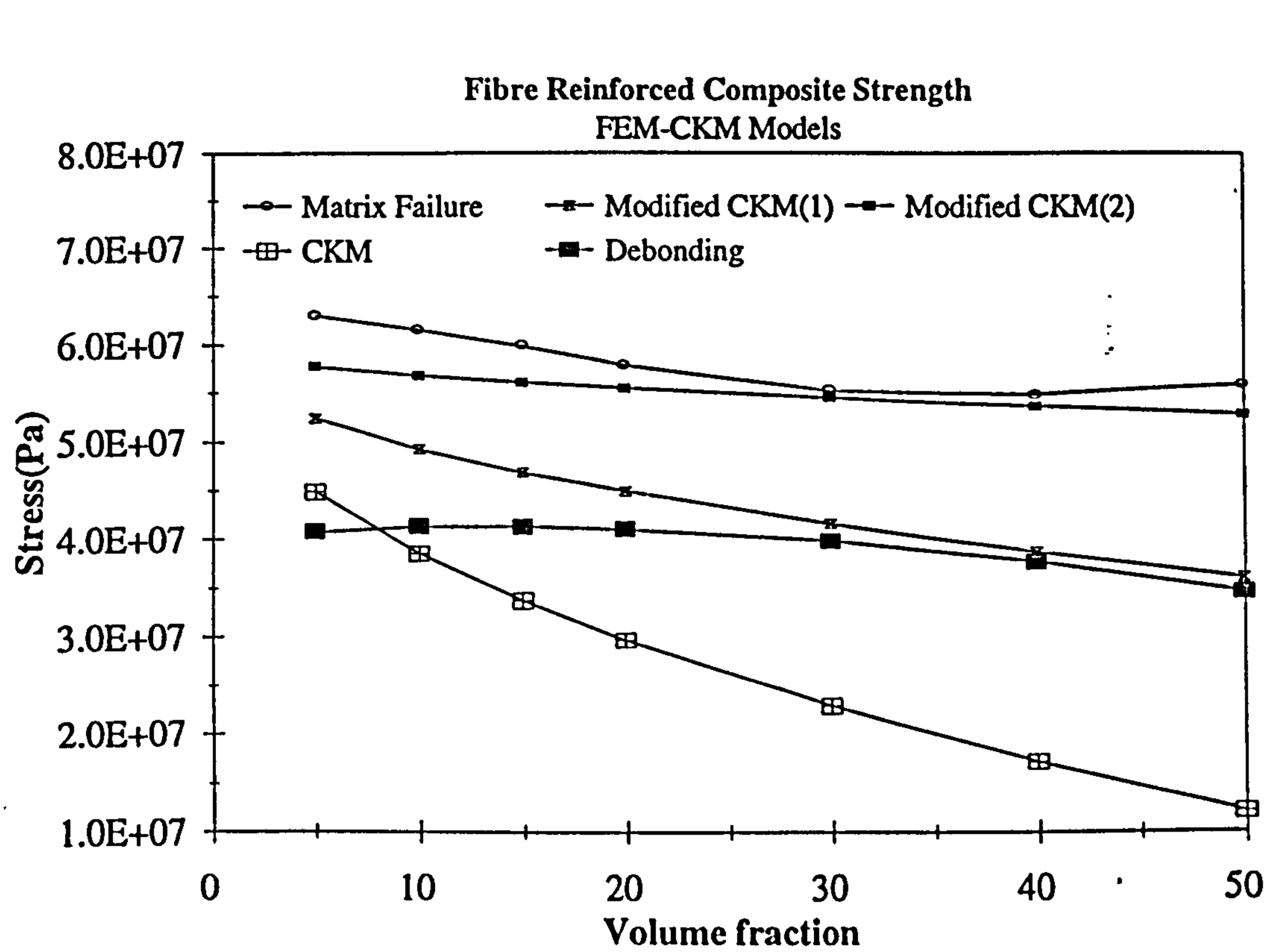

Fig.4.52: Prediction of the failure of the composite by FEM and CKM models (1): Si =0.5.Sm , (2):Si=0.85.Sm

where σ_r and $\tau_{r\theta}$ are the normal (radial) and shear interfacial stresses, respectively, and R and S are the corresponding interfacial strengths with respect to tension and shear. Debond failure resulting from any combination of stresses is thus expected to occur when the left hand side of *equation 4.16* is equal to or greater than unity. Since the values of R and S are not available, in order to define the failure criterion ideal bonding is assumed by taking the values of R and S as the tensile and shear strength of the matrix.

A failure hypothesis may be defined by assuming that the ultimate transverse failure of the composite occurs in response to an externally applied stress once an interfacial debond forms. A debond initiating stress, is the tensile stress necessary to make the left hand side of the interfacial failure criterion equal to unity. The maximum interfacial radial stress occurs in the direction of the applied stress at the pole, while the interfacial shear stress is zero at this angle. Since the maximum interfacial shear stress is less than the maximum interfacial radial stress and the interface is expected to be weaker in tension than in shear, the radial stress will govern the initiation of a debond. The applied stress capable of initiating interface debonding for different fibre volume fractions are calculated and presented in *figure 4.50*. As it can be seen in this figure the applied stress required to initiate debonding decreases with increasing volume fraction of fibres.

In composites with a weak interface and/or ductile matrix, the transverse strength of the composite is expected to be more closely linked to the strength of the matrix. This is specially true if the failure of the matrix is analysed using Von Mises failure theory which is based on the definition of Von Mises stress expressed as:

$$\sigma_e = \frac{1}{\sqrt{2}}\left[(\sigma_1-\sigma_2)^2+(\sigma_2-\sigma_3)^2+(\sigma_3-\sigma_1)^2\right]^{1/2} = \sigma_m \qquad (4.17)$$

where σ_e is the effective stress, σ_i (I=1,2,3) are the principal stresses, and σ_m is the tensile strength of the matrix. The Maximum Von Mises stress and the tensile strength of the matrix are used to calculate the strength of the composite for the range of volume fraction of the fibre. These results are shown in *figure 4.51*. In *figure 4.51* a

comparison of the applied stresses initiating the debond failure and the stresses calculated from the Von Mises criterion are made. The stress initiating the debonding calculated using *equation 4.16* is less than the stress obtained by Von Mises criteria for all volume fractions.

Transverse failure stresses are also calculated using Cooper-Kelly model (CKM) (Cooper and Kelly, 1969) developed for the prediction of transverse strength of the composite. For a composite with a weak interface, the matrix will fail at the minimum matrix cross section at the equator in response to an external stress given by the following equation:

$$S_c^T = \sigma_m\left(1-\sqrt{4\frac{V_f}{\pi}}\right) \tag{4.18a}$$

where S_c^T is the transverse strength of the composite, V_f is the volume fraction of the fibres and σ_m is the tensile strength of the matrix. If the fibre/matrix interface strength is taken into account, the CKM is modified to .

$$S_c^T = \sigma_m\left(1-\sqrt{4\frac{V_f}{\pi}}\right)+\sigma_i\sqrt{4\frac{V_f}{\pi}} \tag{4.18b}$$

where σ_i is the average tensile stress necessary to separate the fibre from the matrix. It should be noted that in the limit when $\sigma_i = \sigma_m$ *equation 4.18b* can be considered to be the upper limit of the transverse strength of the composite.

In *figure 4.52* the strength of the composite obtained by Cooper-Kelly model can be compared with the results of our model for debonding failure and Von Mises failure. The curve obtained from *equation 4.18a* lies much lower than the other predictions on the same graph. When the value $\sigma_i = 0.5\sigma_m$ is used, the results of the *equation 4.18b* is close to the interface debonding curve. Raising the interfacial strength value to $\sigma_i = 0.85\sigma_m$ via *equation 4.18b* gives a variation which is in good agreement with the prediction of our model based on Von Mises criteria.

The experimental transverse tensile strength at the 53% volume fraction is $37_{\pm}$ 4.6 MPa (Pomies, 1992). The transverse tensile strength is predicted by our model at 50%

volume fraction as 35MPa for interface debonding and 56 MPa for matrix yielding. Our model predictions using interface debonding mechanism is in perfect agreement with the experimental results. This confirms that the interface debonding and brittle failure are the dominant mechanism governing the failure of the fibre reinforced composite in this case.

4.5.2 Transverse shear loading

4.5.2.1 Modulus

A shear loading in the transverse direction of the fibre is applied to the composite. The transverse shear modulus of continuous glass fibre reinforced epoxy is given in *figure 4.53*. Both square and hexagonal arrays are examined. The results of square array are in close agreement with the results calculated from Halpin-Tsai model (Halpin and Tsai, 1969). In the case of hexagonal array, both constrained and unconstrained boundary conditions are investigated. The hexagonal array shows less reinforcement at the same volume fraction compared to the square array. The unconstrained boundary condition gives lower values for the transverse shear modulus.

4.5.2.2 Stress distribution and strength

The stress distribution at the interface of the fibre and matrix is shown in *figure 4.54* for the 30% volume fraction of continuous fibres. The maximums of the shear and Von Mises stress concentrations are found at the pole of the fibre. The maximum of the radial stress is at 45°.

The distribution of Von Mises stress concentration is presented in *figure 4.55* for different volume fractions. The maximum of the Von Mises stress concentration occurs at the pole. The Von Mises stress distributions found for different volume fractions are very close to each other and a slight decrease in the maximum value is observed as the volume fraction increases.

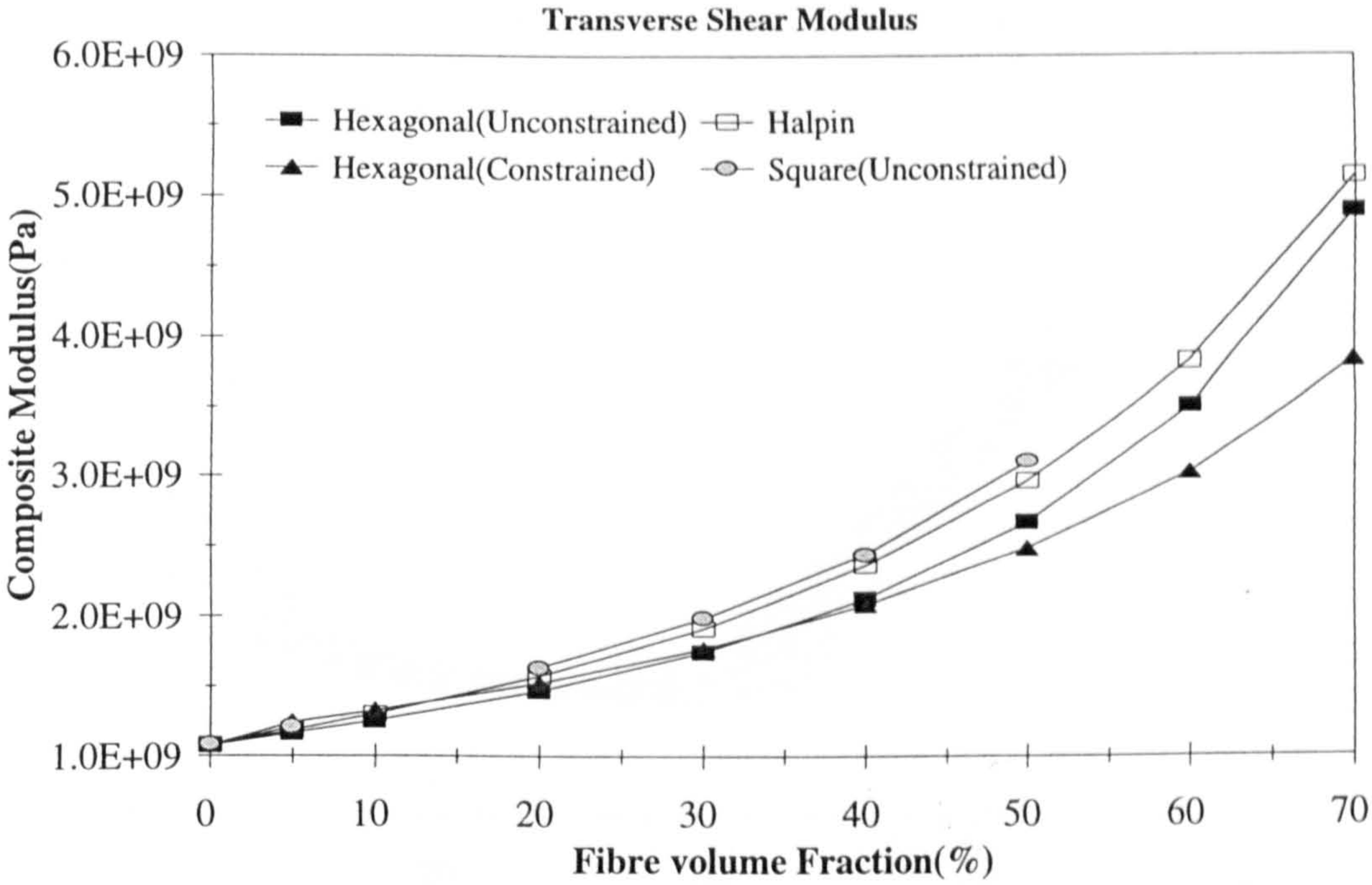

Fig.4.53: Transverse shear modulus at the range of volume fraction for continuous fibre reinforced composites

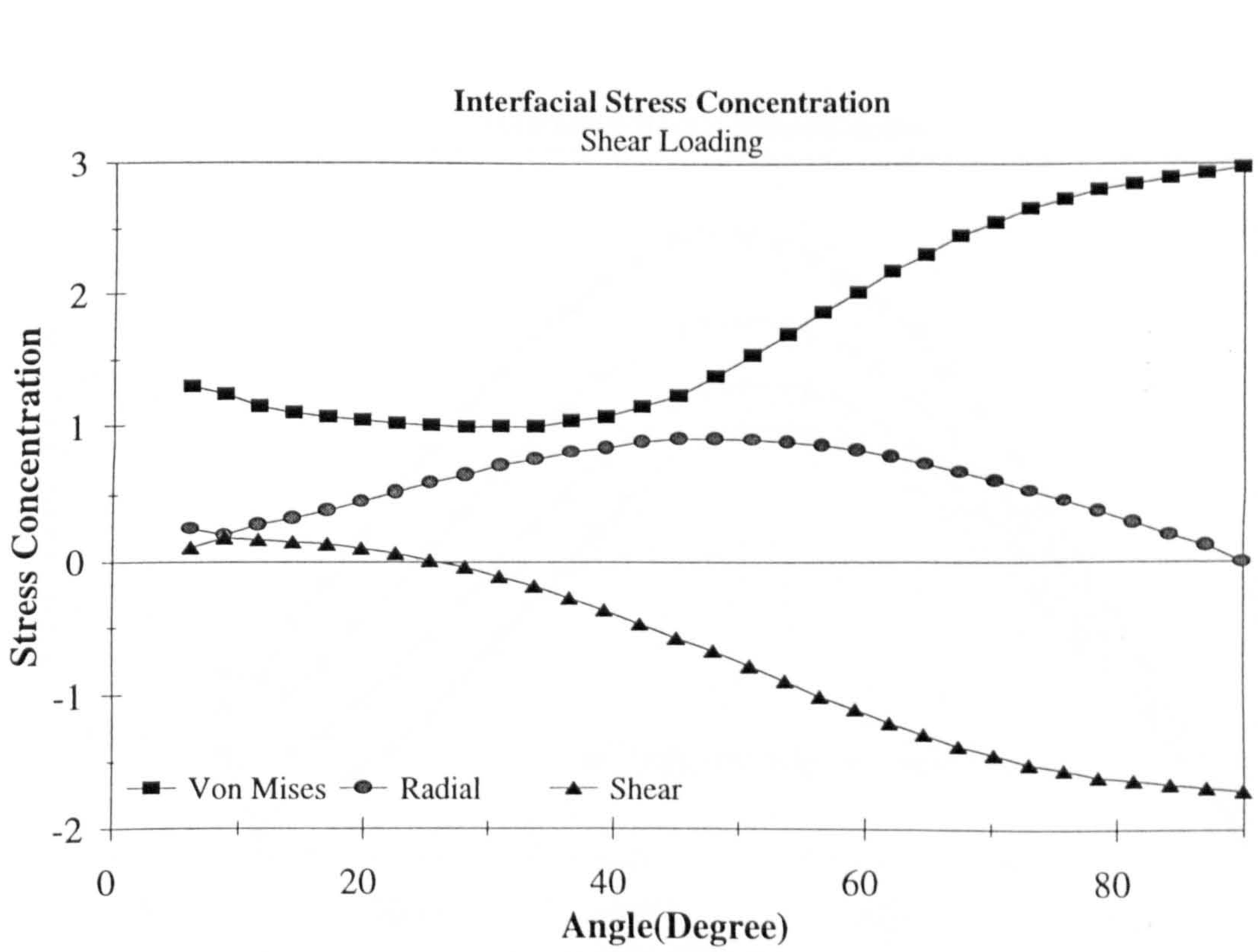

Fig.4.54: Interfacial stress concentration for 30% fibre volume fraction of continuous fibre reinforced composite.

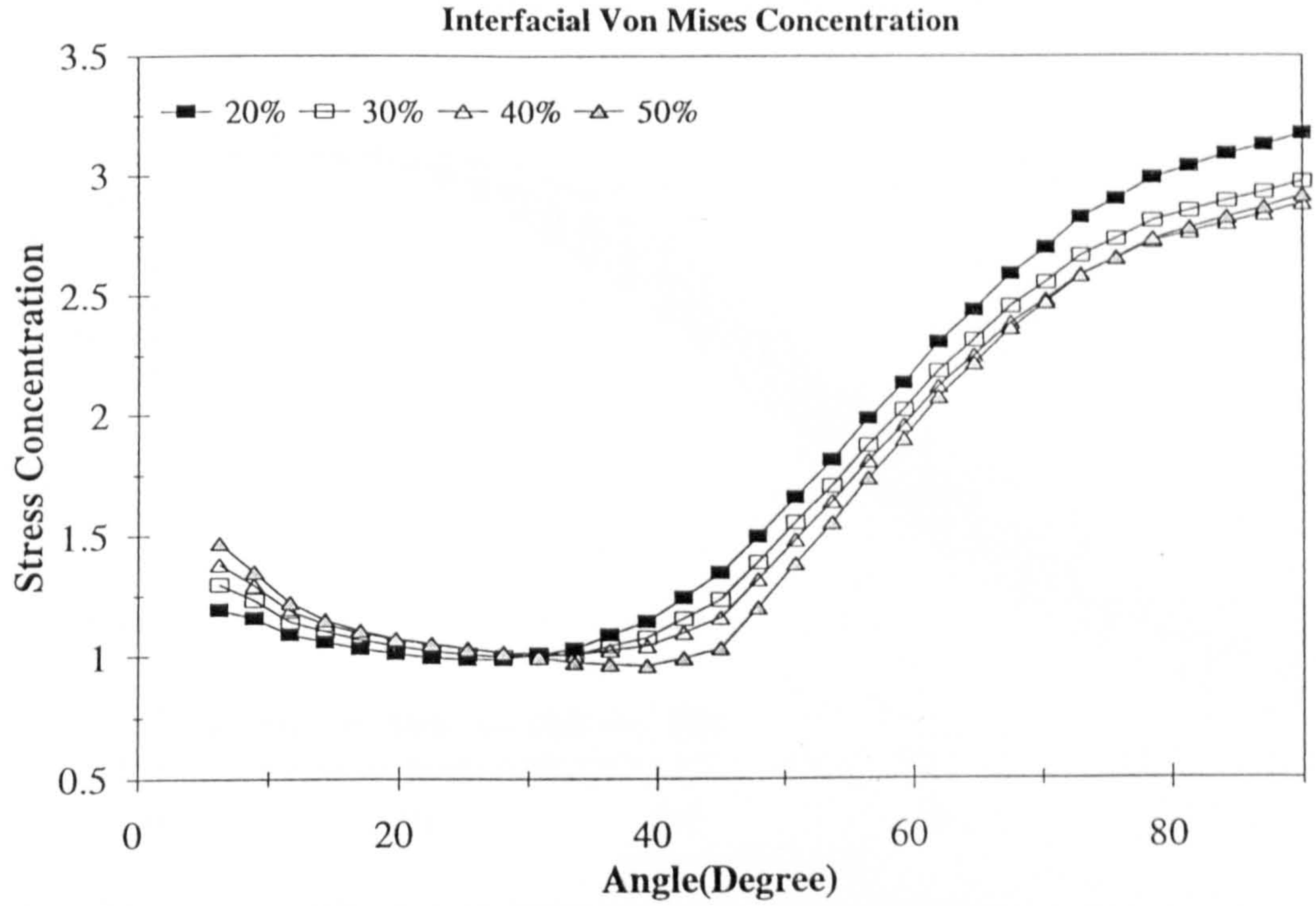

Fig.4.55: Interfacial Von Mises stress concentration for different fibre volume fractions of fibre reinforced composite.

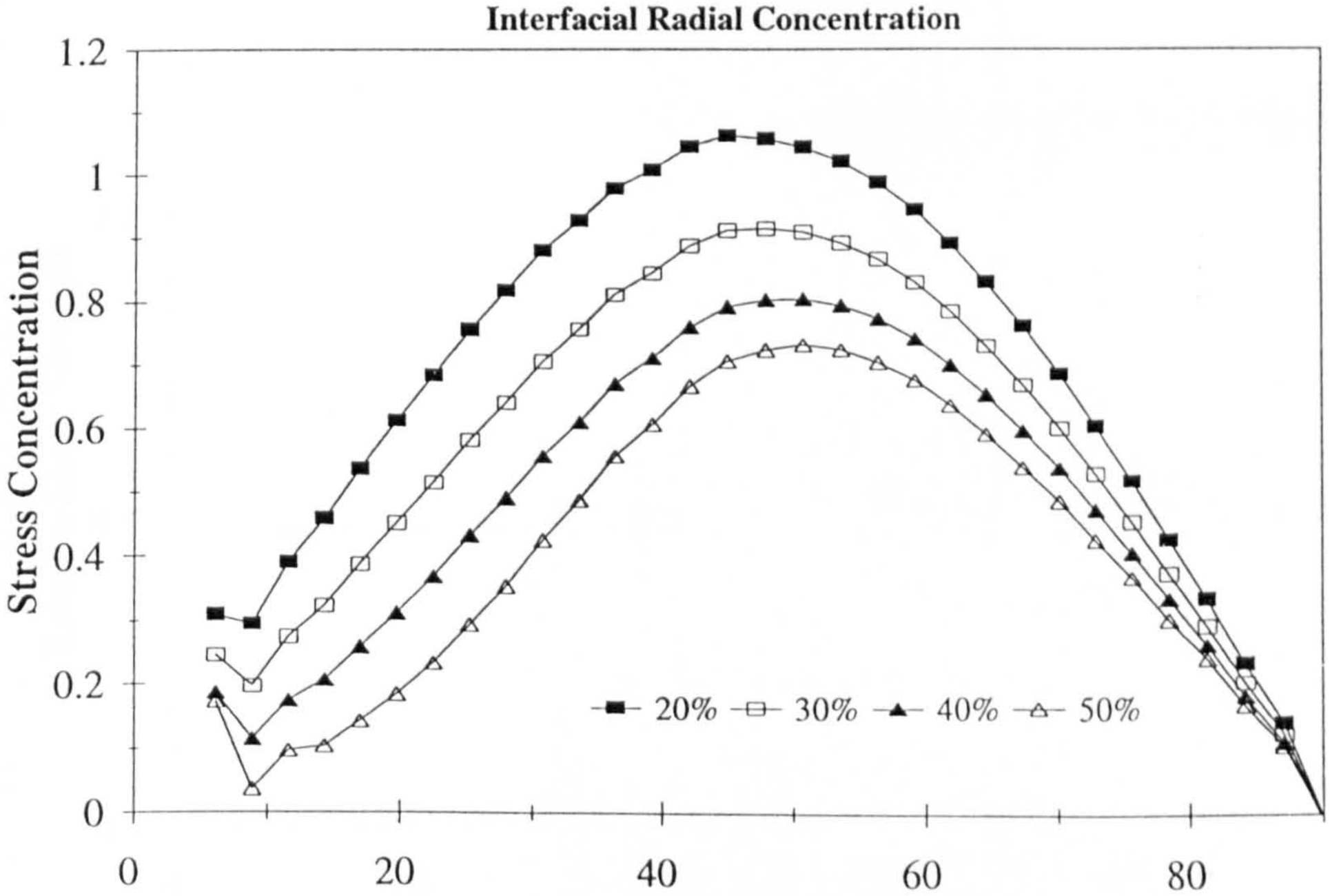

Fig.4.56: Interfacial radial stress concentration for different fibre volume fractions of fibre reinforced composite.

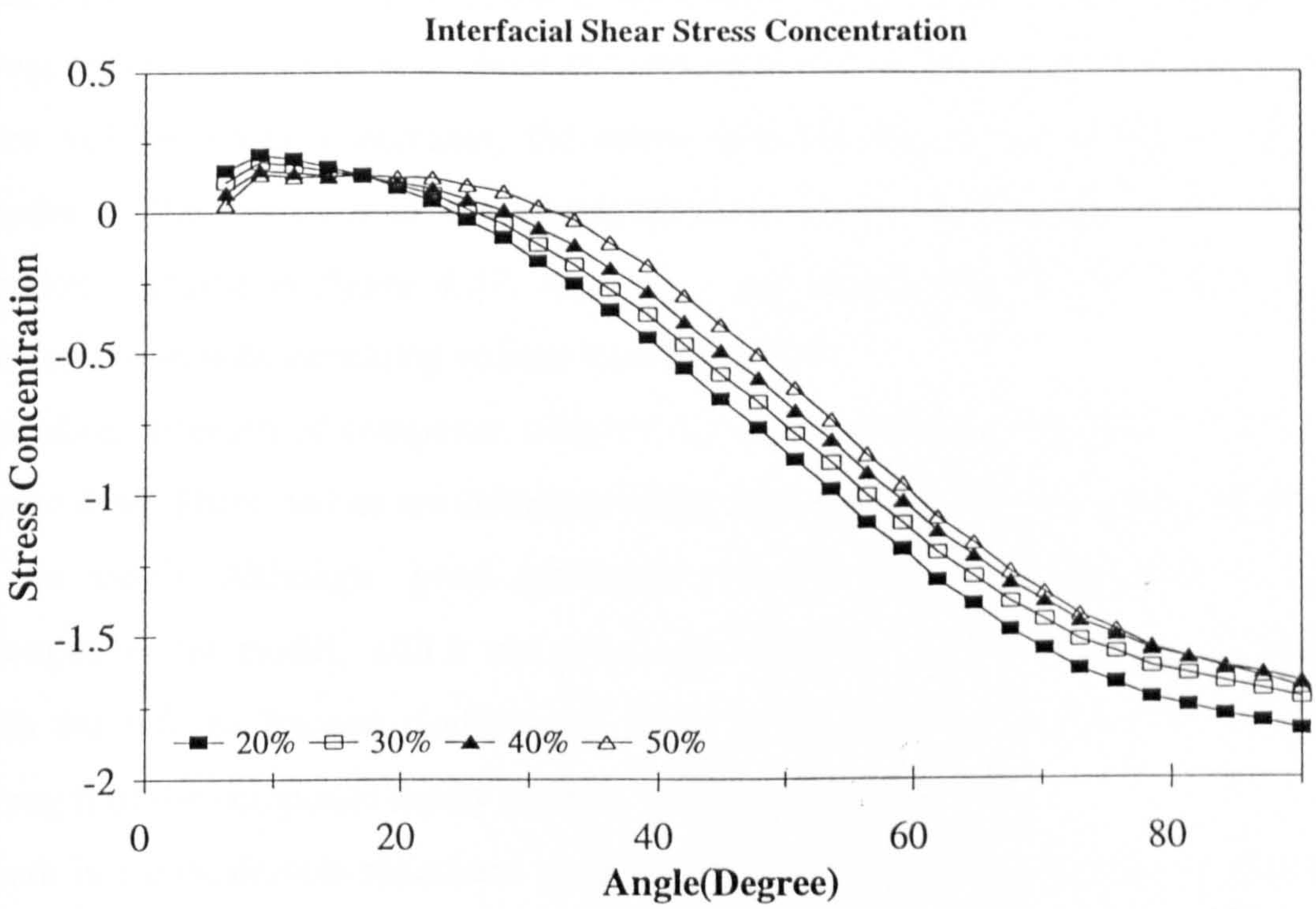

Fig.4.57: Interfacial Shear stress concentration for different fibre volume fractions of fibre reinforced composite

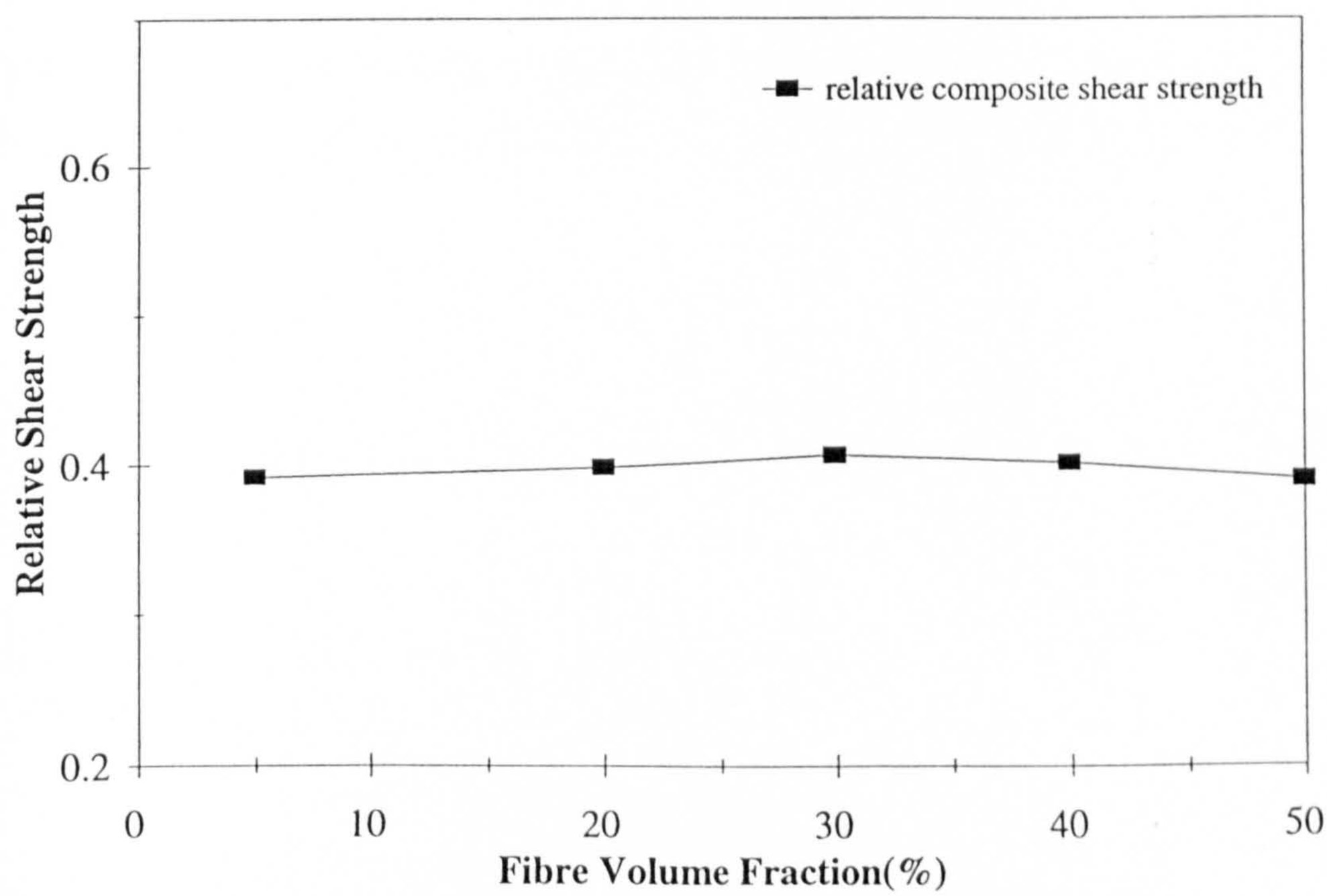

Fig.4.58: Transverse shear strength of continuous fibre reinforced composite.

The distribution of the radial stress concentrations at the interface of the fibre and matrix for different volume fractions is shown in *figure 4.56*. In this case the maximum stress concentration occurs at about 45° of the pole for all the volume fractions. As the fibre volume fraction increases, the stress concentration at the interface becomes smaller. The variation of the interfacial shear stress concentration with volume fraction, shown in *figure 4.57*, indicates an insignificant increase of the stress concentration with increasing volume fraction of fibre.

The shear strength of composite obtained for different volume fractions is shown in *figure 4.58*. These values are calculated using the maximum Von Mises concentrations in the matrix. Although good quantitative predictions are not obtained for shear strength by our model, still it can give a prediction for the variation of the strength with the volume fraction qualitatively. As it can be seen in *figure 4.58* the shear strength of the composite hardly changes with the volume fraction.

There is a considerable resistance to shear fracture of the fibres. Hence this mode of fracture is unlikely to occur and matrix failure can be blunted by fibres.

4.6 SHORT FIBRE REINFORCED COMPOSITES

4.6.1 Modulus

The model results obtained for Young's modulus of fibre reinforced composites show that it strongly depends on the geometrical arrangement of the fibres within the matrix. This arrangement is characterised by the volume fraction of fibres, the fibre aspect ratio and the fibre spacing parameter. Here we assume that the fibres are distributed uniformly in the matrix and there is no overlapping of the fibre ends. Under this condition the tensile load is transferred between cells only through the end sections of the cells.

In *figure 4.59* the Young's modulus of glass-epoxy composite obtained using the finite element analysis is compared with the values calculated from the shear lag model over a range of the volume fraction. The aspect ratios of the glass fibres and cell are equal to 5 in these calculations.

In the shear lag model it is assumed that the stress is transferred from matrix to fibre via the interfacial shear stresses. In modified shear lag model the transfer of normal stress across fibre ends is also considered and the force balance equation is modified. The shear lag model gives an estimate for the tensile stress in the fibres as:

$$\sigma_i = E_i \varepsilon_{3c}[1-\cosh(nz/r)\sec h(ns)] \tag{4.19}$$

and the shear stress at the interface is given using this model as:

$$\tau_i = \frac{n\varepsilon_{3c}}{2} E_i \sinh(\frac{nz}{r_o})\sec h(ns) \tag{4.20}$$

where ε_{3c} is the overall composite strain and n is a dimensional constant defined as:

$$n = \left[\frac{2E_m}{E_i(1+\nu_m)\ln(1/f)}\right]^{1/2} \tag{4.21}$$

where s is the aspect ratio, f is the volume fraction of the fibre, z is the distance from the fibre centre and r is the radial distance.

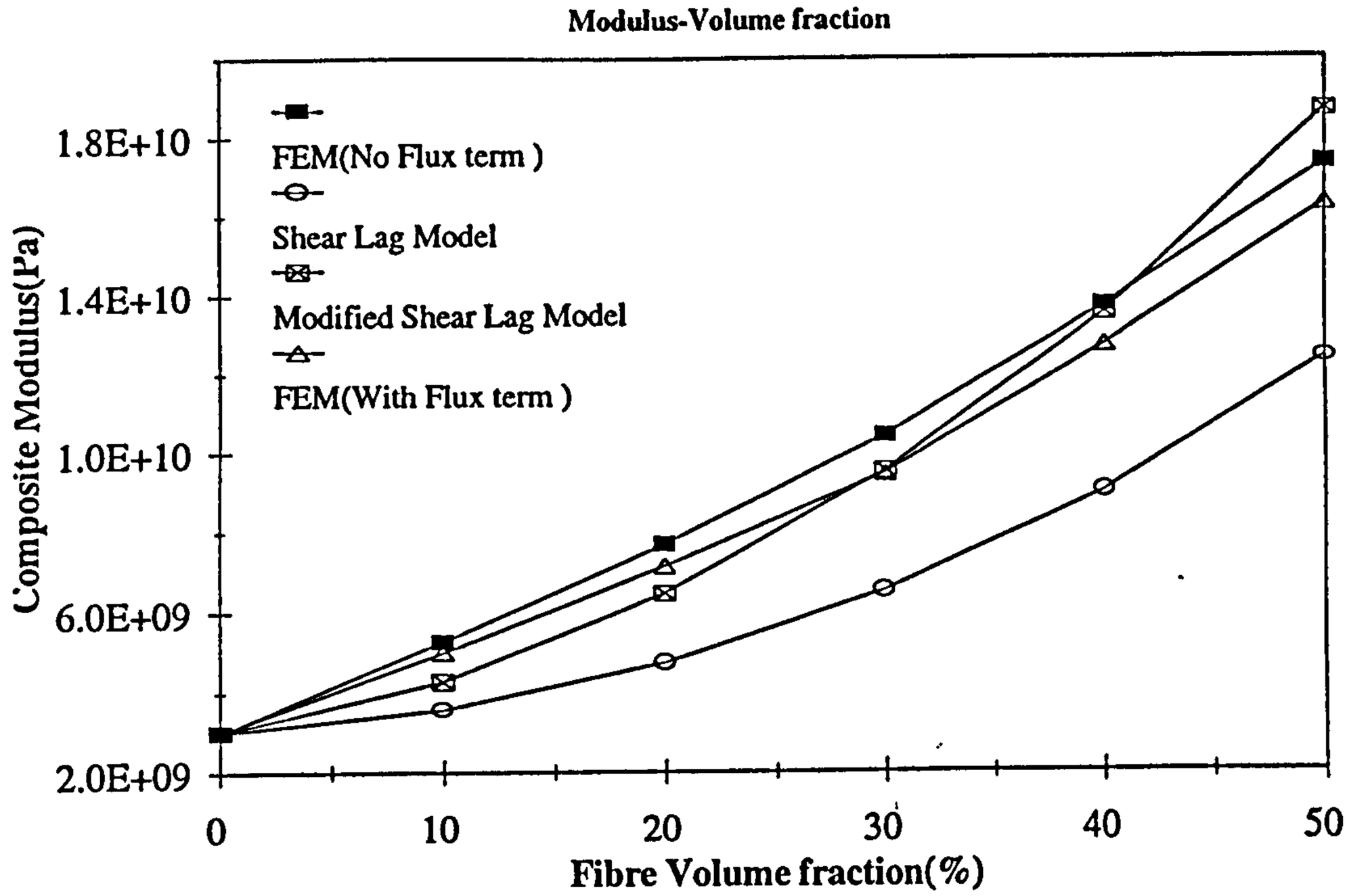

Fig.4.59: Modulus of short fibre filled composite predicted by FEM and shear lag model

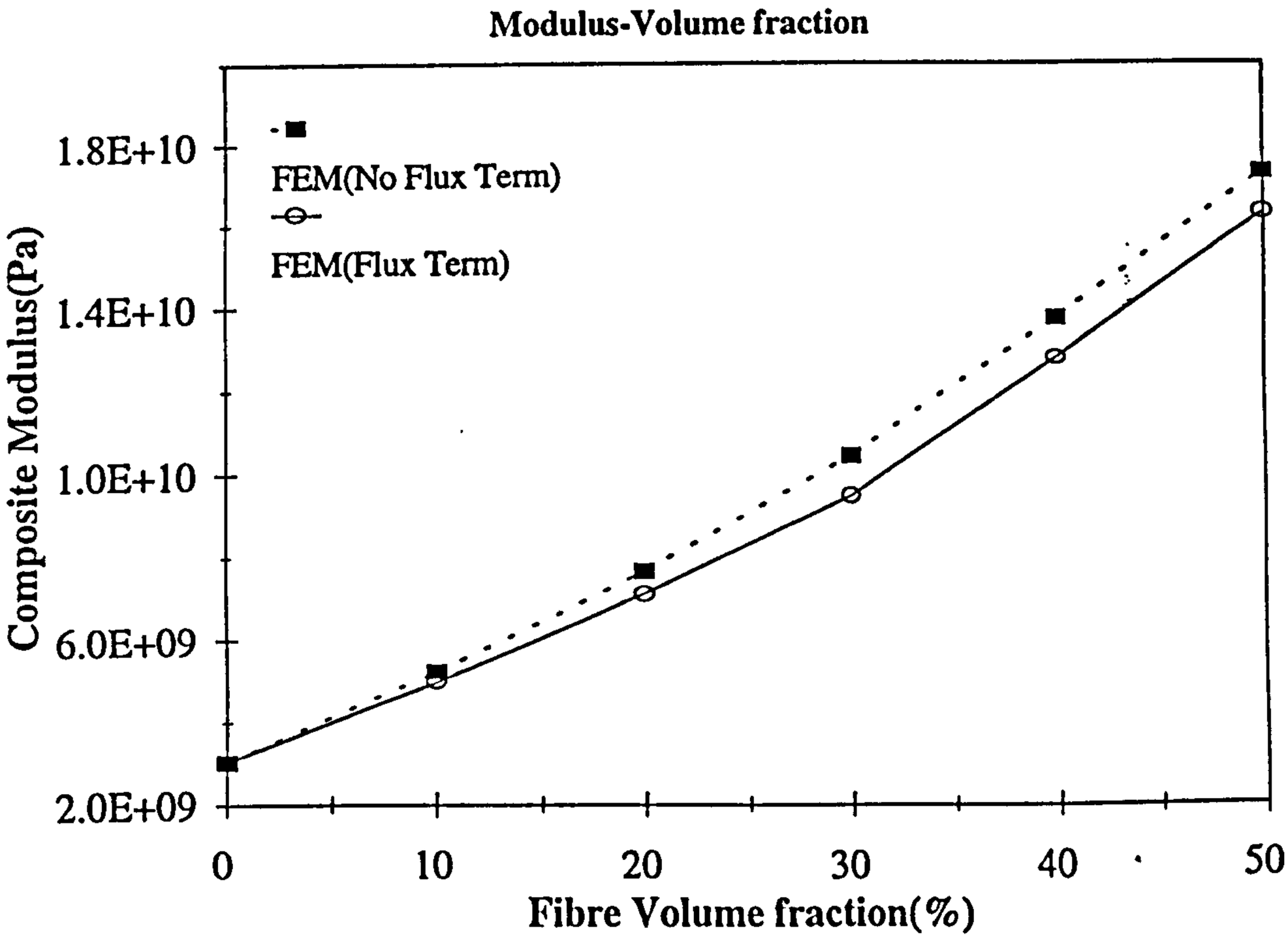

Fig.4.60: Modulus of short fibre filled composite by FEM taking flux terms into account and ignoring them.

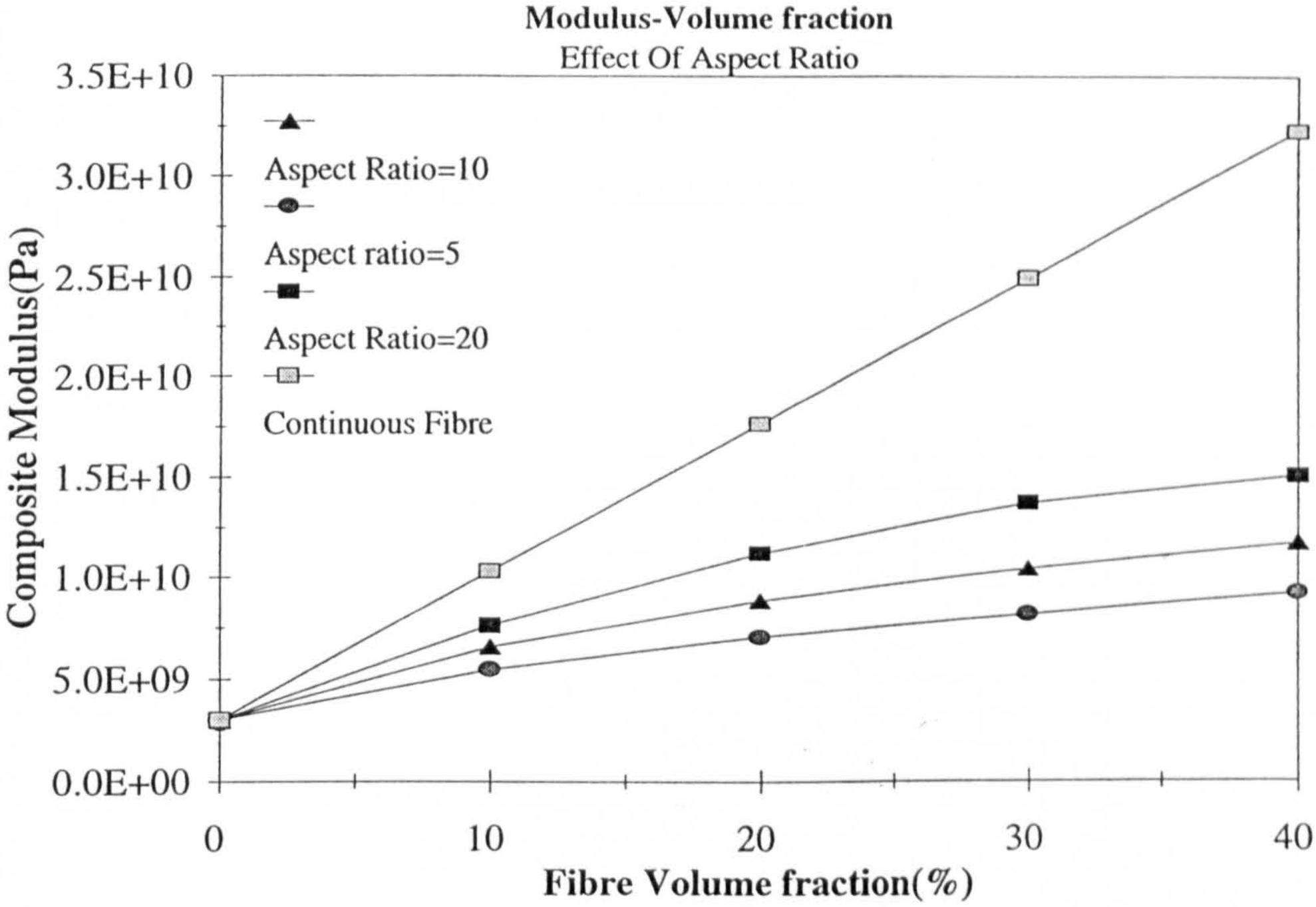

Fig.4.61: Comparison of the modulus of composite filled with fibres of 5, 10 and 20 aspect ratio and the longitudinal modulus of the continuous fibre reinforced composite

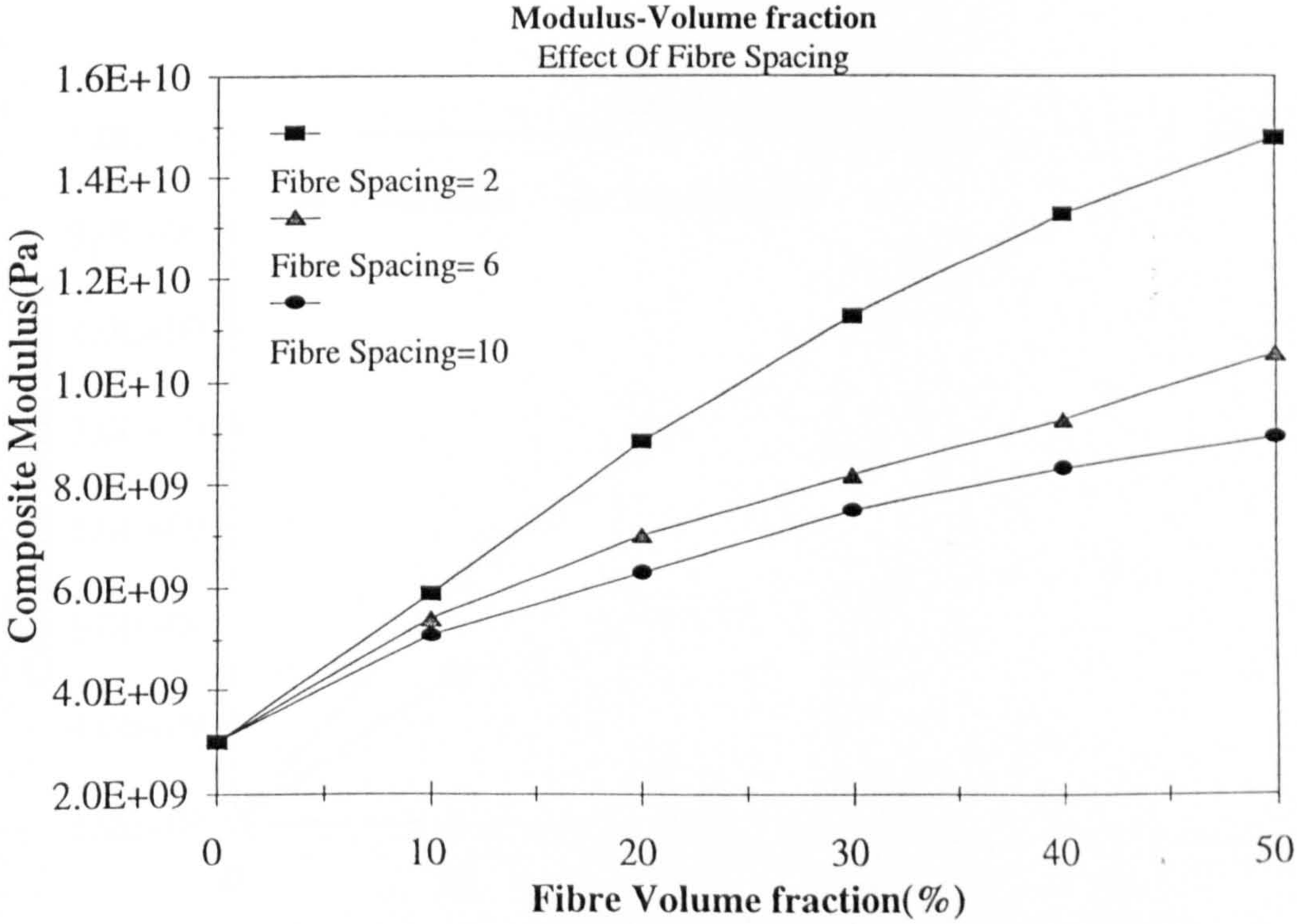

Fig.4.62:The effect of fibre spacing on the modulus of the short fibre filled composite.

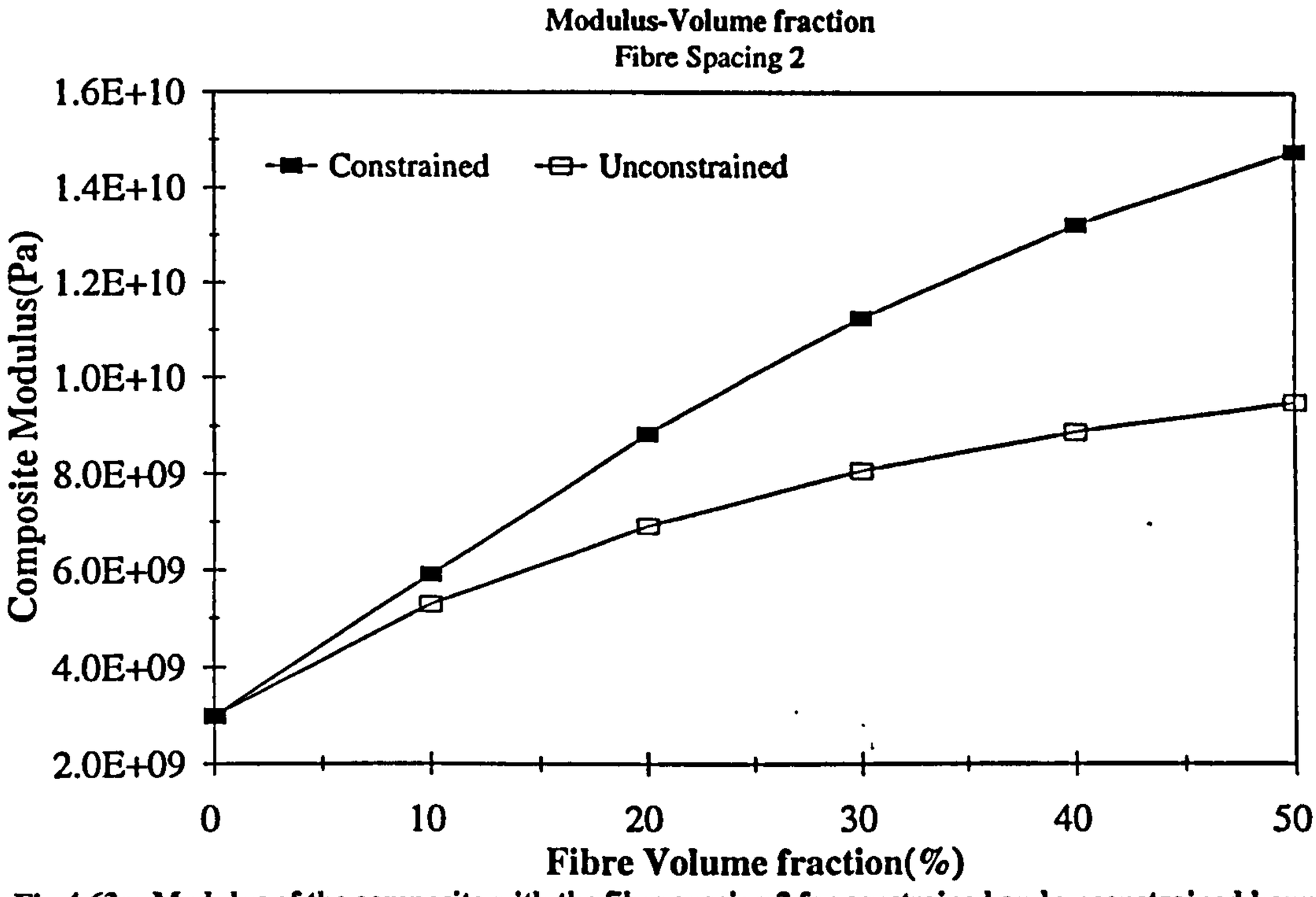

Fig.4.63a: Modulus of the composite with the fibre spacing 2 for constrained and unconstrained boundary conditions.

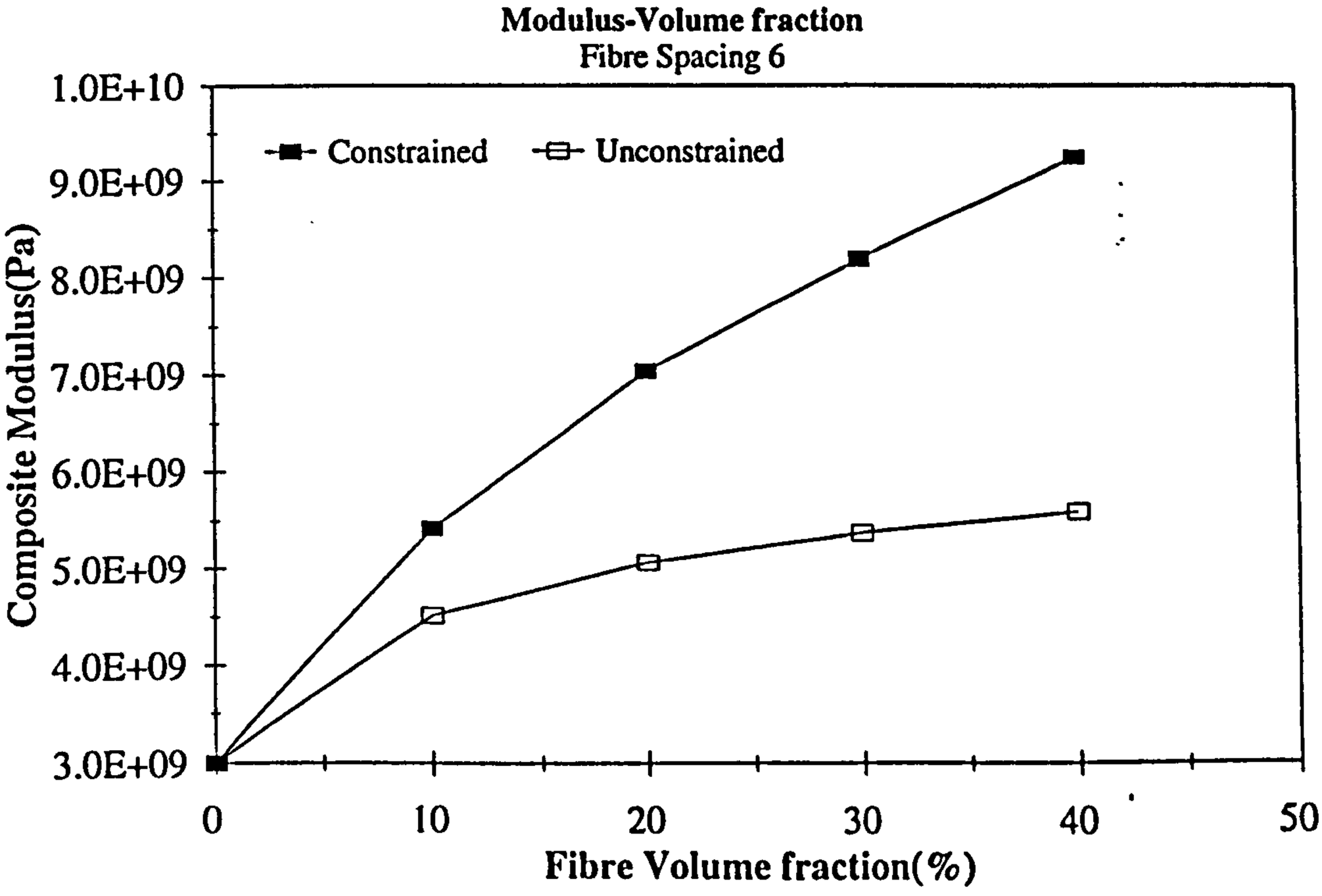

Fig.4.63b: Modulus of the composite with the fibre spacing 6 for constrained and unconstrained boundary conditions.

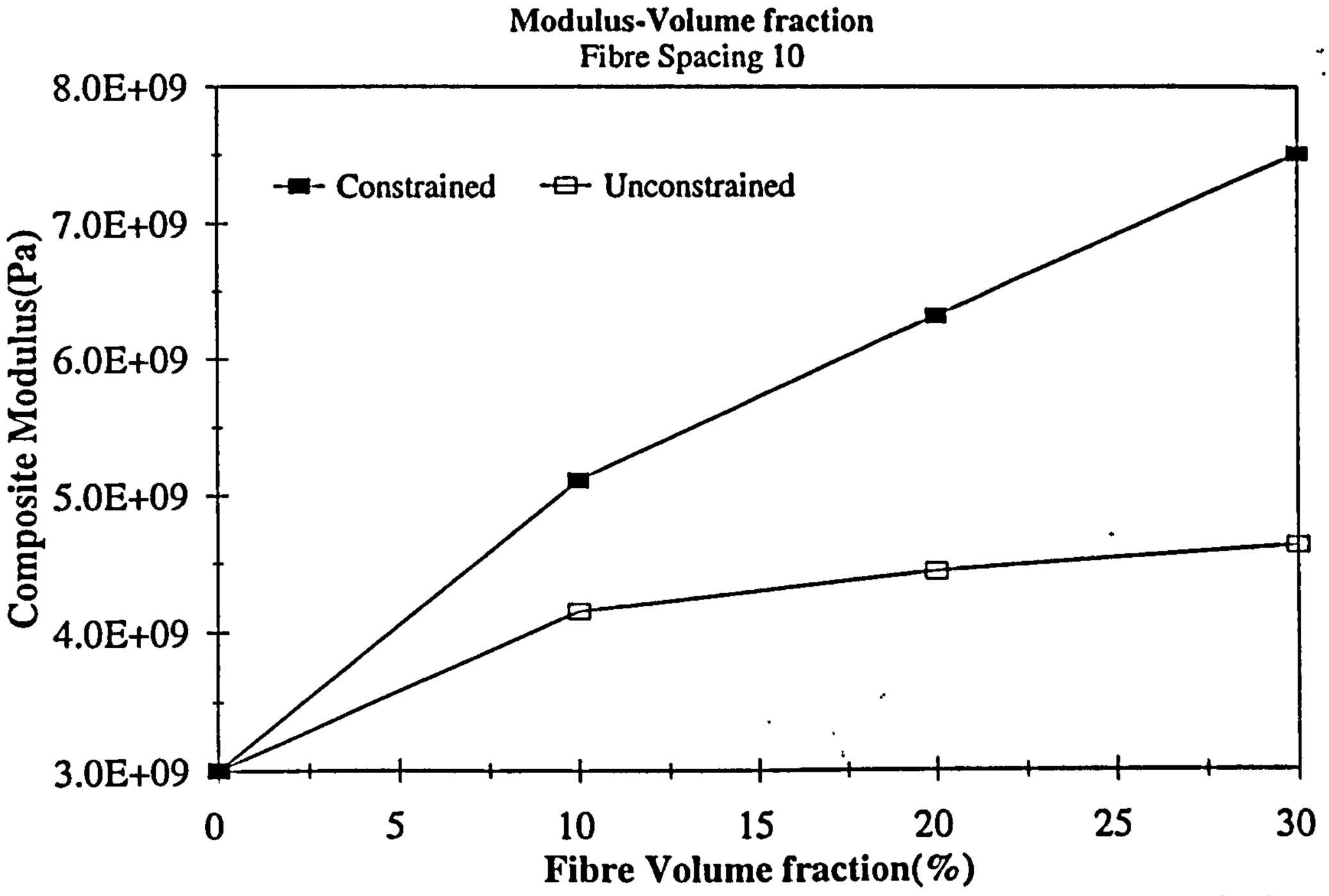

Fig.4.63c: Modulus of the composite with the fibre spacing 10 for constrained and unconstrained boundary conditions

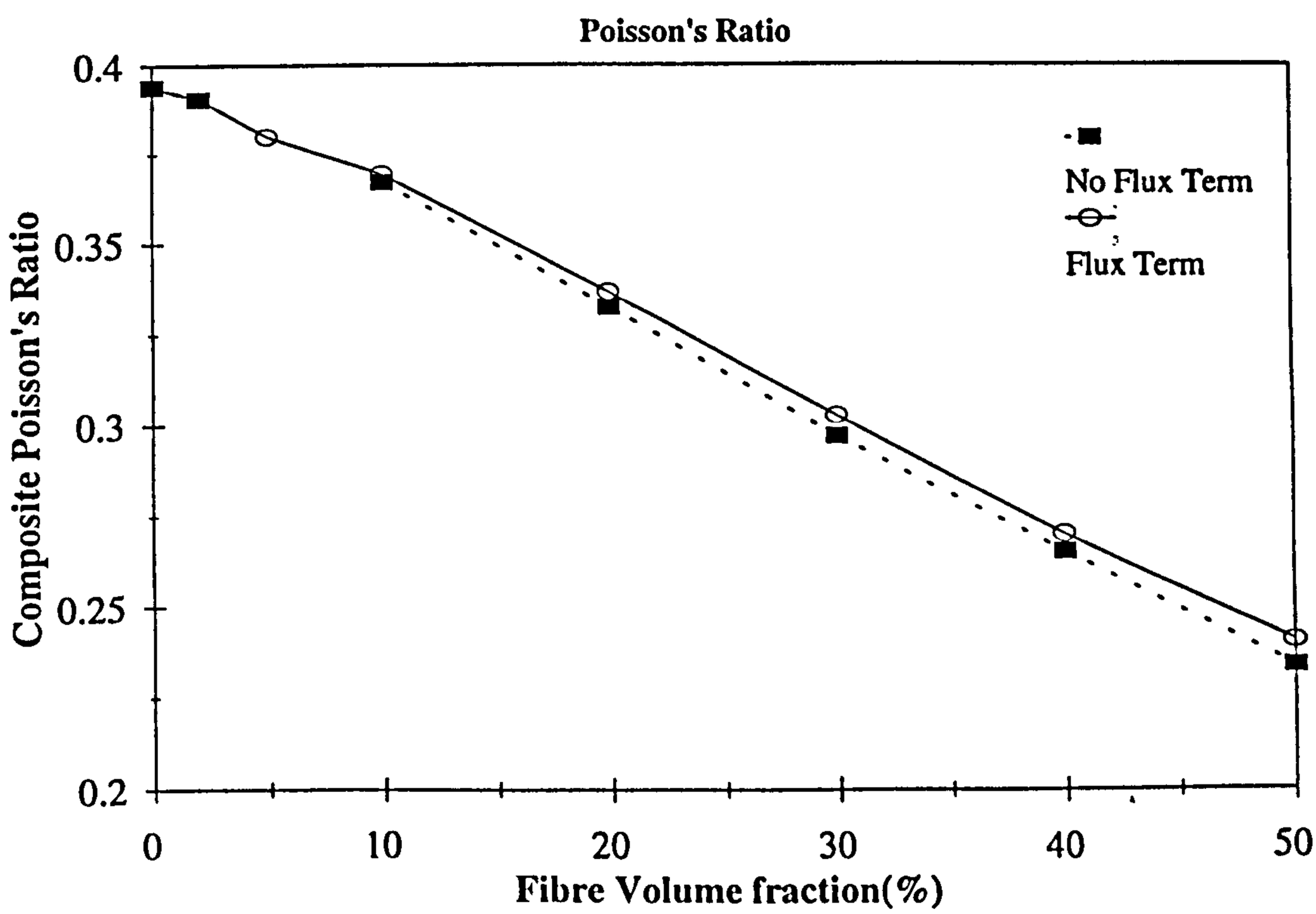

Fig.4.64: Poisson's ratio of short fibre reinforced composite calculated from FEM results

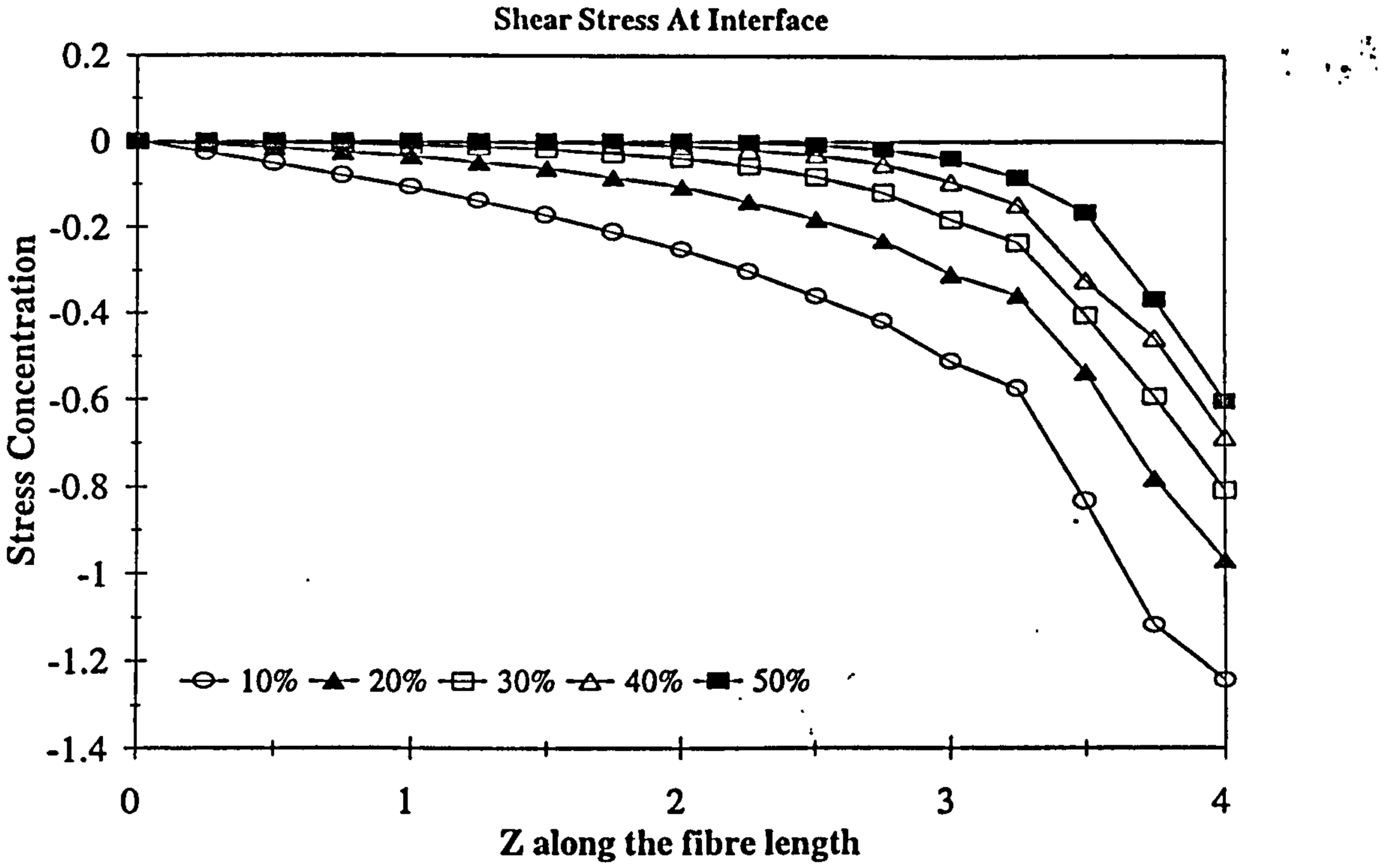

Fig.4.65: Shear stress along the interface of the fibre and matrix for different fibre volume fractions

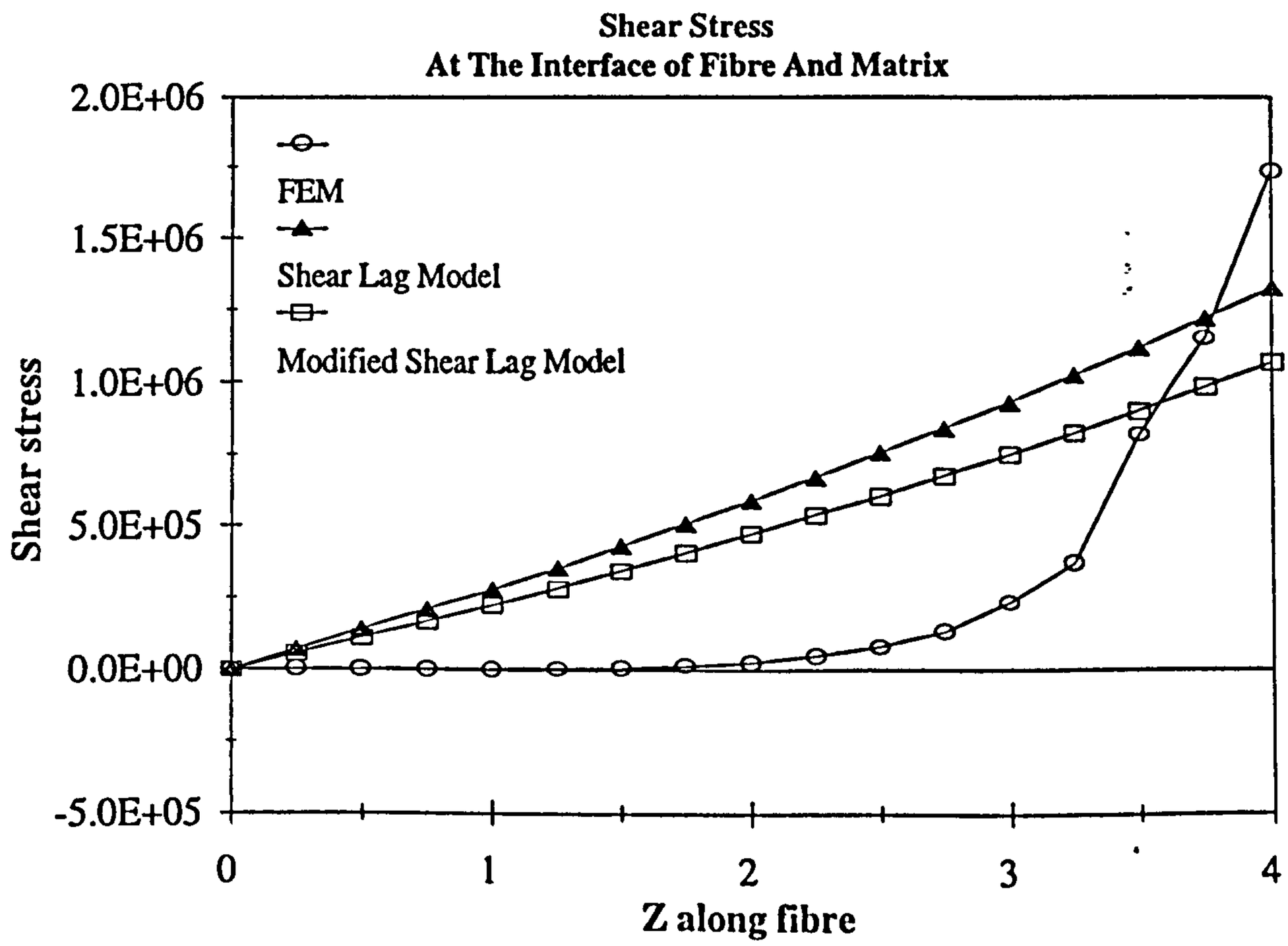

Fig.4.66: Shear stress at the interface of fibre and matrix predicted by FEM and Shear lag model

The shear lag model gives much lower values for modulus. The values of moduli found by modified shear lag model are closer to the finite element results.

In implementing the finite element analysis first the boundary tractions at the interface of the fibre and matrix are ignored. Then the calculations are repeated and the boundary flux terms are considered in the field equations. The moduli values found in the latter analysis are lower than the results obtained from the no boundary traction case. This comparison is shown in *figure 4.60.*

The effect of different fibre aspect ratios at constant fibre spacing on the composite modulus is investigated. In *figure 4.61* the variations of the modulus of glass epoxy composite for the aspect ratios of 5, 10 and 20 are shown. The fibre spacing is 6 in all of these cases. A relative increase of the modulus can be observed with the increase of the aspect ratio. The upper limit is the longitudinal modulus of the continuous fibres that can be achieved by using fibres with high aspect ratio.

The modulus of the composites filled with rod shape particles also depends on the fibre spacing. The variations of the modulus for three different fibre spacing of 2, 6 and 10 at constant aspect ratio of 5 is shown in *figure 4.62*. There is a decrease in modulus as the fibre spacing increases.

The boundary condition on the side wall of the cell can be with constraint. In this case the final stress distribution and effective properties of the composite should be calculated by superimposing the results of the two steps are described in the chapter 3. The unconstrained boundary condition is also modelled. The results of the two sets of the boundary conditions are compared in *figures 4.63a-c.* A remarkable difference can be observed between the two cases. The imposition of unconstrained boundary condition results in much lower values of the modulus.

The Poisson's ratio values are given in *figure 4.64* for both cases of with and without flux terms in the model equations.

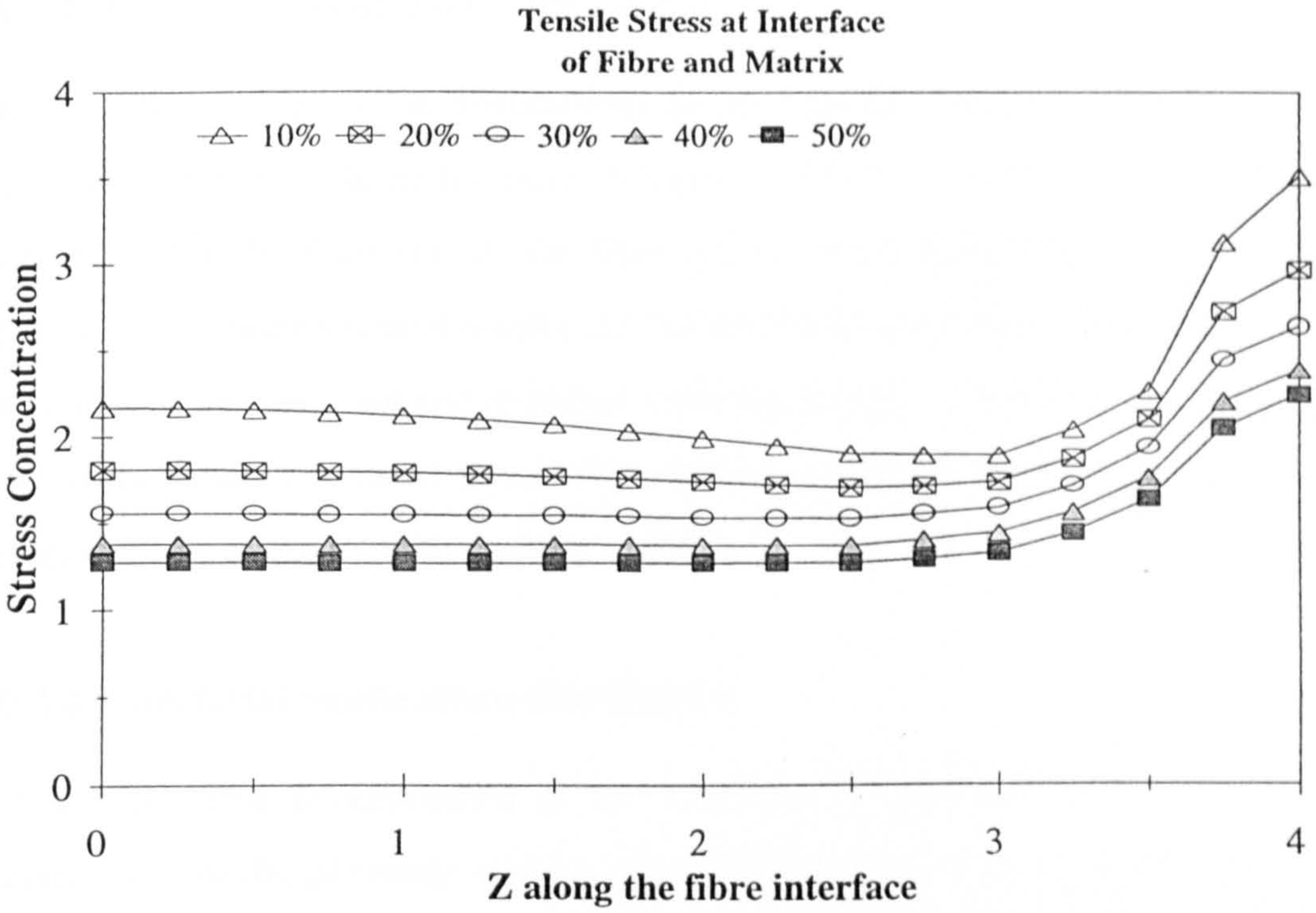

Fig.4.67: Tensile stress concentration at the interface along the fibre length for different fibre volume fractions

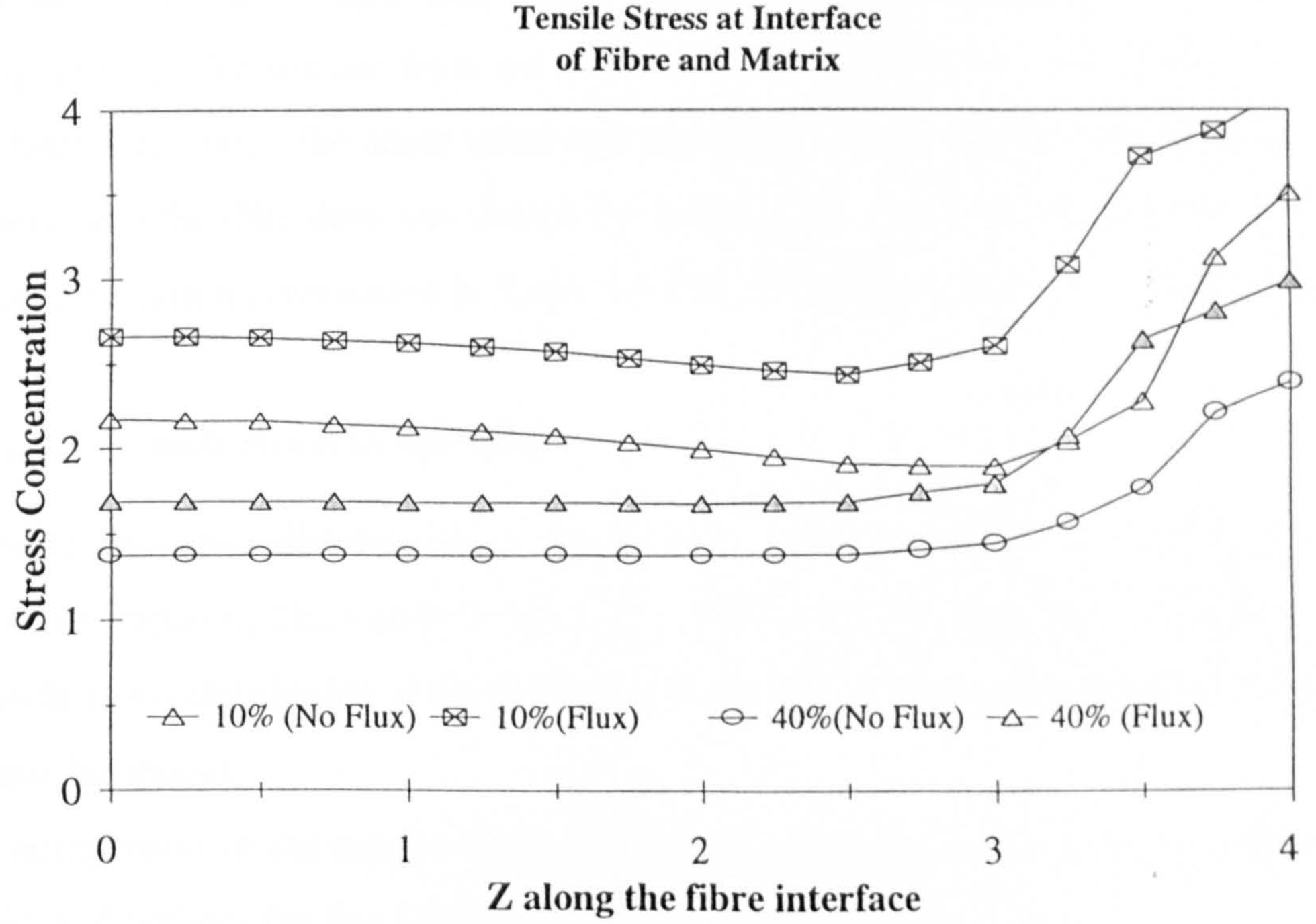

Fig.4.68: Tensile stress concentration at the interface along the fibre length for the 10% and 40% volume fractions comparing the model with and without flux terms

4.6.2 Stress distribution

4.6.2.1 Interfacial shear stress distribution

The normalised shear stress distributions at the interface of the fibre and matrix are shown for different volume fractions in *figure 4.65*. It indicates that the shear stress decreases from the fibre end to the fibre centre where the stress is nearly zero. In *figure 4.66* the finite element results for the interfacial shear stress are compared with the results of the shear lag and modified shear lag model. The shear lag analysis gives much higher shear interfacial stress. The difference between shear lag model and finite element results increases with volume fraction.

4.6.2.2 Interfacial tensile stress distribution

The tensile stress concentration at the interface is maximum at the fibre end. A decrease of interfacial tensile stress concentration can be seen in *figure 4.67* as the volume fraction increases. In *figure 4.68* the interfacial tensile stress concentration resulted from the finite element analyses with and without interfacial flux terms are compared. These comparisons are made for the volume fractions of 10% and 40% respectively. The stresses from the analysis considering flux terms are higher for both volume fractions. The shear stress concentration distribution at the interface of the matrix and the filler does not change by including the flux terms in the field equations. The comparison is presented in *figure 4.69* for the volume fractions of 10% and 40% .

4.6.2.3 Tensile stress in the fibre

The tensile stress distributions in the fibre are shown in *figures 4.70a-b* for different volume fractions. The results of the finite element computations are compared with the tensile stress distribution in the fibre calculated by the shear lag model and the modified shear lag model.

A comparison of the tensile stress distribution resulted from the finite element model with and without the flux boundary terms is made in *figure 4.71*.

The modified shear lag model which considers the tensile stress transferred by the end of fibres gives higher values. The simple shear lag model that assumes the transfer of

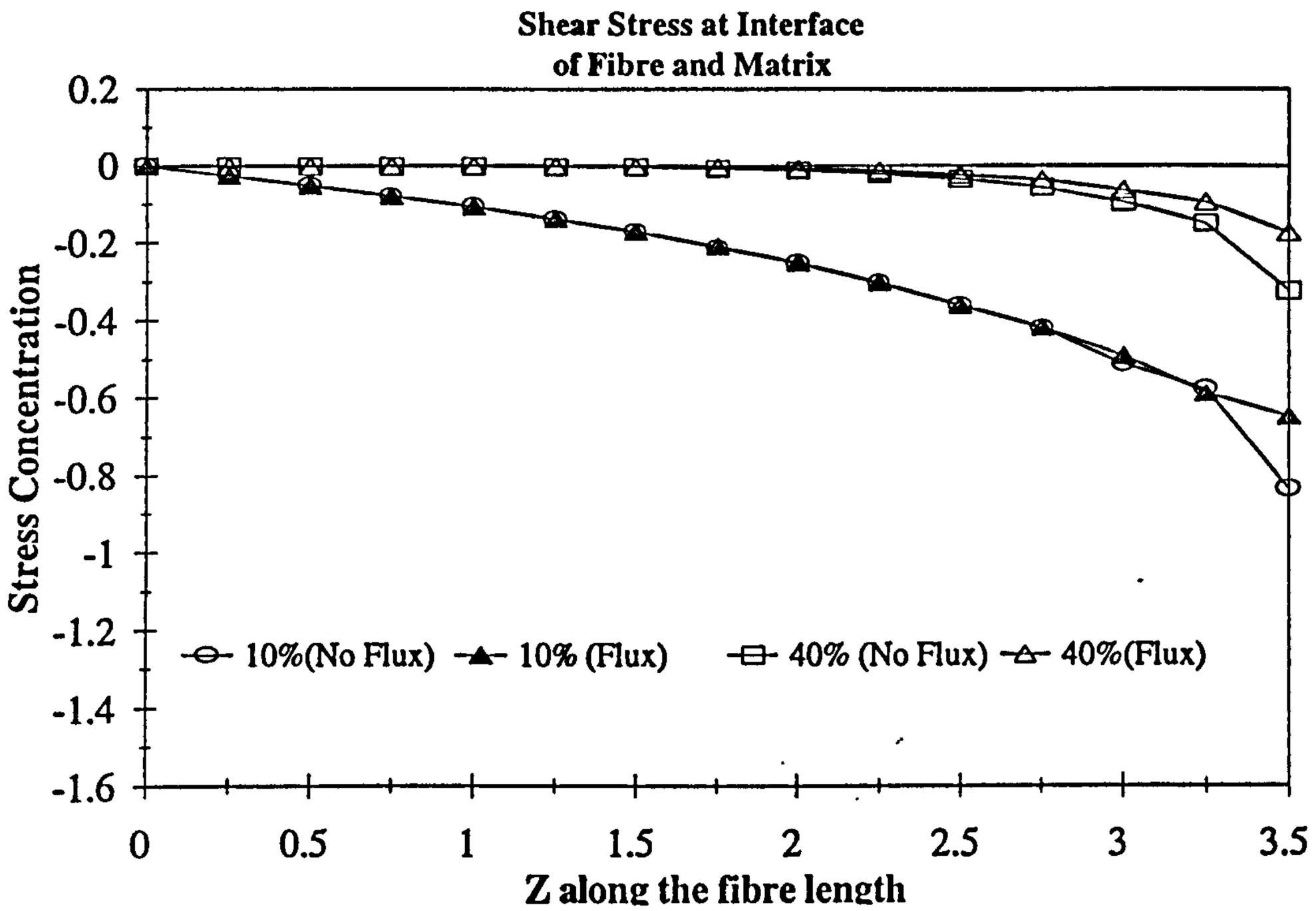

Fig.3.69: Prediction of shear stress along the interface by FEM, Comparison of the results with and without flux boundary terms(Volume fraction 10% and 40%)

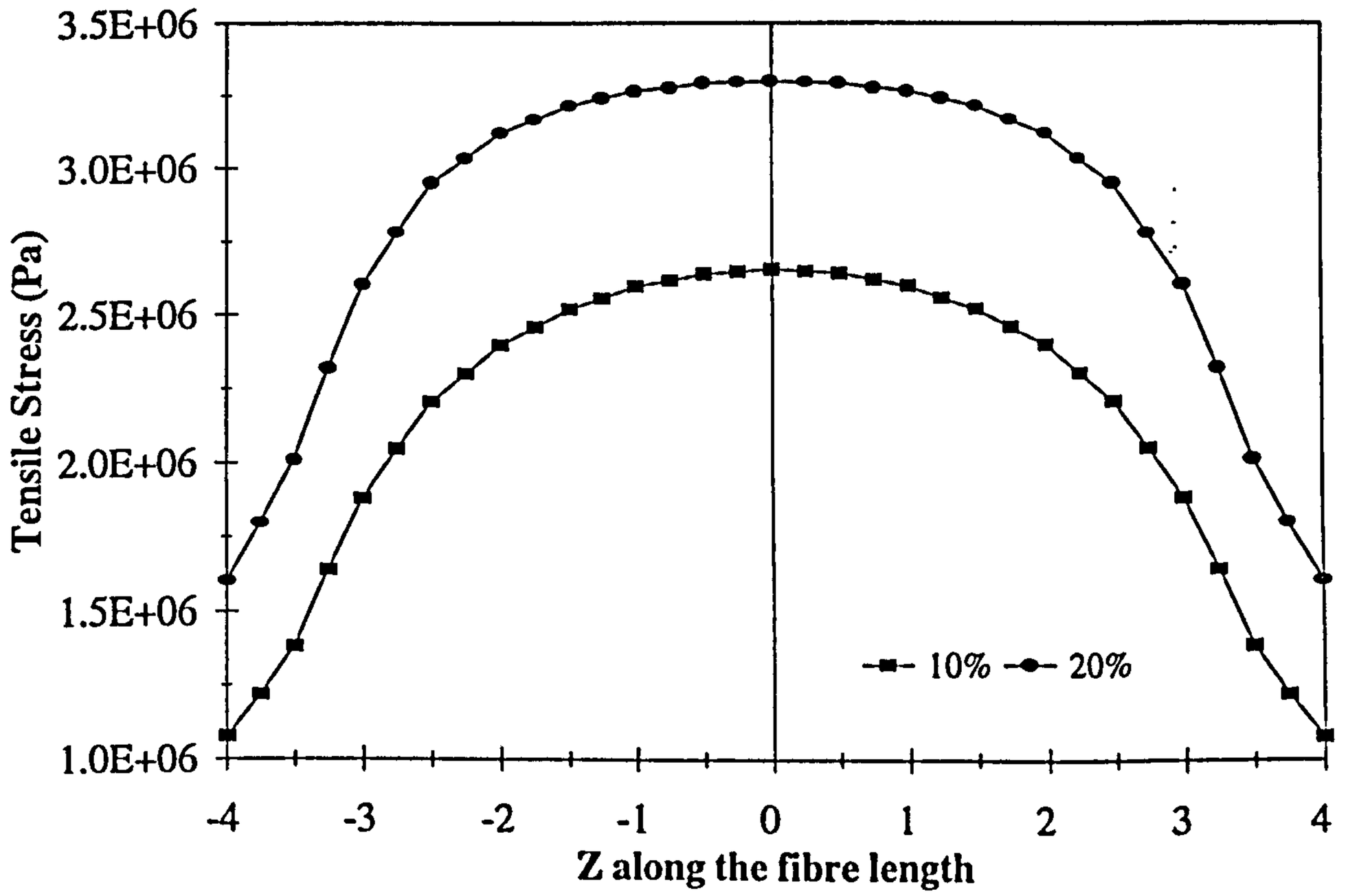

Fig.3.70a: Tensile stress concentration in the fibre for 10% and 20% fibre volume fractions.

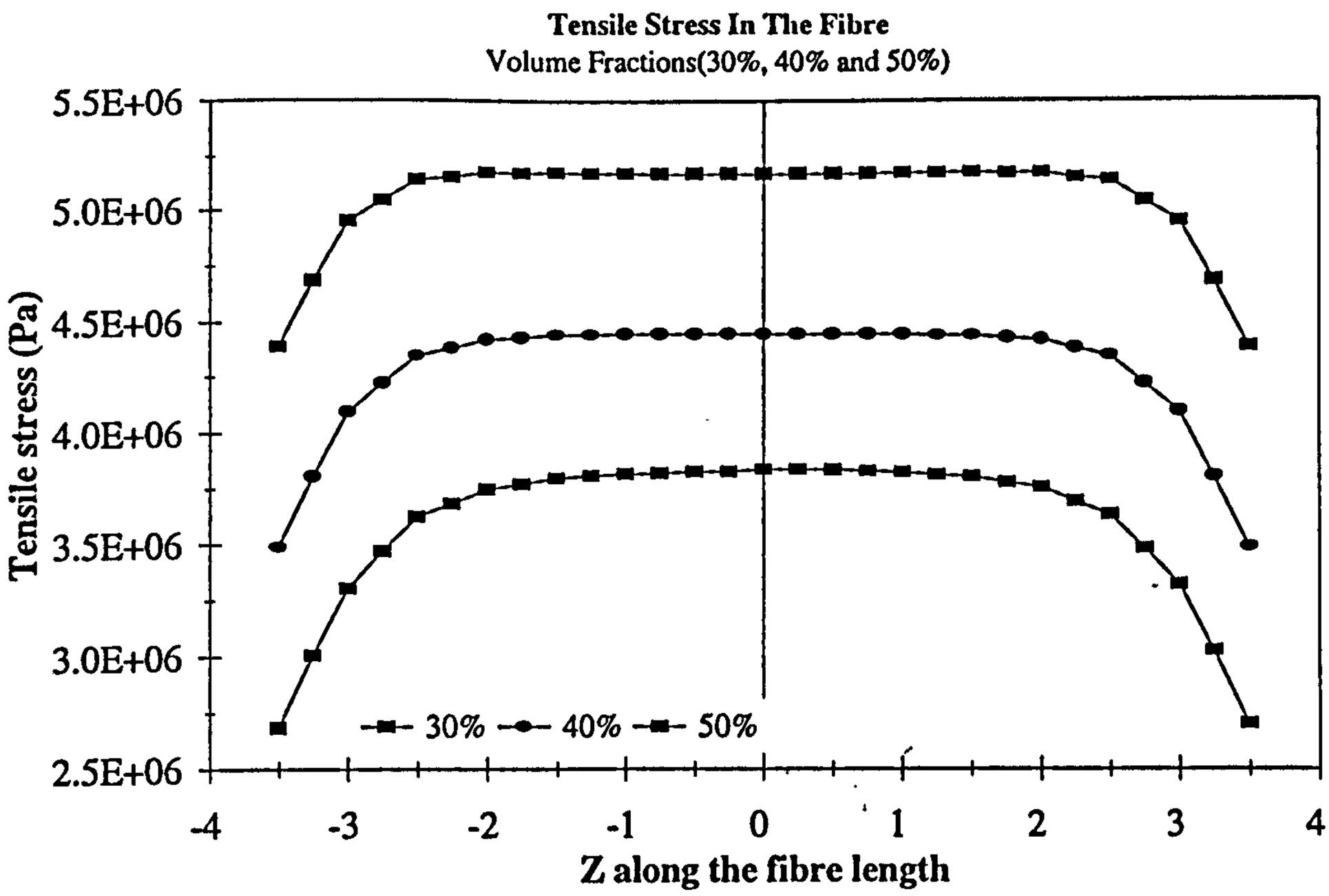

Fig.4.70b: Tensile stress concentration in the fibre for 30%, 40% and 50% fibre volume fractions

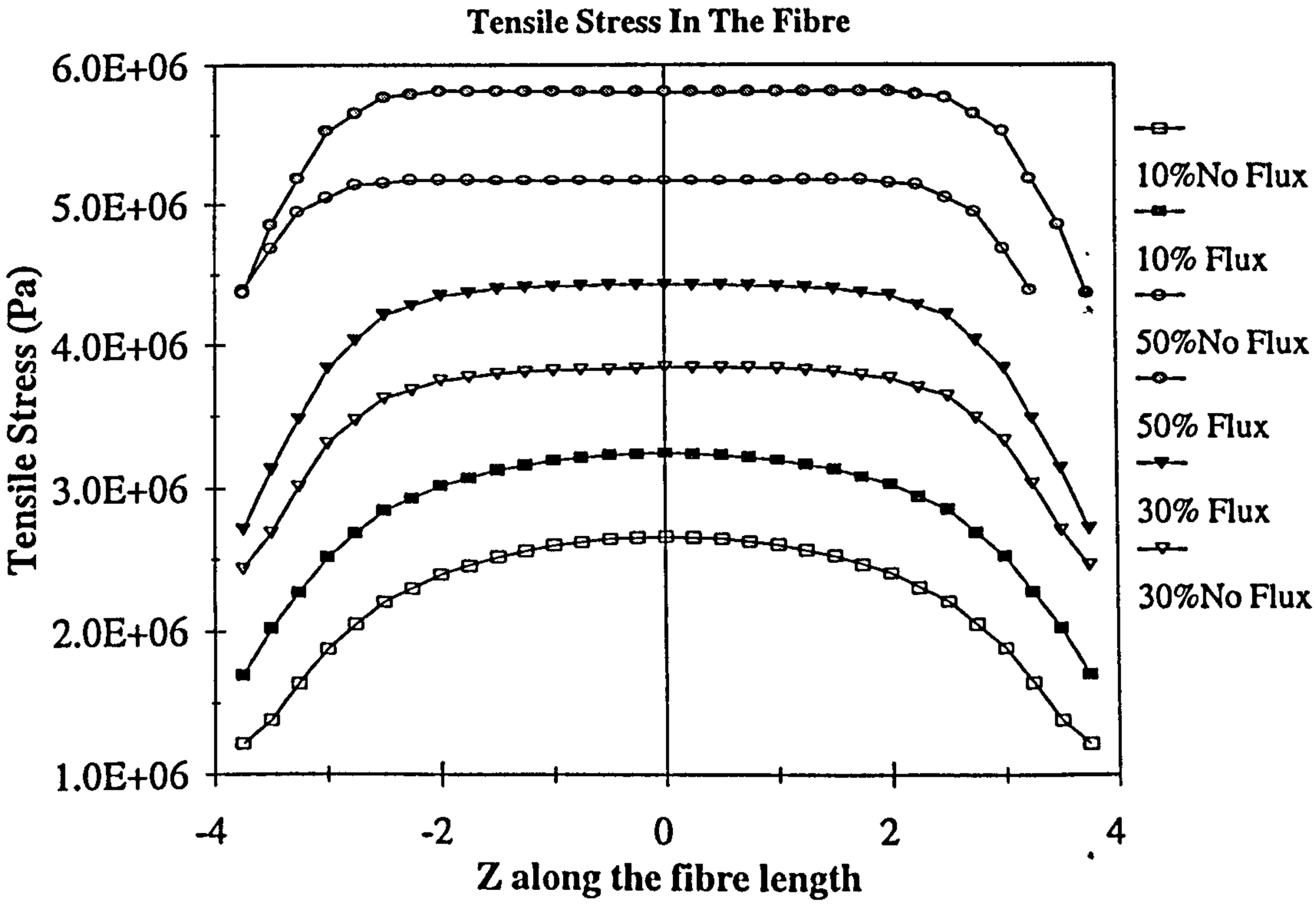

Fig.4.71: Tensile stress concentration in the fibre. Comparison of the FEM predictions with and without flux boundary terms

tensile stress to the fibres is only via shear stress at the interface of the fibre and the matrix gives the lower values for the tensile stress in fibres.

At low volume fractions up to 20% of filler the tensile stress in the fibre found by the finite element model is higher than the shear lag model prediction all over the length of the fibres as it is clear in *figure 4.72a* for 10% fibre volume fraction . *Figure 4.72b* indicates that at the 20% volume fraction of the fibres the finite element results are in close agreement with the modified shear lag model predictions. When the volume fraction rises to 30% the tensile stress distribution of fibres obtained from our model is located between the simple shear lag and modified shear lag models as shown in *figure 4.72c.* For the higher volume fractions the result of our model for tensile stress distribution conforms with the results of the modified shear lag model at the end fibre segment where the tensile stress increases continuously. However it then moves towards the simple shear lag model predictions and reaches a plateau at the central segment of the fibre.

The tensile stress increases from the fibre ends towards the centre of the fibre. For each volume fraction at a certain point along the length of the fibre the tensile stress reaches its maximum and remains almost constant for the rest of the length of the fibre. The point at which the tensile stress reaches its maximum value depends on the volume fraction of the fibres. The higher the volume fraction the closer the peak point is to the fibre end.

4.6.3 Critical length

The minimum length of the fibre at each volume fraction through which the stress rises to its maximum is called the critical length. The critical length plays a great role in characterising the short fibres in order to provide the maximum strength or reinforcement in composite. There are different theoretical approaches for the estimation of the critical fibre length. The definition of the critical length might change from one theory to another. The model proposed by Rosen (Rosen, 1964) defines the critical length as the minimum fibre length or aspect ratio required to reach 0.9 times the maximum fibre strain, about each fibre end in a long fibre. Rosen gives the critical fibre length as:

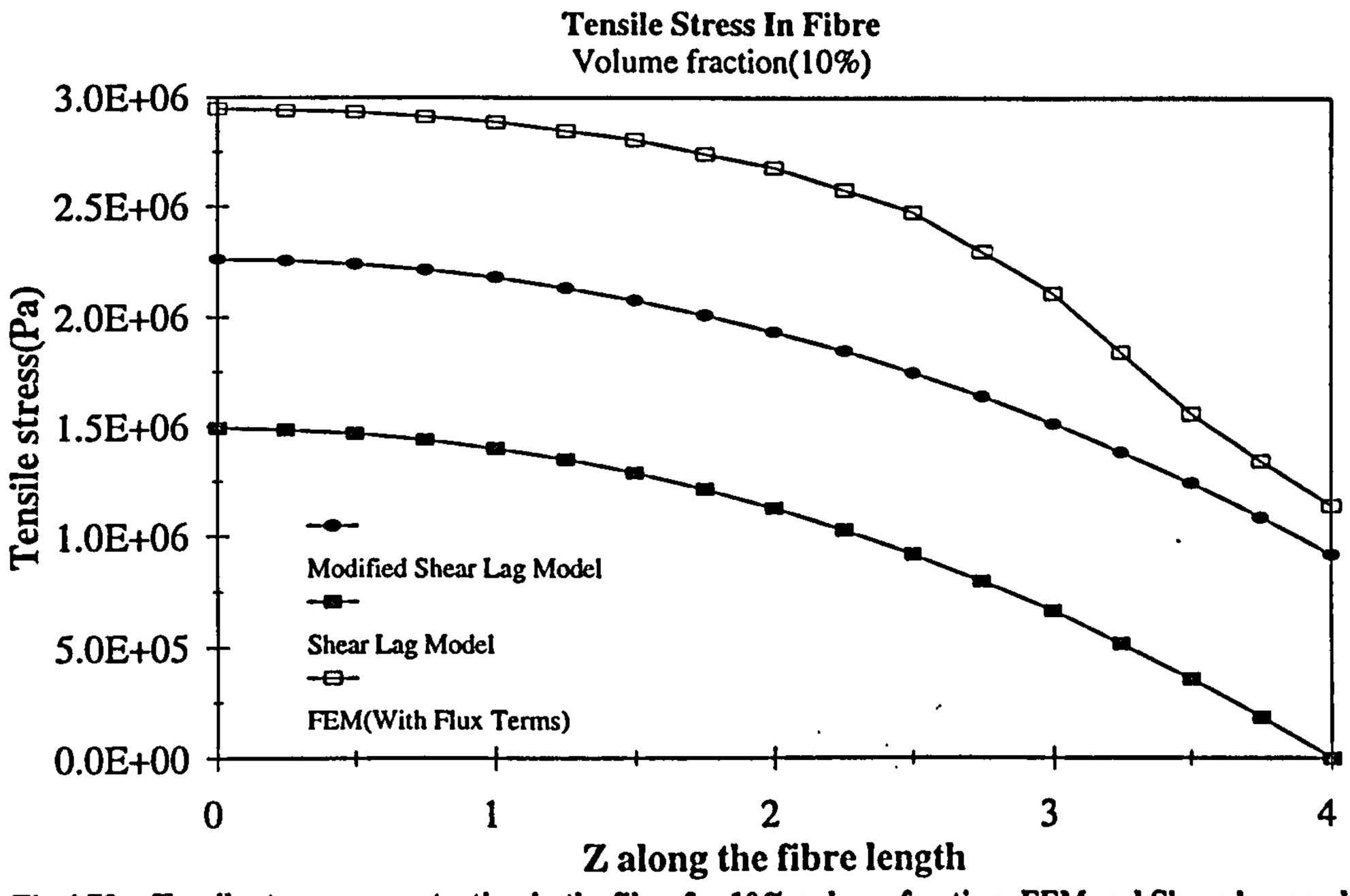

Fig.4.72a: Tensile stress concentration in the fibre for 10% volume fraction. FEM and Shear lag models predictions.

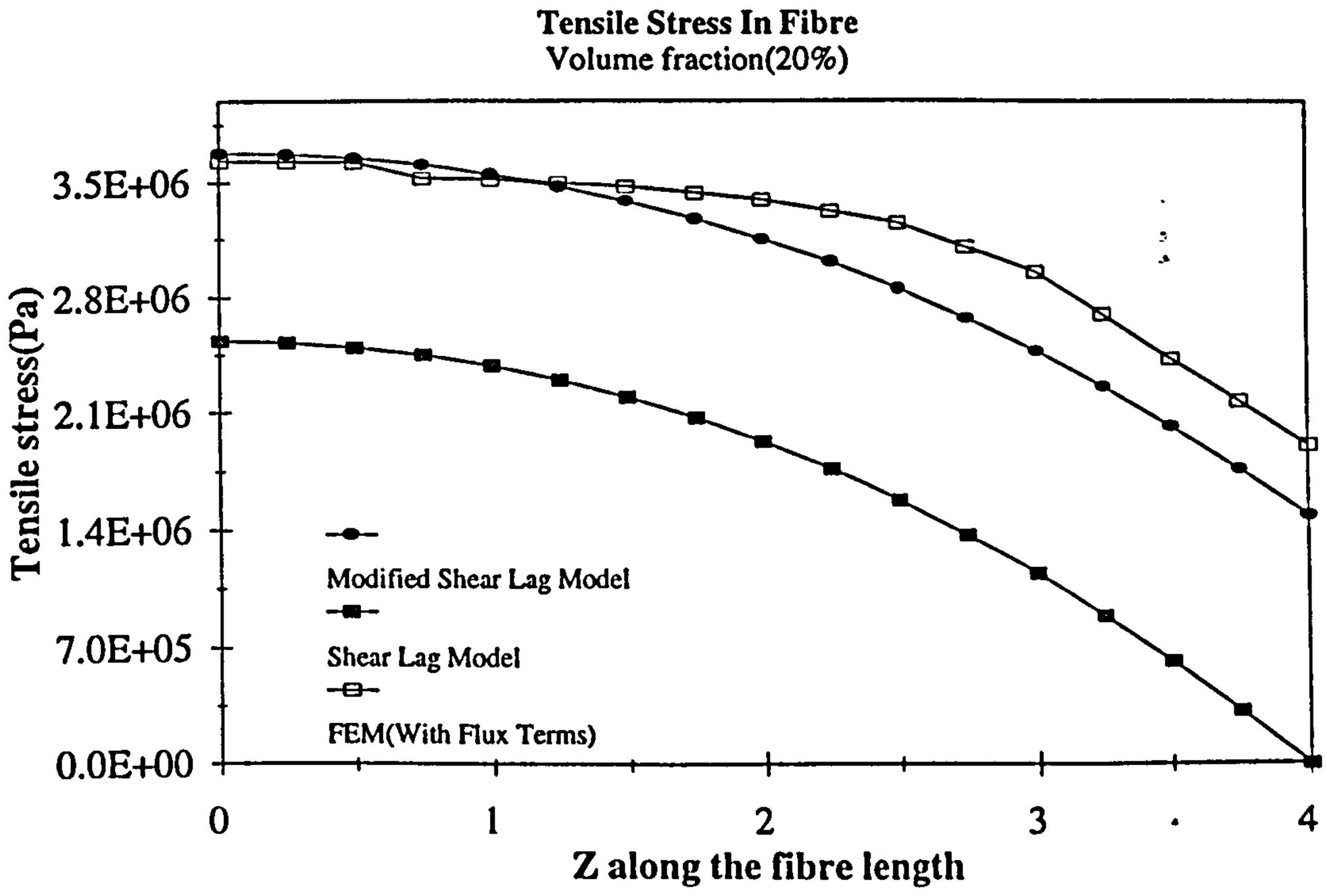

Fig.4.72b: Tensile stress concentration in the fibre for volume fraction 20%. FEM and Shear lag models predictions.

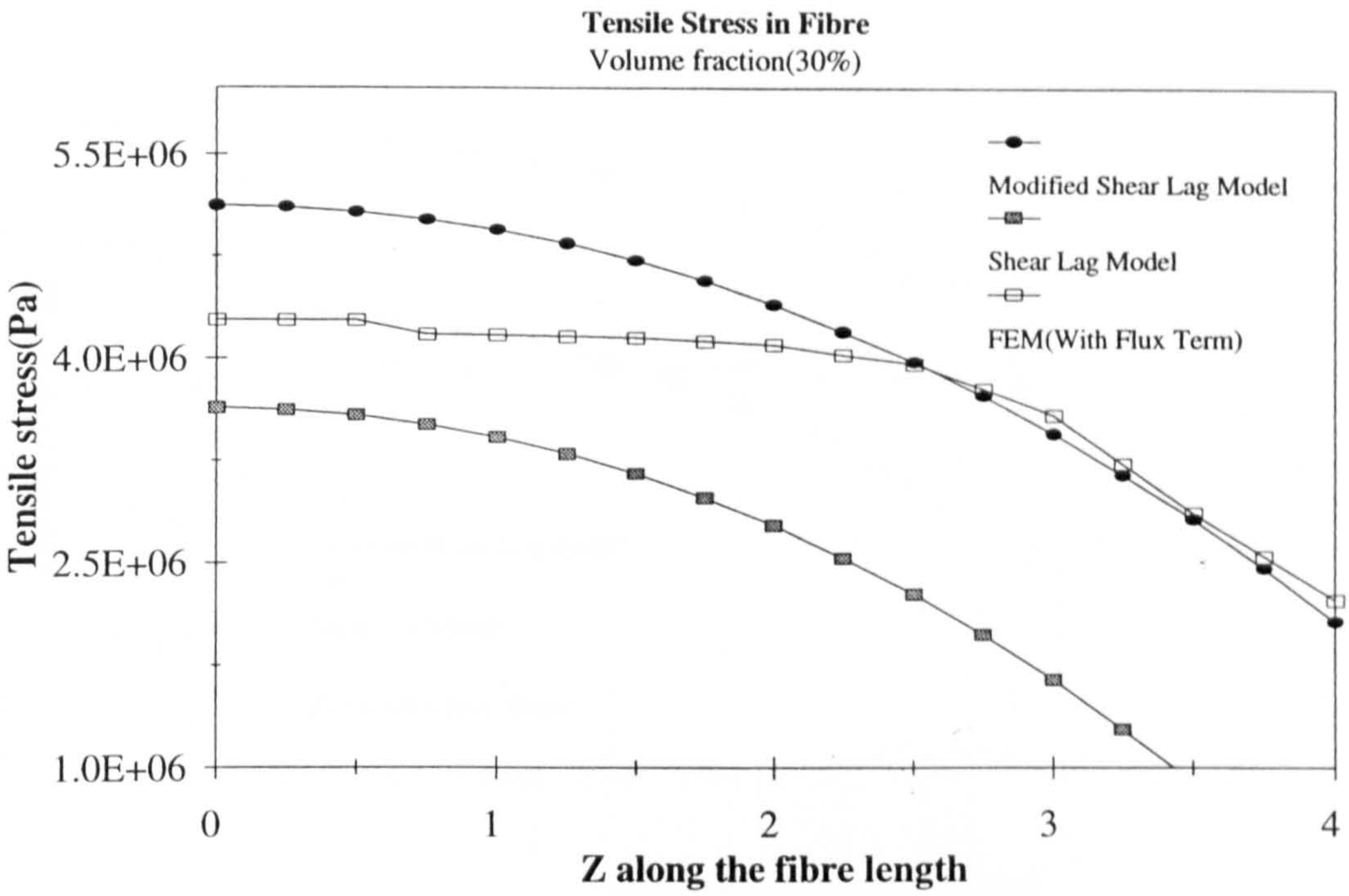

Fig.4.72c: Tensile stress concentration in the fibre 30% for volume fraction. FEM and Shear lag predictions.

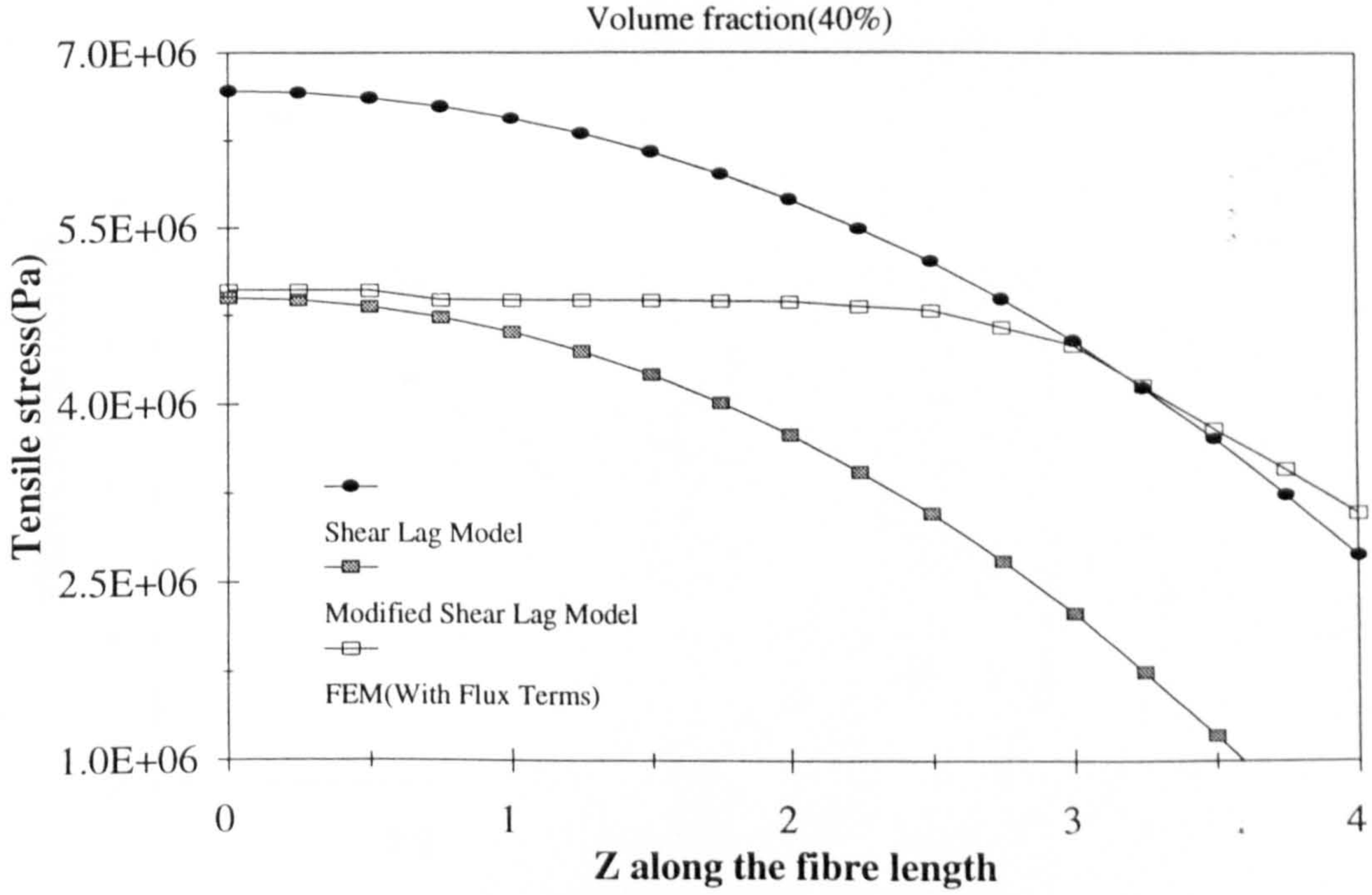

Fig.3.72d: Tensile stress concentration in the fibre for 40% volume fraction. FEM and Shear lag model predictions.

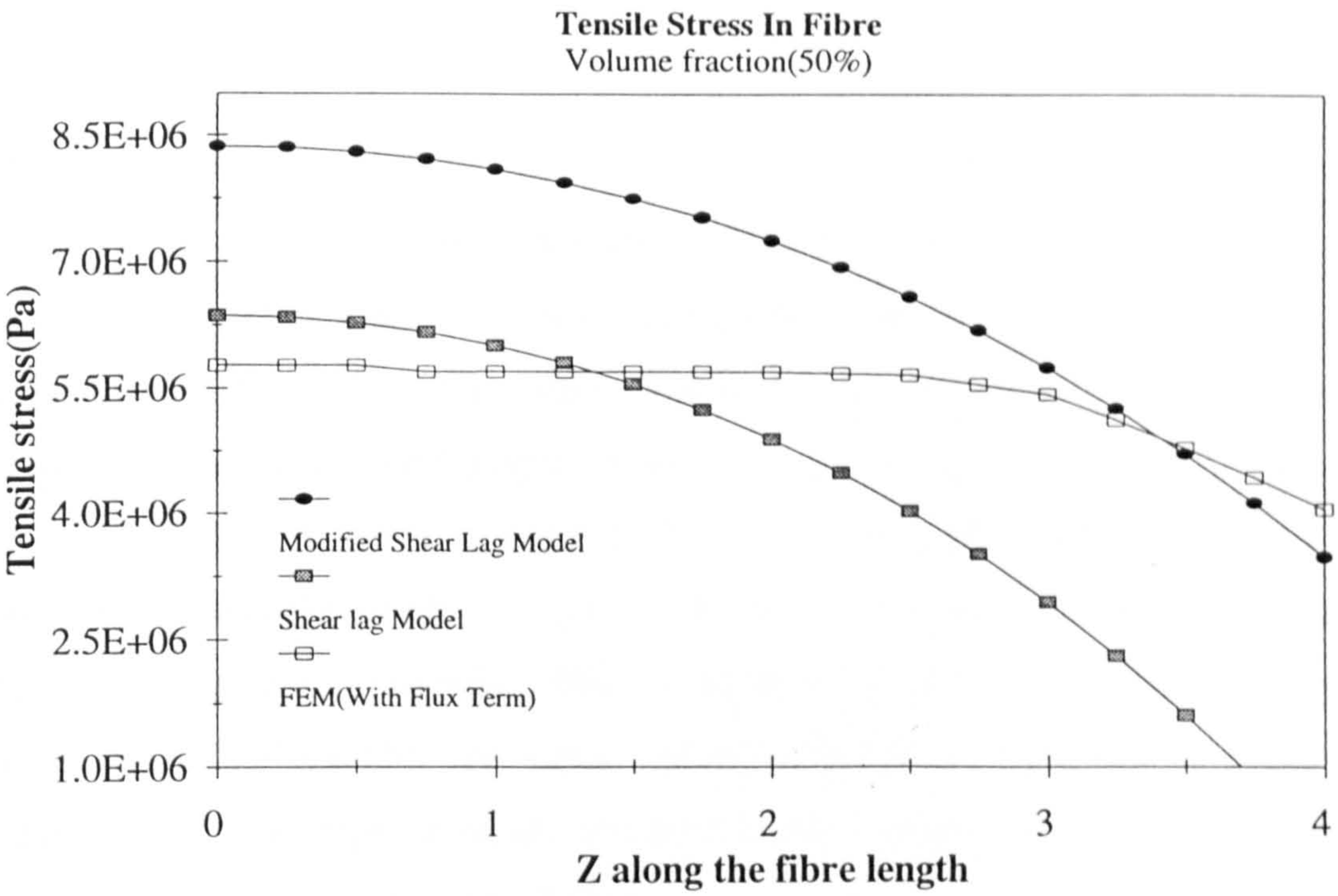

Fig.4.72e: Tensile stress concentration in the fibre for volume fraction 50%. FEM and Shear lag predictions.

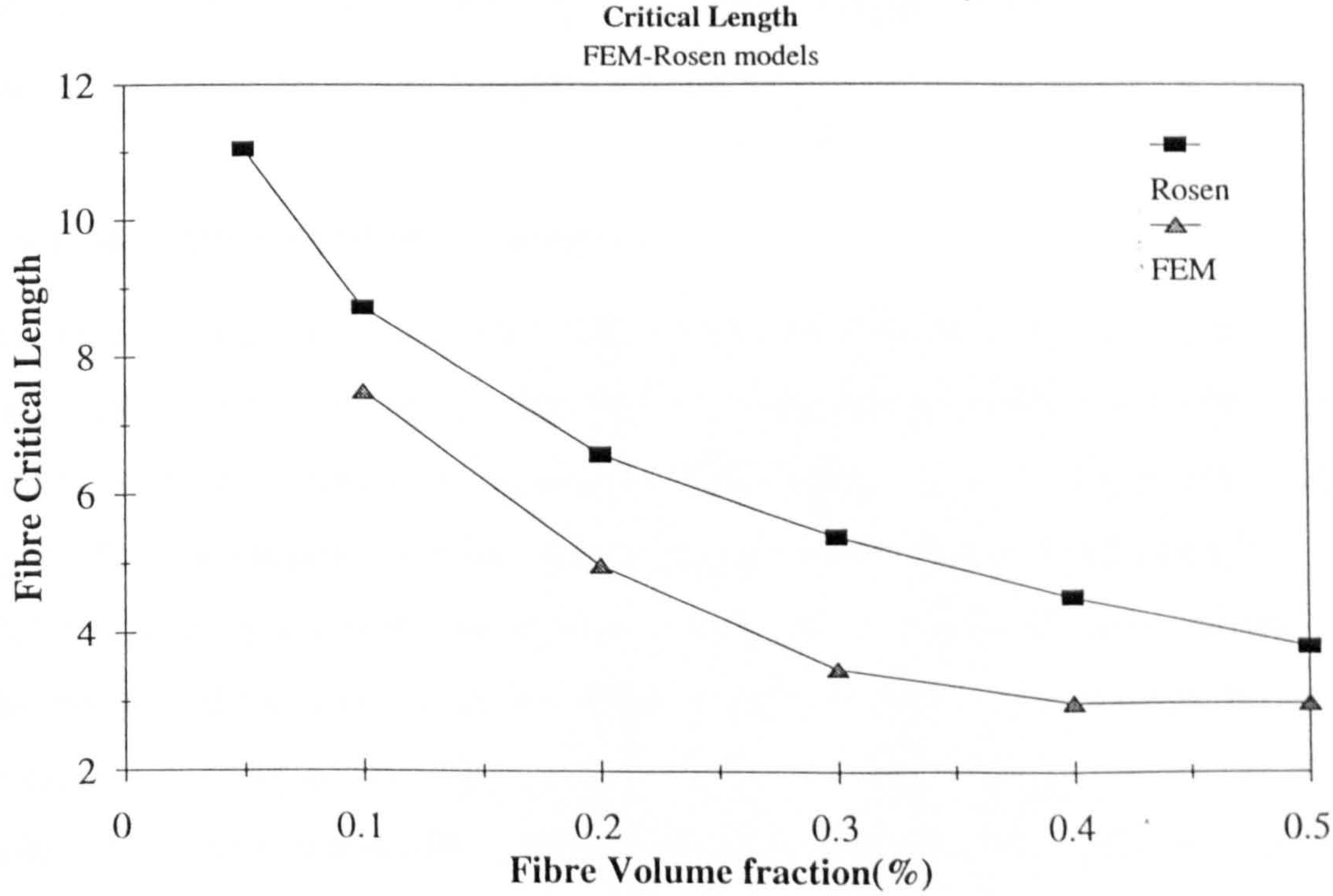

Fig.3.73: Critical length of fibres versus volume fraction

$$l_c = d\left[\frac{E_f(1+\nu_m)}{E_m}\right]^{1/2}\left(\frac{1-V_f^{1/2}}{V_f^{1/2}}\right)^{1/2} \qquad (4.22)$$

where d is the fibre diameter, E_f and V_f are fibre Young's modulus and volume fraction , ν_m and E_m are matrix Poisson's ratio and Young's modulus.

Equation 4.22 shows that the critical fibre length depends on the fibre diameter, the square root of the ratio of the tensile moduli and on a term representing the fibre volume fraction. The critical lengths of fibres obtained by the finite element model and Rosen model are compared in *figure 4.73* for a range of filler volume fractions. Our model shows that the tensile stress in the fibre rises to its peak in a shorter length of the fibre. Termonia (Termonia, 1990) concluded that the critical fibre length is a unique function of the fibre and matrix modulus ratio. But our results show that the critical length also depends on the volume fraction. Another model which descirbes the critical length is developed by Kelly as:

$$l_c = \frac{\sigma_{uf}\, d}{2\tau_u}$$

where d is the diameter of fibre, τ_u is the shear strength of the interface or of the matrix and σ_{uf} is the tensile strength of the fibre.

4.6.4 Strength of short fibre composites

Prediction of the strength of short fibre reinforced thermoplastics is a complex but industrially crucial problem. In the case of a composite containing short fibres, the existence of a non uniform stress along the fibre implies that the average stress carried by the fibres at the point of failure will be less than fibre ultimate tensile strength.

Failure occurs by a different mechanism in the short fibre composite which depends on the mechanical properties of the constituents and the tensile and shear strength of the interfacial bonding of the fibres and the matrix. Another deterministic factor in the failure mechanism in short fibre reinforced composites is the fibre aspect ratio or fibre length. There is the possibility of failure in the fibre, in the matrix phase or at the

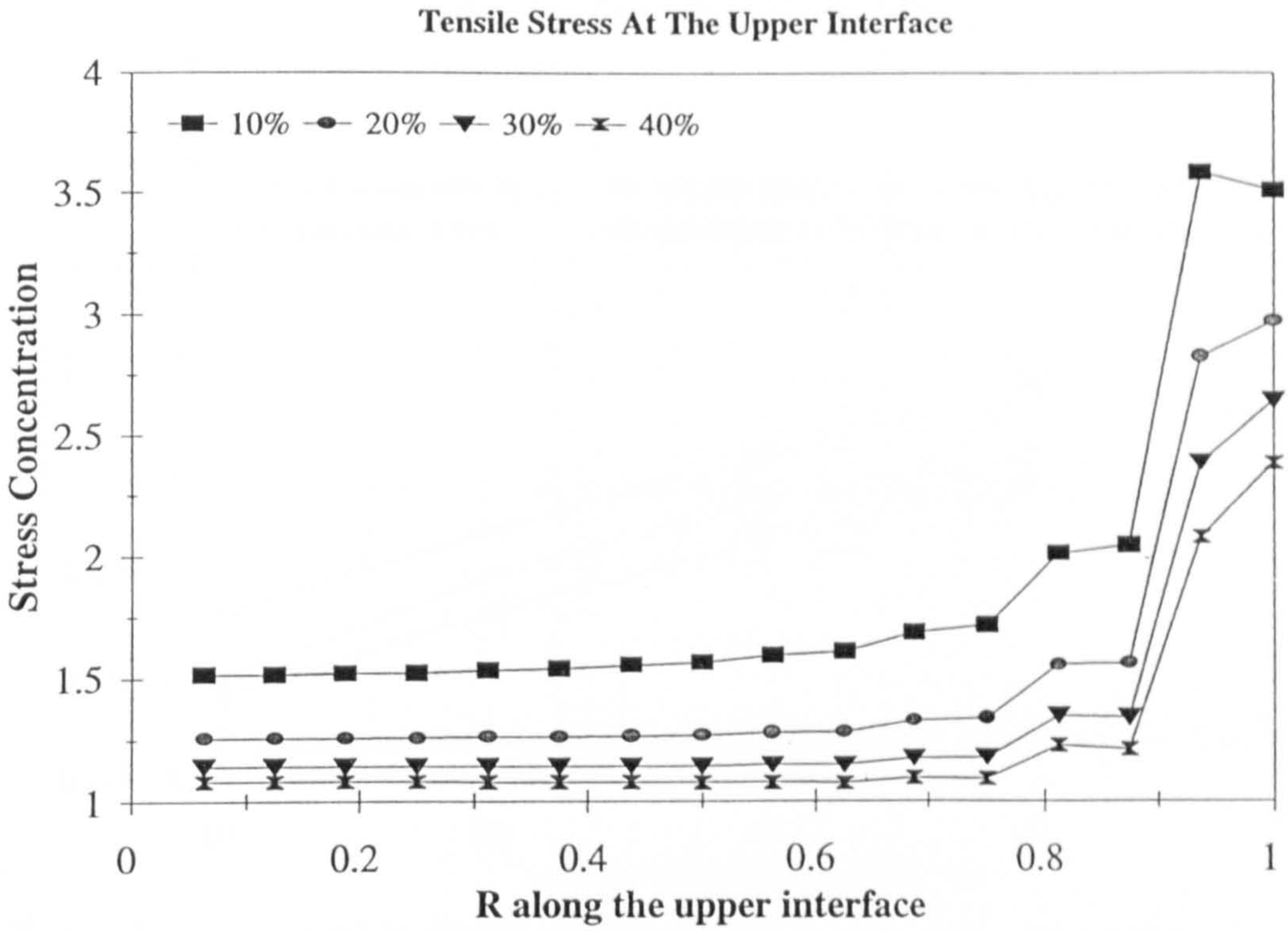

Fig.4.74: Tensile stress concentration at the upper interface

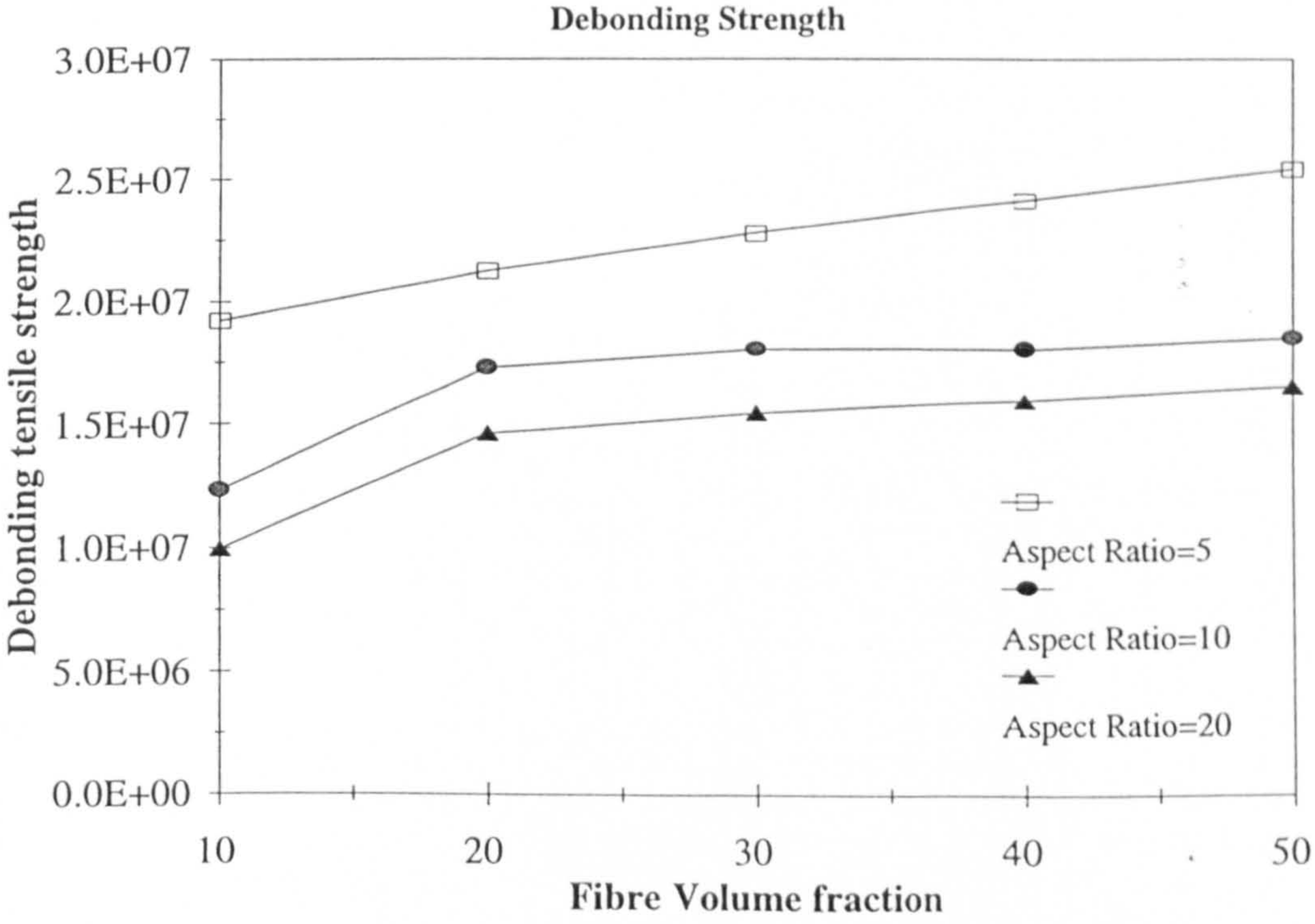

Fig.4.75:Debonding strength prediction by FEM of the fibres with 5, 10 and 20 aspect ratios.

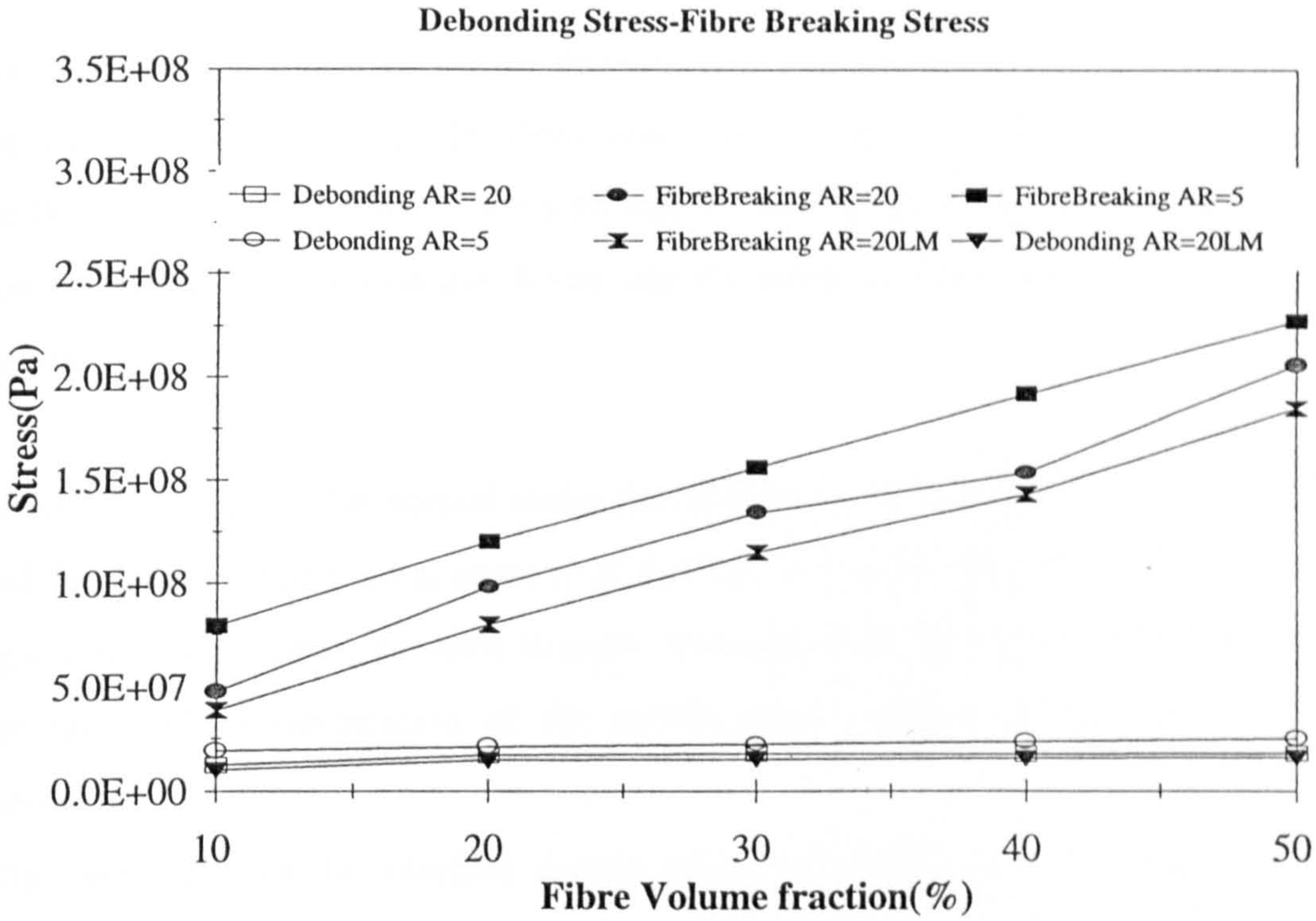

Fig.4.76: Stresses required for debonding and breaking of the fibre with 5 and 20 aspect ratios. (LM: Low Modulus)

fibre/matrix interface. A combination of these mechanisms can lead to the catastrophic failure in the composite.

The significant stress on the lateral interface of the fibre/matrix along the fibre length is the shear stress. Even when the shear stress on this face exceeds the shear strength of the bonding, the compressive forces normal to this interface retain the fibre and matrix closed. The compressive forces are the result of the lateral contraction of the matrix.

Figure 4.74 shows the normal stress distribution at the upper interface of the fibre and the matrix . The normal stresses at this face are tensile and as can be seen in this figure the concentration of these stresses increases from the axis towards the edge of the fibre. The concentration of the tensile stress reduces as the volume fraction increases.

The debonding of the interface occurs when the tensile stress reaches the tensile strength of the interfacial bonding. The debonding stresses obtained by the finite element model are presented in *figure 4.75.* The debonding stresses for the aspect ratios of 5 and 20 are given for the range of the volume fraction. The debonding stress rises as the volume fraction increases. At the aspect ratio of 5 the increase is more significant than the aspect ratio of 20.

The tensile stress required to be applied to the composite to bring the fibres to their failure tensile stress is given in *figure 4.76.* The applied stress to break the fibres is higher for aspect ratio of 5 compared to the values of the aspect ratio of 20. An increase in the stress to breaking point can be observed at higher volume fractions. The stresses at the breaking point are much higher than the debonding stresses for the fibre glass and epoxy matrix. These differences are more remarkable at lower fibre aspect ratios.

Therefore it can be predicted that at low aspect ratios the debonding of the fibres acts as the initiation mechanism for the failure and it is followed by the failure of the matrix near the fibre ends. Since the aspect ratio of short fibre is low, the concentration of the fibre ends is high and then the local cracks merge transversely from the direction of the applied load.

The catastrophic failure of the short fibre filled composite can occur without any breaking of the fibres. At higher aspect ratio, since the breaking stress of the fibres is lower, the failure occurs in two steps. In the first step the interface debonding and tensile failure of the matrix at the fibre ends is observed. However, in contrast to the low fibre aspect ratio case, growing matrix cracks at fibre ends are quickly blunted by neighbouring fibres and hence no catastrophic failure occurs. Because of the cracks and interfacial debonding the modulus of composite drops significantly.

Our model shows that the breaking stress of the fibres reduces at low modulus. Therefore in the second step which corresponds to a decreased modulus the tensile stress in the fibres can easily exceed the failure stress of the fibres leading to the breakage of the fibres.

Chapter Five

CONCLUSION

5.1 CONCLUSIONS OF THE PRESENT WORK

The developed finite element model has proved to be a flexible and cost effective tool for the prediction of properties of polymer composites. The stiffness, stress concentration field, failure mode and strength of different types of composites are studied. The stiffness predictions are in general more accurate than strength values obtained.

5.1.1 Modulus Of Particulate Filled Composites

It has been demonstrated that the modulus of elasticity of a spherical particle reinforced polymer can be accurately predicted using a finite element stress analysis technique. The strength of the composite can also be predicted, but further study is required to account for interfacial bonding effects. The model used to calculate the composite strength may also be extended to simulate fracture mechanism. The degree of bonding influences the strength but not the modulus of elasticity, unless high volume concentrations of particles are present.

The experimental results for effective modulus of the particulate composites agree well with the finite element predictions. The differences can be attributed to the assumptions that have been made in the model, such as agglomeration, dewetting,

adhesion, arrangement and filler particle shape. Another reason for the discrepancy between experimental results and the model predictions can be due to skin effect, which gives higher experimental values of modulus for soft particulate filled composites. The same effect can result in lower experimental modulus values for composites filled with hard particles.

5.1.2 Composite Filled with Hard particles

Our predictive model for particulate filled composite materials containing hard particles has produced interesting and useful results. The finite element model has been validated by the excellent agreement in values of stiffness between our predictions and careful experimental measurements. The predicted stress distributions are validated by exact matching of stresses around the interface. predicted stress distributions for epoxy resin filled with glass spheres have been successfully correlated with previous models and experimental observations. The successful description of the fracture appearance of these materials under various conditions leads to better understanding of their fracture behaviour, which will allow more confident use of these materials under different conditions.

The position and magnitude of the maximum direct stress concentration is found and this can be used to predict the fracture behaviour and the direction and amount of crack growth in the resin. For a well bonded sphere, at low volume fractions, crack growth is attracted to the resin above the pole of the sphere. Smearing of resin around the pole of the sphere is observed.

The amount of resin smearing around the pole of a well bonded sphere would be dependent on the position of the crack with respect to the sphere. Our results show that at low volume fractions the maximum distance is much further away from the sphere than for high volume fractions. Thus the model predicts that more smearing would occur if no spheres are visible in the fracture surface. Greater smearing at low volume fractions has been observed.

The concentration of the radial stress at the interface indicates the possibility of debonding at the interface and the extend of the opening up of the crack at the interface of the matrix and filler particle.
Under compression loading, the absolute value of the

radial stress at the equator is almost an order of magnitude smaller than its value at the pole it may however be sufficient to cause debonding from the equator of the sphere under the condition of the applied compression.

The concentration of the Von Mises stresses shows the position of the formation of shear bands. The state of the stress determines the governing mechanism of plastic deformation. The degree of interfacial adhesion has a profound effect on the competition between craze and shear band formation. In cases where the beads adhesion are perfect craze formation is favoured, whereas for poorly adhering beads shear band formation is dominant. This effect is caused by the difference in local stress situation, craze formation becomes controlling under a triaxial stress state and shear band formation is governing under a biaxial stress state. In the case of an excellently adhering glass bead , the crazes form near the pole. Stress analysis shows that these are regions of maximum dilatation and maximum principle stress. At a perfectly bonded glass bead experimental observations show that the shear bands form near the surface of the bead at 45° from the poles defined by the symmetry axis of maximum principal shear stress and of maximum distortion energy density. Our results confirm these observations.
The tensile strengths predicted by the finite element model and Von Mises criteria are compared with other models. All the models show a decrease in the strength with increasing filler volume fraction. However, since it is assumed that composite failure occurs when the first element fails, the prediction of strength by our model is rather conservative. A more realistic assumption would be that composite failure does not occur until several of the highly stressed elements fail. This allows for crack arrest by neighbouring inclusions and also takes into account the statistical increase in the strength for the small volume of material which is subjected to the stress concentration.

The experimental results show that the strength of the composite depends on the size of the filler particles. In our finite element model, we assume the composite is flawless and hence it predicts the strength of the composite through the stress fields which are independent of the particle size.

5.1.3 Composite Filled with Partially Bonded Particles

An interesting result of the present study is that besides matrix properties, deformation rate and temperature, the nature of the stress concentrating heterogeneities also determines the mode of tensile deformation; the biaxial stress state induced by poorly adhering glass beads promotes ductile shear deformation at the expense of brittle crazing. This insight may be of interest in the development of new composite materials. By avoiding a triaxial stress state at the stress concentrators, a ductile response to tensile deformation might be achieved under test conditions that otherwise would yield a brittle response.

The present study provides a good insight into the factors that determine the stress state near the tip of a curvilinear interfacial crack between a rigid spherical inclusion and a polymer matrix. The maximum stress concentration near the tip of a curvilinear interfacial crack at a further bonded sphere does not simply increase with increasing crack length, but is also determined by the orientation of the crack tip with regard to the applied tension direction. The analyses for a completely unbonded sphere have shown that an interfacial crack at a completely unbonded sphere cannot become larger than a critical length represented by $\theta = 68^0$ to 70^0. The stress state near the tip is biaxial and strongly determined by the extent of interfacial slip along that part of the unbonded interface that remains closed. The values of the elastic failure criteria that rule craze formation substantially increases as the extent of interfacial slip reduces. When relative tangential displacement of the particle and matrix is permitted and partial slip is imposed at the interface of the filler and matrix, the predicted stress concentrations are decreased .

Comparison of the results of the completely unbonded sphere with the physical reality of craze and shear band formation at poorly adhering glass spheres has shown reasonable agreement with respect to the critical interfacial crack length that can maximally be reached until a craze or shear band forms at the tip. Definite conclusion on whether craze and shear band formation occur more easily at the sphere than at an excellently adhering glass sphere could not be made because the extent and character of the interfacial slip between a poorly adhering glass sphere and a polymer matrix are not precisely known.

For a debonded rigid particle the maximum values for direct and Von Mises stress are at the crack tip. This confirms that any further plastic deformation through crazing or shear band formation starts at the crack tip.

Debonding of filler particles reduces the strength of the composite, but the debonded particles still can keep the composite from failure. This results in higher strength of the composite filled with debonded particles compared to that of the porous composite.

5.1.4 Composite Filled With Soft Particles

Comparison of our predictions with experimental results for epoxy resin reinforced with soft particles provides valuable insight into the mechanical behaviour of these materials. The design of optimum particulate reinforced materials in terms of the desired volume fraction of filler and constituent material properties may now be considered.

The experimental values of composite modulus are in comparison higher than our model predictions, this is probably because of some stiffening of the rubber via the epoxy, the inadequate description of the Poisson's ratio of the rubber in the model, and incomplete phase separation leading to a lower rubber volume fraction than the expected theoretical value. The onset of plasticity during the experimental measurements as well as any experimental errors can also cause some discrepancy between the measured and the predicted values. In cases when the experimental value is higher than the predicted results can be due to the skin effect. The restrictions imposed by the walls of molds, leads to an excess polymer at the surface of the test specimens. Thus, in torsion or flexural tests where the maximum stress is at the

surface, the properties of the surface is dominant and determinant the behaviour of the whole sample. This error can be corrected by using thicker specimens which can be extrapolated to infinite thickness, or by using particles of smaller size and extrapolation to zero particle size. The skin effect can produce errors as large as ten to twenty percent depending on the thinness of the specimen.

The effect of the accuracy of the rubber material properties such as the Poisson's ratio, which is used as input for the finite element code, on the result of the calculations is shown.

Linear relationship between Young's modulus and volume fraction is found which is similar to the results of experimental measurements.

The maximum direct and Von Mises stress concentrations are found at the equator of the spherical filler particle.

Shear bands in the resin are expected to grow from the point of the maximum concentration of Von Mises stress, which is predicted to be at the equator of the sphere.

Initiation and growth of the shear bands are largely governed by the concentration of Von Mises stress in the matrix, whereas cavitation, or interfacial debonding, of the rubber particles is largely controlled by the hydrostatic (dilatational) tensile stresses. To analyse the stress field accurately, it is necessary to employ a numerical technique such as the finite element method.

The radial stress at the interface for the soft particles is far smaller than that found for the hard particles. This indicates that there is no tendency for debonding at the interface in composites, which is in contrast to the tendency for debonding in the glass filled material.

Stress distribution in the matrix for resin containing rubber spheres has been found to be very similar to that of a resin containing holes. The values of matrix maximum stress concentration, at the equator for the epoxy resin containing holes or rubber spheres are very close. Shear band formation in the resin would occur in a similar

way for the two materials. However, epoxy resin containing holes is known to be a very poor material. We therefore can postulate that shear band formation is not the only important fracture mechanism for this material. Our results have shown that cavitation of the rubber particles is likely to occur, in agreement with experimental observations; after cavitation the rubber may be stretched. It appears that the process of rubber cavitation and stretching may make important contributions to the overall fracture energy. The magnitude of these contributions is dependent on the modulus of the rubber. Further contributions to the fracture energy of epoxy resin containing rubber spheres may arise from the physical presence of the rubber which would act as a crack stopper to a growing crack attracted to the equator of the sphere by either the concentration of direct stress or the initiation of shear bands.

Cavitation of rubber particles on fracture surfaces is generally found to start from the centre of the sphere. Our predictions do not indicate a preferred point of initiation but clearly show that the imposition of an overall tensile stress of the order of the matrix yield stress places the rubber particles in sufficient hydrostatic tension to initiate cavitations from small flaws. These flaws may be areas of rubber which are not fully polymerised and can not be observed by conventional microscopic techniques. There is some argument as to whether or not the cavitation of the rubber particles is necessary for shear bands to form. The exact stress levels for shear band formation and cavitation will depend upon the values of stress required to form matrix shear bands and cause rubber cavitation for the system under study.

5.1.5 Composites Reinforced With Continuous Fibres

It is observed that the addition of fibres produces a substantial increase in the transverse modulus of the binder material; however, the effect of an increase in fibre modulus is a gradually diminishing one becoming asymptotic to the value obtained for the infinitely rigid fibre. Therefore, at high values of the fibre modulus, The ratio of transverse Young's modulus to longitudinal Young's modulus becomes relatively small which is one of the significant structural problems associated with the use of high modulus filaments in composite structures. If multiple oriented fibre arrays are

utilised to solve the problem of low stiffness in the transverse direction, a decrease in the major stiffness of the fibrous composite follows.

Contours of the direct stress and Von Mises stress for a typical fibre reinforced composite are very similar to that of a particulate filled composite. The maximum concentration of the applied stress is in the matrix above the pole for rigid glass fibre in epoxy resin.

The maximum stress at the interface is the radial stress at the pole. The position of the maximum at the interface moves from about 40° at low volume fraction towards the pole for the higher volume fractions.

Since the failure strength of the interface is expected to be lower than failure strength of the resin, the stress concentration at the interface is considered to be more important for the study of the fracture behaviour than the stress concentration above the pole. The stress distribution in the fibre is almost constant for all volume fractions. The stress concentration reaches a slight maximum at the pole. The concentration of stress may lead to failure via the failure of the fibres in the transverse direction.

The concentration of the stress in the fibre may lead to failure via transverse splitting of the fibres. The concentration of applied stress in the radial direction at the interface may lead to tensile failure of the interface. The fracture strength of the material is predicted to fall with increasing fibre volume fraction.

Interfacial debonding was approached by a quadratic failure criterion based on the magnitudes of the interfacial radial and shear stresses computed by finite element method and the corresponding interfacial strength. The Cooper-Kelly model (CKM) with weak fibre/matrix interface is generally overconservative.

The applied stress needed to cause the debonding of the fibre and matrix is significantly lower than the tensile stress necessary to cause shear failure of the matrix in this case.

Our model predictions using interface debonding mechanism is in perfect agreement with the experimental results. This confirms that the interface debonding and brittle

failure are the dominant mechanism governing the failure of the fibre reinforced composite in this case.

The limited accuracy of the strength predictions is partly attributed to the simplified assumption of a regular microstructure. The sensitivity of the failure predictions to the fibre volume fraction indicates that failure may initiate locally in a region of closely packed fibres. To increase the accuracy of the strength prediction, appropriate strength data for the matrix and interface is needed.

5.1.6 Composites Reinforced With Short Fibre

The stress and strain distribution in unidirectional discontinuous fibre composites have been studied according to a fibre distribution without overlapping of fibres. The stress distributions obtained show that the tensile load applied to the cell is borne essentially by the fibre. Load is transferred between fibres by lateral shear of matrix. The shear load is localised at the fibre and inducing a stress concentration.

The results obtained for young's modulus show that modulus depends strongly on the geometrical arrangement of fibres. Without overlapping of fibres, the tensile load applied to composite is borne by alternate layers of matrix and matrix-fibre, following a scheme of stress equality. So the effective moduli are strongly dependent on the thickness of the matrix layers.

Although shear lag model is very appealing in this task because of its simplicity and also because of its ability to take into account critical factors, such as the reinforcement volume fraction and aspect ratio, it is based on several crude simplifications. the models based on finite element analyses shows that the shear stress is not constant along the reinforcement and matrix interface. The model also takes into account the importance of the stress concentration near fibre ends.

The brittle fracture stress of short glass fibre reinforced composite increases as the adhesion at the fibre-matrix interface increases. Competitive deformation processes between interfacial debonding and matrix cracking at fibre ends is proposed. The increase of interfacial shear strength by coupling prevents early failure at the interface, thus increasing the tensile failure stress of short fibre composites.

The deformation behaviour which shows a sharp drop in stress due to interfacial debonding followed by matrix yielding, is absent in the composites with good coupling at the fibre-matrix interface. The fracture strain after upper shear yielding is higher for the composites with poor coupling.

The model results obtained for Young's modulus of fibre reinforced composites show that it strongly depends on the geometrical arrangement of the fibres within the matrix. This arrangement is characterised by the volume fraction of fibres, the fibre aspect ratio and the fibre spacing parameter.

the finite element results for the interfacial shear stress are compared with the results of the shear lag and modified shear lag model. The shear lag analysis gives much higher shear interfacial stress. The difference between shear lag model and finite element results increases with volume fraction.

The tensile stresses from the analysis considering flux terms are higher for both volume fractions. The shear stress concentration distribution at the interface of the matrix and the filler does not change by including the flux terms in the field equations.

The tensile stress increases from the fibre ends towards the centre of the fibre. For each volume fraction at a certain point along the length of the fibre the tensile stress reaches its maximum and remains almost constant for the rest of the length of the fibre. The point at which the tensile stress reaches its maximum value depends on the volume fraction of the fibres. The higher the volume fraction the closer the peak point is to the fibre end.

The fibre critical lengths obtained by finite element model and Rosen model are compared for a range of filler volume fractions. Our model shows that the tensile stress in the fibre rises to its peak in shorter length of the fibre. Our results show that the critical length also depends on volume fraction.

An increase in the stress to breaking point can be observed at higher volume fractions. The stresses at the breaking point are much higher than the debonding stresses for the fibre glass and epoxy matrix. These differences are more remarkable at lower fibre aspect ratios.

Therefore it can be predicted that at low aspect ratios the debonding of the fibres acts as the initiation mechanism for the failure and it is followed by the failure of the matrix near the fibre ends. Since the aspect ratio is low, the concentration of the fibre ends is high and then the local cracks merge transversely from the direction of the applied load.

Catastrophic failure of the composite then occurs without any breaking of the fibres.

At higher aspect ratio, since the breaking stress of the fibres is lower, the failure occurs in two steps. In the first step the interface debonding and tensile failure of the matrix at the fibre ends is observed.

However, in contrast to the low fibre aspect ratio case, growing matrix cracks at fibre ends are quickly blunted by neighbouring fibres and hence no catastrophic failure occurs. Because of the cracks and interfacial debonding the modulus of composite drops significantly.

Our model shows that the breaking stress of the fibres reduces at low modulus. Therefore in the second step which corresponds to a the decreased modulus the tensile stress in the fibres can easily exceed the failure stress of the fibres leading to the breakage of the fibres.

5.2 SUGGESTIONS FOR FURTHER WORK

One basic assumption made in this analysis is that both the filaments and the matrix are linearly elastic and that no plastic or viscoelastic behaviour occurs. In an actual composite material, localised yielding undoubtedly does occur in the typically weak matrix material, permitting a redistribution of the high localised stresses. Depending on the type of matrix material being considered, either non-linear elastic, inelastic, or viscoelastic behaviour may occur. Thus, a logical extension of the present analysis will be to study this nonconservative material behaviour.

Because strength is affected more than stiffness by material and geometric nonhomogen eity and the resulting local perturbations in the stress and strain distributions. The effects of such local stress and strain perturbations on stiffness are reduced due to the smoothing effect of integration in the effective modulus theories.

On the other hand, material failure is often initiated at the sites of such stress and strain concentrations, so the effect on strength is much greater. The variability of strength in reinforcing fibres alone may be quite significant, and statistical methods must be used for accurate analysis.

The theoretical results obtained for Young's modulus of short fibre reinforced composites depend strongly on the geometrical arrangement of fibres, thus Young's modulus of discontinuous fibre composites cannot be derived from an isolated cell scheme. In our model we have ignored the effect of the overlapping fibres. In order to consider this effect a hexagonal arrangement of fibre should be modelled.

The real arrangement of filler particles or fibres throughout the matrix is normally random. A statistical technique is needed to consider the effect of the random distribution of fibre in the matrix. In our model we assumed that particles and the diameter of fibres are of the same size. Whereas in practice the filler particles and fibre diameters is not the same. This means that in order to get closer to the real microstructure of the composite a unit cell is not enough. and a model geometry containing several particles of different sizes is needed

The findings of the project can be summarised as:

- A FORTRAN code is developed that can be used for studying the behaviour of the polymer composites in the both solid and liquid states. A convenient penalty parameter is used in order to obtain the equilibrium solid mechanic equations starting from the Stokes flow equations.
- The boundary line integral terms are included in the model. Further investigation shows that these terms do not have much effect on the computational result in the case of the particulate filled composites. But for the short fibre composites taking these terms into account can affect the displacements and stresses values considerably.

- The slip boundary condition is imposed at the interface of the filler and matrix in order to simulate the level of adhesion at the boundary of a debonded filler particle and the stress field at the interface is studied. The result are used to predict the further crack propagation in the composite

- The developed model is applied for different types of composites such as composites filled with hard particles or soft particles, composite reinforced with continuous or short fibres. The results are validated by comparing with experimental data and other well established model. The modulus values can be predicted closely and the strength values are generally underestimated. In each case the calculated stress fields are used to predict the failure mechanism. The dominant mechanism of the toughening is predicted in the case of soft particles. For the short fibre composites the critical length is found from the calculations and the effect of fibre aspect ratio and spacing is studied. The crack propagation is predicted for debonded filled composites.

REFERENCES

Adams, D. F., *Fibre Sci. Technol.*, 7, 111, (1974).

Agrawal, B.D. and L.J. Broutman, *Fibre Sci. and Tech.*, 7, 63, (1974)

Agrawal, B.D., G.A. Panizza, L.J. Broutman, *J. Americ. Ceramic Society*, 54, 1, 620, (1971)

Ahmed, S. and F. R. Jones, *J. Mater. Sci.* 25, 4933, (1990).

Berthelot, J.M., A.Cupic and K. A. Brou, *J. Comp. Material*, 27, 14, 1391,(1993)

Bird, R. B., W. E. Stewart and E. N. Lightfoot,*"Transport Phenomena"*, McGraw-Hill (1960)

Brandrup, J., E. H. Immergut, *"Polymer Handbook"*, John Wiley , Vol 8, 9 (1989)

Brassell, G.W., and K. B. Wischmann, *J. Mater. Sci.* 307, (1974)

Broutman, L. J., and R. H. Krock, *"Modern Composite Materials"*, Addison Wesley (1967).

Christensen, R.M., Proceed. IUTAM Symp. *On Mechanics Of Composite Material* (1982), Ed. by Z.

Hashin and C. T. Heracovich, Pergamon press.

Christman, T., A. Needleman, S. Nutt, and S. Suresh, *Material Sci. and Eng.*, A107, 49 (1989)

Cooper, R. D. and A. Kelly, *Interfaces In Composites, ASTM STP 452*, 90 (1969)

Counto, U. J., *Mag. Concr. Res.*, 16, 129, (1964).

Cox, H. L. , *British Journal of Applied Physics*, 3, 72-79 (1952)

Davy, P. J. and F. J. Guild, *J. Mater. Sci.* 24, 298, (1989).

Dekkers, M. E. J. and D. Heikens, *J. Mater. Sci.*, 20, 3865, (1985).

Dekkers, M. E. J. and D. Heikens, *J. Mater. Sci.*, 19, 473, (1984)

Einstein, A., *"Investigation On Theory Of Brownian Motion"*, Dover (1956).

Eischen, J.W., S. Torquato, *J. Appl. Phys.*, 74 (1), 159, (1993)

Frankel, N. A. and A. Acrivos, *Chem. Eng. Sci.*, 7, 847, (1967).

Gardner, S. D. and C. U. Pittman, *Comp. Sci. Technol.*, 46, 307, (1993).

Gent, A. N. and P. B. Lindley, *Proc. R. Soc.*, A 249, 195 (1959)

Gibson, R. F. , *"Principles Of Composite Material Mechanics"*, McGraw-Hill (1994)

Guth, E., *J. Appl. Phys.* 16, 21 (1951).

Halpin, J. C. and Tsai, S. W., *AFMI-TR-67-423* (1969)

Halpin, J. C., *J. Compos. Mater.*, 3, 732, (1969)

Hanson, T. C., *J. Amer. Conc. Inst.*, 62, 193 (1965).

Hashin, Z. and S. Shtrikman, *J. Mech. Phys. Solid*, 11, 127, (1963).

Hashin, Z. and B. W. Rosen, *J. Appl. Mech.* 31, 223, (1964)

Hashin, Z., *Bull. Res. Coun. Israel* 5C, 46, (1955).

Hirsch, T. J., *J. Amer. Conc. Inst.*, 59, 427, (1962).

Huebner, K. H. and E. A. Thornton, *"Finite Element Method For Engineers"*, John Wiley & Sons (1982)

Kerner, E. H., *Proc. Phys. Soc.*, 69B, 808, (1956).

Kunz, S. C., J. A. Sayre, and R. A. Assink, *Polymers Churchill Conference*, Cambridge, 28, 368 (1982)

Leidner, J. and R. T. Woodhams, *J. of Applied Polymer Science*, 18, 1639 (1978)

McCullough, R. L., *Proceed. IUTAM Symp. On Mechanics Of Composite Material* , (1982), Ed. by Z.

Mooney, M., *J. Colloid Sci. 6*, 162, (1951).

Neilsen, L. E., *J. Appl. Polym. Sci.*, 10, 97 (1966)

Neilsen, L.E., *J. Appl. Phys.* Vol 41, No 11, 4626, (1970).

Nicolais, L. and R. A. Mashelkar, *J. Appl. Pol. Sci.*, 20, 561 (1976)

Nicolais, L. and M. Narkis, *Polym. Eng. Sci.*, 11, 194 (1971)

Papanicolaou, G. C. and D. Bakos, *J. of Reinforced Plastics and Composites*, II, Feb.,104-126 (1992)

Piggot, M. R. and J. Leidner, *J. Appl. Pol. Sci.* , 20, 561 (1974)

Piggot, M. R., *"Interfaces in composites "*, Elsevier (1991)

Pomies, F. , *M.S. thesis*, Department of Mechanical Engineering, Florida Atlantic University (1992)

Pomies, F. and L. A. Carlsson, *J. Compos. Mater.*, 28/1, 22-35 (1994)

Quemeda, D., *Rheol. Acta*, 16, 82, (1977).

Rosen, B. W. , *AIAA J.*, 2, 1985 (1964)

Sato, Y. and J. Furukawa, *Rubber Chem. Technol.* 36, 1081, (1963)

Scharger, M., *J. of Applied Polymer Science*, 22, 2379 (1978)

Schwier, C. E., A. S. Argon and R. E. Cohen, *Phil. Mag.*, 52, 581 (1985)

Sheldon, R. P., *"Composite polymeric materials"*, Applied science publishers (1982).

Smallwood, H. M., *J. Appl. Phys.*, 15, 758, (1944).

Spanoudakis, J. and R. J. Young, *J. Mater. Sci.* , 19, 487 (1984)

Sun, C. T. and S. G. Zhou, *J. Reinf. Plast. Comp.*, 7, 515 (1988)

Takayanagi, M., S. Nemura and S. Minami, *J. Polym. Sci.* 5C, 113, (1964).

Termonia, Y., *J. of Mater. Sci.*, 25, 4644-4653 (1990)

Thomas, D. G., *J. Colloid Sci.*, 20, 267, (1965).

Trantina, G. and R. Nimmer, *"Structural Analysis Of Thermoplastic Components"*, John Wiley & Sons (1994).

Tsai, S. W., *U.S. Government Rep., AD 834851*, (1968)

Zienkiewics, o.c. and R.L. Taylor, *"The Finite Element Method "*, Vol. 1, McGraw-Hill (1988)